Bound By
Blissett Bookbinders
020 8992 3965
www.blissetts.com

A SCALE-DOWN EVALUATION OF ADSORPTIVE PROCESS OPTIONS FOR THE RECOVERY AND INITIAL PURIFICATION OF ANTIBODY FRAGMENTS FROM CRUDE *E. COLI* FEEDSTOCKS

A thesis submitted to the University of London
for the degree of Doctor of Engineering
in Biochemical Engineering

by

Samir Bedri Ujam

June 2007

The Advanced Centre for Biochemical Engineering
Department of Biochemical Engineering
University College London
Torrington Place
London WC1E 7JE

ProQuest LLC
789 East Eisenhower Parkway
P.O. Box 1346
Ann Arbor, MI 48106-1346

Abstract

Improvements in fermentation processes, coupled with the rising demand for biologics, are requiring that new ways in which therapeutics are recovered and purified be identified. Column-based approaches are constrained by the need for pre-treatment which leads to decreases in process yield and throughput. By contrast batch adsorption has the potential to handle high solids concentrations and can eliminate the need for pre-treatment. It may offer a viable, robust and simple means to improved process yields and throughput and this forms the central theme to this work.

The thesis presents a scale-down evaluation of the use of both column and batch approaches based upon the adsorption of an antibody fragment (Fab') using ion exchange media.

The particular Fab' used throughout this study was found to bind to cell debris and therefore removal of cell debris had a significant impact on the total process yield. The recovery of the Fab' from unclarified feedstocks, through the use of packed bed columns and stirred tank batch adsorption, was investigated, as was the impact of feedstock ionic strength and solids concentration.

The use of homogenisation and periplasmic heat lysis as distinct product release routes were also investigated and compared via a series of Windows of Operation.

Isotherm data was used to develop an empirical model capable of predicting process performance. From this the effect of cell disruption and feedstock properties, as well as other factors such as the length of the lysis procedure and the number of adsorption cycles, were modelled and the data used to generate Windows of Operation, identifying feasible operating conditions.

The limitations of using packed bed columns for the recovery of Fab' from an unclarified *E. coli* feedstock are discussed. Batch adsorption was found to offer a viable alternative to packed bed chromatography. An analysis of the commercial and regulatory aspects of the use of batch adsorption as an alternative to conventional packed bed adsorption concludes the thesis.

To my loving family

Acknowledgements

Firstly, I would like to thank my supervisor Professor Nigel Titchener-Hooker for his advice, guidance, and patience. His support and encouragement during this study helped me find the tunnel, and then the light at its end.

I would also like to thank Professor Mike Hoare and Dr Daniel Bracewell for their expert advice and time. Their input has been invaluable.

There are many people at the department of Biochemical Engineering who have contributed significantly to my time at UCL. I am grateful for the help and support of Dr Heidi Salte, John Joseph, Dr Kais Lakhdar, Rezwan Islam, Waqar Hussain, Andrew Tustian, Dr Andrew Booth, and the rest of my friends and colleagues at UCL_{BE}.

I am especially grateful to both Andrew Tustian and Andrew Booth for their help with the fermentations, John for his advice on chromatography and modelling, and finally, to Heidi for her continued support, encouragement, and advice on centrifugation and the preparation of this thesis.

Most of all I would like to thank my parents, brothers and sister – without your continued love and support this thesis would not have been possible at all.

The man of knowledge is the one who recognises that what is known is very little compared to what is not known. As a result he considers himself ignorant, and accordingly increases his efforts to know more by going out in search of knowledge.

Imam Ali ibn Abi Talib (a.s.)
(600-661 A.D.)

Table of contents

List of figures

List of tables

Nomenclature

Symbols

A	Absorbance	-
A	Exponential decay amplitude	-
b	Empirical Stickel constant	cm^2/h
c	Σ correction factor to account for non-ideality	-
C_0	Initial solute concentration	mg/mL
C_d	Debris-bound Fab' concentration	mg/mL
C_{d0}	Initial debris-bound Fab' concentration	mg/mL
C_{eq}	Equilibrium solute concentration	mg/mL
C_f	Concentration of debris-bound Fab' per gram debris	mg Fab/g debris
C_{f0}	Initial concentration of debris-bound Fab per gram debris	mg Fab/g debris
C_s	Supernatant Fab' concentration	mg/mL
C_{s0}	Initial supernatant Fab' concentration	mg/mL
C_t	Total equilibrium Fab' concentration	mg/mL
C_{t0}	Initial total available Fab' concentration	mg/mL
D	Column diameter	cm
d_{50}	Mean particle diameter (where 50% of the particles, by volume, are smaller than the stated diameter)	-
f_l	Correction factor for spacer caulks	-
g	Acceleration due to gravity	m/s^2
I	Feedstock ionic strength	mS/cm
K_f	Empirical Freundlich coefficient	-
K_d	Langmuir dissociation constant	mg/mL
K	Linear isotherm distribution coefficient	-
L_0	Settled bed height	cm
L_{crit}	Bed height at which u_{crit} occurs	cm
m	Empirical Stickel constant	cm^2/h
n	Empirical Freundlich coefficient	-
N	Rotational speed	rpm

N_{AD}	Number of active discs in a disc-stack	-
OD	Optical density	-
Q	Volumetric flow rate	L/h
Q_{eq}	Solute concentration on the adsorbent	mg/mL ads
Q_{max}	Maximum binding capacity of the adsorbent	mg/mL ads
R	Percentage Fab' recovery	-
r_1	Inner disc radius	m
r_2	Outer disc radius	m
r_e	Effective radius	m
r_i	Inner radius	m
r_o	Outer radius	m
s_e	Effective settling distance	m
t_1	Exponential decay constant	-
u_{crit}	Critical velocity	cm/h
u_{op}	Packed bed column operating velocity	cm/h
V	Volume	L
V_{lab}	Volume of feed material in laboratory tube	L
V_l	Feedstock load volume	L
V_m	Adsorbent volume	L
x	Adsorbent phase ratio	-
x	Fraction of centrifugation time required for acceleration	-
$\bar{x}$	Mean Fab' concentration	mg/mL
y_0	Exponential decay equation offset	-
y	Fraction of centrifugation time required for deceleration	-
y	Dimensionless concentration	-

Greek letters

λ_{crit}	Critical bed compression	-
θ	Half disc angle	rad
σ	Standard deviation of Fab' concentration	mg/mL
ω	Angular velocity around the centre of rotation	rad/s
Σ	Sigma factor	m^2

1 Introduction

1.1 Research motivation

In May 2005 there were 18 therapeutic monoclonal antibody (mAb) products on the US market, approximately 500 mAbs being developed by more than 200 companies worldwide and approximately 80 mAbs in clinical trials (DrugResearcher.com, 2005). Due to recent technological advances, and the imminent release of several new antibody products, the worldwide market for therapeutic and diagnostic antibodies is expected to reach $26 - $30 billion by 2010 (DrugReasearcher.com, 2005; Evans and Das, 2005). However, the cost of development and commercialisation of such new products can be as high as $800 million (Rathore *et al.*, 2004), with the process taking up to 12 years to complete (Petrides *et al.*, 2002). The manufacture of antibody therapeutics faces several critical challenges including improving the process economics and efficiency, meeting demanding FDA regulations and reducing costs (Roque *et al.*, 2004). As much as 80% of the total manufacturing cost of a therapeutic antibody is incurred during the downstream processing (Roque *et al.*, 2004; Aldridge, 2006). The reduction in the costs of process development and manufacture of an antibody or antibody derivatives is therefore an important factor in the future success of these novel therapeutics. In order to reduce process development costs manufacturers are turning to scale-down methods, including high throughput process screening (HTPS) to evaluate rapidly numerous process options. To improve manufacturing output the integration of primary recovery and initial purification, through the use of batch adsorption unit operations, could now be considered as a viable option. The evaluation of such approaches and for methods which allow for the rapid assessment of adsorptive process options provided the motivation for this research.

Section 1.2 provides general information on antibodies and antibody derivatives, including a description of their structure and commercial application. The production of antibody fragments, based upon expression in *E. coli*, is described in Section 1.3. Section 1.4 examines the various adsorptive methods available for the primary

recovery and initial purification of antibody fragments from fermentation broths and unclarified feedstocks. The main aims and objectives of the thesis are presented in Section 1.5, and finally, Section 1.6 gives a description of the thesis layout.

1.2 Antibodies and antibody fragments

1.2.1 Structure of whole antibodies

The basic structure of all antibodies is a Y-shaped molecule composed of two identical light (L) chains and two identical heavy (H) chains. Inter-chain disulphide bonds and non-covalent interactions hold together the heavy and light chains as well as the two heavy chains (Vaughan *et al.*, 1998). Both the heavy and the light chains can be divided into regions, or domains, based on the variability of their amino acid sequence. Each chain consists of one variable (V) domain, which has a highly variable amino acid sequence and is responsible for antigen binding, as well as one or more constant (C) domains which have a relatively constant amino acid sequence and are responsible for binding effector molecules. Each light chain contains one variable (V_L) domain and a single constant (C_L) domain. The heavy chains contain one variable (V_H) domain and 3 constant (C_{H1}, C_{H2} and C_{H3}) domains (Vaughan *et al.*, 1998). The point at which the chains meet and form the Y-shape of the molecule is called the hinge region, due to the fact that there is some flexibility at this point. There are 5 classes of immunoglobulins, of which class G (IgG) is the most important from a biotechnology perspective (Maynard *et al.*, 2000). Figure 1.1 shows an illustration of the structure of a typical IgG molecule.

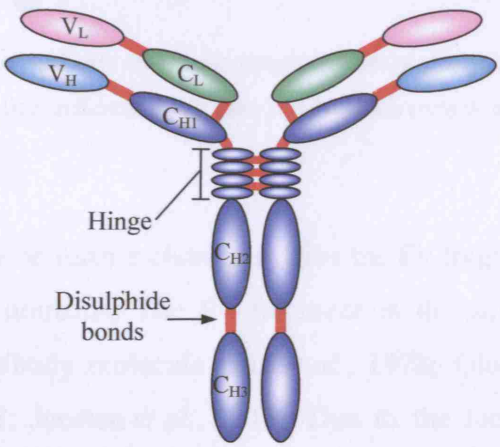

Figure 1.1. The structure of a typical IgG antibody.

1.2.2 *Structure of antibody fragments*

Proteolytic digestion of whole antibodies results in various antibody fragments. Digestion with papain results in the molecule breaking at the hinge region before the heavy chain inter-chain disulphide bond, as seen in A of Figure 1.2. This yields two identical Fab (fragment antigen binding) fragments, each with a single site for antigen binding, as well as a third fragment called the Fc (fragment crystallisable) which lacks the ability to bind antigen (Roitt, 1991). Each Fab fragment contains the light chain and the V_H and C_{H1} domains of the heavy chain. The Fc contains the C_{H2} and C_{H3} domains of the remaining heavy chains. Digestion of the whole antibody with pepsin breaks the heavy chain inter-chain disulphide bonds after the hinge region, as seen in B of Figure 1.2. This results in a Fab' fragment, which is a Fab fragment including portions of the hinge region. Depending on the proteolytic conditions this fragment may be divalent ($F(ab')_2$) or monovalent. The remaining Fc region is digested into peptides.

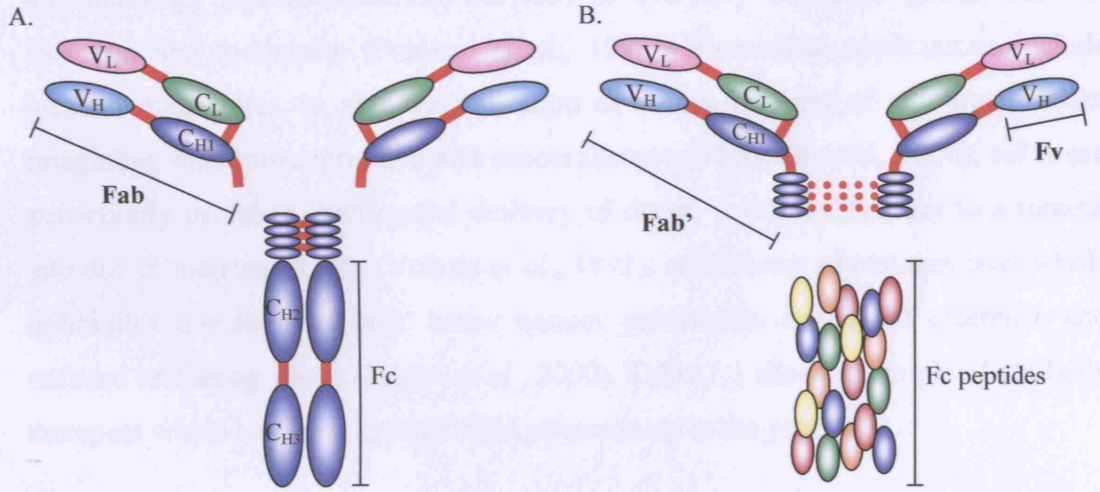

Figure 1.2. An illustration of antibody fragments resulting from proteolytic digestion using A: papain, and B: pepsin. Dashed red line indicates disulphide bonds which may or may not exist, depending on proteolytic conditions.

The Fab fragments can be further cleaved to give the Fv fragment, which consists of only the V_L and V_H domains. The Fv fragment is the smallest active fragment derivable from an antibody molecule (Lin *et al.*, 1978; Glockshuber *et al.*, 1990; Brinkman *et al.*, 1997; Joosten *et al.*, 2003). Due to the lack of disulphide bonds

between the V_H and V_L domains Fv fragments are relatively unstable (Glockshuber *et al.*, 1990). To improve the stability of the Fv fragments the two domains can either be linked through a peptide link to give a single-chain Fv (scFv) (Bird *et al.*, 1988) or a disulphide bridge to give a disulphide stabilised Fv (dsFv) (Glockshuber *et al.*, 1990). The type and length of linkers used has been reported previously (Bird *et al.*, 1988; Huston *et al.*, 1988; Whitlow *et al.*, 1993, 1994; Kortt *et al.*, 1997). The most frequently used linker, $(Gly_4\text{-}Ser)_3$, was introduced by Huston *et al.* (1988) and consists of 15 peptide residues (Kortt *et al.*, 1997). A dsFv is obtained when cysteine residues are introduced at the interface between the V_H and V_L domains forming disulphide bonds which hold the domains together (Glockshuber *et al.*, 1990).

1.2.3 Commercial application of antibodies and antibody fragments

Antibodies are currently used in a wide range of commercial products, not only in biotechnology and biomedicine, but also in everyday consumer goods, such as shampoo and toothpaste (Franken *et al.*, 1998). Biomedical applications include medical diagnostics, in vivo neutralisation of toxins, delivery of radionuclides for imagining, immunosuppression and cancer therapy (Maynard *et al.*, 2000). scFvs are particularly useful in the targeted delivery of drugs, toxins or nuclides to a tumour site due to their small size (Yokota *et al.*, 1992). scFvs have advantages over whole antibodies due to potentially better tumour penetration and blood clearance and reduced immunogenicity (Freyre *et al.*, 2000). Table 1.1 shows a sample of antibody therapies which had been granted FDA approval up to the year 2002.

Antibodies are also used as biosensors and in immunoassays, such as enzyme-linked immunosorbent assay (ELISA), and are being evaluated for use in the food and environmental industries for routine monitoring to detect microbial contaminants or organic pesticides (Maynard *et al.*, 2000). Antibody fragments can be immobilised onto porous supports enabling the purification of a target antigen by affinity chromatography (Berry and Davis, 1992; Loetscher *et al.*, 1992).

Table 1.1. Monoclonal antibody therapies approved by the US Food and Drug Administration (FDA). Adapted from Nature (2002).

Product	Condition	Company	Approved
Orthoclone OKT3	Transplant rejection	Johnson & Johnson	June 1986
ReoPro	Cardiovascular disease	Eli Lilly	December 1994
Rituxan	Non-Hodgkin's lymphoma	Genentech	November 1997
Synagis	Respiratory syncytial virus	MedImmune	June 1998
Remicade	Rheumatoid arthritis/ Crohn's disease	Johnson & Johnson	August 1998
Herceptin	Metastatic breast cancer	Genentech	September 1998
Campath	Lymphocytic leukaemia	Millennium Pharmaceuticals	May 2001
Zevalin	Non-Hodgkin's lymphoma	IDEC Pharmaceuticals	February 2002

1.3 Methods of antibody fragment production

In order to meet the increasing demand for antibody fragments the development of cost effective large scale production methods has become essential. The success of several recent clinical trials has lead to an increased interest in expressing various forms of antibodies. Therapeutic doses are often quite large, exceeding a gram per patient per year (Andersen *et al.*, 2004) and so an expression system capable of high production levels is needed. There are a number of expression systems capable of expressing antibody fragments including mammalian, yeast, insect and bacterial (Verma *et al.*, 1998). The expression of antibody fragments in transgenic plants and animals has also been developed (De Neve *et al.*, 1993; Fiedler *et al.*, 1997; Larrick *et al.*, 2001; Peeters *et al.*, 2001).

Each expression system has its advantages and disadvantages. The use of mammalian cells for the production of antibodies is well established and can achieve product titers of up to 1 g/L at large scale using recombinant CHO and COS cells (Maynard *et al.*, 2000). However, large scale production of antibodies using mammalian cells is expensive and time-consuming (Joosten *et al.*, 2003). The use of plants as large scale antibody production systems provides an easy, low cost method of obtaining large quantities of antibodies. The advantages of the plant system include capital cost savings, production flexibility to suit market needs and the lack of mammalian pathogens (Andersen *et al.*, 2004). The disadvantages of such a

system include the long lead time for production, regulatory uncertainties and an expensive and laborious downstream processing route (Joosten *et al.*, 2003; Andersen *et al.*, 2004). Bacterial systems have become the most commonly used methods of producing recombinant antibody fragments. The technology is well established, and is relatively cheap and quick (Roque *et al.*, 2004).

1.3.1 E. coli expression of antibody fragments

The use of *Escherichia coli* as an expression system for the production of antibody fragments has been the focus of much of the research into antibody fragment production. The main advantages of using this system include the ability to produce rapidly large amounts of protein, using simple cheap media, in large microbial fermenters (Weir *et al.*, 2002; Joosten, *et al.*, 2003). Other benefits of this system include the fact that genetic manipulations of *E. coli* are relatively straightforward, production of cell lines is quick and easy when compared to eukaryotic cell lines and production can progress rapidly from antibody selection to good manufacturing practice (GMP) (Joosten, *et al.*, 2003; Andersen *et al.*, 2004). However, *E. coli* expression systems do have disadvantages, such as an inability to glycosylate proteins, which means whole antibodies can not be produced in *E. coli* as they are glycosylated in the C_{H2} domain (Verma *et al.*, 1998; Joosten *et al.*, 2003).

Expression of antibody fragments produced in *E. coli* can be achieved in a number of ways, such as the generation of cytoplasmic inclusion bodies, which then require *in vitro* folding, or expression within the cytoplasm followed by secretion of the fragments into the culture medium and/or the periplasm (Joosten *et al.*, 2003).

Cytoplasmic expression of antibody fragments can lead to extensive aggregation and the formation of large insoluble intracellular particles, known as inclusion bodies. Due to their large size and density the inclusion bodies can be easily separated from the other cell components (Maynard *et al.*, 2000). As the inclusion bodies contain the unfolded protein the development of refolding methods is required to recover the antibody fragment (Verma *et al.*, 1998). Often this consists of solubilising the inclusion body in a strong denaturant, such as Guanidine Hydrochloride or Urea, and

a reducing agent, such as β-mercaptoethanol or dithiothreitol (DTT). The subsequent removal of the denaturant by dilution or dialysis results in the correctly folded antibody fragments (Verma *et al.*, 1998; Maynard *et al.*, 2000). However, this refolding process is cost-intensive and laborious, and leads to a significant decrease in the yield of the antibody fragments (Joosten *et al.*, 2003).

An alternative method involves attaching leader peptides to the N terminus of the antibody fragment, which direct the secretion of the antibody fragment to the periplasm. The periplasm provides an oxidising environment in which folding, assembly, and disulphide bond formation can occur, resulting in the antibody fragment refolding into the functional state (Verma *et al.*, 1998; Weir *et al.*, 2002; Joosten *et al.*, 2003). The periplasmically expressed antibody fragments can then be recovered by cell lysis. Although periplasmic expression can achieve levels of antibody fragments in excess of 1-2 g/L the level of expression can vary greatly, especially as scFv fragments often fail to fold properly or aggregate in the periplasm (Maynard *et al.*, 2000). Other problems associated with this method include the leaking of antibodies from the periplasm through the outer membrane into the culture medium, and toxicity of the antibody towards the host cell (Verma *et al.*, 1998; Maynard *et al.*, 2000; Joosten *et al.*, 2003).

1.4 Recovery and purification of antibody fragments from *E. coli* fermentation broths

The unit operations which are typically utilised during the downstream processing of antibody fragments are described in this section.

1.4.1 Objectives of downstream processing

The recovery and purification of antibody fragments, from the culture medium to the point where it is suitable for its end use, is the ultimate objective of downstream processing (DSP). DSP is usually divided into a number of key steps which are often determined by a number of factors such as the characteristics of the fermentation

broth, the source of the product, the physical and chemical properties of the product and its intended end use. The first of these key steps is primary recovery. The methods involved in primary recovery depend on the location of the antibody fragment. For extracellular fragments the aim is to separate the cells from the culture medium through the use of centrifugation and/or filtration. The primary recovery of periplasmically expressed antibody fragments and inclusion bodies is often a three stage process including the recovery of cells from the fermentation broth by centrifugation and/or filtration; the release of the products by various cell disruption techniques; and finally the removal of cells or cell debris. However, prior to further purification, the inclusion bodies need to be processed as described in Section 1.3.1. Following primary recovery, purification of the antibody fragments by one or more chromatographic steps is performed, with the most commonly used techniques being ion exchange and affinity chromatography.

To minimise capital and operating costs and maintain product yield, a downstream process should include as few a steps as possible. The use of integrated recovery processes such as batch adsorption and expanded bed adsorption, as well as aqueous two-phase systems, combine clarification, concentration and initial purification. The use of integrated recovery processes minimises the number of steps and can lead to increased product yield and process throughput.

1.4.2 Cell recovery and feedstock clarification

For many antibody production processes the removal of cells from the fermentation broth is the first step in the recovery process. The cell recovery and clarification methods used during DSP depend on the amount of cells present as well as the affect any residual cell debris may have on subsequent processing methods. For example, the use of high resolution purification methods requires the feedstock to be free of all particulate material. The removal of cells and cell debris is most often performed using centrifugation and/or filtration.

1.4.2.1 Centrifugation

Solid-liquid separation through the use of centrifugation is widespread in bioprocessing. Centrifugation can be used to remove cells from the culture medium after fermentation, as well as further downstream for the removal of cell debris, spheroplasts and inclusion bodies from the liquid phase. Centrifugation utilises the density difference between the solid and liquid phases. Rotating the solid-liquid mixture at high speeds creates a centrifugal force which leads to an increase in the density gradient. Laboratory scale centrifuges are often low volume batch systems which are capable of achieving high centrifugal forces and hence good levels of clarification. However, industrial scale clarification requires centrifuges which can handle large volumes of process feed. These machines generate lower centrifugal forces and offer shorter residence times and as a result are less efficient at clarification than laboratory scale centrifuges. The main types of centrifuges used in industrial bioprocessing are the tubular-bowl, multi-chamber bowl and disc-stack centrifuges.

Tubular-bowl centrifuges are amongst the simplest types of large scale centrifuges and are widely used in the biopharmaceutical industry. Although a continuous stream of feed material is applied to the centrifuge, tubular-bowl centrifuges are operated as batch centrifuges, as they must be stopped in order to remove the solids. Typically tubular-bowl centrifuges are used for small scale cell harvest, clarification of cell debris and the recovery of inclusion bodies.

A multi-chamber bowl centrifuge is effectively comprised of a number of tubular-bowls, and so has a larger capacity for solids. However, as a result of frequent stopping and emptying of the tubular-bowl and multi-chamber bowl centrifuges the use of these machines is often limited to feed solutions which have a relatively low solids concentration. Feed solutions with higher solids concentrations can be clarified using a disc-stack centrifuge.

Disc-stack centrifuges contain a stack of conical-shaped metal discs which provide a large surface area for the sedimentation of solids. The ability to discharge the solids

continuously through nozzles, or intermittently with the use of valves which open when the bowl capacity is reached, enables the disc-stack centrifuge to operate continuously.

The use of centrifugation for the processing of antibody fragments has several disadvantages including high investment and energy costs, incomplete biomass removal, damage to the product caused by shear, and aerosol production.

1.4.2.2 Membrane filtration

Even in a situation where centrifugation was able to remove 99% of cell debris the remaining particulates would cause problems during subsequent high resolution purification. Centrifugation of homogenate solutions is particularly difficult due to the small particle size and often negligible density difference. Filtration separates solids from a solid-liquid mixture according to their size and not density differences. Microfiltration is often used as an alternative to centrifugation and can achieve nearly particulate-free solutions. Dead-end filtration is the simplest form of microfiltration and involves the feedstock flowing perpendicular to the filter membrane. During dead-end filtration solids are deposited on the membrane surface; however, over time this eventually leads to membrane fouling and reduced performance. The use of cross-flow filtration is often preferred to dead-end filtration for the removal of cell debris as it overcomes the problem of solids accumulation and membrane blockage. During cross-flow filtration the feedstock flows parallel to the filter membrane and cell debris which can not flow through is swept away by the incoming feedstock.

Microfiltration membranes with a pore size of 0.1-0.2 μm are often used for the separation of particulates in the range of 0.1-10 μm. As well as the membrane pore size, the membrane area, material of construction and membrane configuration (for example hollow fibre, flat sheet or rotary drum) can all impact the process efficiency. The properties of the feedstock such as the pH, ionic strength and viscosity will also affect the efficiency of the filtration process. The development of an effective filtration process requires the screening of a number of filter units, solution

conditions and operating conditions such as the cross-flow velocity and transmembrane pressure.

Although the use of filtration can achieve an essentially particulate-free solution the method is often limited by fouling of the membrane which causes a decrease in the flux per unit area of membrane and, therefore, the process efficiency. As a result large membrane areas are needed which can result in substantial operating costs.

1.4.3 Release of intracellular antibody fragments

For intracellularly expressed antibody fragments the next stage in the recovery process is cell disruption, in order to release the antibody fragments into solution. This can either be achieved through the use of mechanical cell disruption or by selective periplasmic release.

1.4.3.1 Mechanical cell disruption – high pressure homogenisation

The high pressure homogeniser is the most widely used industrial disruption device (Sauer *et al.*, 1989). A homogeniser consists of a positive displacement pump with one or more adjustable restricted orifice discharge valves. During operation the cell suspension is forced at high pressure through the discharge valve. Cell disruption is thought to result from a number of mechanisms, such as the high shear levels, impingement and cavitation (Sauer *et al.*, 1989). The degree of cell breakage may also be affected by the operating temperature, valve unit design, number of passes through the device, the disruption pressure, the nature of the organism and the culture medium (Sauer *et al.*, 1989; Keshavarz-Moore *et al.*, 1990). The cell breakage efficiency is increased when homogenisation is performed at high pressures. However, repeated passes through the device at high pressures can produce very fine cell debris particles which can reduce the efficiency of subsequent clarification steps. The release of all cellular contents into the feedstock is also a disadvantage of homogenisation as it affects the further purification due to the release of numerous contaminants. The release of proteases can also lead to product loss due to degradation.

1.4.3.2 *Selective periplasmic release*

Complete cell disruption by homogenisation can expose periplasmically expressed proteins and antibody fragments to cytoplasmic proteases, which increase the risk of proteolytic degradation. The release of cytoplasmic contents including proteases, DNA and lipids also complicates subsequent purification methods. The use of periplasmic extraction facilitates the selective release of the periplasmic contents without the release of contaminating cytoplasmic proteins and intracellular material. Unlike homogenisation, periplasmic extraction maintains cell wall integrity and does not produce fine cell debris particles which can impact the efficiency of subsequent clarification steps.

Numerous methods of periplasmic release have been reported in the literature including the use of chemical methods using detergents such as Triton X-100 and guanidine (Naglak and Wang, 1990), EDTA (Ryan and Parulekar, 1991), chloroform (Lall *et al.*, 1989), and glycine (Yu *et al.*, 1991); biological methods using lytic agents such as lysozyme (French *et al.*, 1996; Pierce *et al.*, 1997; Selisko *et al.*, 2004); physical methods such as osmotic shock (Neu and Heppel, 1965; Beacham, 1979), freeze/thaw (Johnson and Hecht, 1994), and heat treatment (Tsuchido *et al.*, 1985). Weir and Bailey (1997) describe a method of periplasmic release which combines a chemical approach using EDTA with heat treatment. It is this latter method which will be used in this thesis.

1.4.4 *Initial antibody fragment purification*

After the periplasmic release of the antibody fragments the process stream can either be clarified by centrifugation or filtration, or be processed directly through the use of batch or expanded bed adsorption. However, at this stage of the recovery process the product is usually present in the process stream as a dilute solute. In order to reduce the process volume a concentration step is often the next stage in the purification sequence. Two of the most commonly used methods for product concentration are ultrafiltration and adsorption.

1.4.4.1 *Ultrafiltration*

Ultrafiltration is used to concentrate dissolved molecules of different sizes. Lee *et al.* (1986) reported that the monoclonal antibody murine IgG_{2a} was concentrated 10-20 fold using ultrafiltration. The membranes used in ultrafiltration have pores which allow the passage of salt ions, buffers and water, but prohibit the passage of the target protein. Another application of ultrafiltration membranes is diafiltration which is used for buffer exchange, similar to dialysis. However, unlike dialysis, with the use of ultrafiltration membranes, buffer exchange can occur rapidly and easily at large scale (Wheelwright, 1991).

The performance of ultrafiltration is limited by the effects of concentration polarisation at the surface of the membrane and fouling (Sofer and Hagel, 1997). Adsorption chromatography provides an alternative, more selective method of initial concentration and purification of the antibody fragments.

1.4.4.2 *Adsorption chromatography*

Chromatography is considered to be one of the most important techniques used in protein purification (Yamamoto, 1995). It is often the only technique used in modern processes (Rehm and Reed, 1993). The term *chromatography* refers to a group of separation techniques that are characterised by the distribution of the molecules to be separated between two phases, one stationary and the other mobile (Janson and Jönsson, 1998). There are two main mechanisms for chromatography: adsorption, which involves the binding of solutes onto a chromatographic medium, and non-adsorption, such as gel filtration, which are based on the different rates of diffusion of solutes of different sizes in a porous matrix (Wheelwright, 1991).

For the purpose of this study the emphasis of this section will be adsorption chromatography techniques.

Adsorption chromatography occurs as a result of diffusion of molecules from the process feed onto the surface of a solid adsorbent. Adsorption relies on the reversible

interaction between solute molecules and a ligand immobilised on the adsorbent. Contaminants and products are separated according to their affinity for the ligand. The attraction between the solutes and the adsorbent can be due to a number of different types of interactions. The main types of interactions utilised in antibody purification are charge (ion exchange) and biospecific affinity (affinity) interactions. However, this study utilised only ion exchange methods since these are generic and relatively inexpensive. A brief description is provided below.

1.4.4.2.1 Ion exchange chromatography (IEC)

Of all the chromatographic techniques, ion exchange chromatography (IEC) has become the most important and widely used method for purifying proteins (Rehm and Reed, 1993). The main reasons for the popularity of IEC include its widespread applicability, ease of use, high resolution and yield of active material, as well as its ability to concentrate the process stream and be easily optimised to suit specific process requirements.

In IEC proteins are separated according to differences in their surface charges. The separation depends upon the reversible adsorption of charged solute molecules, Pr^+, to immobilised ion exchange groups of opposite charge, A, as shown in Equation 1.1.

$$Pr^+ + NaA \rightleftharpoons PrA + Na^+ \qquad 1.1$$

where NaA and PrA represent ion exchange adsorbent sites filled with a sodium ion and a protein molecule, respectively. This would suggest that all the binding sites are filled, which results in the following equilibrium:

$$K = \frac{[PrA][Na^+]}{[Pr^+][NaA]} \qquad 1.2$$

where K is an equilibrium constant.

As the concentration of binding sites, $\bar{A}$, on the adsorbent is fixed:

$$[\bar{A}]=[PrA]+[NaA] \tag{1.3}$$

which gives the following equilibrium for the ion exchange adsorption of a target charged solute:

$$[PrA]=\frac{K[\bar{A}][Pr^+]}{[Na^+]+K[Pr^+]} \tag{1.4}$$

The following section describes the characteristics of ion exchange adsorbents and how the feedstock properties affect the immobilised charged groups and influence the performance of the adsorbent.

The characteristics of the adsorbent are vitally important, as they will determine chromatographic properties such as the efficiency, capacity and recovery. An ion exchange adsorbent consists of an insoluble porous matrix to which charged groups have been covalently bound. The porous matrix may be based around inorganic compounds, synthetic resins or polysaccharides such as agarose. There are two main types of ion exchangers: anion exchangers, which are positively charged, and cation exchangers, which are negatively charged. Within each type of ion exchanger there are variations in the ligand chemistry and density of adsorption sites. The most common anion exchangers are diethylaminoethyl (DEAE) and quaternary amino ethyl (Q). DEAE is a weak anion exchanger, whereas Q is a strong anion exchanger. Two of the most common cation exchangers are carboxymethyl (CM) and sulphopropyl (SP). CM adsorbents are weak cation exchangers and SP are strong cation exchangers. The main parameters controlling ion exchange adsorption are the ionic strength and pH of the process feed, and are used to influence the ion exchange process. In general, a reduction in the ionic strength of the process feed leads to an increase in the binding of solutes to the adsorbent. This is due to the reduced number of ions which compete with the protein for binding sites. Reducing the ionic strength of the feedstock is normally achieved through the use of diafiltration, dialysis or dilution. The pH of the process feed affects the adsorbents in different ways. For

example, if the pH of the process feed is above the p*I* of the solute the net charge is negative, resulting in successful binding to an anion exchanger, but no binding to a cation exchanger. A solution pH below the p*I* of the solute gives a net positive charge which results in no binding to an anion exchanger, and successful binding to a cation exchanger. The ionic strength and pH of the feedstock must be adjusted to give a balance between the adsorption of the product and contaminants.

The fact that humanised Fab' fragments tend to have a basic p*I*, whilst periplasmic material tends to have acidic p*I*'s, makes ion exchange purification of Fab' an attractive option (Humphreys *et al.*, 2004). There are numerous examples in the literature of ion exchange chromatography being used for the purification of antibodies and antibody fragments (Mhatre *et al.*, 1995; Humphreys *et al.*, 2004; Staby *et al.*, 2004; Chen *et al.*, 2006a, Harinarayan *et al.*, 2006; Melter *et al.*, 2007; Stein and Kiesewetter *et al.*, 2007; Ljunglöf *et al.*, 2007). Fab' purification methods using the cation exchanger SP Sepharose FF (GE Healthcare, Uppsala, Sweden) were already well established at UCL, and were therefore used throughout this study.

1.4.4.2.2 Adsorption isotherms

The analysis of adsorption processes such as IEC is based on equilibria and mass balances, as described in Section 1.4.4.2.1. Adsorption isotherms are graphical representations of the equilibrium distribution of molecules between the mobile phase and adsorbent. Figure 1.3 presents three of the simplest and most commonly used adsorption isotherms; the linear, Freundlich and Langmuir isotherms.

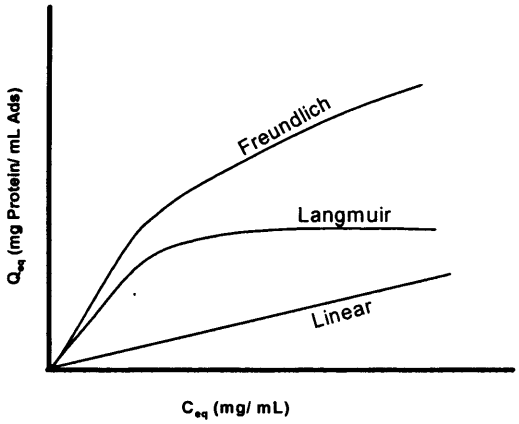

Figure 1.3. The typical adsorption isotherms observed in protein adsorption (Belter *et al.*, 1988).

The x- and y-axes in Figure 1.3 represent the solute liquid concentration, C_{eq}, and the solute concentration on the adsorbent, Q_{eq}, respectively. An adsorption isotherm which is concave towards the x-axis is said to be favourable, due to the fact that strong binding occurs even when the feed stream solute concentration is low. An adsorption isotherm which is concave towards the y-axis is described as unfavourable (Belter, *et al.*, 1988). The three isotherms presented in Figure 1.3 are described in greater detail in Section 4.1.1.

Several other adsorption isotherms may be used to describe adsorption processes including; the BET isotherm (Brunauer *et al.*, 1938) which unlike the Langmuir isotherm accounts for multilayer solute adsorption; the Temkin isotherm which assumes that the adsorption is characterised by a uniform distribution of binding energies (Sharma and Agarwal, 2001); and the Steric Mass Action (SMA) isotherm (Brooks and Cramer, 1992) which takes into account the steric hindrance of salt counterions upon protein binding.

As the effect of ionic strength is a central theme of this study a brief description of the SMA isotherm is provided. However, despite the fact that the SMA model may be the most suited to the type of analysis which is being carried out in this study, the complexity of this particular isotherm and the fact that a more generic approach was desired for this study, precludes it from consideration.

Brooks and Cramer (1992) presented the SMA model to describe nonlinear ion exchange adsorption. The model is based on the combination of the stoichiometric displacement model (Drager and Regnier, 1986) with the concept of macromolecule steric shielding. Chen *et al.* (2006b) state that the main assumptions on which the model is based include: A) the adsorption is an exchange reaction between a free protein molecule and a certain number of bound ions, which accounts for the steric hindrance of salt counterions upon protein binding. B) The binding of protein molecules causes steric hindrance of salt counterions bound to the ion exchanger. C) The adsorbent beads are spherical, with uniform size and density, and the ion exchange ligands are evenly distributed throughout the interior surface of the beads.

D) The multipointed nature of protein binding can be described by the characteristic charge, ν (Velayudhan and Horváth, 1988).

1.4.5 Chromatographic modes of operation

The recovery of antibodies and antibody fragments is typically performed using packed bed, expanded bed or batch adsorption. Suspended bed adsorption (Levison *et al.*, 2000) which is a hybrid system incorporating batch adsorption and packed beds has recently been developed.

1.4.5.1 Packed bed chromatography

Purification strategies have long been dominated by packed bed chromatography (Przybycien *et al.*, 2004). A chromatography column is a hollow cylinder, typically constructed of glass or stainless steel, into which the adsorbent material is packed. The end of the column often has adjustable adaptors which contain porous frits that retain the adsorbent particles whilst allowing the mobile phase to flow through unhindered (Levison *et al.*, 2000). To achieve good chromatographic performance it is essential to ensure the adsorbent is well packed and the column packing methods are reproducible. Once the adsorbent has been packed a number of tests can be performed in order to assess the quality and reproducibility of the packing. Often such tests include the use of a tracer molecule such as acetone to determine the height equivalent to one theoretical plate (HETP) and the peak asymmetry (Sofer and Hagel, 1997).

Protein recovery using packed bed columns requires the feedstock to be clarified and free of particulate material in order to avoid blocking the voids of the bed. This is achieved through the use of centrifugation and/or filtration as described in Section 1.4.2. Typically industrial centrifuges are less than 100% efficient, therefore it is often essential to incorporate a filtration step into the purification strategy in order to obtain a feedstock which is free of particulates prior to loading onto a packed bed column. The use of filtration will result in a particulate-free feedstock however, membrane fouling and the resulting drop in flux will lead to increased processing times, and the increased risk of product degradation due to proteolytic

attack. The inclusion of clarification as yet another process step will also lead to reduced process yields.

The direct capture of antibody fragments from unclarified process feeds removes the need for any clarification steps and therefore minimises the number of unit operations required during a purification strategy. The application of unclarified feedstocks to packed bed columns results in operational problems such as clogging of the packed bed system and an increase in the pressure drop across the bed. The particulate material is also likely to accumulate at the surface of the packed bed and may lead to further bed compression.

The direct capture of antibody fragments through the use of expanded bed, suspended bed and batch adsorption potentially reduces the number of unit operations required, and also overcomes the problems associated with loading particulate material onto a packed bed.

1.4.5.2 Expanded bed adsorption (EBA)

Expanded bed adsorption enables the direct capture of proteins from particulate containing feedstocks, such as fermentation broths and unclarified homogenates (Chase, 1994). EBA combines clarification, concentration and initial purification into one unit operation (Chase, 1994; Barnfield-Frej *et al.*, 1994; Hjorth, 1997; Blank *et al.*, 2001). By avoiding traditional time-consuming solid-liquid separation and primary purification unit operations, EBA can lead to significant improvements in downstream process efficiency. The use of centrifugation and/or filtration can lead to a reduction in the product yield, and the time spent on these unit operations can result in further losses through denaturation (Chase, 1994).

EBA is based on the fluidisation of adsorbent beads. The adsorbent beads are lifted and separated from each other by an upward liquid flow, which leads to an increased void fraction as the bed expands. As the unclarified feedstock is applied to the bed the cells, cell debris and other particulate material pass through the void space of the column unhindered, while the target protein binds to the adsorbent (Barnfield-Frej, 1996; Anspach *et al.*, 1999). In order to achieve the stable

fluidisation required for good chromatographic performance EBA requires specially designed columns and adsorbents. Draeger and Chase (1990) were able to obtain a stable fluidised (expanded) bed by using a column fitted with a specially designed liquid distribution system. The liquid distributor resulted in plug flow through the column, which is an essential element of EBA. The adsorbents used in EBA are specially designed to give stable expansion, even at relatively high flow rates. To achieve this stability, and to prevent the bed from expanding too far, the adsorbent beads have a density higher than that of traditional adsorbents, usually due to a quartz or steel core. The density and size of the adsorbent beads is also well characterised and normally distributed (EBA Handbook, GE Healthcare).

Successful applications of EBA have been reported for the initial capture of monoclonal antibodies from unclarified mammalian cell culture (Fahrner *et al.*, 1999; Feuser *et al.*, 1999a; Gonzalez *et al.*, 2003), hybridoma cell culture broth (Thömmes *et al.*, 1996), and transgenic tobacco plants (Valdes *et al.*, 2003). There are numerous other examples of the wide application of EBA including the recovery of: streptokinase from *E. coli* inclusion bodies (Goyal *et al.*, 2006); the fibroblast growth factor Saporin Mitotoxin from *E. coli* lysates (McDonald *et al.*, 1996); alcohol dehydrogenase (ADH) from yeast cell homogenate (Smith *et al.*, 2002); the clotting factor IX from human plasma (Chang *et al.*, 2006); and an interleukin-1 receptor antagonist from an *E. coli* lysate (Zanette *et al.*, 1998).

Although EBA is capable of handling particulate material, problems can occur when the particulates are large enough to cause blockage of the flow adaptors or fluid distributors. This would result in channeling which leads to reduced bed stability and adsorption performance. The processing of high viscosity materials is also problematic as it results in over-expansion of the expanded bed, which reduces the adsorption performance. Other disadvantages of EBA include the need for specialist equipment, which can often cost more than conventional packed bed equipment. The specially designed, high density adsorbents are more expensive than standard packed bed adsorbents. The adsorbent lifetime is often reduced as a result of irreversible fouling and the application of harsh CIP reagents and procedures (Feuser *et al.*, 1999b).

1.4.5.3 Suspended bed adsorption (SBA)

Suspended bed adsorption is a recent development in process-scale chromatography. SBA is designed to be used in processes where large volumes of process feed are being contacted with a relatively small mass of adsorbent, or in systems where either the adsorption kinetics or pressure-flow performance of the adsorbent prevent the use of high flow rates. The use of low flow rates will lead to long process times. Suspended bed chromatography can also be used in systems where the process solution contains unstable compounds, or could be prone to proteolytic degradation (Quinones-Garcia *et al.*, 2001).

The system works by combining the benefits of batch adsorption, such as the short processing time, with those of an enclosed column system. The process relies on recent developments in column design which enable pump-packing and unpacking of the adsorbent matrix (Levison *et al.*, 2000). The operation is carried out in three main stages: firstly, during the adsorption stage the process feed is mixed in a stirred tank with the adsorbent. Once the adsorption stage is complete the adsorbent-product slurry is packed into an empty packed bed column, in the same way as fresh adsorbent would be during packed bed chromatography. Finally, standard chromatographic techniques are then used to wash and elute the product from the packed bed (Quinones-Garcia *et al.*, 2001).

Ling *et al.* (2003) describes the use of the SBA method for the anion exchange capture and chromatographic fractionation of glyceraldehyde-3-phosphate dehydrogenase (G_3PDH) from crude baker's yeast disruptate.

The drawbacks of the SBA method include the potential loss of product during the transfer of the adsorbent-product slurry from the batch contactor to the packed bed. There is also a risk of trapping particulate material within the packed bed prior to the wash and elution stages. This could affect the quality of the packing and impact the flow pattern within the packed bed, and therefore the product yield and quality.

1.4.5.4 Stirred tank batch adsorption

Batch adsorption is a very effective, simple and rapid method for the recovery of proteins from large volumes of unclarified feedstocks. The method simply involves mixing the adsorbent beads with the feedstock in a stirred tank for an appropriate length of time. Once the adsorption stage is complete the adsorbent is separated from the depleted feedstock, traditionally through the use of filtration, settling or centrifugation (Lyddiatt, 2002). Washing and elution can then be carried out in batch mode.

The use of batch adsorption has several advantages over both packed bed column chromatography and EBA. Due to the immediate and uniform contact of the adsorbent and feedstock, batch adsorption can be performed faster than both column chromatography and EBA. Levison *et al.* (1992) reported that the adsorption stage of a batch system lasted 30-60 min regardless of scale. The rapid separation of a target protein from large volumes of feedstock is essential in a situation where the product has limited stability or is exposed to proteolytic attack. The ability to handle viscous and/or unclarified feedstocks without the need for clarification or dilution is also an advantage of the stirred tank batch system, as dilution of the feedstock is often necessary in EBA. Process scale batch adsorption offers the opportunity to utilise cheaper adsorbents which lack the geometric refinement, rigidity and density needed in packed bed and expanded bed adsorption. Such adsorbents would be ideal for single-use, disposable systems and would remove the need for cleaning and cleaning validation (Lyddiatt, 2002).

The main limitations of batch adsorption include the lower purification resolution and efficiencies, due to incomplete adsorption, when compared to column chromatography (Chase, 1994). Pierce *et al.* (1999) reported problems with adsorbent mixing during batch adsorption. Traditionally batch adsorption systems have been labour intensive and required the use of centrifugation and/or filtration to separate the adsorbent from the depleted feed. However, with increasing interest in process integration, and the wide range of potential applications of batch adsorption, the bioprocess industry is slowly beginning to embrace batch adsorption again. Bio-Rad (California, USA), a manufacturer of conventional column chromatography

units, has recently developed a series of batch adsorption systems called "Batch Columns". These are fully automated, enclosed systems which require no manual filling, draining or transfer of adsorbent. They are designed to be easy to operate and validate. Such systems would overcome the problems associated with batch adsorption.

Batch adsorption has been used in a wide range of applications, including the recovery of the anti-tumour antibiotic kedarcidin from a clarified fermentation broth (Lam *et al.*, 1994), lactoferrin from raw whole milk (Fee and Chand, 2005), and recombinant α-amylase expressed in the periplasm of *E. coli* (Pierce *et al.*, 1999).

1.5 Project aims and objectives

In order to meet the rising demand for biologics the bioprocess industry is having to evaluate new methods and to re-visit existing ways of recovering and purifying therapeutic proteins. The most commonly used methods involve the use of packed bed columns, which are constrained by the need for substantial pre-treatment of the feedstock. The use of batch adsorption provides an alternative process option and allows the direct capture of the target protein from unclarified feedstocks.

This study aims to develop scale-down adsorptive methods in order to assess rapidly various process options for the adsorptive recovery of Fab' antibody fragments from unclarified *E. coli* feedstocks. Of particular interest is the potential use of batch adsorption as an alternative to conventional packed bed columns. The periplasmically expressed Fab' is released from *E. coli* by selective periplasmic release or high pressure homogenisation. The impact of the cell disruption method and resulting feedstock properties on the ion exchange adsorption of Fab' is also investigated.

In order to assess the various process options data from the scale-down adsorptive methods will be used to form an empirical model. The model will then be used to predict the performance of each process option, which is then visualised through the use of Windows of Operation.

1.6 Thesis layout

This section briefly describes the structure of the thesis. Each chapter begins with an abstract briefly describing its aims and outcomes. This is followed by a brief introduction, providing background information and any relevant theory. The results are then presented and discussed, before the main findings are finally summarised.

Chapter 2 provides details of the experimental materials and methods used during this study. The experimental results are then presented in Chapters 3-6.

Chapter 3 describes the use of several unit operations utilised during the preparation of industrially relevant feedstocks for use in the investigation of adsorptive methods. The methods used and the resulting feedstocks are characterised, along with the primary assay used during the study (protein G assay).

In Chapter 4 a scale-down adsorption isotherm method is used to investigate the effect of feedstock properties, including the feedstock ionic strength and solids concentration, on the ion exchange adsorption of Fab'. The adsorption isotherm data is then used to develop and compare two different empirical models capable of predicting adsorption isotherms. [The most effective model is then selected and used in Chapter 7.]

In Chapter 5 the impact of linear velocity, and feedstock solids concentration and ionic strength on the recovery of Fab' within packed bed columns is investigated. The effect of column packing is presented along with a laboratory scale mimic of industrial scale packed columns.

Chapter 6 describes the development of scale-down batch adsorption methods for the recovery and initial purification of Fab' from *E. coli* feedstocks. The effect of feedstock properties on the adsorption of Fab' is investigated using a bespoke microwell filterplate. The results of the microwell plate adsorptions (each well has a volume of 0.2 mL) are then compared to data obtained from laboratory scale stirred tank batch adsorptions, performed at 15 and 135 mL scale.

Chapter 7 uses the model developed in Chapter 4 to compare different process options for the recovery and initial purification of Fab' from particulate containing feedstocks. This chapter is separated into a series of case studies, each one investigating certain process options:

1. Comparing high pressure homogenisation and selective periplasmic release as methods of cell disruption,
2. Optimisation of the batch adsorption process,
3. A stirred tank batch adsorption process is compared to a conventional packed bed process,
4. Model sensitivity analysis investigating the effect lysis time and Fab' partitioning has on the process flowsheets.

The different process options are compared on the basis of total process time, yield and throughput. These performance parameters are then used to generate Windows of Operation in order to visualise feasible operation conditions.

Chapter 8 considers the commercial benefits of implementing batch adsorption and the scale-down screening and optimisation methods developed in this study.

Chapter 9 describes the validation concerns and issues which need to be considered when a batch adsorption system is incorporated into a downstream processing route.

Chapter 10 summarises the main observations and conclusions of the study and, suggestions for future work are given in Chapter 11.

2 Materials and methods

This chapter describes the materials, experimental equipment and methods, as well as analytical techniques that have been used during this study.

Unless otherwise stated, all chemicals were of analytical grade and were purchased from Sigma-Aldrich (Poole, Dorset, UK). Reverse osmosis (RO) water was used at all times in the preparation of buffers and solutions.

2.1 Fermentation

Fab' expressed in *E. coli* was produced as described below. The fermentations were carried out with the help and support of fellow UCL EngD student Andrew Tustian.

The following protocol has been taken from Salte (2006).

2.1.1 E. coli strain and plasmid for expression of a Fab' antibody fragment

The industrial *E. coli* strain W3110 containing the plasmid pTTOD A33 IGS2 was kindly donated by UCB Celltech Ltd (Slough, UK).

2.1.2 Culture media

Recipes are quoted per L of final media, unless otherwise stated.

Complex media for starter cultures: Complex media was used for starter cultures and contained 16 g Phytone (Becton-Dickinson Life Science Research Ltd, UK), 10 g yeast extract and 5 g NaCl.

SM6G$_c$ defined media: SM6G$_c$ was prepared as follows: 5.2 g $(NH_4)_2SO_4$, 4.4 g $NaH_2PO_4.H_2O$, 4.03 g KCl, 1.04 g $MgSO_4.7H_2O$, 4.16 g citric acid,

0.25 g $CaCl_2.2H_2O$, 112 g glycerol, and 0.01% trace elements solution. pH was adjusted to 6.95 with 15% ammonia.

100 x trace element solution: 104 g citric acid, 5.22 g $CaCl_2.2H_2O$, 2.06 g $ZnSO_4.7H_2O$, 2.72 g $MnSO_4.4H_2O$, 0.81 g $CuSO_4.5H_2O$, 0.42 g $CoSO_4.7H_2O$, 10.06 g $FeCl_3.6H_2O$, 0.03 g H_3BO_3, 0.02 g $Na_2MoO_4.2H_2O$.

2.1.3 45 L fermentation

Starter cultures were grown in 200 mL of complex media containing 10 μg/mL tetracycline for 4 h at 37 °C. This culture was used as a 10% inoculum for $SM6G_c$ defined media shake flasks, which were incubated for 22 h at 30 °C, 200 rpm, with 10 μg/mL tetracycline, until an OD_{600} of 3-4 was achieved.

1 L of culture from the defined media shakes described above was used to inoculate 40 L of $SM6G_c$ media in a 75 L fermenter (Series 2000 LH 75 L, Inceltech, Reading, UK). The pH was maintained at 6.95 using 15% (w/v) ammonia solution and 20% (v/v) H_2SO_4. Dissolved oxygen was maintained at 30% with the addition of 40% oxygen when necessary. The culture temperature was maintained at 30 °C for ~32 h (OD_{600} ~ 42), after which it was reduced to 25 °C for the remaining duration of the fermentation. Between OD_{600} of 42-88 multiple salt additions were given to maintain Mg^{2+} and PO_4^{2-} concentrations. When an OD_{600} of ~88 was achieved, dissolved oxygen tension (DOT) spiking and demand for acid indicated complete utilisation of the glycerol carbon source. At this point Fab' production was induced by the addition of 25 mL of 15.3 g/L isopropyl β-D-thiogalactopyranoside (IPTG). After induction carbon was supplied to the culture for Fab' synthesis and cell maintenance by a 16 mL/h glycerol feed. The culture was then harvested 36 h post-induction.

2.2 General downstream processing

2.2.1 Cell Harvest

E. coli cells were harvested from the fermentation broth by solid–liquid separation using a CSA-1 disc-stack centrifuge (Westfalia Separator, AG, Oelde, Germany) operated at 9,800 rpm at a flow rate of 25 L/h). The resulting cell paste was then packed in aliquots of approximately 200 g and stored at -80 °C.

2.2.2 Intracellular product release

Cell disruption was required to release Fab' from the periplasm of the *E. coli* cells. High pressure homogenisation was performed at small and pilot scale as described in Section 2.2.2.1 and Section 2.2.2.2, respectively. Selective periplasmic extraction was performed using a heat chemical lysis, as described in Section 2.2.2.3.

2.2.2.1 Small scale high pressure homogenisation

A Lab 40 high pressure homogeniser (APV Ltd., Crawley, UK) was used to prepare small volumes of *E. coli* homogenate. Thawed cell paste was resuspended in RO water to minimise the ionic strength of the resulting homogenate and homogenised for five discrete passes at 500 bar using the standard Lab 40 valve unit. A sample of the slurry/homogenate was taken after each pass in order to measure the mean particle diameter, as described in Section 2.3.4. The temperature was maintained at approximately 4 °C through the use of glycol cooling.

2.2.2.2 Pilot scale high pressure homogenisation

The slurry was prepared as described in Section 2.2.2.1 and homogenised for five passes at 500 bar using a Lab 60 high pressure homogeniser (APV Ltd., Crawley, UK) fitted with a "cell disruption" (CD) valve unit. The temperature was maintained at approximately 4 °C through the use of glycol cooling.

2.2.2.3 *Periplasmic extraction – heat lysis*

The selective release of Fab' was achieved through the use of periplasmic extraction. Thawed cell paste (prepared as described in Section 2.2.1) was resuspended in periplasmic extraction buffer (100mM Tris, 10mM EDTA at pH 7.4) to give a solids concentration of approximately 10% (ww/v). The slurry was then heated to 60 °C for 16 h in a 3 L Chemap stirred tank fermenter (Chemap, Alpha Laval Engineering Ltd., Middlesex, UK).

2.2.3 *Diafiltration*

The ionic strength of the unclarified lysate was reduced to approximately 3.2 mS/cm using constant volume diafiltration. A 10 kDa cut-off Xampler hollow fibre membrane, with a membrane area of 0.011 m^2, (GE Healthcare, Uppsala, Sweden) was connected to and controlled by an ÄKTAcrossflow™ automated crossflow filtration system (GE Healthcare, Uppsala, Sweden). The diafiltration was performed at a constant transmembrane pressure (TMP) of 1 bar. RO water was used as the diafiltration buffer and the temperature was maintained at 20 °C using ice packs and an ice bath.

2.3 Feedstock preparation and system characterisation

2.3.1 *Feedstock solids concentration*

2.3.1.1 *Determining feedstock solids concentration (wet weight)*

The feedstock solids concentration was determined on a wet cell weight per volume basis (ww/v) by filling a pre-weighed 2.2 mL Eppendorf tube with 1 mL of sample feedstock and spinning it at 14,000 rpm for 15 min in an Eppendorf 5810R bench top centrifuge with a T-60-11 rotor fitted (Eppendorf UK Ltd., Cambridge, UK). The resulting supernatant was discarded and the solids concentration determined by re-weighing the Eppendorf tube.

2.3.1.2 *Sample preparation*

E. coli homogenate and lysate feedstocks were prepared according to Section 2.2.2. For experiments requiring clarified feedstocks, clarification was performed by centrifugation at 10,000 rpm for 90 min in a Beckman J2-M1 centrifuge with a JA 10 rotor fitted (Beckman Coulter Ltd. High Wycombe, UK).
When solutions containing solids were required the feedstocks were centrifuged for various lengths of time using an Eppendorf 5810R bench top centrifuge with a T-60-11 rotor fitted (Eppendorf UK Ltd., Cambridge, UK).

2.3.2 *Feedstock ionic strength*

The conductivity of all feedstocks and buffers was measured using a Jenway Conductivity meter (Jenway, Essex, UK) at a given reference temperature (18, 20 or 25 °C).
The ionic strength of the lysate was reduced as described in Section 2.2.3. As stated in Section 2.2.2.1, in preparation for homogenisation the thawed cell paste was resuspended in RO water to minimise the ionic strength of the homogenate and avoid the need for diafiltration.

To prepare feedstocks of varying ionic strength NaCl was added until the desired ionic strength was obtained.

2.3.3 *Optical density*

The optical density of feedstock samples was measured in triplicate using a Genesys™ Series 10 spectrophotometer (ThermoSpectronic, Cambridge, UK). A quartz cuvette was used when the optical density was measured at 280 nm for total protein measurements, and the spectrophotometer was blanked using RO water. If necessary the samples were diluted with the appropriate buffer or RO water to keep the absorbance reading (A) within the range of the spectrophotometer ($A < 1.0$).

2.3.4 Particle size distribution by laser light defraction

The particle size distributions were measured using a Malvern Mastersizer 2000 laser sizer (Malvern Instruments, Worcestershire, UK). The instrument uses a Low Angle Laser Light Scattering (LALLS) method to measure particles in the range of 0.1 to 2,000 μm. The samples were diluted and dispersed in RO water to achieve an obscuration of approximately 10-12%. The data of interest obtained from the instrument was the d_{50}, which is defined as the point within the particle distribution where 50% of the particles, by volume, are smaller than the stated diameter.

2.3.5 Fab' quantification

2.3.5.1 Protein G assay

The concentration of Fab' present in all feedstocks was measured using the Protein G assay. An Agilent 1100 Series HPLC system (Agilent Technologies UK Ltd, West Lothian, UK) was modified to allow the connection of a Hi-Trap Protein G column (GE Healthcare, Uppsala, Sweden). The sample being analysed was spun for 15 min at 14,000 rpm in an Eppendorf 5810R bench top centrifuge with a T-60-11 rotor fitted (Eppendorf UK Ltd., Cambridge, UK). The resulting supernatant was filtered into glass sample vials using 0.2 μm sterile syringe filters (VivaScience AG, Hannover, Germany). The column was equilibrated with 20 mM Sodium Phosphate at pH 7.4 (Buffer A) prior to sample loading. The built-in autosampler was programmed to collect the samples from a vial tray in the desired sequence. The samples were then loaded onto the column using an injection volume of 50 μL[1]. Finally, elution was performed using 20 mM Sodium Phosphate at pH 2.5 (Buffer B). Integration of the peaks recorded on the chromatogram was performed to obtain the peak area for the Fab' sample. The Fab' concentration was then

[1] The standard sample injection volume was 100 μL. A series of standard curves were obtained using injection volumes of 25, 50 and 100 μL in order to assess the possibility of using a lower injection volume.

determined from a standard curve generated from Fab' samples of known concentration.

2.3.5.2 *Determining the concentration of total available Fab'*

The "total available Fab'" method was developed in order to measure the total concentration of Fab' in a sample of an unclarified feedstock. A known volume of the unclarified feedstock sample was spun in an Eppendorf tube for 15 min at 14,000 rpm in an Eppendorf 5810R bench top centrifuge with a T-60-11 rotor fitted (Eppendorf UK Ltd., Cambridge, UK). The resulting supernatant was then removed and assayed as described in Section 2.3.5.1 using the protein G assay to give the supernatant Fab' concentration (C_s). The remaining cell debris pellet was then resuspended in 1M NaCl and mixed on an IKA Vibrax orbital shaker (IKA Works, Inc, Wilmington, USA) for 15 min at 1,800 rpm. The volume of NaCl used was equal to the initial volume of the sample. Once the pellet had been fully resuspended, the sample was spun again for 15 min at 14,000 rpm in an Eppendorf 5810R bench top centrifuge. The resulting supernatant was then assayed for Fab' as described in Section 2.3.5.1 to give the debris-bound Fab' concentration (C_d).

2.3.5.3 *Optimising elution conditions for debris-bound Fab'*

In order to determine the number of elution steps and molarity of the eluting NaCl solution required to elute fully the debris-bound Fab', a series of 2.2 mL Eppendorf tubes containing 1 mL of the homogenate prepared as described in Section 2.2.2.1 were spun for 15 min at 14,000 rpm in an Eppendorf 5810R bench top centrifuge, and the resulting supernatant discarded. The cell debris pellets were assayed for debris-bound Fab' as described in Section 2.3.5.2, however the molarity of the NaCl solution used to elute the Fab' was either 1.0 or 2.5 M with RO water used as a control. The procedure was repeated to obtain the debris-bound Fab' concentration for the second elution step.

2.3.6 Characterising cell debris-Fab' interactions and Fab' stability

2.3.6.1 The effect of ionic strength

1 mL homogenate solutions at 3.0, 3.6, 4.2, 5.5 and 11.0 mS/cm were assayed for total available Fab' using the method described in Section 2.3.5.2.

2.3.6.2 The effect of buffer ionic strength on Fab' concentration during feedstock dilution

2.2 mL Eppendorf tubes containing diafiltered lysate with an ionic strength of 3.1 mS/cm were diluted with 20 mM Sodium Acetate at an ionic strength of 1.4 or 3.1 mS/cm to give dilutions ranging from 0 to 100%, in 10% intervals. NaCl was added to the Sodium Acetate in order to obtain the 3.1 mS/cm solution. The Eppendorf tubes were then placed on a Vibrax orbital shaker and mixed for 15 min at 1,800 rpm. The total available Fab' method, as described in Section 2.3.5.2, was used to determine the Fab' concentration for each dilution and buffer solution.

2.3.6.3 The effect of storage conditions on Fab' stability

A series of 2.2 mL Eppendorf tubes were filled with the freshly prepared homogenate and lysate feedstocks. A sample of each feedstock was stored at +4, -20 and -80 °C for 7 days. The total available Fab' method was used to determine the Fab' concentration of the fresh and stored samples.

2.4 Methods for the ion exchange adsorption of Fab'

The methods for the use of microwell filterplates, packed bed columns and stirred tank batch adsorption are described in this section.

The ion exchange adsorbent used in all experiments in this study was the cation exchanger SP Sepharose FF (GE Healthcare, Uppsala, Sweden). The equilibration buffer used was 20 mM Sodium Acetate (pKa 4.76 at 25°C, buffer range pH 4-6) (Sigma product information sheet), adjusted to pH 5.5 using Acetic Acid.

2.4.1 Microwell filterplate

In order to perform adsorption experiments in a microwell format it was necessary to use a microwell filterplate (MWFP) to separate the adsorbent from the feedstock. However, standard filterplates which contain membranes or frits with a pore size ranging from 0.2 to 25 μm were found to prevent the passage of unclarified feedstock. To overcome this problem a standard 96 well 800 μL MWFP obtained from Seahorse Labware (formerly Innovative Microplate) (Chicopee, USA), shown in Figure 2.1, was modified to allow the rapid separation of the adsorbent from the feedstocks.

Figure 2.1. A photograph of the MWFP prior to modification.
Taken from http://www.multiwell.com/Blueprints/F20064-Data.pdf

2.4.1.1 Filterplate modification

The bottom plate of the MWFP was carefully removed in order to replace the membrane discs with stainless steel mesh discs cut out of Betamesh 25 (25 μm pore size) (Bopp & Co. Ltd., Derbyshire, UK). The bottom plate was then re-attached to the microwell plate and sealed with silicon adhesive, as shown in Figure 2.2.

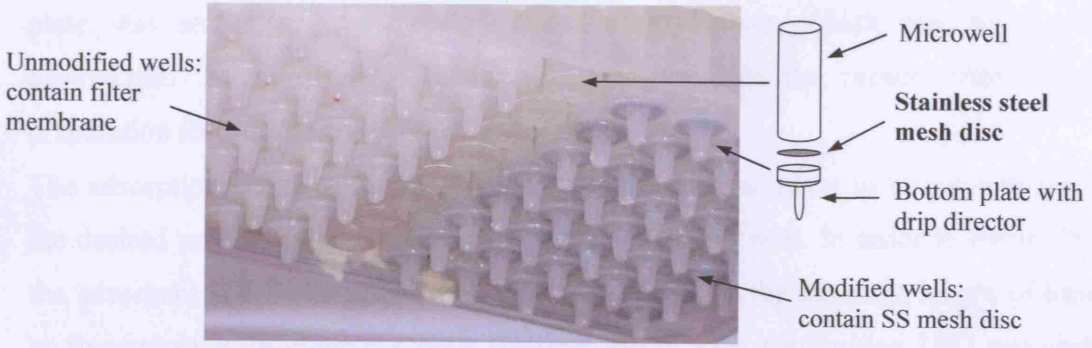

Figure 2.2. A photograph of the MWFP during modification, and a schematic showing the location of stainless steel (SS) mesh disc.

In order to carry out adsorption experiments using the modified MWFP the outlets of the wells had to be sealed in a way that prevented the loss of material during the experiments, but did not delay the drainage and removal of the sample once the experiments were completed. This was achieved by placing a sheet of silicon rubber covered in a thick piece of Parafilm® M (Pechiney Plastic Packaging Company, Chicago, USA) under the drip directors of each well. The drip directors are nozzles extending out from the outlet of the wells and were crimped to restrict the liquid flow. Pressure was applied from above with the use of a clamp attached to the Thermomixer Comfort (Eppendorf UK Ltd., Cambridge, UK) on which the MWFP was mixed.

2.4.1.2 General microwell methods

The first step in the method developed for MWFP-based adsorption experiments is the preparation of a 50% (v/v) slurry of the adsorbent, using 20% (v/v) Ethanol in a sealable tube. The MWFP was then placed onto a Multiscreen vacuum manifold (Millipore, Watford, UK). At this stage of the method, no collection plate was placed beneath the MWFP. Using a standard, calibrated laboratory pipette the required volume of the well-mixed slurry was applied to each well, with the slurry being mixed by inversion between each aspiration. Equilibration of the adsorbent was then carried out by adding 500 μL equilibration buffer (20 mM Sodium Acetate, pH 5.5) to each well. The addition of the liquid provided sufficient agitation to mix the slurry. A vacuum was then applied and the buffer removed from the wells. This was repeated to give a total of three equilibration steps. The MWFP was then removed from the vacuum manifold, and using the method detailed in Section 2.4.1.1, the plate was sealed and positioned on the Thermomixer, which was set to the desired rpm. A collection plate was then placed inside the vacuum manifold in preparation for sample collection.

The adsorption phase of the method required the Thermomixer to be rotating while the desired volume of feedstock was pipetted into each well. In order to ensure that the adsorbent and feedstock in each well was contacted for the same length of time, an Eppendorf multi-channel pipette (Eppendorf UK Ltd., Cambridge, UK) was used. At the end of the adsorption phase the Thermomixer was stopped and the MWFP

released from the clamp. The bottom seal was then removed and the plate positioned onto the vacuum manifold and a vacuum applied for 0.5 min. The sample was then collected in the collection plate and the Fab' concentration measured using the methods described in Section 2.3.5.1 and Section 2.3.5.2.

Section 2.4.1.4 describes the portion of the MWFP method which is specific to the adsorption isotherms, whereas the use of MWFP for the scale-down batch adsorption of Fab' is described in Section 2.4.1.5.

2.4.1.3 Determining Thermomixer rotational speed

The rotational speed of the Thermomixer required to achieve sufficient mixing to ensure suspension of the adsorbent was determined by using the MWFP method at rotational speeds ranging from 400 to 1,000 rpm. 200 µL of feedstocks was contacted with 50 µL of the adsorbent. Fab' concentration was measured using the total available Fab' method, as described in Section 2.3.5.2.

2.4.1.4 Adsorption isotherms

The equilibrium adsorption isotherms were determined using the general MWFP method described in Section 2.4.1.2, however, with the following adjustments made to the method. The method developed in this study was based on maintaining a constant feedstock concentration and volume and a varying adsorbent volume. In this case each microwell contained 200 µL of feedstock and a varying volume of adsorbent, ranging from 0.1 to 20 µL. The MWFP was mixed overnight using the Thermomixer set at 950 rpm. The top of the wells were sealed using Parafilm® M to reduce evaporation.

2.4.1.5 Microwell scale-down batch adsorption

The general MWFP method was used to investigate the effect of phase ratio and feedstock solids concentration. For the phase ratio experiments utilising the homogenate feedstock, the load volume was fixed at 200 µL and the adsorbent

volume ranged from 20 to 60 μL, resulting in phase ratios between 0.1 and 0.3. In the case of the lysate feedstock the adsorbent volume was fixed at 10 μL and the feed volume ranged from 300 to 700 μL, giving phase ratios between 0.01 and 0.03. Different methods were used due the fact that the lysate experiments were carried out prior to the optimisation of the MWFP method and a lack of time and material meant it was not possible to carry out repeat experiments.

For the investigation into the effect of solids concentration, feedstocks of varying solids concentration were prepared as described in Section 2.3.1.2. 200 μL of feedstock was contacted with 60 μL of adsorbent, to give a phase ratio of 0.3.

In order to minimise the time taken to carry out the experiments the adsorption stage of the general MWFP method was modified. The feedstock was applied to the microwells containing adsorbent in reverse order, such that the sample for the final time point was applied first, and the first time point, applied last. This method enabled all the samples to be vacuum filtered at the same time.

2.4.2 Packed bed adsorption

Packed bed adsorption studies were performed using Tricorn 15 (TC15) and XK16 columns connected to and controlled by an ÄKTA Explorer 100 chromatography system (GE Healthcare, Uppsala, Sweden). A method for obtaining breakthrough curves was programmed into the software package Unicorn, which controls the ÄKTA Explorer system.

Samples of the flow-through were collected by a FRAC-950 fraction collector and assayed for Fab' using the methods described in Section 2.3.5.1 and Section 2.3.5.2 (diluting with equilibration buffer if necessary), and the solids concentration measured as described in Section 2.3.1.1.

Section 2.4.3.1 describes the methods used to obtain breakthrough curves using the TC15 column, whereas Section 2.4.3.2 describes the use of the XK16 column to investigate the effect of column packing and wall support.

2.4.2.1 Fab' breakthrough curves

Fresh adsorbent was used for each run and flow packed into the TC15 column at linear velocities 20% greater than the desired loading linear velocity to give a bed height of 15 cm, and column volume (CV) ~ 2.95 mL. The adsorbent was then equilibrated with 20 mM Sodium Acetate, pH 5.5, for approximately 30 min at the desired loading linear velocity (100, 200 and 300 cm/h for the investigation into the effect of linear velocity and solids concentration, and 300 cm/h for the investigation into the effect of feedstock ionic strength). Feedstocks prepared as described in Section 2.3.1.2 and Section 2.3.2 were loaded onto the column at the desired linear velocity using the sample pump. Once the loading step was complete the adsorbent was washed with approximately 4-5 CV equilibration buffer (or until the OD_{280} trace had reached the baseline). Fab' elution was performed using approximately 5 CV 20 mM Sodium Acetate + 1 M NaCl, pH 5.5, at a linear velocity of 150 cm/h.

2.4.2.2 Effect of column packing and wall support

The use of an XK16 column to investigate the effect of packing flow rate on the loading and breakthrough curves of unclarified feedstocks is described in this section.

2.4.2.2.1 Critical velocity (u_{crit}) determination

A 50% (v/v) slurry of adsorbent was gravity packed in an XK16 column (0.16 cm i.d) to give a gravity settled bed height of 12.5 cm. In order to flush out the 20% (v/v) Ethanol which is used to prepare the slurry, the column was equilibrated with 20 mM Sodium Acetate, pH 5.5, at a nominal linear velocity of 60 cm/h. The top adaptor of the column was then lowered to the top of the adsorbent bed. The column was then equilibrated at incrementally higher flow rates until an increase in flow rate no longer caused an increase in the pressure drop. Flow rate, bed height and pressure drop measurements were recorded in order to calculate u_{crit}.

The same procedure was repeated for an empty XK16 column, containing no adsorbent, in order to obtain the pressure drop across the ÄKTA Explorer system,

which is then deducted from the calculation of u_{crit}. In this case the system pressure data was kindly provided by fellow UCL EngD student John Joseph.

2.4.2.2.2 u_{crit}-based loading and Fab' breakthrough

An XK16 column was flow packed with fresh adsorbent at the start of each of the experiments described in this section. The packing linear velocity used was 1230 cm/h, which was 80% of the experimentally determined u_{crit}. The adsorbent was equilibrated for approximately 30 min with 20 mM Sodium Acetate, pH 5.5. Unclarified homogenate, prepared as described in Section 2.3.1.2, was then loaded at two linear velocities. Firstly, at a linear velocity of 985 cm/h, which was 80% of the packing linear velocity, and secondly at 300 cm/h, which was 24% of the packing linear velocity.

2.4.2.2.3 Industrial packing mimic

Section 5.2.4.3 describes how the Stickel model (Stickel *et al.*, 2001) was used to obtain a packing linear velocity which provides a laboratory scale column prediction of industrial scale pressure drop. As a result of the calculations a packing linear velocity of 1380 cm/h was used, prior to loading a homogenate feedstock, prepared as described in Section 2.3.1.2, at a linear velocity of 1155 cm/h.

2.4.3 Stirred tank batch adsorption methods

2.4.3.1 Amicon Stirred Cell modification

Batch adsorption was carried out using two modified Amicon Stirred Cells; 8050 (50 mL) and 8200 (200 mL) (Millipore, Watford, UK). The ultrafiltration membrane which is normally used was replaced by a stainless steel Betamesh 25 disc (Bopp & Co. Ltd., Derbyshire, UK). As well as replacing the membrane, the stirrer was replaced with a 4-blade pitched-blade impeller, attached to a Eurostar Digital Overhead Stirrer (IKA Works, Inc, Wilmington, USA). The pitched-blade impeller was custom built and designed to have a diameter which is 85% of the diameter of

the stirred cell. The impeller was positioned approximately 1 cm above the base of the vessel. Figure 2.3 shows a selection of the components and how the Stirred Cells are assembled.

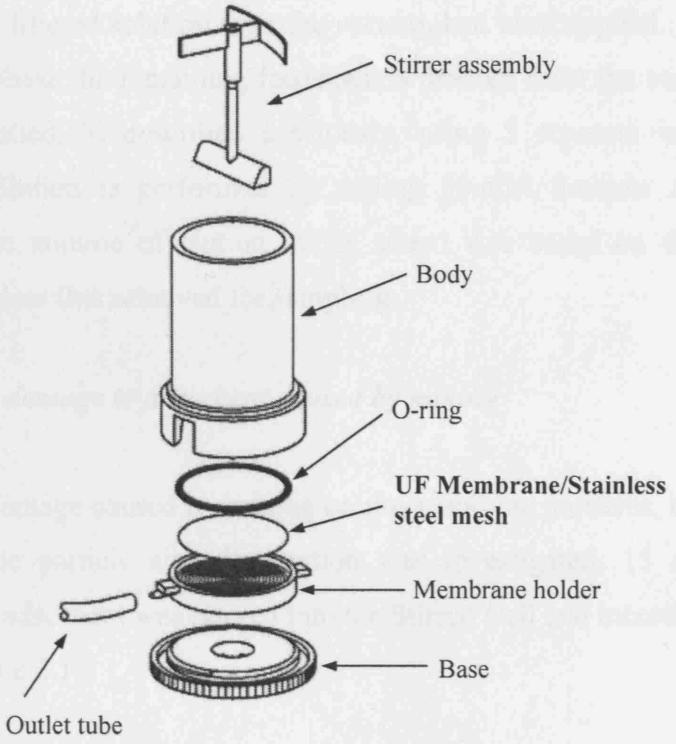

Figure 2.3. A schematic of an Amicon Stirred Cell, modified from the version available at: http://www.millipore.com/catalogue.nsf/docs/C3259

2.4.3.2 General batch adsorption methods

The first step in the stirred tank batch adsorption method is the equilibration of the adsorbent. This was achieved by pouring the desired volume of adsorbent into the stirred cell with the outlet open to allow the 20% (v/v) Ethanol, used to prepare the slurry, to drain out. With the outlet tube clamped 1 batch volume (BV) of equilibration buffer (20 mM Sodium Acetate, pH 5.5) was applied to the adsorbent, which was then mixed for 2 min at 300 rpm, before the clamp was removed and the buffer allowed to drain. This process was repeated to give a total of 3 equilibration steps. With the stirrer still operating and the outlet tube clamped, the required volume of feedstock was then added. Samples were taken at intervals and assayed for Fab' as described in Section 2.3.51 and Section 2.3.5.2.

As the samples taken from the stirred tank contained both the feedstock and adsorbent, the MWFP was used to separate the adsorbent from the supernatant. As described in Section 2.4.1.2, a collection plate was placed beneath the vacuum manifold to receive the filtered solution after the vacuum had been applied. After the end of the adsorption phase the remaining feedstock is drained from the outlet tube, and the adsorbent washed, as described previously, using 3 separate washes of equilibration buffer. Elution is performed by adding 20 mM Sodium Acetate + 1 M NaCl, pH 5.5. The volume of elution buffer added was based on the initial feedstock load volume less that removed for sampling.

2.4.3.3 Assessing the damage to adsorbent caused by mixing

In order to assess the damage caused by mixing on the adsorbent particles, the effect of agitator type on the particle size distribution was investigated. 15 mL of a 50% (v/v) slurry of the adsorbent was poured into the Stirred Cell and mixed with the impellers shown in Table 2.1.

Table 2.1. The impeller type, stirrer speed and length of mixing used to assess the damage caused to adsorbent beads during agitation in a 20 mL stirred tank. 15 mL of a 50% (v/v) adsorbent slurry used.

Stirrer	Speed (RPM)	Time (min)
6-blade Rushton	1,500	80
3-blade Marine	1,500	80
4-blade Pitched-blade	1,000	15
Magnetic	Level 8	25

The 4-blade pitched-blade impeller was then used to mix 15 mL 50% (v/v) slurry for 2 min, at stirrer speeds ranging from 100 to 1,000 rpm. The particle size distribution was measured as described in Section 2.3.4.

2.4.3.4 *The effect of agitation on Fab' adsorption*

The 4-blade pitched-blade impeller was used to mix 1.5 mL adsorbent with 15 mL unclarified lysate, for 2 min at stirrer speeds ranging from 50 to 500 rpm. The adsorbent and feedstock were separated as described in Section 2.4.4.2 using the MWFP and vacuum manifold. The Fab' concentration was then measured as described in Section 2.3.5.1. The total available Fab' method was used to measure the debris-bound Fab' concentration.

2.4.3.5 *The effect of phase ratio*

The general batch adsorption method was used to investigate the effect of phase ratio on the adsorption of Fab' using the modified 8020 Amicon Stirred Cell. 15 mL of the homogenate feedstock, prepared as described in Section 2.2.2.2, was mixed with 1.5, 4.5 and 7.5 mL adsorbent using the 4-blade pitched-blade impeller at 300 rpm.

2.4.3.6 *The effect of feedstock properties on Fab' adsorption*

The general batch adsorption method was used to investigate the effect of feedstock solids concentration and ionic strength on the adsorption of Fab' using the modified 8020 Amicon Stirred Cell. 15 mL of the feedstock, prepared as described in Section 2.3.1.2 and Section 2.3.2, was mixed with 4.5 mL adsorbent using the 4-blade pitched-blade impeller at 300 rpm.

2.4.3.7 *Geometric scale-up of batch adsorption*

The modified 8200 Amicon Stirred Cell was used to perform batch adsorptions using 135 mL of homogenate feedstock mixed with 40.5 mL adsorbent. The rate of agitation, impeller type and the ratio of impeller to tank diameter was kept constant. The Fab' concentration was measured as described in Section 2.3.5.2.

3 Feedstock preparation and system characterisation

Abstract

The ability to produce industrially relevant feedstocks at small scale is of increasing importance when developing a purification process for the recovery of high value products such as antibody fragments. In order to minimise the volume of feedstock required for this study, a number of unit operations were performed at both laboratory and pilot scale. This chapter describes the characterisation of operations of cell lysis, homogenisation, centrifugation and diafiltration used in order to obtain feedstocks suitable for further purification by ion exchange adsorption, either by conventional column chromatography or stirred tank batch adsorption. No attempt was made to optimise these unit operations during this study.

3.1 Introduction

It is essential for a study such as this to use feedstocks which are both industrially relevant and well characterised as this will aid the assessment of the adsorptive methods being investigated. The production of such feedstocks through the use of small, or lab-scale mimics of industrial scale processes is the focus of this chapter.

This chapter describes a series of unit operations utilised in the production of two alternative process streams, both originating from the same *E. coli* fermentation. In order to quantify the effects of the production methods on the Fab' concentration a suitable analytical method is developed and its robustness tested in Section 3.1.1. Section 3.1.2 gives a brief outline of the fermentation process. The cell harvest and product release methods are described in Section 3.1.3 and Section 3.1.4, respectively. A description of diafiltration and how the ionic strength of the feedstock solutions must be reduced prior to ion exchange adsorption is given in Section 3.1.5. A key observation of earlier work using Fab' (Novais, 2001) was that the Fab' partitions to the cell debris. The quantification of this interaction between

cell debris and Fab' is discussed in Section 3.1.6. Finally, the effect of storage conditions on the feedstock properties is described in Section 3.1.7.

3.1.1 Protein G assay for Fab' quantification

This section describes the development of the protein G assay, including the reduction of the standard injection volume and analysis of its robustness and reproducibility. The operating procedure is described in Section 2.3.5.1.

The protein G assay used in this study was developed at UCB Celltech Ltd (Slough, UK) and is based on the use of a HiTrap protein G Sepharose™ High Performance column (GE Healthcare, Uppsala, Sweden). Protein G is a cell surface protein of Group G *streptococci*. GE Healthcare recombinant protein G is produced in *E. coli* and contains two IgG binding regions. Protein G is known to bind immunoglobulins at both the Fc region and the C_{H1} domain of the Fab' fragment (Gronenborn and Clore, 1993; Derrick and Wigley, 1994; Lian *et al.*, 1994).

The linear region of the standard curve for the protein G-based assay was determined by assaying a series of Fab' solutions ranging from 0 to 1 mg/mL.
As major elements of this doctoral study were conducted at ultra scale-down (USD) it was necessary to minimise the sample volumes required for the assay. It was essential, therefore, to establish whether the assay could perform satisfactorily when small volumes of the process sample were loaded on to the protein G column. This was tested by obtaining a standard curve for three injection volumes; 25, 50 and 100 µL, with 100 µL being the standard volume used previously in the protocol.
An important aspect of any assay is its reproducibility. The ability to achieve reliable and consistent results depends on both the assay itself and the ability of the operator carrying out the test. In order to assess the reproducibility of the method a sample of the lysate feedstock was assayed nine times and the resulting Fab' concentrations used to calculate the mean ($\bar{x}$), standard deviation (σ) and coefficient of variance (CV). The coefficient of variance gives a measure of the precision of the assay, i.e. how close the replicates are to one another. The lower the CV, the better

the precision, with a value of 10% or less being deemed acceptable. CV is defined by Equation 3.1:

$$CV = 100 \times \left(\frac{\sigma}{\bar{x}} \right) \qquad 3.1$$

3.1.2 *E. coli fermentation*

The *E. coli*-Fab' fermentation procedure is performed routinely at UCL and the system well characterised. The biomass used in this project was obtained from a 45 L fermentation carried out with the help of fellow EngD student Andrew Tustian, according to the methods described in Section 2.1.
As the sole purpose of the fermentation was to provide the biomass and Fab' necessary for the studies into the downstream processing of Fab', no attempt to optimise the fermentation was made in this study.

The procedure was based on the use of a defined culture medium and glycerol as the carbon source. In order to reduce the leakage of Fab' from the cells Mg^{2+} and PO_4^{2-} were added throughout the fermentation to strengthen the cell walls. IPTG was used to induce Fab' production and the culture was harvested 36 h post-induction.

3.1.3 *Cell Harvest*

There are several methods available for achieving the primary recovery of cells from fermentation broths. This normally consists of the separation of solids from the liquid broth, either by filtration or by centrifugation. Due to the short processing times, centrifugation was the method of choice for the production of the feedstocks utilised in this study. As stated in Section 2.2.1, *E. coli* cells were harvested from the fermentation broth using a CSA-1 disc-stack centrifuge (Westfalia Separator, AG, Oelde, Germany) operated at 9,800 rpm at a flow rate of 25 L/h ($Q/c\Sigma = 1.09 \times 10^{-8}$ m/s). The harvested cell paste was then packed in aliquots of approximately 200 g and stored at -80 °C.

3.1.4 *Intracellular product release*

When products are expressed intracellularly, cell disruption must be performed in order to release the desired product. There are numerous methods available, as described in Chapter 1. As described in Section 2.2.2 high pressure homogenisation and periplasmic extraction, by means of a heat lysis, were used as the product release methods. Both methods offer particular process advantages and disadvantages, such as process time, energy and equipment requirements, and therefore offer different process options. These will be discussed in more detail in Chapter 7.

The method of cell disruption will yield feedstocks with specific physical and chemical properties. These differences can significantly affect the selection of unit operations and process conditions further downstream. For this study the ionic strength and particle size of the resulting feedstock were chosen as the main parameters to be investigated. The particle size distribution is critical to this study as it will have a major impact on the ability to process unclarified materials by packed bed adsorption. The ionic strength of the feedstock will affect the binding of Fab' to the ion exchange adsorbent as discussed in Chapter 1.

3.1.5 *Feedstock ionic strength*

Cell disruption affects the chemical properties of the resulting feedstock, especially the ionic strength. The importance of adjusting the ionic strength of the feed prior to ion exchange adsorption has been discussed in Chapter 1. There are numerous ways of adjusting the ionic strength of the feedstock, including the use of diafiltration. As with all unit operations, there are process considerations that dictate which method is employed. This can have major implications when considering the productivity of the total process.

In order to minimise the ionic strength of the resulting homogenate, *E. coli* cell paste was resuspended in ultra pure water prior to high pressure homogenisation.

The ionic strength of the unclarified *E. coli* lysate was reduced by diafiltration using a hollow fibre membrane system as described in Section 2.2.3.

3.1.6 Clarification

In order to investigate the effect of solids concentration on the performance of the adsorptive processes, feedstock solutions of varying solids concentration were needed. The *E. coli* homogenate and lysate solutions were clarified to different degrees using laboratory centrifuges according to Section 2.3.1.2.

3.1.7 Cell debris-Fab' interactions

During the course of this study yields greater than 100% were being obtained during the purification of Fab' from unclarified material. It has been hypothesised (Novais, 2001) that cell debris acts as an ion exchanger and binds Fab' from solution. The debris-bound Fab' contributes to the amount of Fab' being adsorbed to the media, resulting in yields greater than 100%. Previously the measurement of Fab' concentration had been limited to analysis of the supernatant and the concentration of Fab' bound to the debris was unknown. Therefore, a method of measuring the total available Fab' was developed, which took into account the concentration of Fab' bound to the cell debris as well as that in the supernatant.

The development of this method, which includes the optimisation of the molarity of the elution buffer, the number of elution steps required, as well as a reproducibility analysis is described in Section 2.3.5.2. The effect of ionic strength on the cell debris-Fab' interaction is also investigated, along with the effect of the ionic strength of a diluting buffer on cell debris-Fab' interactions during the dilution of feedstocks.

3.1.8 Feedstock storage and Fab' stability

To minimise the variability in the properties of the feedstocks used during this study the aim was to freeze a stock solution of both the homogenate and lysate and use small volumes as and when needed. In order to be able to confidently use the stock solution it was important to assess the effect of the storage conditions on the Fab' concentration and *E. coli* cell particle size distribution. The Fab' concentration and particle size distribution of freshly produced homogenate and lysate were measured prior to storage for one week at +4, -20 and –80 °C.

3.2 Results and discussion

The results of the feedstream preparation and characterisation are presented and discussed in the following sections. Section 3.2.1 presents the results of the development and assessment of the protein G assay used during this study for the quantification of Fab' concentration. Section 3.2.2 states the results of the fermentation, and Section 3.2.3 compares the physical properties of the feedstocks obtained after periplasmic product release. Section 3.2.4 describes the results from the investigation into the interaction between cell-debris and Fab', and how the method of total system Fab' measurement was developed. Finally, in Section 3.2.5 the effect of the storage conditions on the Fab' concentration and particle size distribution are discussed.

3.2.1 Protein G assay characterisation

This section will describe the development, characterisation and optimisation of the primary assay used in this study. The aim was to determine the linear region of the standard curve, the optimal sample injection volume, and the reproducibility of the assay.

3.2.1.1 Determining the linear region of the standard curve

The determination of the linear region of the Fab' standard curve was performed using purified Fab' solutions in a concentration range of 0 to 1.0 mg/mL. For the purpose of this experiment an injection volume of 100 μL was used.
As seen in Figure 3.1, the standard curve was linear in the concentration range 0 to 0.5 mg/mL, and based on these results all future standard curves were performed using Fab' concentrations in the range of 0 to 0.5 mg/mL.

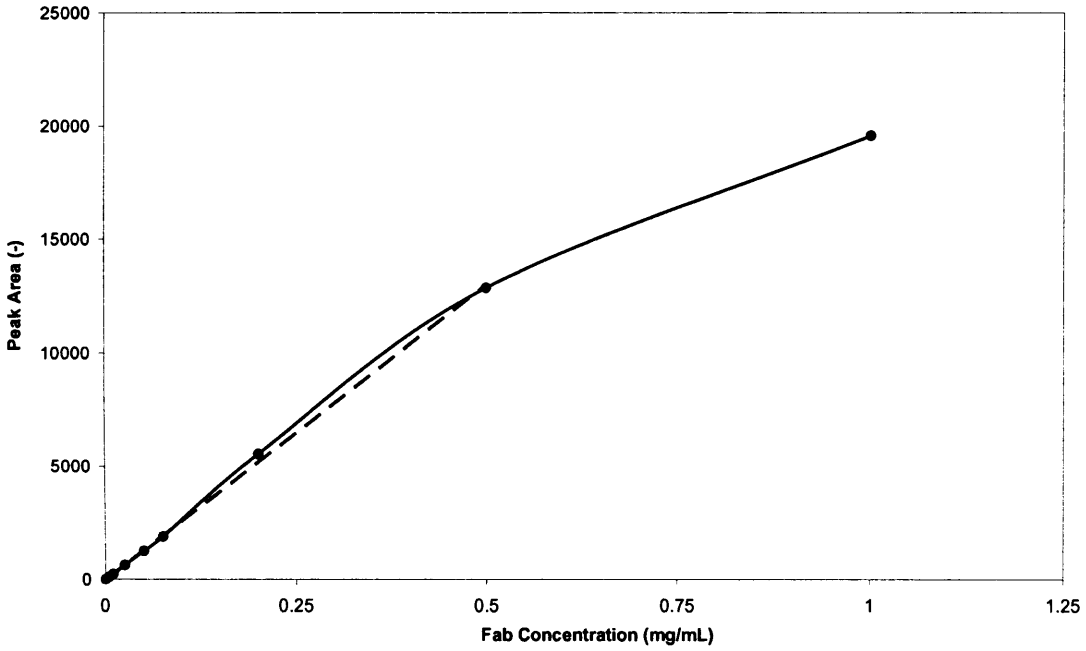

Figure 3.1. Fab' standard curve for the protein G assay. The line (---) represents the trendline obtained from standard solutions in the concentration range 0 to 0.5 mg/mL Fab'. The equation of this line was $y = 26{,}000x$, with an R^2 of 0.999. 100 µL injection volume.

3.2.1.2 Optimising sample injection volume

Figure 3.2 shows the standard curves obtained when loading 25, 50 or 100 µL of the same Fab' standard solution. Each standard curve was obtained using standard solutions in the concentration range 0 to 0.5 mg/mL. As in Section 3.2.1.1 linear regression was used to obtain an equation for each standard curve. Table 3.1 shows the regression equations and corresponding R^2 values.

The results show that reducing the injection volume by half leads to a 50% drop in the peak area of the eluted Fab' standard. Reducing the injection volume from 100 to 50 µL appears to have no adverse affect on the performance of the assay. The use of an injection volume of 50 µL for all samples was selected for all future work.

Table 3.1. Summary of the regression equations and R^2 values obtained during the loading of Fab' standards at three different injection volumes, where y is the integrated peak area and x is the Fab' concentration (mg/mL).

Injection Volume (μL)	Regression Equation	R^2
100	y = 28600x	0.999
50	y = 14400x	0.999
25	y = 7300x	0.997

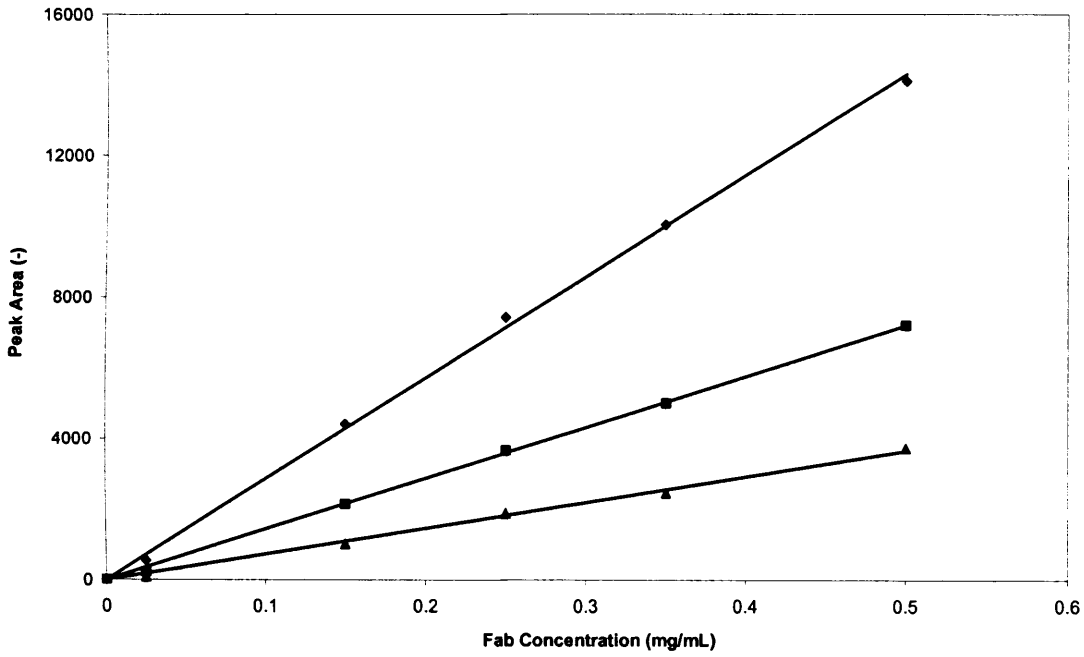

Figure 3.2. The effect of sample injection volume on the standard curves of Fab' using the Protein G assay. Standard curves for 25 (▲), 50 (■) and 100μL (♦) Fab' standards, in the concentration range of 0 to 0.5 mg/mL.

3.2.1.3 Assessing the assay reproducibility

To assess the reproducibility of the assay the standard deviation (σ) and coefficient of variance (CV) were calculated from Fab' concentration data obtained from assaying the same sample nine times. The results are summarised in Table 3.2. These results confirm a high level of assay reproducibility.

Table 3.2. Mean Fab' concentration and corresponding standard deviation and coefficient of variance for nine lysate feed samples used in the assessment of the reproducibility of the protein G assay.

$\bar{x}$ (mg/mL)	σ (mg/mL)	CV (%)
0.10	4.2E-4	0.4

3.2.2 *E. coli Fab' fermentation*

The production of antibody fragments expressed in *E. coli* was briefly discussed in Chapter 1 and the fermentation protocol described in Section 2.1. The fermentation yielded approximately 40 L of fermentation broth, which had a solids concentration of approximately 18% (ww/v). The Fab' produced was expressed in the periplasm of the *E. coli* cells, and virtually none had leaked into the fermentation medium.
The resulting Fab' had a molecular weight of 47 kDa and an isoelectric point, p*I*, of 7.6.

3.2.3 *Periplasmic product release*

High pressure homogenisation was performed at small scale using a Lab 40 (APV Ltd., Crawley, UK) homogeniser and at pilot scale using a Lab 60 homogeniser, as described in Section 2.2.2.1 and Section 2.2.2.2. The material obtained from the Lab 40 was used to demonstrate how the number of passes through the homogeniser affects the mean particle diameter (d_{50}, volume basis). It was also used for characterisation experiments, including studying cell debris-Fab' interactions (Section 3.2.4) and feedstock storage analysis (Section 3.2.5). The material from the homogenisation using the Lab 60 was used for all adsorptive work carried out in the study. Selective periplasmic extraction was performed in a 3 L stirred tank fermenter as described in Section 2.2.2.3.

The following section describes how the periplasmic product release methods used in this study determine the properties of each feedstream. The effect of homogenisation and periplasmic extraction on the mean particle diameter and ionic strength of the resulting feedstocks are compared and discussed. The release of Fab' into solution during the periplasmic extraction will also be presented.

3.2.3.1 Post-cell disruption particle size distribution

The particle size distribution (PSD) was measured as described in Section 2.3.4. Figure 3.3 shows the PSD of the homogenate as a function of the number of passes through a Lab 40 homogeniser. It appears that complete cell disruption was achieved after only two passes at 500 bar as the d_{50} remained constant for further passes (Figure 3.3 inset).

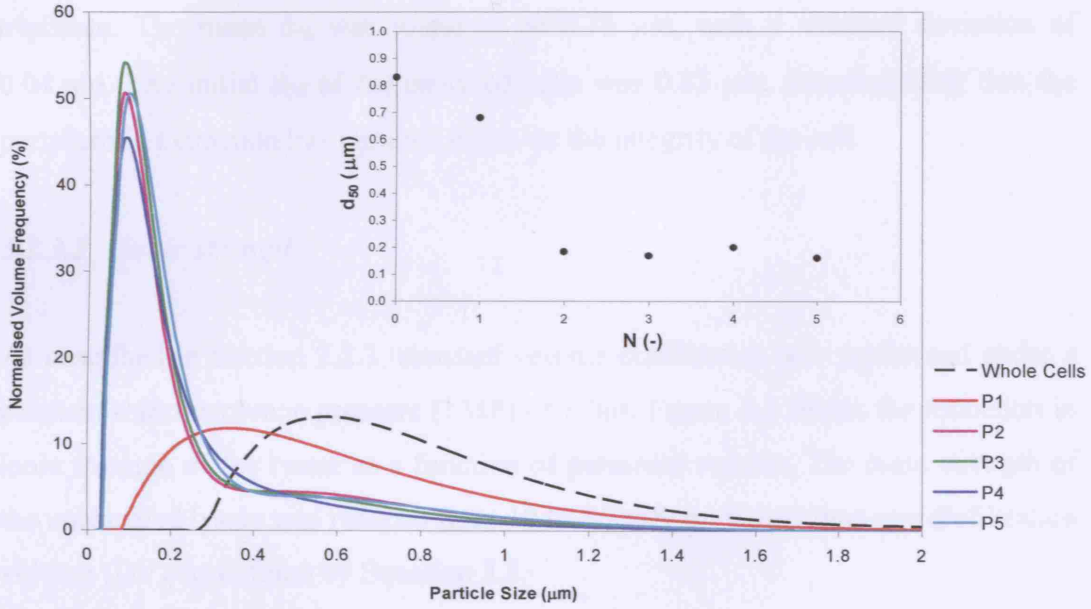

Figure 3.3. *E. coli* particle size distribution and, inset, d_{50} plotted against number of passes (N) for disruption by a Lab 40 high pressure homogeniser.

The initial d_{50} for the resuspended cell paste was 0.83 µm. After five passes this had decreased to 0.16 µm. The equivalent d_{50} for the cell debris resulting from homogenisation using the Lab 60 was 0.37 µm. This result suggests a difference in the performance of the two homogenisers when operated under the same conditions. A comparison of the particle size distributions obtained from the two homogenisers used in this study has been previously carried out by Siddiqi *et al.* (1996) who reported that the particle size distribution of disrupted baker's yeast is independent of scale of operation and valve head design. It is then reasonable to assume the results observed in this study are due to operational reasons, such as operator error or equipment failure. One source of such a discrepancy is the valve unit of the homogeniser. Keshavarz *et al.* (1990) showed that the valve unit design has a

significant effect on cell breakage. Kleinig *et al.* (1996) report that 80% of *E. coli* cell disruption is due to valve unit geometry. Valve units are susceptible to wearing, and worn valves are known to cause discrepancies in the degree of cell breakage (personal communication, Dr. Keshavarz-Moore). The valve units on the Lab 60 homogeniser were therefore inspected, and showed evidence of wear and tear. It is reasonable to attribute the observed difference in d_{50} to the wear and tear on the valve unit on the Lab 60 homogeniser.

The d_{50} of the *E. coli* cell debris after periplasmic extraction was measured in triplicate. The mean d_{50} was found to be 0.76 μm, with a standard deviation of 0.04 μm. The initial d_{50} of the un-lysed cells was 0.83 μm, demonstrating that the periplasmic extraction has minimal effect on the integrity of the cell.

3.2.3.2 Ionic strength

As described in Section 2.2.3, constant volume diafiltration was performed under a constant transmembrane pressure (TMP) of 1 bar. Figure 3.4 shows the reduction in ionic strength of the lysate as a function of permeate volume. The ionic strength of the unclarified lysate was reduced from 10 to 3.2 mS/cm in less than one diafiltration volume (DV), as defined by Equation 3.2.

$$\text{Diafiltration Volume (DV)} = \frac{\text{permeate volume}}{\text{feed volume}} \qquad 3.2$$

Figure 3.5 shows the drop in flux over time as the hollow fibre membrane becomes fouled. The permeate flux decreased from 22 L/m^2/h to a steady flux of 11 L/m^2/h in 1 h.

As stated in Section 3.1.5, resuspending the *E. coli* cell paste in ultra pure water prior to homogenisation helped to reduce the ionic strength. The ionic strength of the cell suspension was 2.9 mS/cm both before and after homogenisation. No further conditioning was necessary for the homogenate.

For experiments where solutions of varying ionic strength were required, NaCl was added to increase the ionic strength.

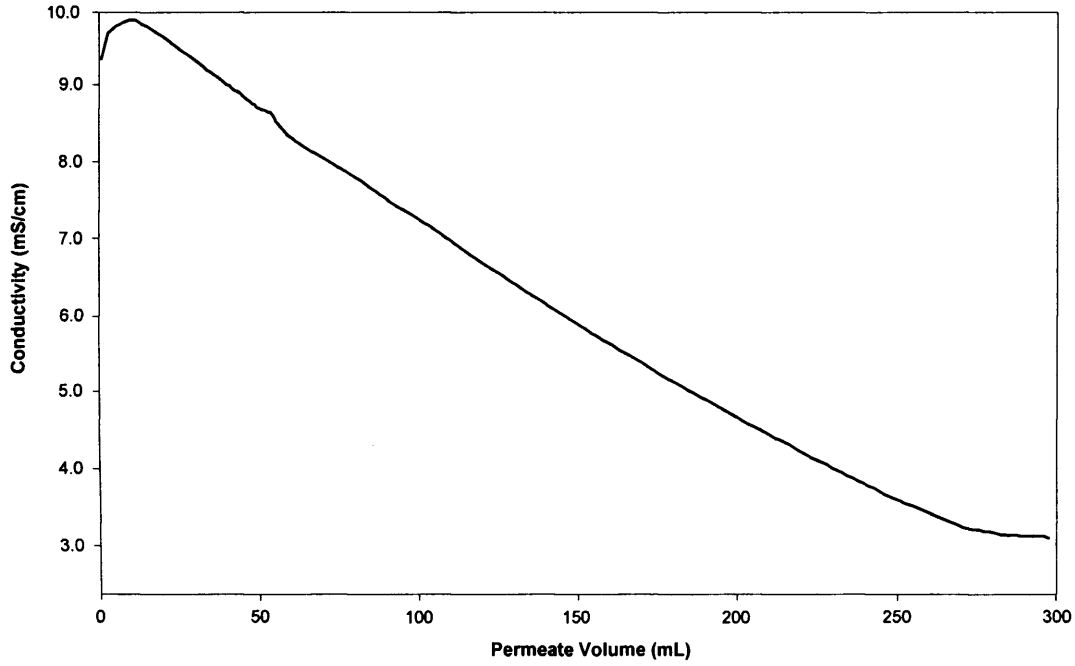

Figure 3.4. Reduction of ionic strength of unclarified *E. coli* lysate using constant volume diafiltration. The volume of unclarified lysate (feed) was 350 mL.

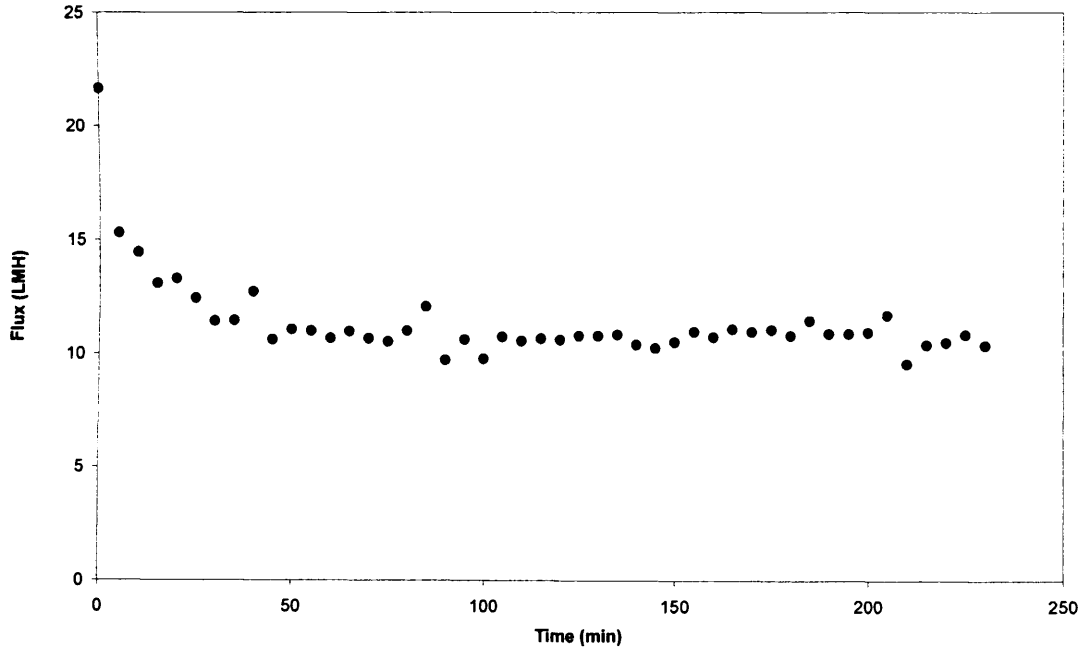

Figure 3.5. The drop in flux of the hollow fibre membrane due to fouling caused by the *E. coli* lysate feedstock, pH 7.2. 10 kDa membrane operated at a constant TMP of 1 bar.

3.2.3.3 *Fab' release during periplasmic extraction*

Figure 3.6 and Table 3.3 show the release of Fab' and total protein during the periplasmic extraction process performed in a 3 L stirred tank fermenter. Release of Fab' follows rapidly on addition of the cell paste to the extraction buffer. The concentration of Fab' falls steadily from the maximum which is achieved within 30 min as the temperature of the solution rises. The extraction process holds the cell suspension at a temperature of 60 °C for up to 16 h, a step which is designed to purify the periplasmic extract. Unlike correctly formed, disulphide-bonded Fab', incomplete Fab', free heavy and light chain fragments are degraded at 60 °C (Weir *et al.*, 1997; Bowering *et al.*, 2002). These contaminant fragments are able to bind to the protein G assay as they contain the correct binding regions. As the temperature of the cell suspension rises, these incomplete Fab' fragments begin to degrade, which results in the observed drop in the measured Fab' concentration. In reality then the concentration of active Fab' is essentially constant within 30 min of extraction.

Table 3.3. Monitoring the periplasmic extraction of Fab' from *E. coli* using a 3 L stirred tank fermenter.

Time (h)	Temperature (°C)	OD_{280}	Fab' Concentration (mg/mL)
0	20.0	45.8	0.59
0.5	52.0	73.5	0.69
1.0	59.7	77.1	0.65
1.5	60.6	82.2	0.65
2.5	60.7	82.9	0.64
4.5	60.7	89.3	0.62
5.5	60.7	87.8	0.62
6.5	60.7	91.1	0.60
19.5	60.6	98.4	0.61

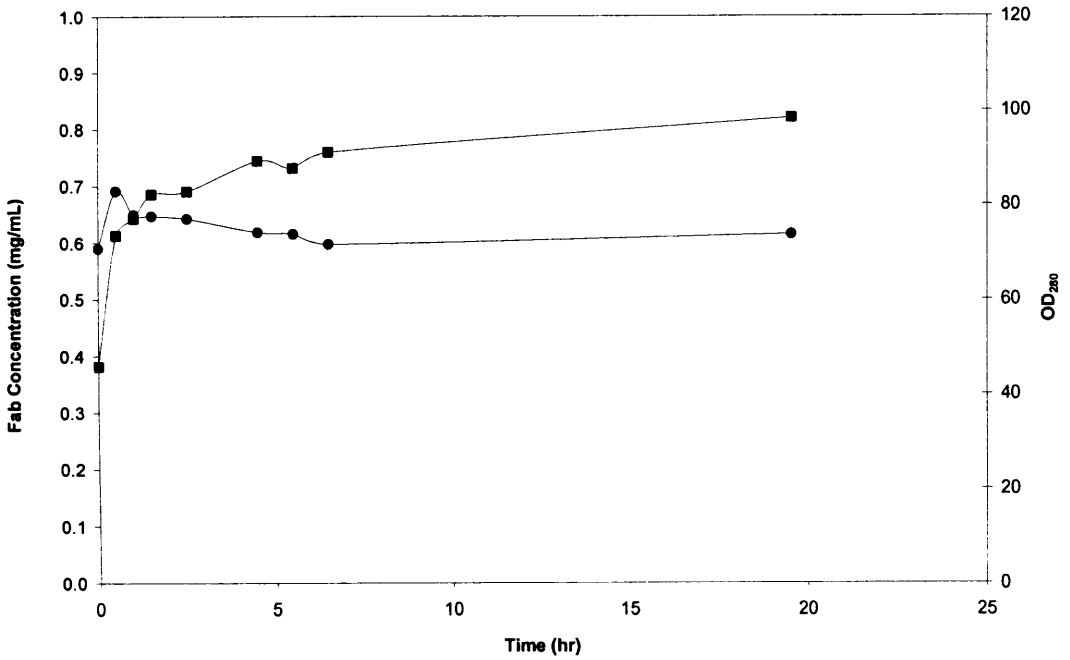

Figure 3.6. Comparing the release of Fab' (•) and total protein (■) during periplasmic extraction performed in a 3 L stirred tank fermenter operated at 60 °C and 400 rpm.

3.2.4 Cell debris – Fab' interactions

As described in Section 2.3.5.2 the method of total available Fab' measurement is based on the resuspension of a cell pellet in an eluting buffer, effectively washing the pellet and stripping it of Fab'. The choice of eluting buffer, the number of elutions and the reproducibility of the method will be discussed in this section as well as an investigation of the effect ionic strength has on the cell debris-Fab' interactions.

As the method of total available Fab' measurement will be used throughout this project it is important to define the terms used to characterise the total available Fab'.

The following definitions were used when determining Fab' concentration:

- Supernatant Fab' concentration (mg/mL): C_s
- Debris-bound Fab' concentration (mg/mL): C_d
- Total available Fab' concentration (C_s + C_d) (mg/mL): C_t

3.2.4.1 Total available Fab' method: Buffer molarity and number of elution steps

Figure 3.7 presents the elution of cell debris-bound Fab' as a function of Sodium Chloride molarity and number of elutions. As described in Section 2.3.5.3, debris pellets obtained from the centrifugation of 1 mL of the unclarified homogenate were resuspended in 1 mL 1, and 2.5 M NaCl, with RO water used as a control. After resuspension and mixing the solutions were centrifuged again and the Fab' concentration assayed. This procedure was repeated to determine the number of repeat elutions required to release all debris-bound Fab'. Figure 3.7 shows that maximum Fab' release is obtained when elution is performed using 1 M NaCl. Although it appears that Fab' release is incomplete after one elution, 94% of the total Fab' eluted from the cell debris using 1 M NaCl was released during the first elution. It was deemed that one elution using 1 M NaCl was the most efficient and appropriate way to perform this assay. A second elution would double the analytical burden, which in this study could lead to many hundreds of samples and hinder the investigation.

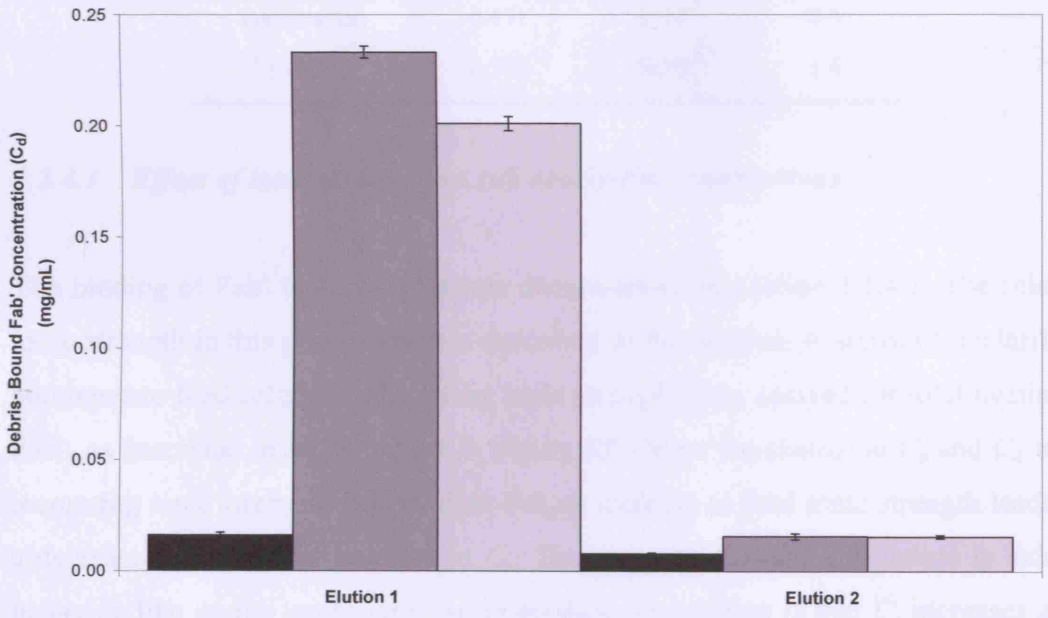

Figure 3.7. Elution of Fab' from homogenate cell debris as a function of buffer molarity and number of elutions. RO water (■), 1 M NaCl (■) and 2.5 M NaCl (■) used to elute Fab' from the debris of a feed with supernatant Fab' concentration of 0.33 mg/mL at an ionic strength of 3.5 mS/cm and pH 5.8. Feed solids concentration 6.4% (ww/v). Error bars shown represent the standard deviation.

3.2.4.2 Total available Fab' method: Method reproducibility

The mean Fab' concentration, standard deviation and coefficient of variance (CV) of ten homogenate feed samples were used to assess the reproducibility of the total available Fab' method. Table 3.4 shows that the standard deviation and CV for the debris-bound Fab' measurements are higher than those of the supernatant measurements, which suggests that there is some error associated with measuring the concentration of debris-bound Fab'. However, both values are relatively low and a CV of 1.4% indicates that the method is highly reproducible.

Based on these findings this method can be used to determine total available Fab' with a high degree of confidence.

Table 3.4. Mean ($\bar{x}$) supernatant (C_s) and debris-bound (C_d) Fab' concentrations, with corresponding standard deviation (σ) and coefficient of variance (CV) for ten homogenate feed samples. Lab 60 homogenate, feed solids concentration 5.5% (ww/v) at an ionic strength of 3.4 mS/cm and pH 5.8.

Fab' Source	$\bar{x}$ (mg/mL)	σ (mg/mL)	CV (%)
Supernatant	0.451	$3x10^{-3}$	0.6
Debris	0.363	$5x10^{-3}$	1.4

3.2.4.3 Effect of ionic strength on cell debris-Fab' interactions

The binding of Fab' to cell debris was demonstrated in Section 3.2.4.1. The role of ionic strength in this phenomenon is described in this section. A series of unclarified homogenate feed solutions of varying ionic strength were assayed for total available Fab', as described in Section 2.3.6.1. Figure 3.8 shows the change in C_s and C_d with increasing ionic strength. It is evident that an increase in feed ionic strength leads to a decrease in C_d and an increase in C_s. This suggests that the cell debris is indeed behaving like an ion exchanger. An interesting observation is that C_t increases as a function of ionic strength. This may be due to irreversible binding leading to incomplete elution of the debris-bound Fab' during the measurement of C_d at the lower ionic strength solutions. These results are based on single 1 M NaCl elutions of Fab' from cell debris. As shown in Figure 3.7, when the feed ionic strength is as low

as 3.5 mS/cm, not all Fab' is eluted from the cell debris in one elution volume. Complete Fab' elution from cell debris may be easier to achieve at higher feed ionic strengths.

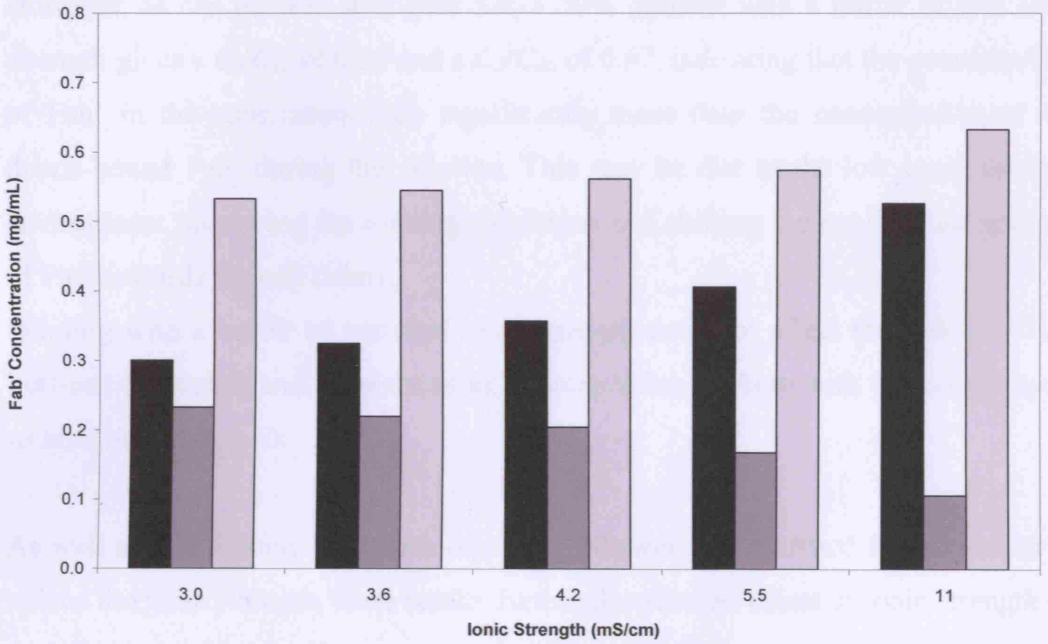

Figure 3.8. Supernatant (■), debris-bound (■) and total (■) Fab' concentration as a function of homogenate ionic strength. Feed solids concentration 6.4% (ww/v), pH 5.75. Debris-bound Fab' eluted using one, 1 mL 1 M NaCl elution.

3.2.4.4 Feedstock dilution and cell debris-Fab' partition

The reduction of feedstock ionic strength by dilution with low ionic strength buffers is common practice in downstream processing. However, in the specific case investigated in this study, this may lead to an increase in cell debris-Fab' interactions. Figure 3.8 has shown that reducing the ionic strength of a feedstock increases the concentration of debris-bound Fab'. To investigate the effect of feedstock dilution on cell debris-Fab' interactions a lysate feed with an ionic strength of 3.1 mS/cm was diluted with two Sodium Acetate solutions of different ionic strength, as described in Section 2.3.6.2. The first dilution was designed to mimic a typical dilution of a feedstock and was carried out using a buffer with an ionic strength of 1.4 mS/cm. As a control, a second feed sample was diluted with a buffer with an ionic strength identical to that of the feed, 3.1 mS/cm.

The effect of the ionic strength of the diluting buffer on cell debris-Fab' interactions is presented in Figure 3.9 and Figure 3.10, where dimensionless concentration is plotted against dilution. When carrying out a 50% dilution of the feed, both C_s and C_d are expected to fall to 50% of their original values, i.e. C_s/C_{s0} and $C_d/C_{d0} = 0.5$. However, as can be seen in Figure 3.9, a 50% dilution with a buffer of low ionic strength gives a C_s/C_{s0} of 0.20 and a C_d/C_{d0} of 0.67, indicating that the concentration of Fab' in the supernatant falls significantly more than the concentration of the debris-bound Fab' during this dilution. This may be due to the low ionic strength environment improving the binding conditions and shifting the equilibrium position of Fab' towards the cell debris.

Diluting with a buffer of identical ionic strength does not affect the Fab' partition between cell debris and supernatant as the correlation for both with dilution is linear as seen in Figure 3.10.

As well as highlighting the issues regarding dilution of unclarified feeds in order to reduce the ionic strength, these results further describe the effect of ionic strength on the behaviour of Fab' with regards to binding to cell debris.

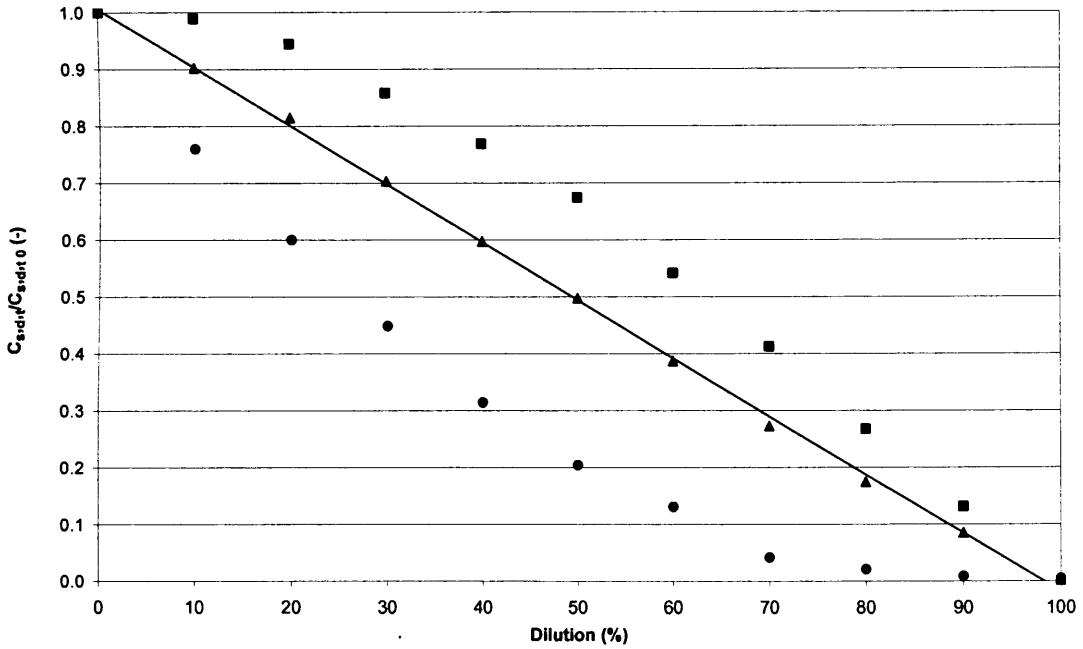

Figure 3.9. Dilution of lysate feed with low ionic strength buffer (1.4 mS/cm). C_s (●), C_d (■) and C_t (▲) normalised to give dimensionless concentration. The line represents a linear fit of the C_t data and confirms that the correlation between the total available Fab' and feed dilution is linear.

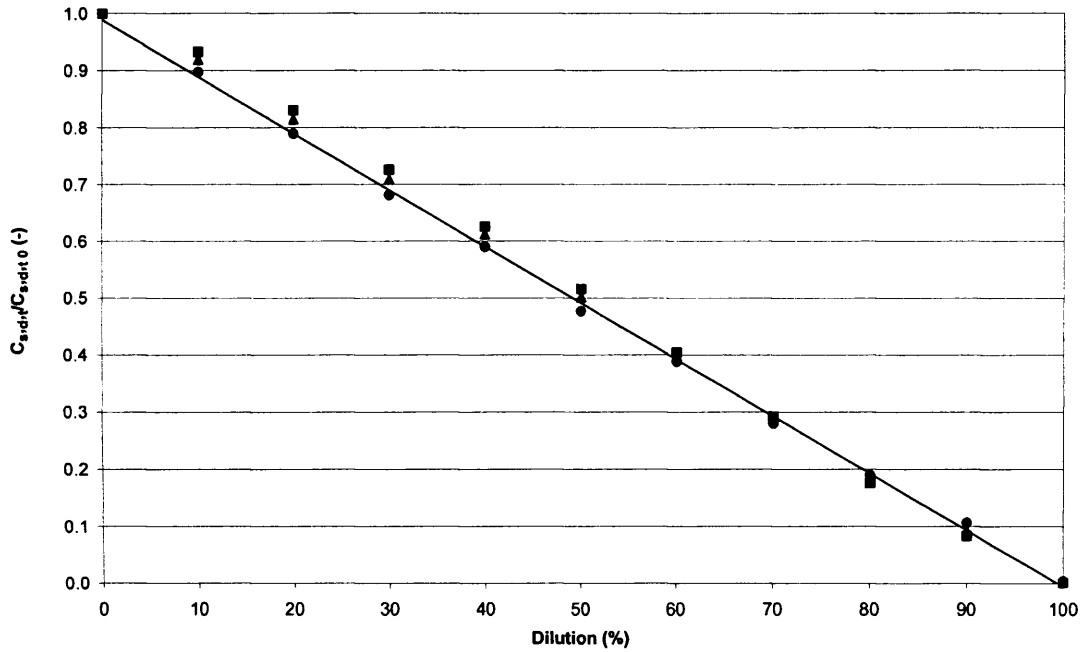

Figure 3.10. Dilution of lysate feed with a buffer of similar ionic strength (3.1 mS/cm). C_s (•), C_d (■) and C_t (▲) normalised to give dimensionless concentration. The line represents a linear fit of C_t.

3.2.5 Short term storage analysis

The impact of storage temperature on homogenate Fab' concentration is presented in Figure 3.11. Storage of the unclarified feed at +4 °C for seven days led to a drop in Fab' concentration. This is most likely as a result of protease enzymes being released in to the feed during homogenisation. Freezing the feed straight after homogenisation reduces the impact of the protease attack and the Fab' concentration remains constant after seven days storage at -20 and -80 °C.

Figure 3.12 shows that the storage temperature affects the Fab' concentration of the lysate feed in a different manner. Storage for seven days at +4 °C had almost no affect on the Fab' concentration. This is in contrast with the homogenate where a drop in Fab' concentration was observed. One reason for this difference is the fact that the lysis procedure does not release protease enzymes in to the feed and so the Fab' remains relatively stable at this temperature. It is interesting to note that freezing the unclarified lysate leads to a slight increase in Fab' concentration. A possible explanation for this is that cell breakage can occur during freezing, possibly releasing any remaining intracellular Fab' which may not have been extracted during the lysis.

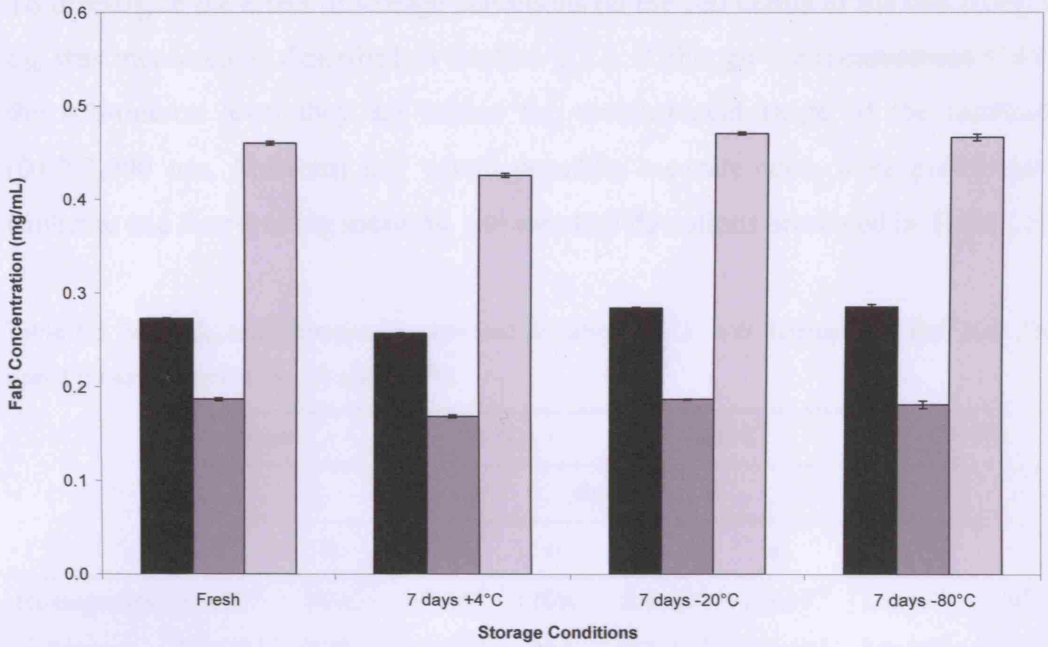

Figure 3.11. Homogenate supernatant (■), debris-bound (■) and total (■) Fab' concentration measured after storage for seven days at +4, -20 and -80 °C. Feed solids concentration 2.6% (ww/v), ionic strength 3.2 mS/cm.

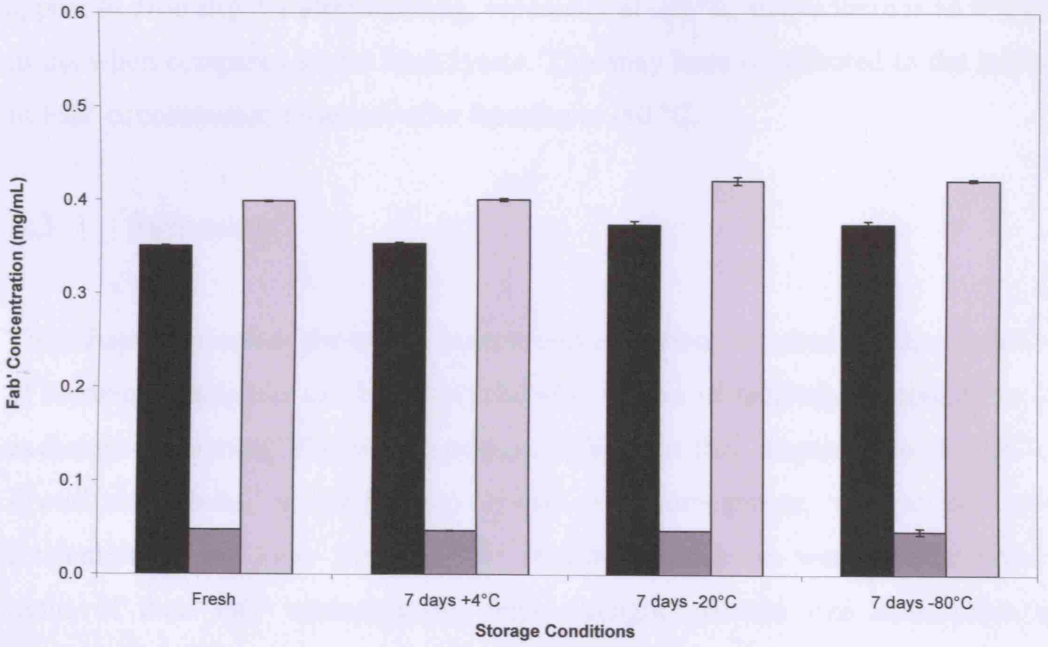

Figure 3.12. Lysate supernatant (■), debris-bound (■) and total (■) Fab' concentration measured after storage for seven days at +4, -20 and -80 °C. Feed solids concentration 14% (ww/v), ionic strength 9.0 mS/cm (unconditioned feed).

To investigate the effect of storage conditions on the cell debris of the two feeds, the d_{50} was measured as described in Section 2.3.4. Although the measurements are in the sub-micron level they are within the measurement range of the instrument (0.02-2,000 μm, Malvern) and where possible, measurements were performed in triplicate and the resulting mean d_{50} and standard deviations presented in Table 3.5.

Table 3.5. Mean d_{50} and corresponding standard deviations for *E. coli* homogenate and lysate feeds stored for seven days at +4, -20 and -80 °C.

	Fresh		**+4 °C**		**-20 °C**		**-80 °C**	
	d_{50} (μm)							
	$\bar{x}$	σ	$\bar{x}$	σ	$\bar{x}$	σ	$\bar{x}$	σ
Homogenate	$1.6x10^{-1}$	N/A	$1.7x10^{-1}$	N/A	$1.6x10^{-1}$	$1.0x10^{-3}$	$1.6x10^{-1}$	$1.5x10^{-3}$
Lysate	$7.6X10^{-1}$	N/A	$6.1x10^{-1}$	N/A	$7.3x10^{-1}$	$3.4x10^{-2}$	$7.0x10^{-1}$	$3.1x10^{-2}$

Table 3.5 shows that the mean particle diameter of the homogenate cell debris remains constant, which is to be expected as complete cell breakage should already have occurred. However, the mean particle diameter of the lysate cell debris does appear to drop slightly after freezing, especially at -80 °C, where there is an 8% drop in d_{50} when compared to the fresh lysate. This may have contributed to the increase in Fab' concentration observed after freezing at -80 °C.

3.3 Summary

This chapter describes the use of several unit operations required for the production of feedstocks suitable for the successful purification of antibody fragments by ion exchange adsorption. The unit operations utilised in this chapter have yielded two *E. coli* feedstocks, a periplasmic lysate and homogenate, of varying solids concentration and ionic strength. The resulting feedstocks were characterised in terms of their Fab' concentration, ionic strength, particle size distribution and stability.

The protein G assay used in this study was found to be highly reproducible and robust. It was possible to successfully reduce the sample volume required for this assay.

Product release was performed using both high pressure homogenisation and periplasmic extraction. The effect of these two methods on the physical properties of the resulting feeds were investigated and compared. High pressure homogenisation yielded a feed of low ionic strength, requiring minimal further conditioning. However, the periplasmic lysate required substantial conditioning, and diafiltration was shown to be an efficient way to reduce the ionic strength of the solution. The ionic strength of both feedstocks was found to influence the concentration and level of partitioning of Fab' within the unclarified feeds. For feedstocks of low ionic strength, antibody fragments were found to bind preferentially to the cell debris. This phenomenon had to be accounted for and a method to determine the concentration of debris-bound Fab' was developed and assessed in this chapter.
Short term storage was also found to influence the concentration and particle size distribution of the feeds. Unlike the homogenate, the lysate mean particle diameter was found to decrease slightly after storage at -80 °C. This was thought to be due to cell breakage, which was also the reason for a slight increase in Fab' concentration, as previously un-extracted Fab' may have been released from the cells.

Having characterised the range of feedstocks Chapter 4 will now look at the effect of these unit operations on the equilibrium adsorption isotherms of antibody fragments when binding to ion exchange media. Chapter 5 will investigate their effects on column chromatography and Chapter 6 will develop and assess batch adsorption as an alternative to column chromatography.

4 The determination of equilibrium isotherms for the adsorption of antibody fragments from crude *E. coli* homogenate and lysate solutions

Abstract

A method of data analysis and modelling which enables the prediction of adsorption isotherms was developed and the resulting data used to predict the effect of two process variables, the feedstock ionic strength and solids concentration, on the performance of the ion exchange media. In order to achieve this, equilibrium isotherms performed in a bespoke microwell plate, utilising minimal volumes of the feedstocks prepared through the work carried out in Chapter 3 are presented and discussed.

4.1 Introduction

An introduction to adsorption and equilibrium adsorption isotherms was given in Chapter 1. In this chapter the feedstock solutions prepared in Chapter 3 were used to investigate the effect of the feedstock properties on the adsorption isotherms. The impact of the feed ionic strength and solids concentration of both the *E. coli* lysate and homogenate is assessed and compared. The experimental data was processed prior to fitting to established isotherm models and used to generate models which will allow the prediction of process yields and productivity.

Section 4.1.1 provides a description of the theoretical background to equilibrium adsorption.

4.1.1 Adsorption Isotherms

A critical parameter needed for any investigation into adsorptive processes is the adsorption isotherm. The isotherm is an important part of modelling protein adsorption as well as process design, including process efficiency and economics.

(Dechow, 1989). Therefore, accurate determination and representation of the isotherms is essential (Miyabe *et al.*, 2004). As stated in Chapter 1, there are many different types of adsorption isotherms and several authors have already carried out substantial and detailed reviews (Freundlich, 1906; Langmuir, 1916; Giles *et al.*, 1960; Seidel-Morgenstern, 2004) to name only a few. The focus of this study will be aimed at linear, Freundlich and the single component Langmuir isotherms. As acknowledged in Chapter 1, the Steric Mass Action (SMA) isotherm would perhaps provide a more detailed and realistic description of the effects of ionic strength on Fab' adsorption. However, since the aim of this thesis is to provide a generic and simple analysis of Fab' adsorption and the effect of both feedstock ionic strength and solids concentration the complexity of the SMA approach precludes it from consideration. Figure 4.1 shows the three isotherms which are considered in this chapter.

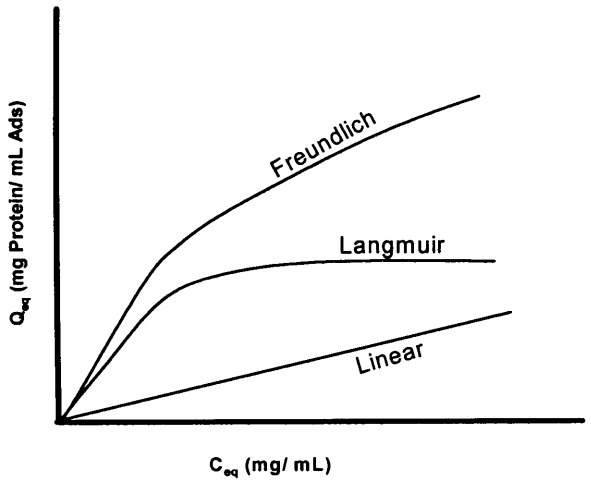

Figure 4.1. The common adsorption isotherms observed in protein adsorption (Belter *et al.*, 1988).

4.1.1.1 Linear isotherm

The linear isotherm, given by Equation 4.1, is the simplest form of adsorption isotherm and is normally observed when the solute concentration is low and the solutes are not competing. The amount of solutes bound to the adsorbent is directly proportional to the concentration of the solutes in solution (Sofer and Hagel, 1997).

$$Q_{eq} = K \cdot C_{eq} \qquad 4.1$$

where Q_{eq} is the concentration of protein bound to the adsorbent, C_{eq} is the equilibrium protein concentration (left in solution), and K is an equilibrium constant (distribution coefficient) (Belter *et al.*, 1988). Q_{eq} is calculated using experimental C_{eq} data and the following equation:

$$Q_{eq} = \frac{(C_0 - C_{eq})V_l}{V_m} \qquad 4.2$$

where C_0 is the initial solute concentration, V_m is the volume of adsorbent and V_l is the feed load volume.

4.1.1.2 Freundlich isotherm

The Freundlich isotherm is a relatively simple, empirical isotherm, as defined by Equation 4.3. The use of the Freundlich equation to characterise several protein systems has been reported recently (Finette *et al.*, 1997; Sharma and Agarwal, 2001; Bayramoglu *et al.*, 2005). The Freundlich isotherm also appears to be very popular in the heavy metal and environmental management industries where numerous articles are available describing its application to heavy metal adsorption.

$$Q_{eq} = K_f \cdot C_{eq}^n \qquad 4.3$$

where K_f and n are empirical coefficients, determined experimentally. The best way to determine K_f and n is through a log-log plot of Q_{eq} versus C_{eq}, where the slope gives the exponent n. A value of n greater than 1 indicates that the adsorption is unfavourable. Favourable adsorption is achieved when n is less than 1 (Belter *et al.*, 1988). The Freundlich isotherm does have some limitations, such as the concentration of bound solute increases indefinitely with increasing concentration of solute in solution (Finette *et al.*, 1997).

4.1.1.3 Langmuir isotherm

The Langmuir isotherm is commonly observed in liquid chromatography (Sofer and Hagel, 1997). Despite initially intended for the description of adsorption of gases to glass, mica and platinum surfaces (Langmuir, 1916), the Langmuir isotherm has been used widely in the description of simple cases of protein adsorption. There are numerous examples of its use in this field (Skidmore *et al.*, 1990; Skidmore and Chase, 1990; Finette *et al.*, 1997; Chang and Lenhoff, 1998; Lan *et al.*, 2001; Hahn *et al.*, 2003; Seidel-Morgenstern, 2004; Jozwik *et al.*, 2005).

The Langmuir isotherm, described by Equation 4.4, is based on several assumptions, of which the following are most commonly stated (Dechow, 1989; Annadurai and Krishnan, 1997; Fargues *et al.*, 1998; Jozwik *et al.*, 2005):

- Solutes are adsorbed onto one adsorption site and the number of sites is fixed.
- All adsorption sites are identical.
- Only one layer of solutes is adsorbed (monolayer).
- Adsorption at one site is not influenced by adjacent sites (no interaction between adsorbed molecules).

$$Q_{eq} = \frac{Q_{max} \cdot C_{eq}}{K_d + C_{eq}} \qquad 4.4$$

where Q_{max} is the maximum binding capacity of the adsorbent and K_d is the dissociation constant, the ratio of the forward and backward rate constants ($K_d = k_2/k_1$) as shown in Equation 4.5. Equation 4.5 shows the adsorption of a protein, P, to an adsorption site within the ligand, S.

$$P + S \underset{k_2}{\overset{k_1}{\rightleftharpoons}} P \cdot S \qquad 4.5$$

4.2 Data processing and modelling

The development of two methods of data processing and modelling are described and compared in this section. Section 4.2.1 describes a reproducibility analysis performed on the experimental method used to obtain isotherm data, while Section 4.2.2 describes the development of two models and the subsequent selection of one for use in the processing of all experimental data.

4.2.1 Isotherm method reproducibility

Adsorption isotherms using unclarified lysate were performed in triplicate as described in Section 2.4.1.4. As the feedstock was unclarified, the total available Fab' method was used to measure Fab' concentration both in solution and bound to cell debris. Therefore, to calculate Q_{eq} Equation 4.2 is redefined to give Equation 4.6:

$$Q_{eq} = \frac{(C_{t0} - C_t)V_l}{V_m} \qquad 4.6$$

where C_{t0} is the initial total available Fab' concentration (mg/mL) and C_t is the total equilibrium Fab' concentration (mg/mL).

As stated in Section 3.1.1 the Coefficient of Variance (CV), as defined by Equation 3.1, is a measure of the precision of a set of replicated samples. Table 4.1 shows the CV for the measured C_t and the corresponding Q_{eq} as a function of the phase ratio, V_m/V_l (adsorbent volume/load volume). The CV is below 5% and indicates that the measurement of C_t is reproducible and can be used with confidence. The observed increase in CV with increasing phase ratio is due to C_t approaching zero as the volume of adsorbent increases. It is worth noting that due to the nature of Equation 4.6 and the small volumes of adsorbent (V_m) utilised in this study, minor errors in C_t can lead to large discrepancies in Q_{eq}. This will become apparent in later sections of this chapter.

Table 4.1. Isotherm method reproducibility analysis. Coefficient of variance for isotherms performed in triplicate using 200 µL unclarified lysate at 3.1 mS/cm and pH 5.6. Adsorbent volume ranged from 0.1 to 20 µL.

	CV (%)	
V_m/V_l $(x10^{-3})$	C_t	Q_{eq}
0	0.3	n/a
0.5	1.0	6.1
1.0	0.5	2.4
2.5	1.0	4.9
5.0	2.5	5.6
10	2.4	2.3
25	4.2	1.8
50	3.8	1.0

4.2.2 Isotherm data processing and modelling

Adsorption isotherms were measured as described in Section 2.4.1.4 using both the homogenate and lysate feedstocks. Both feedstocks were prepared to give solutions of varying ionic strength. The aim of the following section is to detail the choice of the data processing approach adopted through presenting an example of the experimental results and describing the two methods of data processing and modelling used. One of these will then be selected to analyse all subsequent isotherm data.

Figure 4.2 shows a flowsheet of the steps taken during the processing and modelling of the experimental isotherm data for a clarified homogenate performed at various feed ionic strengths.

The steps involved in the modelling process will be detailed firstly in Section 4.2.2.1, which outlines the data processing technique which utilised a 1st order exponential decay equation. Section 4.2.2.2 then describes the results obtained from the second modelling technique which utilises an empirical isotherm-type model. Finally, a conclusion will be drawn as to the most appropriate form of data processing to be used.

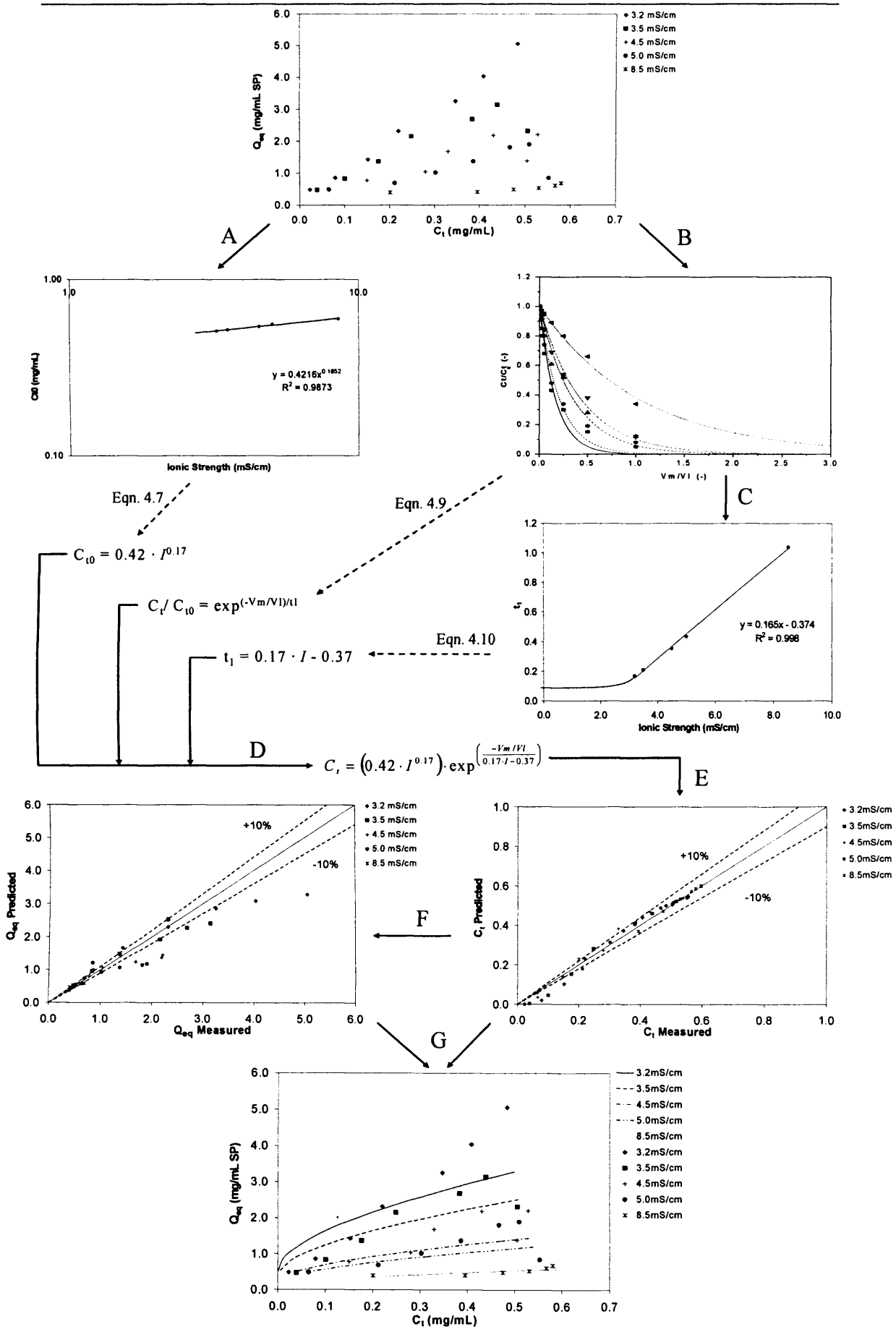

Figure 4.2. A flowsheet showing the steps involved in the data processing and modelling of equilibrium isotherm data. Data shown is for a clarified homogenate feed at increasing ionic strength.

4.2.2.1 Exponential decay model (ExpDec model)

Figure 4.3 shows an example of experimental isotherm data obtained in this study. For the purpose of this section the trends and significance of the result will not be discussed but merely presented as part of the development of the model.

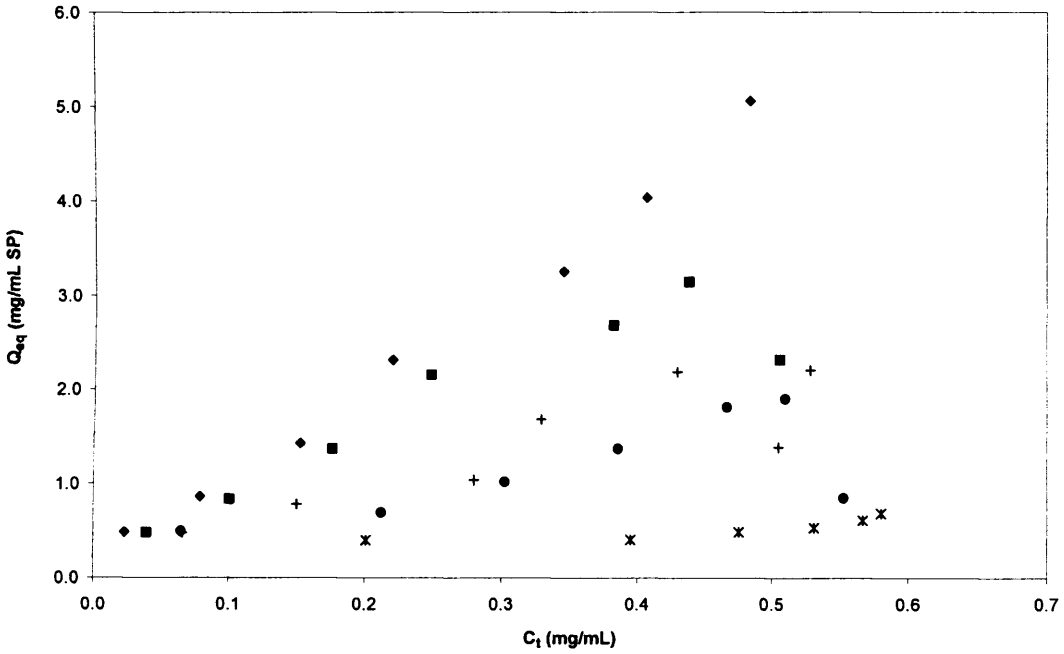

Figure 4.3. Experimental adsorption isotherm data for clarified homogenate at pH 5.5 and ionic strength of 3.2 (♦), 3.5 (■), 4.5 (+), 5.0 (●) and 8.5 (x) mS/cm.

The first stage of the modelling process is concerned with modelling the initial total Fab' concentration (C_{t0}). As described in Section 3.2.3.3 there is an increase in C_{t0} with increasing ionic strength. There is also an increase in C_t with increasing feed solids concentration. In order to model accurately the effect of ionic strength and feed solids concentration on adsorption isotherms, the effect of these feedstock properties on C_{t0} must be incorporated into the model. This example is concerned with the effect of ionic strength on the adsorption isotherms. Figure 4.4 shows Stage A of the flowsheet (Figure 4.2) and the correlation between C_{t0} and ionic strength. In this specific case there is a power law relationship and Figure 4.4 is plotted with logarithmic scales. As the model is empirical, the correlations and linear regression equations are system-specific.

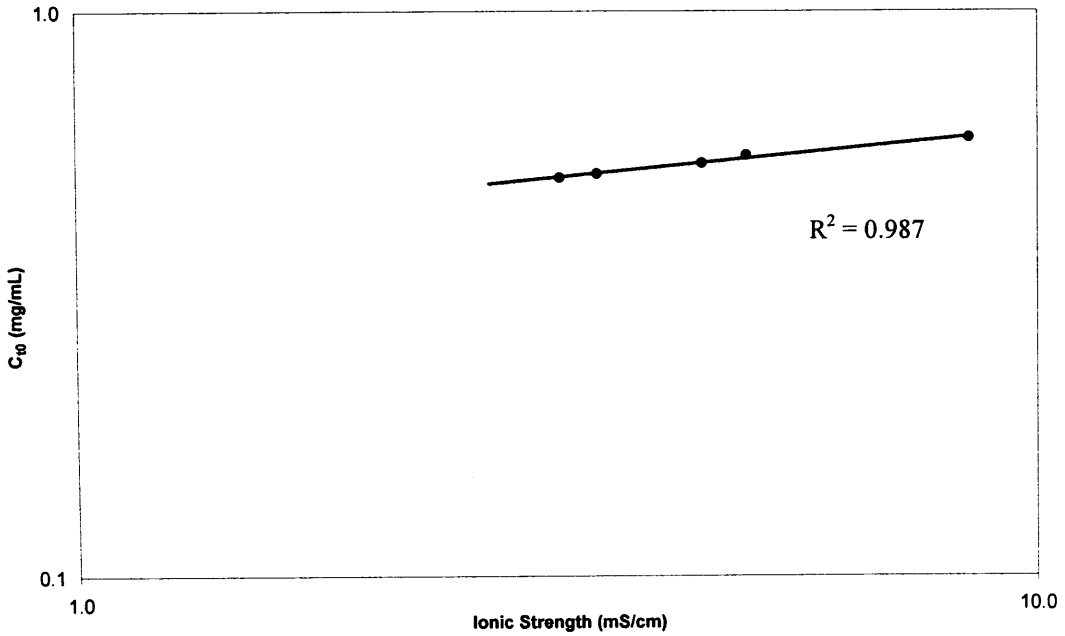

Figure 4.4. Stage A of the ExpDec model development, correlating C_{t0} and feed ionic strength.

As a result of the linear regression C_{t0} can be predicted using Equation 4.7.

$$C_{t0} = A \cdot I^B \qquad 4.7$$

where I is the feed ionic strength (mS/cm) and A and B are empirical constants.

During Stage B of this model the adsorption of Fab' (C_t/C_{t0}) as a function of phase ratio (V_m/V_l) was fitted to a 1st order exponential decay model (Equation 4.8) using a Levenberg-Marquard least squares estimation of a non-linear curve using the software package Origin™ (Microcal Software Inc., Northampton, USA).

$$y = A \cdot \exp^{\left(\frac{-x}{t1}\right)} + y_0 \qquad 4.8$$

where y is the dimensionless concentration (C_t/C_{t0}), A is the amplitude, x is the phase ratio (V_m/V_l), t_1 is the exponential decay constant and y_0 is the equation offset. Fitting to Equation 4.8 is based on two assumptions:

- $A = 1$
- $y_0 = 0$

The offset, y_0 equals zero due to the assumption that within the range of ionic strength tested, complete adsorption of Fab' will occur if an excess of adsorbent is used. The amplitude is fixed to 1 as the x-axis is dimensionless concentration and can not be greater than 1.

Equation 4.8 can be rearranged to make C_t the subject, giving Equation 4.9.

$$C_t = C_{t0} \cdot \exp^{\left(\frac{-Vm/Vl}{t1}\right)} \qquad 4.9$$

Figure 4.5 presents the experimental data fitted to Equation 4.8.

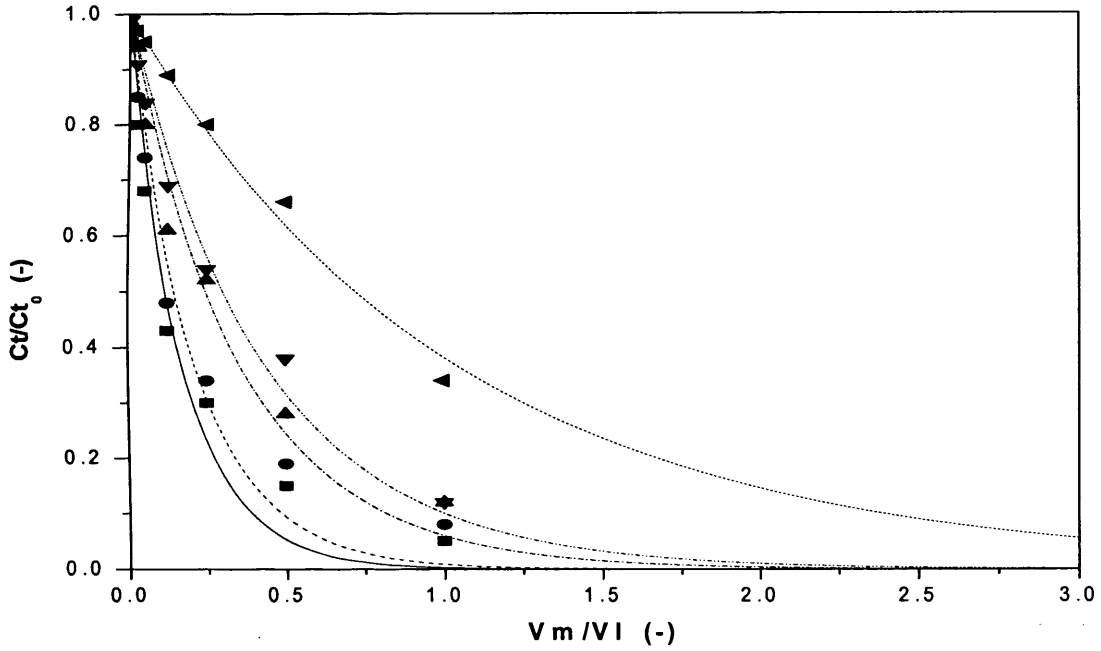

Figure 4.5. Stage B of the ExpDec model, fitting the experimental data to the first order exponential decay equation to obtain the decay constant as a function of ionic strength. Average $R^2 = 0.978$.

Stage C of the model takes the exponential decay constant, t_1, from each of the curves in Figure 4.5 and correlates these with the feed ionic strength as seen in Figure 4.6. Within the range of feed ionic strength tested, the relationship between t_1 and ionic strength is linear and the correlation is very strong as indicated by the R^2 of 0.998. Due to a lack of experimental data at very low ionic strengths, the relationship between t_1 and ionic strength is unknown at low ionic strengths. The dashed line (---) in Figure 4.6 represents an assumed relationship between t_1 and feed

ionic strength. The model is therefore limited in the range of ionic strengths it can cope with ($3.2 < I < 8.5$).

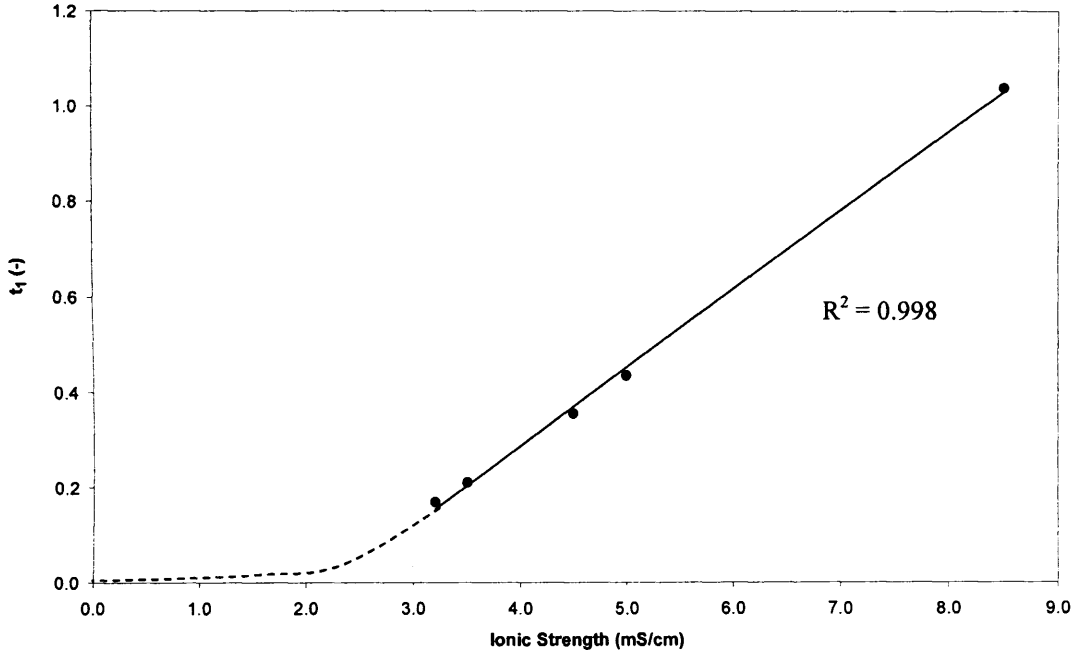

Figure 4.6. Stage C, the relationship between feed ionic strength of the clarified homogenate and the exponential decay constant, t_1.

Linear regression was used to enable the accurate prediction of t_1 between 3.2 and 8.5 mS/cm.

$$t_1 = C \cdot I - D \qquad 4.10$$

where C and D are empirical constants.

Figure 4.7 compares the predicted and experimental t_1 values in a parity plot. The experimental and predicted values are very closely matched.

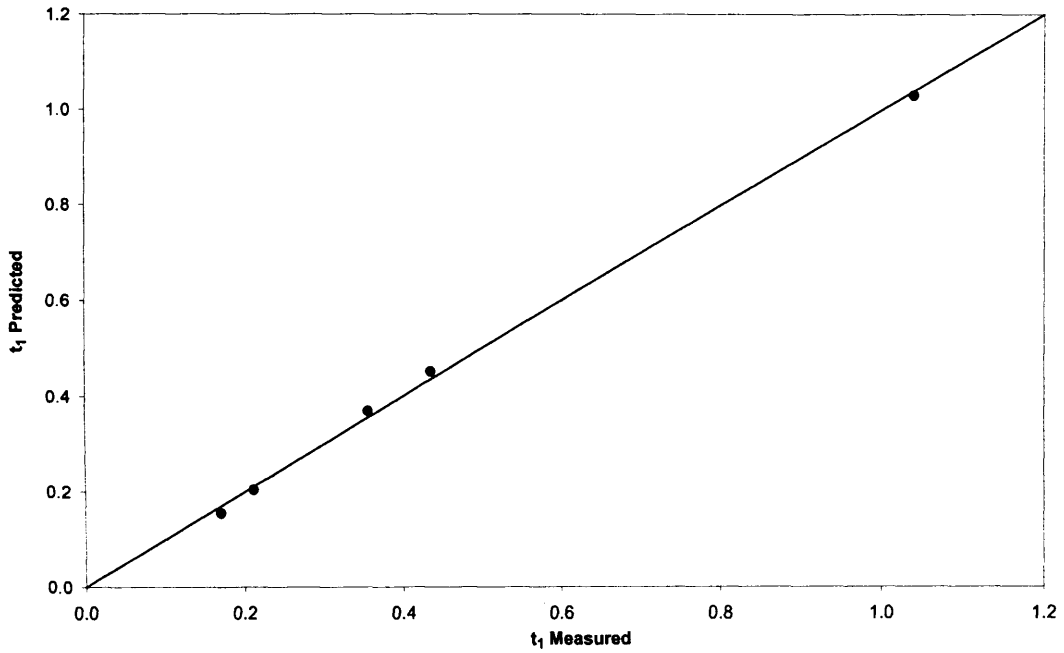

Figure 4.7. A parity plot showing the measured and predicted exponential decay constant, t_1.

The next stage of the model, Stage D, combines Equation 4.7, Equation 4.9 and Equation 4.10. Substituting C_{t0} (Equation 4.7) and t_1 (Equation 4.10) into Equation 4.9 gives Equation 4.11:

$$C_t = \left(A \cdot I^B\right) \cdot \exp^{\left(\frac{-Vm/Vl}{C \cdot I - D}\right)} \qquad 4.11$$

Using Equation 4.11 it is now possible to predict the equilibrium Fab' concentration as a function of ionic strength and phase ratio. The predicted C_t can now be used to calculate a predicted Q_{eq} and give the equilibrium adsorption isotherms.

In order to test the accuracy of the model Stage E generates a parity plot of experimental and predicted C_t (Figure 4.8) and Stage F generates a parity plot of the corresponding Q_{eq} (Figure 4.9).

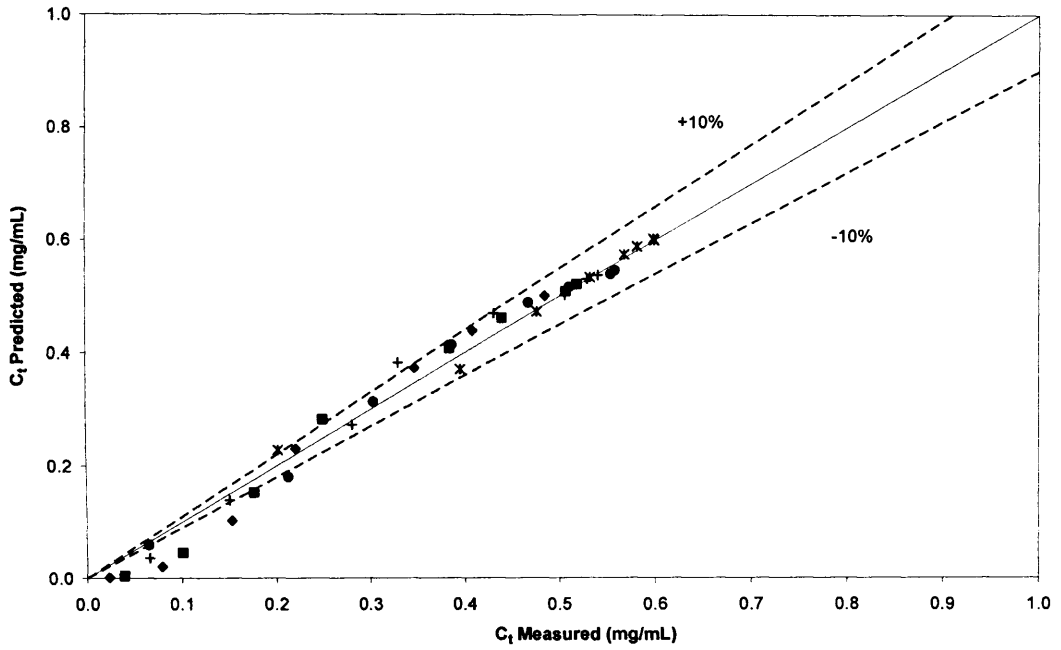

Figure 4.8. A comparison of the experimental and predicted data for C_t showing 10% error limits. Clarified homogenate feed at ionic strengths of 3.2 (♦), 3.5 (■), 4.5 (+), 5.0 (●) and 8.5 (x) mS/cm.

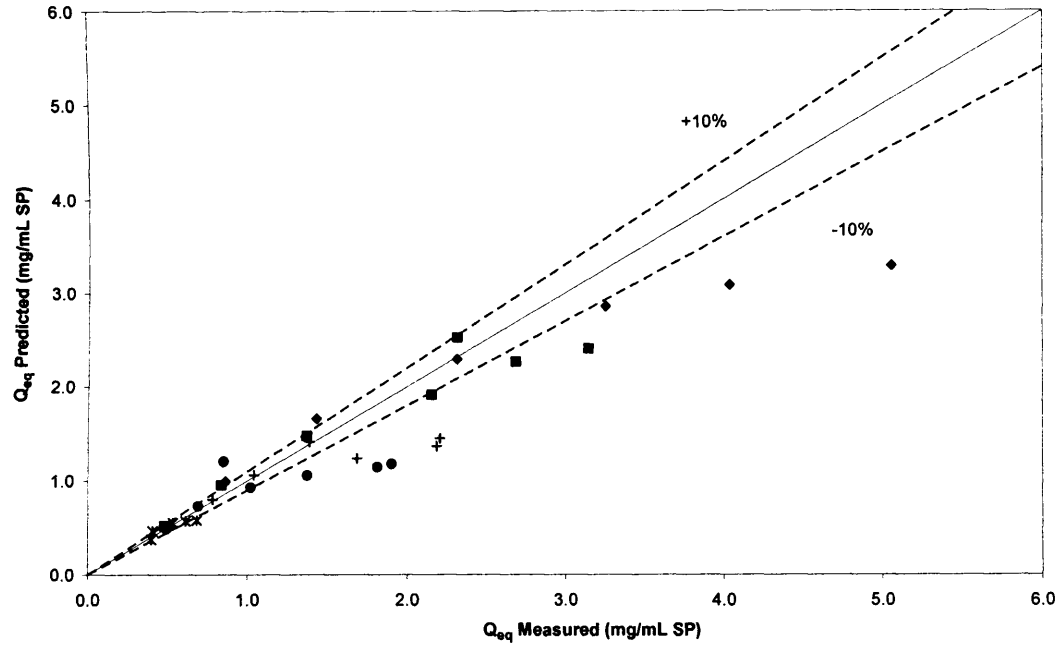

Figure 4.9. A comparison of the experimental and predicted data for Q_{eq} showing 10% error limits. Clarified homogenate feed at ionic strengths of 3.2 (♦), 3.5 (■), 4.5 (+), 5.0 (●) and 8.5 (x) mS/cm.

Figure 4.8 shows that the majority of the predicted C_t values are within ± 10% of the experimental data. The model appears to under-predict C_t at the lower concentrations and for all ionic strengths tested. A reason for this could be the way the data is fitted in Stage B of the model. As stated previously, when the data is fitted to Equation 4.8 the amplitude and offset are fixed. Fixing the amplitude should have no effect on the fitting as the x-axis is dimensionless concentration and so the maximum value can only be 1. However, fixing the offset to zero forces the model through points which deviate away from the experimental data. This can be seen in Figure 4.5 where the line of best fit for the 3.2 and 3.5 mS/cm data sets deviates significantly from the experimental points between the phase ratios (V_m/V_l) of 0.25-1.0. The data fitting is essentially over-predicting the degree of adsorption, which leads to the model under-predicting C_t, as seen in Figure 4.8.

Figure 4.9 shows that there are also significant deviations in the parity plot for Q_{eq}. A possible explanation for these deviations was touched upon in Section 4.2.1. Due to the nature of Equation 4.6 and the extremely low volumes of adsorbent being used (0.001-0.2 mL), small errors in the calculation of C_t are magnified when calculating Q_{eq}.

The final step in the model is Stage G, where the predicted C_t and Q_{eq} are plotted to give the equilibrium adsorption isotherms. Figure 4.10 shows the experimental and predicted isotherms for clarified homogenate. It is clear to see that although Figures 4.8 and Figure 4.9 suggest the model predicts C_t and Q_{eq} to an acceptable degree of accuracy, the overall model fails to predict the shape of the isotherm in situations were binding of Fab' is occurring. Significant deviations occur at low ionic strength, conditions which are better suited for binding. Figures 4.8-4.10 show that when the ionic strength is high and little or no binding occurs, the model predicts very accurately. This inaccuracy and failure to predict the correct isotherm shape is probably due to the exponential decay equation used in Stage B of the model. The exponential decay model results in the predicted isotherms being curved, when the experimental isotherms are in fact linear. To overcome this problem an alternative equation was investigated for Stage B of the model.

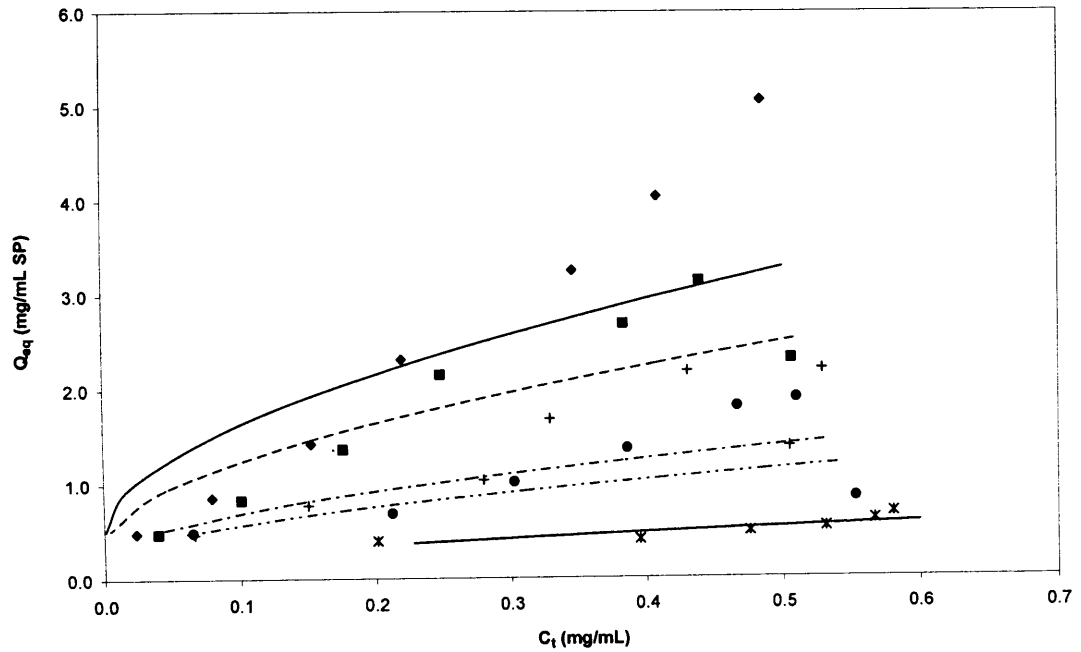

Figure 4.10. A comparison of the experimental and predicted adsorption isotherms for clarified homogenate feed at ionic strengths of 3.2 (♦), 3.5 (■), 4.5 (+), 5.0 (●) and 8.5 (x) mS/cm. Isotherms predicted at 3.2 (—), 3.5 (- -), 4.5 (- · -), 5.0 (—··—) and 8.5 (—) mS/cm using ExpDec model.

4.2.2.2 Distribution coefficient-based model (K-model)

This section describes the development of the "*K*-model". As there are few, but significant, differences between the two models this section will only highlight and detail the differences and present results of the *K*-model. The main difference between the two models is the equation used in Stage B.

In the linear region of an isotherm the distribution coefficient, K, is related to the equilibrium concentration, C_t and equilibrium capacity, Q_{eq}, by the following equation.

$$Q_{eq} = C_t \cdot K \qquad 4.12$$

As described in Section 4.1.1.1 Q_{eq} can be calculated using the Equation 4.6:

$$Q_{eq} = \frac{(C_{t0} - C_t)V_l}{V_m}$$

To show the relationship between the distribution coefficient, K, and adsorption isotherms, the following derivation of the K-model is provided.

Rearranging Equation 4.6 to make C_{t0} the subject gives:

$$C_{t0} = \frac{Q_{eq} \cdot V_m}{V_l} + C_t \qquad 4.13$$

Dividing both sides by C_t gives Equation 4.14:

$$\frac{C_{t0}}{C_t} = \frac{Q_{eq}}{C_t} \cdot \frac{V_m}{V_l} + 1 \qquad 4.14$$

Rearranging Equation 4.14 gives:

$$\frac{C_t}{C_{t0}} = \frac{1}{\left(\frac{Q_{eq}}{C_t} \cdot \frac{V_m}{V_l}\right) + 1} \qquad 4.15$$

From the curve fitting in Stage B of the model $y = C_t/C_{t0}$ and $x = V_m/V_l$ and rearranging Equation 4.12 gives $K = Q_{eq}/C_t$. Substituting x, y and K into Equation 4.15 gives Equation 4.16:

$$y = \frac{1}{(K \cdot x) + 1} \qquad 4.16$$

Therefore, to simplify the model and obtain the distribution coefficient as a function of ionic strength and the phase ratio, Equation 4.16 was used for Stage B of the modelling.

Figure 4.11 presents the results of the data fitting performed using a least squares estimation of a non-linear curve using Equation 4.16. This model provides a better fit when compared to Figure 4.5 where the equivalent data fitting was performed using an exponential decay model.

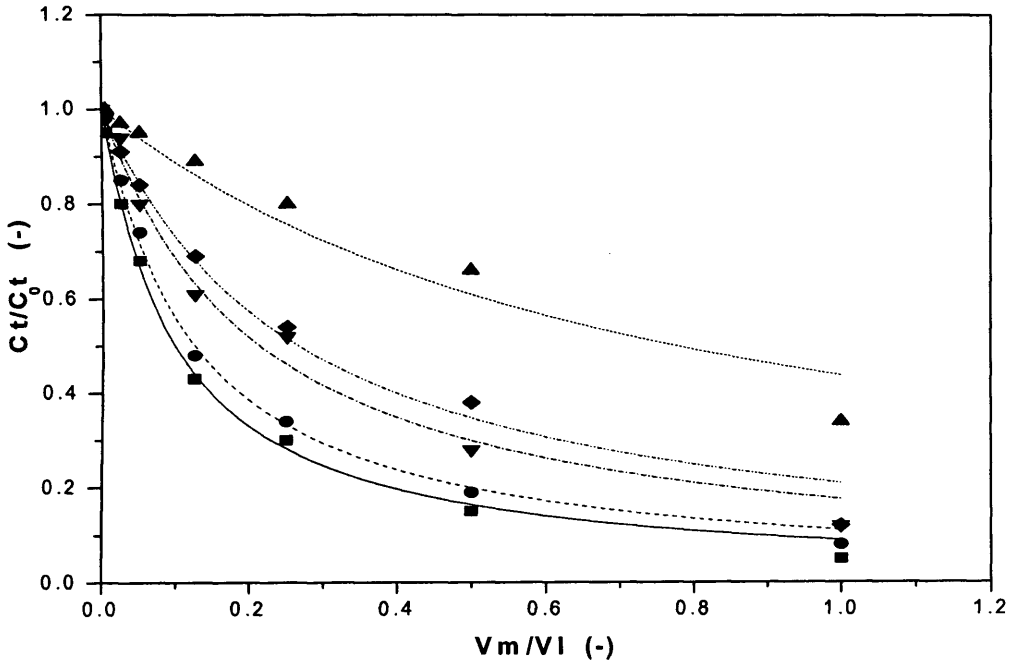

Figure 4.11. Stage B of the *K*-model, fitting experimental isotherm data to obtain the constant K as a function of feed ionic strength. Average $R^2 = 0.990$.

The K constants obtained from this data fitting were then correlated with the feed ionic strength (Stage C of the model) as presented in Figure 4.12. In this instance the correlation has a power law relationship, with an R^2 of 0.998. Equation 4.17 was then obtained which enables the prediction of K as a function of feed ionic strength.

$$K = E \cdot I^{-F} \qquad 4.17$$

where I is the feed ionic strength (mS/cm) and E and F are empirical constants.

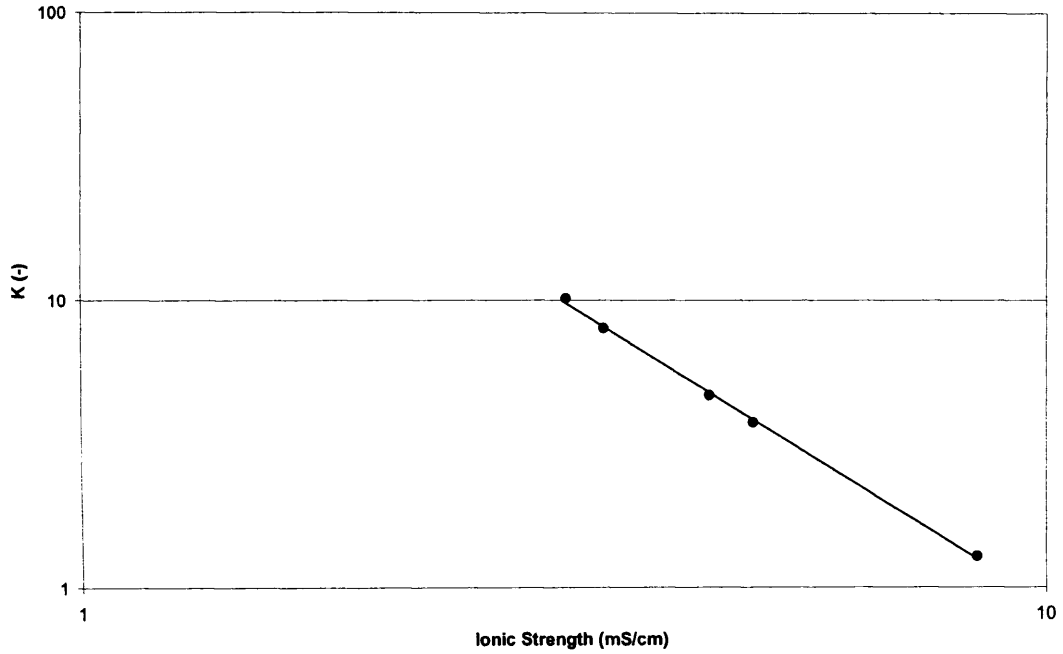

Figure 4.12. Stage C of the *K*-model. Correlating the K constant with the feed ionic strength. $R^2 = 0.999$.

Stage D of the *K*-model combines the equations needed to generate the final model. Firstly, C_t/C_{t0} and V_m/V_l are substituted into Equation 4.12 to give Equation 4.18.

$$\frac{C_t}{C_{t0}} = \frac{1}{\left(K \cdot \frac{V_m}{V_l}\right) + 1} \qquad 4.18$$

Equation 4.18 is then rearranged to make C_t the subject:

$$C_t = \frac{C_{t0}}{\left(K \cdot \frac{V_m}{V_l}\right) + 1} \qquad 4.19$$

C_{t0} and K are then substituted into Equation 4.19 to give the final model:

$$C_t = \frac{A \cdot I^B}{\left(E \cdot I^{-F}\right) \cdot \frac{V_m}{V_l} + 1} \qquad 4.20$$

Equation 4.20 makes it possible to predict the equilibrium Fab' concentration as a function of ionic strength and phase ratio. As with the exponential decay model, the predicted C_t is now used to calculate a predicted Q_{eq} and give the equilibrium adsorption isotherms.

Once again parity plots were used to assess the accuracy of the model (Stages E and F of the model). Figure 4.13 presents the parity plot of the experimental and predicted C_t obtained through the *K*-model. When compared to Figure 4.8, it is evident that the predicted C_t now matches the experimental to a much greater extent. This can be seen in Figure 4.13 where almost all the data points are tightly aligned along the parity line.

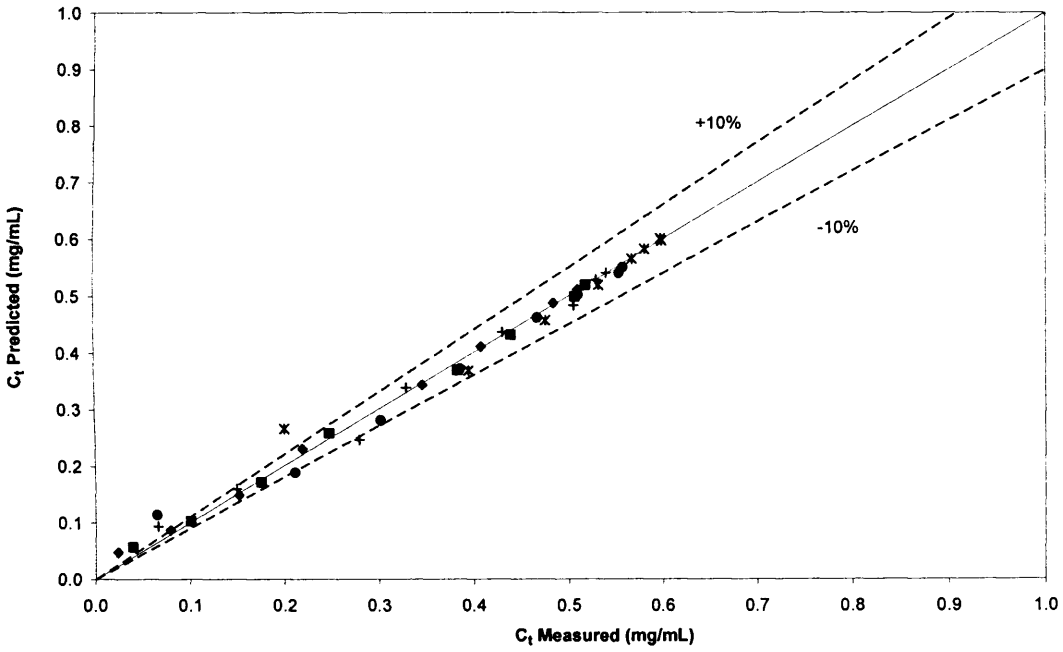

Figure 4.13. A comparison of the experimental and predicted (*K*-model) data for C_t from clarified homogenate feed at ionic strengths of 3.2 (♦), 3.5 (■), 4.5 (+), 5.0 (●) and 8.5 (x) mS/cm. 10% error limits shown.

Figure 4.14 presents the parity plot of the experimental and predicted Q_{eq} obtained through the *K*-model. In this case, almost all the predicted Q_{eq} data points lie within ± 10% of the experimental Q_{eq}. When compared to Figure 4.9, the parity plot of the Q_{eq} obtained through the exponential decay model, the predictions are clearly a much better match to the experimental data.

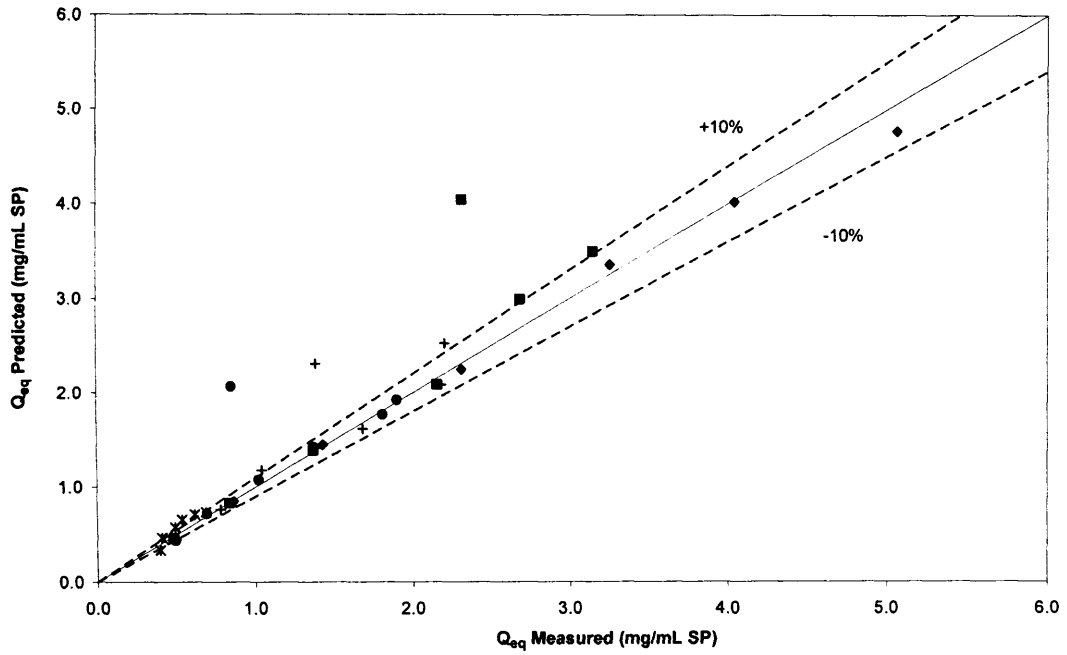

Figure 4.14. A comparison of the experimental and predicted (K-model) data for Q_{eq} from clarified homogenate feed at ionic strengths of 3.2 (♦), 3.5 (■), 4.5 (+), 5.0 (●) and 8.5 (x) mS/cm. 10% error limits shown.

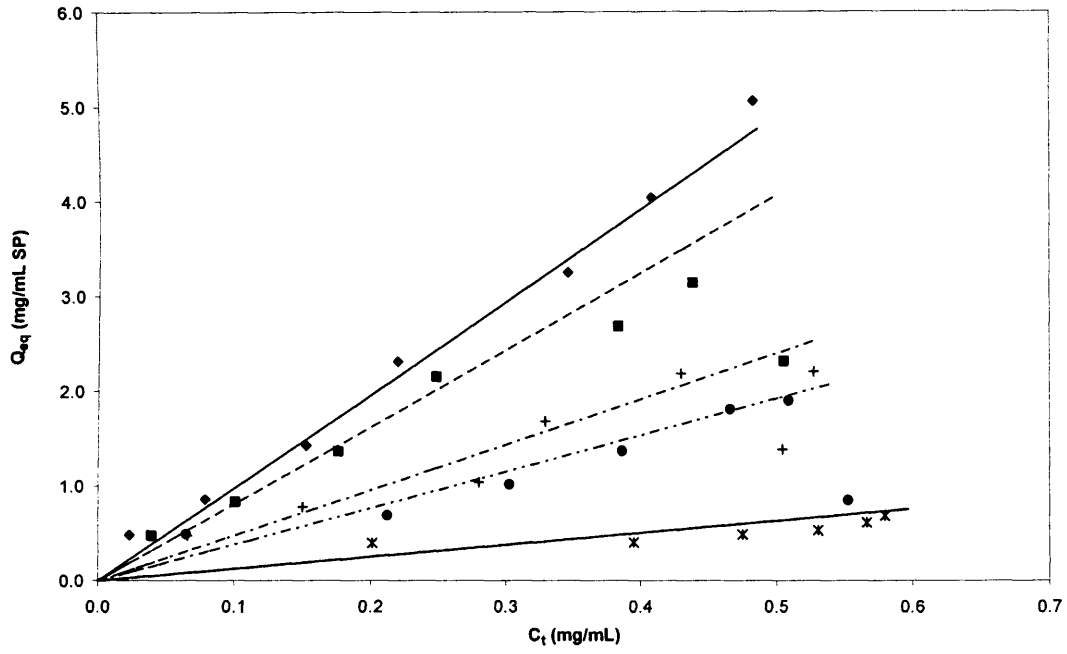

Figure 4.15. A comparison of the experimental and predicted adsorption isotherms for clarified homogenate feed at ionic strengths of 3.2 (♦), 3.5 (■), 4.5 (+), 5.0 (●) and 8.5 (x) mS/cm. Isotherms predicted at 3.2 (—), 3.5 (- -), 4.5 (- · -), 5.0 (— · —) and 8.5 (—) mS/cm using K-model model.

Based on the parity plots, the *K*-model appears to be a significant improvement on the exponential decay model. This is confirmed by Figure 4.15 which shows the experimental data plotted with the predicted isotherms. The fits are now good and follow the correct shape of the experimental data at all ionic strengths tested.

Another advantage of this method of data processing is that the model predicts the distribution coefficient of an isotherm, *K*, without the need for any further modelling or data fitting. The distribution coefficient, as defined by Equation 4.13, is the ratio between the concentrations of Fab' bound to the adsorbent and Fab' remaining in solution (Kaltenbrunner, 1996). The *K* values obtained in Stage B of the model give the slope of the adsorption isotherm, which is the distribution coefficient. When correlated with ionic strength (Stage C) the model predicts the distribution coefficient at any ionic strength, within the range tested.

As a result of the success of the model at predicting C_t, and the fact it can provide the distribution coefficient with no further modelling, the *K*-model was used to analyse all experimental isotherm data. All data was treated in the same manner, following the steps outlined in Figure 4.2 and Section 4.2.2. However, in the case of the feed solids concentration, the prediction of C_{t0} was performed using a linear relationship, and not a power-law, as this gave the best fit.

A standard method of assessing adsorption isotherms is to compare the isotherm parameters, such as the maximum binding capacity, Q_{max}, and the dissociation constant, K_d. Previous results (not shown) suggested that the adsorption of Fab' follows a Langmuir-type isotherm. In this specific case is it likely the isotherm experiments were performed at a Fab' concentration which is within the initial linear region of the Langmuir isotherm. Accordingly, the distribution coefficient was used to quantify the effects of feed ionic strength and solids concentration on the adsorption equilibrium.

4.3 Results and discussion

The effect of feedstock properties on equilibrium adsorption isotherms is presented and discussed in this section. The *K*-model developed in this chapter is used to process experimental data in order to describe the impact of feedstock ionic strength (Section 4.3.1) and solids concentration (Section 4.3.2) on equilibrium adsorption isotherms. Finally, Section 4.2.3 describes the calculation and prediction of process yields and throughput through the use of the *K*-model.

4.3.1 The effect of feedstock ionic strength

The effects of feedstock ionic strength on adsorption of Fab' to the cation exchanger SP Sepharose FF is shown in Figures 4.16 to 4.19. Figure 4.16 and Figure 4.17 show the effect of feedstock ionic strength on the adsorption of Fab' from a clarified and unclarified *E. coli* homogenate respectively. Figure 4.18 and Figure 4.19 show the effect of feedstock ionic strength on the adsorption of Fab' from a clarified and unclarified *E. coli* lysate respectively. In all cases the range of ionic strength investigated was 3.2-8.5 mS/cm at pH 5.5.

It is evident from Figures 4.16 to 4.19 that in this case the equilibrium isotherms are linear. The effect of the feedstock ionic strength is the same on all feedstocks tested. An increase in ionic strength leads to a decrease in the slope of the isotherm, as presented in Table 4.2, which shows the distribution coefficient, as well as the equilibrium binding capacity calculated at an equilibrium concentration of 0.1 mg/mL. Several trends can be seen in these results. Firstly, the effect of ionic strength is more pronounced in the case of the clarified feedstocks. As ionic strength increased from 3.2 to 8.5 mS/cm the distribution coefficient for the clarified homogenate dropped by 87% as compared to 76% for the unclarified. The effect of increasing ionic strength on the distribution coefficient for the lysate is greater. The distribution coefficient dropped by 97% for the clarified lysate and 95% for the unclarified. Although there is little, if any, literature reporting the effects of ionic strength on the ion exchange adsorption of Fab' from crude feedstocks, these results are in agreement with the findings of several groups who have investigated the effect

of ionic strength on the adsorption of Lysozyme (Chang *et al.*, 1998; Hashim *et al.*, 1995; Dziennik *et al.*, 2005), hCTRB (Thömmes *et al.*, 2001), Fab (Ljunglöf *et al.*, 2007), BSA (Kaltenbrunner *et al.*, 1996; Lan *et al.*, 2001; Linden *et al.*, 2001) and HHb (Kondo *et al.*, 1998). Hashim *et al.* (1995) investigated the effect of ionic strength on adsorption of Lysozyme to three strong cation exchangers, one of which was SP Sepharose FF. They reported that increasing ionic strength leads to a decrease in the binding capacity for Lysozyme in all the ion exchangers tested. They attribute this decrease in binding capacity to competition for negatively charged binding sites between the positive ions of the buffer and the positive charges on Lysozyme. Both Hashim *et al.* (1995) and Linden *et al.* (2002) state that an increase in ionic strength causes the buffer ions to shield the surface charges, therefore reducing the strength of the ionic interactions between the protein and the adsorbent. Lan *et al.* (2001) attributed the decrease in the binding capacity of BSA on the anion exchanger Diaion HPA25 to interactions between the salts ions and protein molecules as well as between the salt ions and the adsorbent. Such effects impact the electrostatic and Van der Waals interactions between the protein and the ion exchanger (Stahlberg *et al.*, 1992).

It is also clear to see from Table 4.2 that at a given ionic strength the distribution coefficient is higher for the clarified feed over the unclarified. The clarified feedstocks have a higher distribution coefficient and Q_{eq} than their corresponding unclarified solutions. This is probably due to cell debris binding to the adsorbent surface and blocking binding sites.

When comparing the two methods of feedstock preparation, the distribution coefficients and equilibrium binding capacities are higher for the lysate feedstock. The reason for this is that the lysate is a purer feed and there are fewer contaminants competing for binding sites. As described in Chapter 3 the lysis protocol used in this study includes a period of raised temperature which effectively purifies the lysate further. This can be seen by the fact that at the lowest ionic strength tested, 3.2 mS/cm, the distribution coefficient for the lysate feedstock is almost an order of magnitude greater than that of the homogenate, for both the clarified and unclarified solutions.

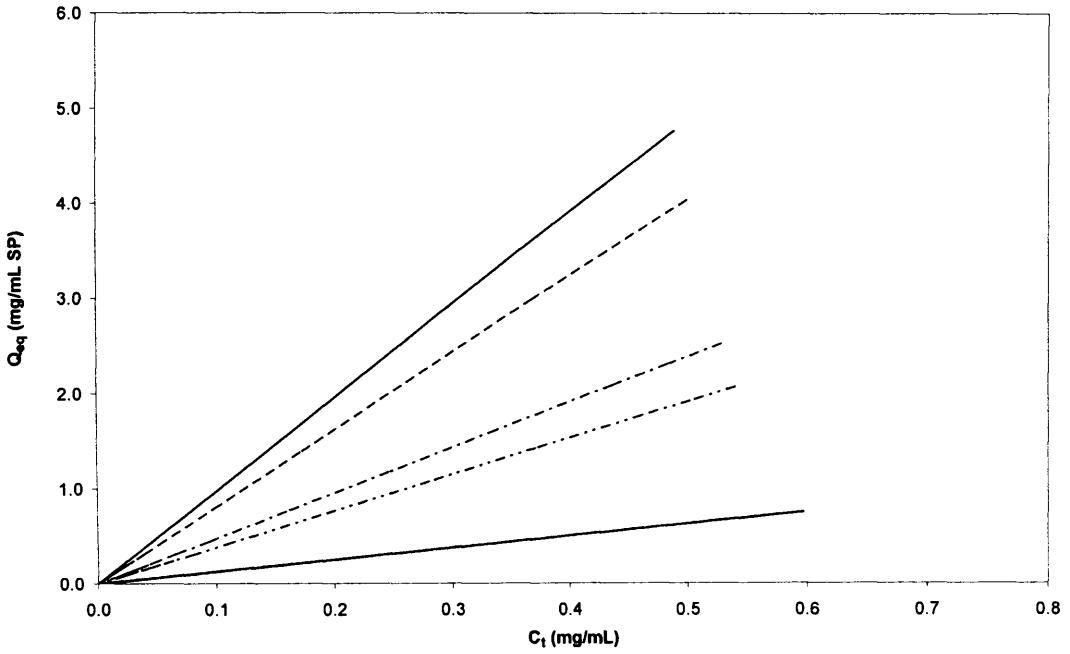

Figure 4.16. Predicted adsorption isotherms for clarified homogenate at various feed ionic strengths. Isotherms predicted isotherms at 3.2 (—), 3.5 (- -), 4.5 (- · -), 5.0 (— · —) and 8.5 (—) mS/cm using the *K*-model model.

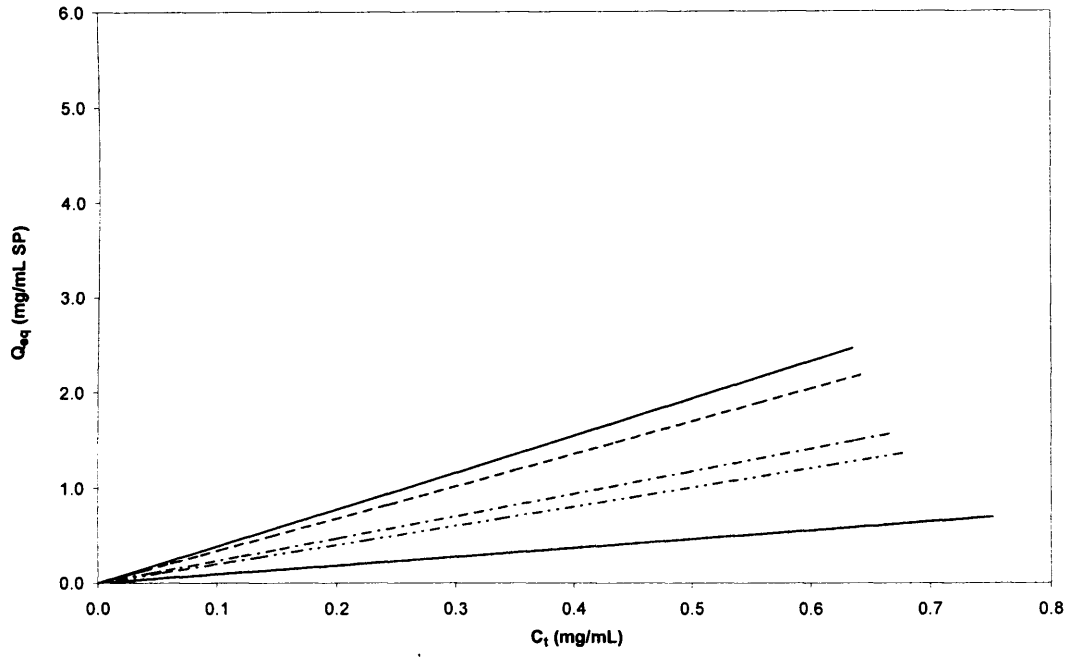

Figure 4.17. Predicted adsorption isotherms for unclarified homogenate at various feed ionic strengths. Isotherms predicted isotherms at 3.2 (—), 3.5 (- -), 4.5 (- · -), 5.0 (— · —) and 8.5 (—) mS/cm using the *K*-model model.

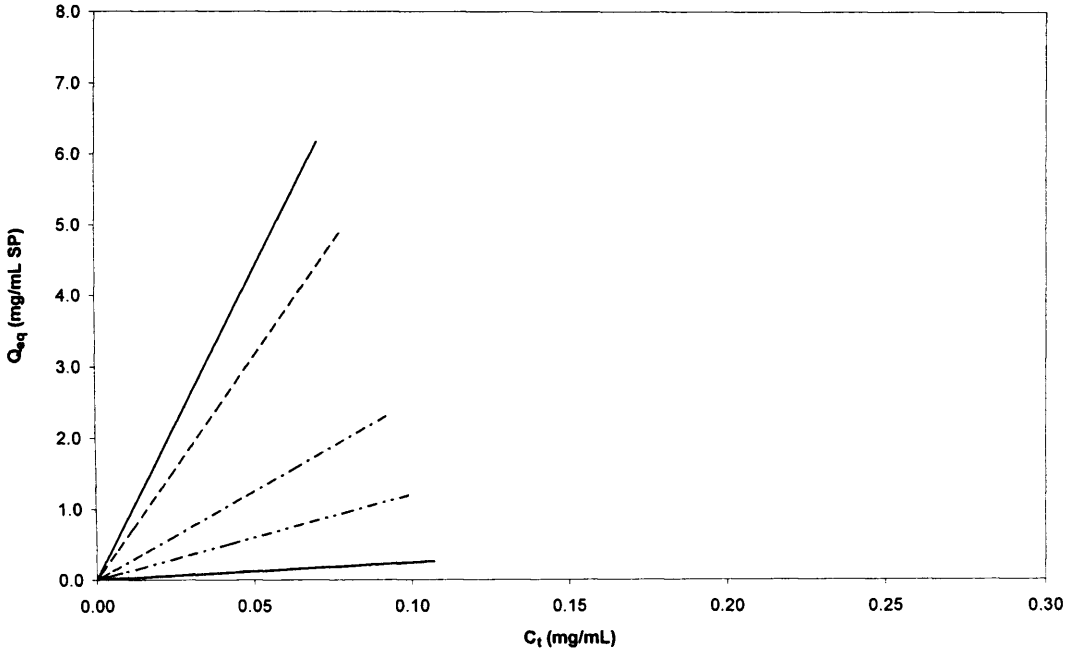

Figure 4.18. Predicted adsorption isotherms for clarified lysate at various feed ionic strengths. Isotherms predicted isotherms at 3.2 (—), 3.5 (- -), 4.5 (- · -), 5.0 (-··-) and 8.5 (—) mS/cm using the *K*-model model.

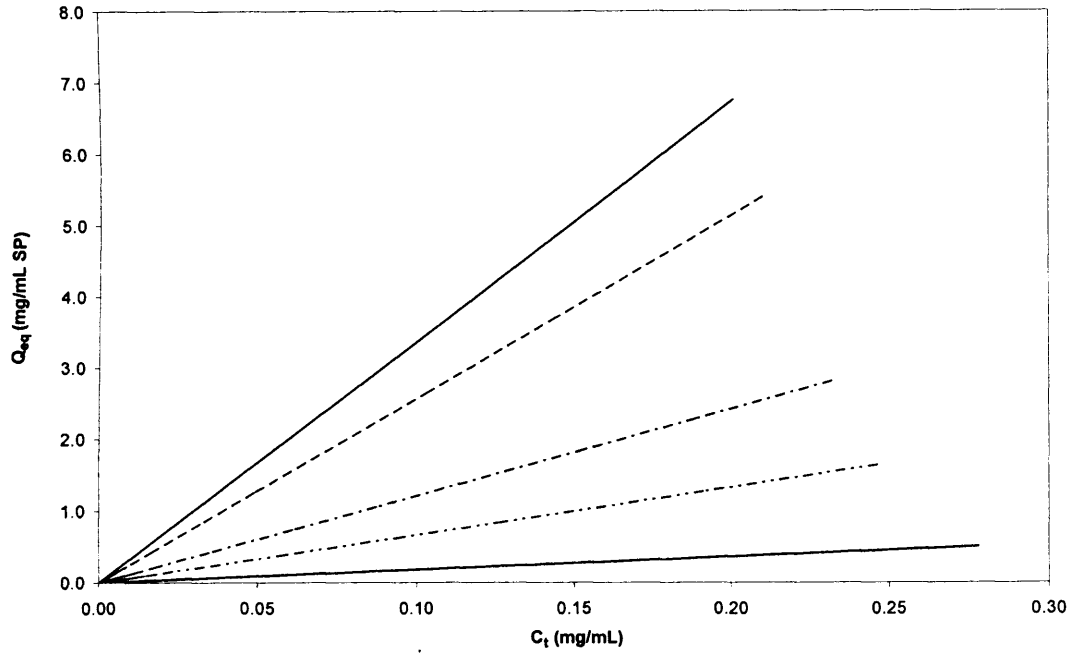

Figure 4.19. Predicted adsorption isotherms for unclarified lysate at various feed ionic strengths. Isotherms predicted isotherms at 3.2 (—), 3.5 (- -), 4.5 (- · -), 5.0 (-··-) and 8.5 (—) mS/cm using the *K*-model model.

Table 4.2. The effect of feedstock properties on the adsorption distribution coefficient, K, obtained from the modelling of experimental data. Q_{eq} (mg/mL SP) was calculated at $C_t = 0.1$ (mg/mL). Feed solids concentration of both feedstocks was 6.4% (ww/v).

Ionic Strength (mS/cm)	K (-)	Q_{eq} (mg/mL SP)
Homogenate		
Clarified		
3.2	9.78	0.98
3.5	8.10	0.81
4.5	4.78	0.48
5.0	3.83	0.38
8.5	1.26	0.13
Unclarified		
3.2	3.87	0.39
3.5	3.39	0.34
4.5	2.35	0.24
5.0	2.01	0.20
8.5	0.92	0.09
Lysate		
Clarified		
3.2	87.85	8.79
3.5	63.22	6.32
4.5	25.12	2.51
5.0	12.02	1.20
8.5	2.43	0.24
Unclarified		
3.2	33.57	3.36
3.5	25.68	2.57
4.5	12.10	1.21
5.0	6.64	0.66
8.5	1.80	0.18

4.3.2 *The effect of feedstock solids concentration*

Adsorption isotherms were obtained for homogenate and lysate feedstocks of varying solids concentration at a fixed ionic strength of 3.2 mS/cm. The effect of solids concentration on the equilibrium isotherms of the feedstocks is shown in Figure 4.20 and Figure 4.21. Table 4.3 summarises the distribution coefficient and equilibrium binding capacity at an equilibrium concentration of 0.1 mg/mL for both feedstocks.

Once again comparing the two feedstocks it is evident that the distribution coefficient for the lysate is almost an order of magnitude greater than that of the homogenate. Decreasing the homogenate solids concentration from 9.1 to 0.5% (ww/v) using centrifugation leads to a 70% increase in the distribution coefficient. Decreasing the lysate solids concentration from 7.0 to 0.3% (ww/v) leads to almost a tripling in the distribution coefficient. It is interesting to note that the unclarified lysate (7.0% ww/v solids) achieves a higher distribution coefficient than the clarified homogenate. This would suggest that the presence of intracellular contaminants in the homogenate feed affects the adsorption of Fab' greater than whole cells. However, not only does the homogenate feed contain intracellular contaminants which increase the competition for binding sites but also cell debris which can physically block the binding sites and reduce the ability of the adsorbent to bind Fab', hence the reduction in the equilibrium binding capacity.

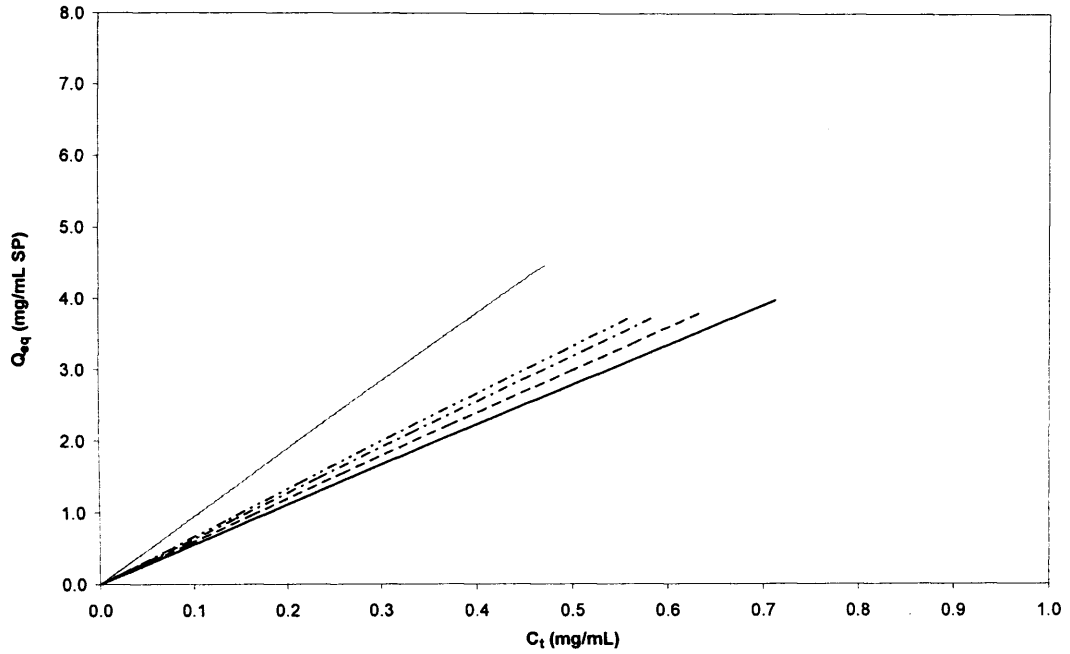

Figure 4.20. The effect of homogenate feed solids concentration on Fab' adsorption isotherms. Isotherms predicted at 0.5 (—), 3.5 (-··-), 4.4 (-·-), 6.2 (- -) and 9.1 (—) % solids (ww/v) using the *K*-model model.

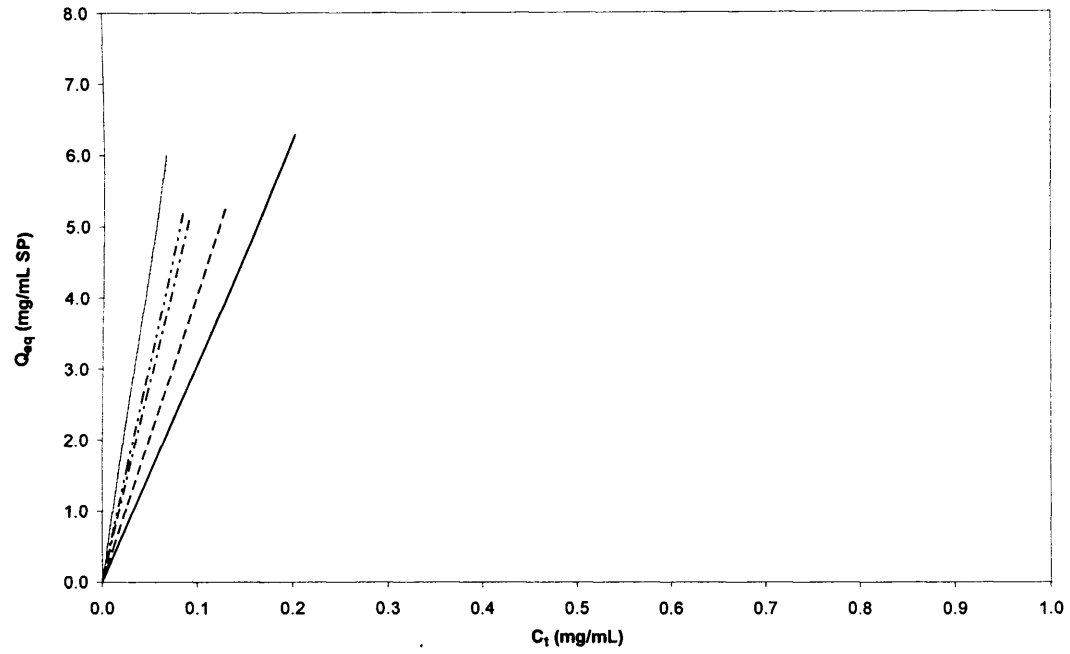

Figure 4.21. The effect of lysate feed solids concentration on Fab' adsorption isotherms. Isotherms predicted at 0.3 (—), 1.0 (-··-), 1.2 (-·-), 3.1 (- -) and 7.0 (—) % solids (ww/v) using the *K*-model model.

The binding of cell debris to adsorbents has been investigated and reported by numerous groups, most commonly investigating the use of expanded bed adsorption (EBA). The recovery of proteins from crude feedstocks is most often performed using EBA. Several studies have been carried out investigating the effect of solids concentration and cell debris on protein adsorption. Evidence of cell debris binding to the adsorbent and influencing the binding capacity has been reported by Chase and Draeger (1992) who stated that the presence of *S. cerevisiae* caused a reduction in the equilibrium capacity of BSA to a fluidised anion exchanger. They attributed this to cells binding to the outer surface of the adsorbent, as well the penetration of small cells or cell debris into porous adsorbents. Feuser *et al.* (1999a) reported that hybridoma cells are adsorbed onto the surface of Streamline SP during the expanded bed adsorption of IgG_1, while Feuser *et al.* (1999b) reported evidence of *E. coli* adsorbing to Streamline SP at pH 7.0. It would appear from the findings of these groups that the adsorption of cell debris to adsorbents is due to electrostatic interactions between the cell surface and the oppositely charged adsorbent. Indeed, Ujam *et al.* (2000) showed that it is possible to separate *E. coli* and *S. cerevisiae* based on their net surface charge using Streamline DEAE. Figure 4.22 is a detailed scanning electron microscope image showing *E. coli* and *S. cerevisiae* bound to the surface of an adsorbent bead (reproduced with permission of the authors).

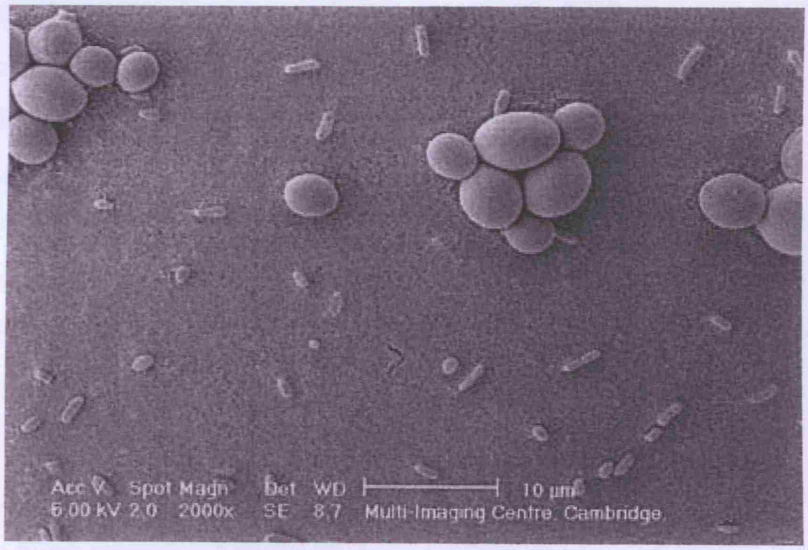

Figure 4.22. A detailed scanning electron microscope image showing *E. coli* and *S. cerevisiae* bound to the surface of DEAE. Ujam *et al.*, (2000).

Table 4.3. The effect of feedstock solids concentration on the adsorption distribution coefficient, K, of an *E. coli* homogenate and lysate. Feed ionic strength 3.2 mS/cm and pH 5.5. Q_{eq} (mg/mL SP) calculated at C_t = 0.1 (mg/mL).

% Solids (ww/v)	K (-)	Q_{eq} (mg/mL SP)
Homogenate		
0.5	9.49	0.95
3.5	6.66	0.67
4.4	6.38	0.64
6.2	5.99	0.60
9.1	5.57	0.56
Lysate		
0.3	90.87	9.09
1.0	62.48	6.25
1.2	56.85	5.69
3.1	41.05	4.10
7.0	30.85	3.09

4.3.3 The K-model as a predictive tool

The *K*-model can be used as a predictive tool in a number of ways. Firstly, as the equilibrium adsorption isotherms are performed in batch mode in microwell plates, each data point is essentially a single batch adsorption. Each isotherm is comprised of 8 data points and 5 feed ionic strengths were tested for each feedstock, both clarified and unclarified. When the number of data points required for the solids concentration analysis are included the total number of individual batch adsorptions equals 240. With the use of the *K*-model this data makes it possible to predict the equilibrium concentration at the end of batch adsorptions for a wide range of feed ionic strengths, solids concentration, phase ratio (assuming perfect mixing), load volume and initial concentration.

The model is also able to predict the effect of feedstock ionic strength and solids concentration on the yield, productivity, and throughput of an adsorptive process.

Spreadsheets were created which allowed the visualisation of the impact that process variables, such as process time, volume and feed properties have on the performance of the overall adsorptive process. These are examined in greater detail in Chapter 7,

however, the model equations will now be outlined and an example of their use described in this section.

The basic equations used in the development of the models are given below.

$$\text{Mass loaded (g)} = V_l \cdot C_{t0} \tag{4.21}$$

$$\text{Mass bound (g)} = V_l \cdot (C_{t0} - C_t) \tag{4.22}$$

$$\text{Mass eluted (g)} = V_l \cdot R \cdot (C_{t0} - C_t) \tag{4.23}$$

where R is the percentage Fab' recovered.

$$Yield\ (\%) = 100 \cdot \left(\frac{mass\ eluted}{mass\ loaded} \right) \tag{4.24}$$

$$Throughput\ (g/h) = \frac{mass\ eluted}{time} \tag{4.25}$$

$$Productivity\ (g/h/L\ ads) = \frac{throughput}{V_m} \tag{4.26}$$

Model equations:

$$C_t = \frac{C_{t0}}{\left(K \cdot \frac{V_m}{V_l} \right) + 1} \tag{4.27}$$

$$Q_{eq}\ (mg/mL\ ads) = \frac{V_l}{V_m} \cdot \left[C_{t0} - \left(\frac{C_{t0}}{\frac{K \cdot V_m}{V_l} + 1} \right) \right] \tag{4.28}$$

$$Yield\ (\%) = \frac{100 \cdot R \cdot \left[C_{t0} - \left(\frac{C_{t0}}{\frac{K \cdot V_m}{V_l} + 1} \right) \right]}{C_{t0}} \quad 4.29$$

$$Throughput\ (g/h) = \frac{V_l \cdot R}{time} \cdot \left[C_{t0} - \left(\frac{C_{t0}}{\frac{K \cdot V_m}{V_l} + 1} \right) \right] \quad 4.30$$

$$Matrix\ Productivity\ (g/h/L\ ads) = \frac{V_l \cdot R}{time \cdot V_m} \cdot \left[C_{t0} - \left(\frac{C_{t0}}{\frac{K \cdot V_m}{V_l} + 1} \right) \right] \quad 4.31$$

In order to incorporate the effect of feed properties, the correlations from the *K*-model were substituted into the relevant equations to obtain the desired performance output.

$$C_{t0} = A \cdot I^B \quad 4.32$$

$$K = E \cdot I^{-F} \quad 4.33$$

Where I is the feed ionic strength, A, B, E and F are empirical constants obtained from correlations detailed in the model development.

The same data set used to generate the models earlier in this chapter is shown here as an example of how the equilibrium isotherm data can be used to predict process performance. As we are considering an initial capture step, the main process performance criteria of interest is the yield. The impact of feed ionic strength on yield, as defined by Equation 4.24, is shown in Figure 4.23. A 95% recovery was assumed in this example. The model has been used to obtain data for feed ionic strengths in the range 3.0 to 8.0 mS/cm.

A number of conclusions can be drawn from Figure 4.23. Firstly, decreasing the feed ionic strength from 8.0 to 3.0 mS/cm causes a significant increase in the process yield. For example, at a phase ratio of 0.30, which is a feasible industrial phase ratio, the yield improves from 24 to 73%. The reasons for the improved adsorption have already been discussed in Section 4.2.3.

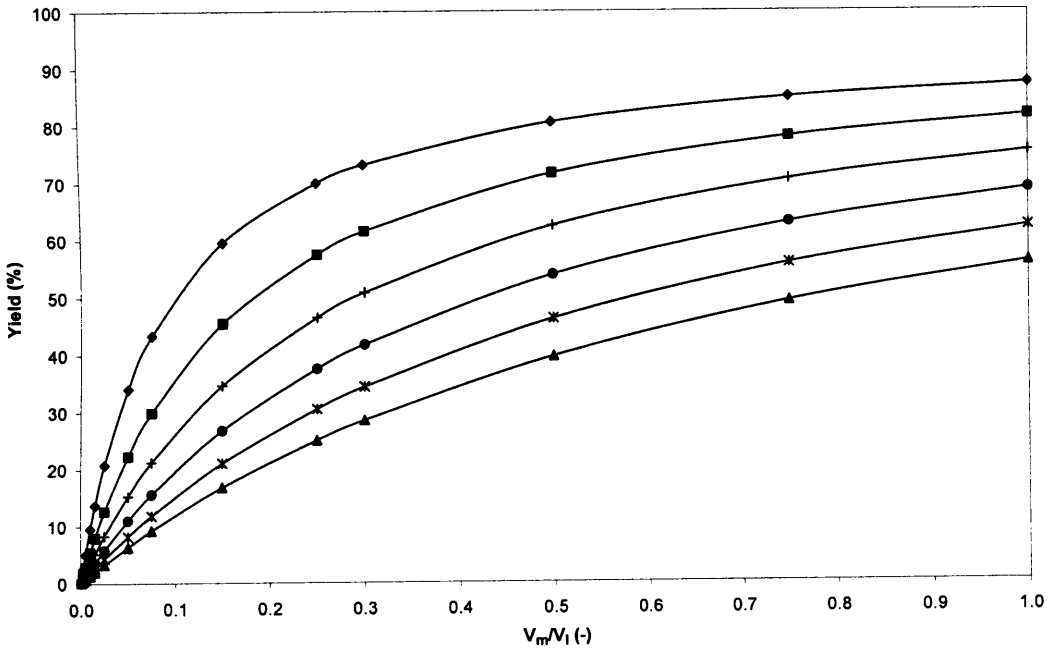

Figure 4.23. The effect of ionic strength on the predicted yield of a Fab' adsorption process. Yield predictions for a clarified homogenate at 3.0 (♦), 4.0 (■), 5.0 (+), 6.0 (●), 7.0 (x) and 8.0 (▲) mS/cm.

Secondly, it is evident that under the conditions tested incomplete Fab' adsorption was achieved, even at a phase ratio of 1.0 the yield is less than 90%. This is common in batch adsorption and is likely to be due to the adsorbent and Fab' reaching an equilibrium, which is normally avoided in column chromatography. The shape of the isotherms can also explain this result as linear isotherms suggest the interaction between Fab' and adsorbent are not as strong as they would need to be for efficient and favourable binding. Alternatively, the Fab' concentration, and therefore the mass of Fab' present in each adsorption, is high and the saturation binding capacity of the adsorbent is reached, preventing further Fab' adsorption. Figure 4.23 can be used as a crude design tool, enabling a design engineer to determine, for example, which phase ratio is most efficient. For example, at 3.2 mS/cm the increase in yield as a function of phase ratio is greatest in the range 0 to 0.50, where the yield

reaches 80%. Increasing the phase ratio from 0.50 to 1.0 only increases the yield by another 7%. The effect this would have on the process productivity and economics would be significant. The *K*-model also predicts the effect of feed ionic strength and phase ratio on the process productivity. Figure 4.24 presents an example of the effect feed ionic strength has on the matrix productivity (MP) of the adsorption process. The MP is a measure of the utilisation of the adsorbent.

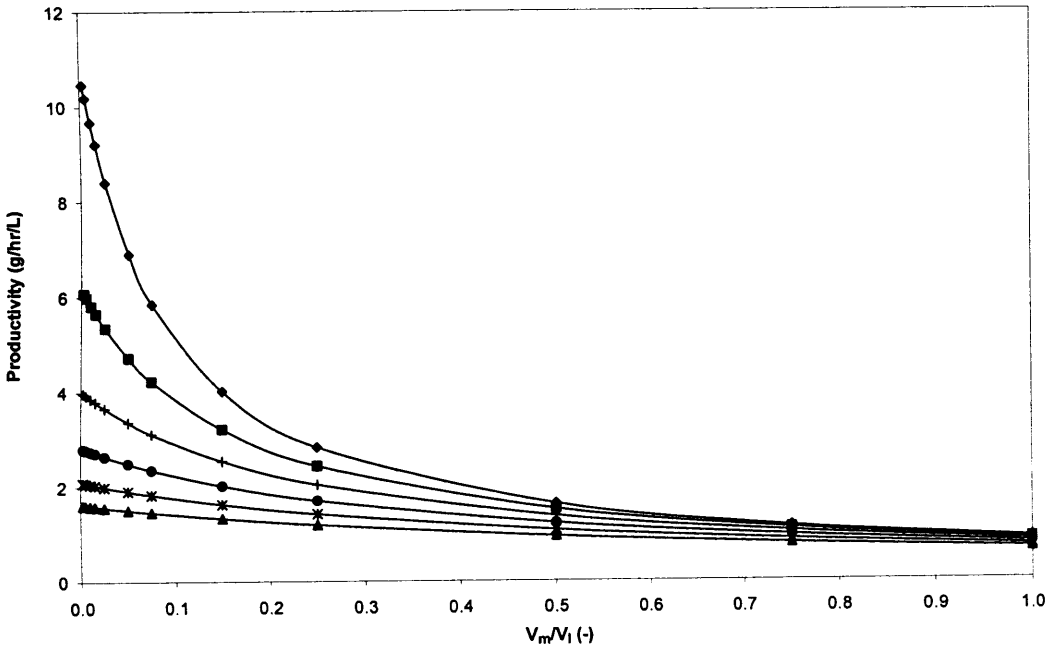

Figure 4.24. The predicted effect of ionic strength on the matrix productivity of a Fab' adsorption process. The matrix productivity predictions for a clarified homogenate at ionic strengths of 3.0 (♦), 4.0 (■), 5.0 (+), 6.0 (●), 7.0 (x) and 8.0 (▲) mS/cm.

In order to obtain this data, a recovery of 95% and adsorption time of 30 min were assumed. When the MP is calculated as a function of phase ratio, it is clear to see that the MP falls rapidly with increasing phase ratio and ionic strength. In a phase ratio range of 0 to 0.5 MP drops from 10.5 to 1.6 g/h/L ads. Although these figures are system-specific and based on simple assumptions the method does provide a clear visual examination of the data. Chapter 7 will use the isotherm data and models developed in this chapter to generate a more sophisticated method of analysis via Windows of Operation.

4.4 Summary

This chapter has demonstrated how equilibrium isotherms established at small scale can be used to investigate the affect of process variables in order to determine rapidly the effect of feedstock properties on the purification of antibody fragments. The conditions, and operating strategies, which could potentially lead to the satisfaction of pre-determined performance criteria are identified. The performance of the adsorption processes is modelled as the basis from which to generate a data set to be tested in the following chapters.

The binding conditions determined in this chapter will be used for the purification of antibody fragments using conventional packed bed chromatography and stirred tank batch adsorption.

Chapter 5 investigates the effect of these operating conditions on the purification of antibody fragments using laboratory scale packed bed columns.

5 The purification of Fab' antibody fragments from *E. coli* feedstocks using packed bed chromatography

Abstract

The previous chapter used equilibrium isotherms in batch mode to determine the binding conditions required for the successful purification of antibody fragments. This chapter investigates the effect of key operating conditions on the performance of conventional column chromatography. The influence of linear velocity, feed solids concentration and ionic strength on the breakthrough of antibody fragments using packed bed chromatography is investigated.

The purification of antibody fragments from an unclarified *E. coli* feedstock, using laboratory scale packed bed columns is described. The effect of column packing, including an industrial scale packing mimic designed to account for the effect of adsorbent bed support, is used to investigate the feasibility of loading unclarified material at industrial scale.

5.1 Introduction

The use of packed bed chromatography was discussed in Chapter 1. In this chapter packed beds are used to capture Fab' from the feedstock solutions prepared in Chapter 3. Section 5.1.1 describes the effect of feedstock solids concentration on packed beds, and Section 5.1.2 describes the significance of column packing and laboratory scale mimics of industrial column packing.

5.1.1 The effect of feed solids concentration on packed beds

As stated in Chapter 1 the use of packed bed adsorption is extremely popular and widespread in the bioprocess industry. The typical operation of a packed bed requires the complete clarification of feedstocks prior to loading onto the column. This would involve a number of unit operations such as centrifugation and filtration. However, each step contributes to the drop in product yield. This becomes more apparent in a

situation, such as this, where the product is bound to the cell debris. Removal of cell debris therefore also impacts the total product yield. To overcome this problem the primary recovery and initial purification of the product have been integrated in unit operations such as magnetic separations, aqueous two-phase systems, and expanded bed adsorption (EBA) (Dainiak *et al.*, 2004). As with all unit operations, each has its advantages and disadvantages. Dainiak *et al.* (2004) described the concerns and issues of each of the integrated systems:

1. Magnetic separations
   - Require special equipment and costly magnetic adsorbents
   - Limitations in magnetic capacity limit technique to mainly small scale
2. Aqueous two-phase
   - Poor separation efficiency due to batch-wise operation
   - Difficulty collecting product due to material gathering at interface of the two phases
3. EBA
   - Column verticality is essential
   - Long equilibrium times
   - Feedstock may require dilution/pre-treatment
   - Conventional EBA adsorbents prone to fouling and cell binding
   - Cost of EBA system can be higher than conventional route

Wlad *et al.* (2001) showed that the direct capture of a mouse Fab fragment was possible when a diluted unclarified *E. coli* homogenate was loaded onto a packed bed of SP Sepharose Big Beads.

This chapter aims to avoid the problems associated with specialist integrated systems and describes how conventional packed beds, packed with a standard ion exchange adsorbent, can be used to capture Fab' from an unclarified *E. coli* homogenate.

5.1.2 Column packing

Column packing is an important aspect of packed bed chromatography. The quality of the packing can significantly affect the process efficiency, product yield, and

purity. Any irregularities in the packing may cause uneven flow within the bed, which results in band broadening, and loss of product yield and quality. There are many factors which influence the quality of column packing, including; media factors such as the particle size and homogeneity, and bed compression; column factors such as the bed height and column diameter; mobile phase factors such as the pH, ionic strength, viscosity and chemical compatibility; and finally, system factors such as tubing, pump quality and the presence of a bubble trap to reduce pulsations (BioPharm International, 2003). The packing method can also influence the quality and structure of the packed bed. Flow packing is one of the most commonly used methods of column packing, and often involves packing the media at a flow rate 20-30% greater than the operating flow rate in order to reduce the risk of post-packing bed compression (BioPharm International, 2003).

The critical velocity, u_{crit}, defined as the superficial fluid velocity at which the pressure-flow curve starts to rise to infinity (Stickel *et al.*, 2001), is often used to determine the flow rates required for column packing and loading. Sofer and Hagel (1997) suggest that the packing flow rate should be approximately 90% of u_{crit}, with the operating flow rate being no more than 80% of the packing flow rate.

5.1.2.1 Laboratory scale mimic of industrial scale column packing

Chromatographic process development is often performed at laboratory scale using columns of diameters (D) less than 3 cm. Scale-up typically involves increasing the column diameter to accommodate the increased volume of process feed, while the bed height and superficial fluid velocity are maintained (Sofer and Hagel, 1997). As many of the chromatographic media available today are compressible the large increase in the aspect ratio leads to increased pressure drops and bed compression as a result of decreasing wall support (Stickel *et al.*, 2001). Stickel *et al.* (2001) developed an empirical correlation of wall effects on media compression, as well as a model to predict the pressure drop of compressible packed beds at varying scales. The use of such models would provide valuable information and aid the design and development of an industrial scale chromatography process.

The following is a description of the model put forward by Stickel *et al.* (2001).

Following the development of a pressure-flow curve u_{crit} is multiplied by the gravity settled bed height (L_0) to give the term $u_{crit}L_0$, which is then plotted against the aspect ratio (L_0/D), as seen in Figure 5.1.

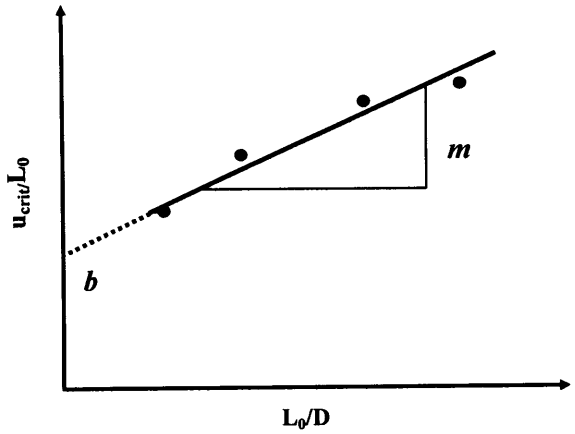

Figure 5.1. Critical velocity, u_{crit}, as a function of column scale.

The linear relationship observed in Figure 5.1 results in the following empirical correlation:

$$u_{crit}L_0 = m\left(\frac{L_0}{D}\right) + b \qquad 5.1$$

where m and b are empirical constants determined through linear regression. The empirical constant b provides a numerical indication of the compressibility of a chromatographic medium under given operating conditions. The slope m is indicative of the changing wall support with scale.

In order to predict u_{crit} for a chromatographic system significant experimentation is required (Tran and Joseph *et al.*, 2007). However, using Equation 5.1 and the published empirical constants enables the prediction of u_{crit} for industrial scale packed beds through the use of small scale laboratory columns.

5.2 Results and discussion

Section 5.2.1 describes the effect of linear velocity on the breakthrough of Fab' from clarified feedstocks. The effect of feedstock solids concentration on Fab' breakthrough and system back pressure is discussed in Section 5.2.2. Section 5.2.3 describes the impact feedstock ionic strength has on the breakthrough of Fab' when purified from a clarified *E. coli* homogenate. A mimic of industrial scale column packing and feed loading is described in Section 5.2.4 in order to assess the feasibility of loading solids onto an industrial scale packed bed.

5.2.1 The effect of linear velocity

Fab' breakthrough curves were obtained as described in Section 2.4.2 using a Tricorn 15 column (GE Healthcare, Uppsala, Sweden) connected to an ÄKTA Explorer 100 chromatography system (GE Healthcare, Uppsala, Sweden). The column was packed to a bed height of 15 cm with fresh adsorbent for each run as described in Section 2.4.2.1 and equilibrated with 20 mM Sodium Acetate pH 5.5. The ionic strength of the feedstocks was 3.4 and 3.3 mS/cm for the homogenate and lysate feed, respectively. Due to limited feedstock availability it was not possible to load to 100% Fab' breakthrough in all cases.

Table 5.1 summarises the experiments performed and describes the experimental conditions of the investigation into the effect of linear velocity of clarified feedstocks on Fab' breakthrough.

Table 5.1. Experimental conditions and outputs for the recovery of Fab' from clarified feedstocks as a function of linear velocity.

Linear velocity (cm/h)	BT %	Residence Time (min)	% Solids (ww/v)	CV loaded (-)	Fab' applied (mg)
Homogenate					
100	100	7.4	0.5	48	51.2
300	100	2.9	0.5	65	61.6
Lysate					
100	10	7.4	0.3	51	14.4
300	14	2.9	0.3	58	19.0

Table 5.1 shows the number of column volumes (CV) loaded and mass of Fab' applied in each run. Loading clarified feedstocks within the range of linear velocities tested did not lead to bed compression or system over-pressure.

Figure 5.2 shows an example chromatogram of the loading, washing and elution stages performed during the capture of Fab' from the clarified homogenate feed at 100 cm/h.

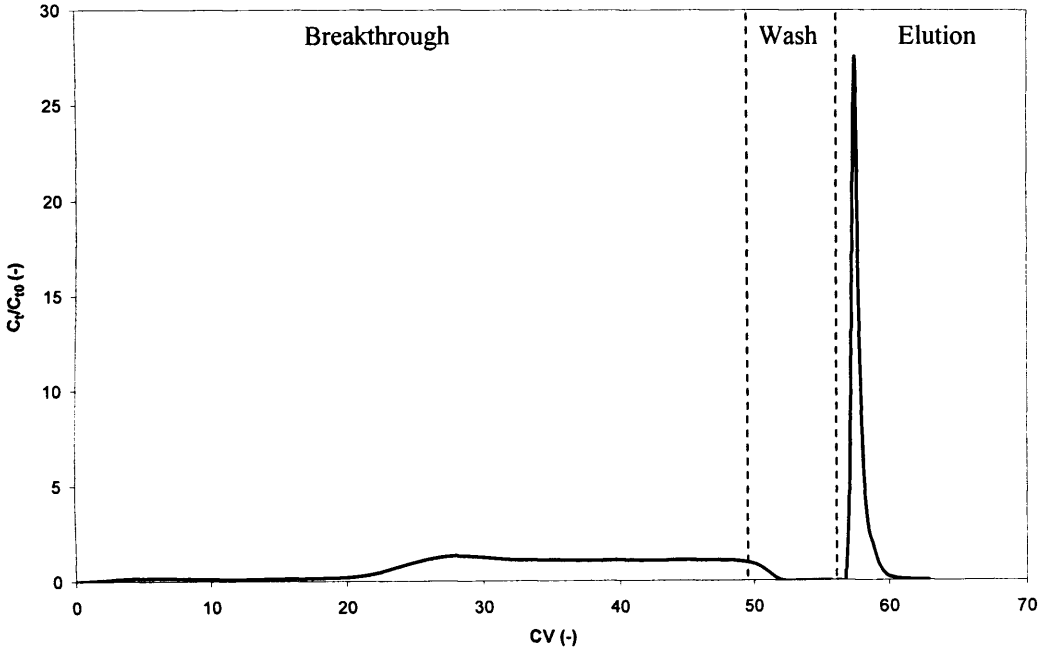

Figure 5.2. The recovery of Fab' from a clarified homogenate using a TC15 column of 15 cm bed height operated at 100 cm/h, showing the breakthrough, wash and elution stages.

Figure 5.3 presents breakthrough curves obtained at 100 and 300 cm/h for the clarified homogenate feedstock. At both the linear velocities tested there appears to be an initial breakthrough which occurs after 1 column volume (CV) then a period of sustained adsorption, as seen by the plateau between 5 and 20 column volumes. A similar plateau has been reported by Staby *et al.* (1998) during the purification of an insulin precursor from a fermentation broth using SP Sepharose BB. Figure 5.3 shows that the breakthrough curves appear to be unaffected by the linear velocity during this plateau. At the point where the plateau ends, the breakthrough curve at 300 cm/h is the first to appear, which is as expected.

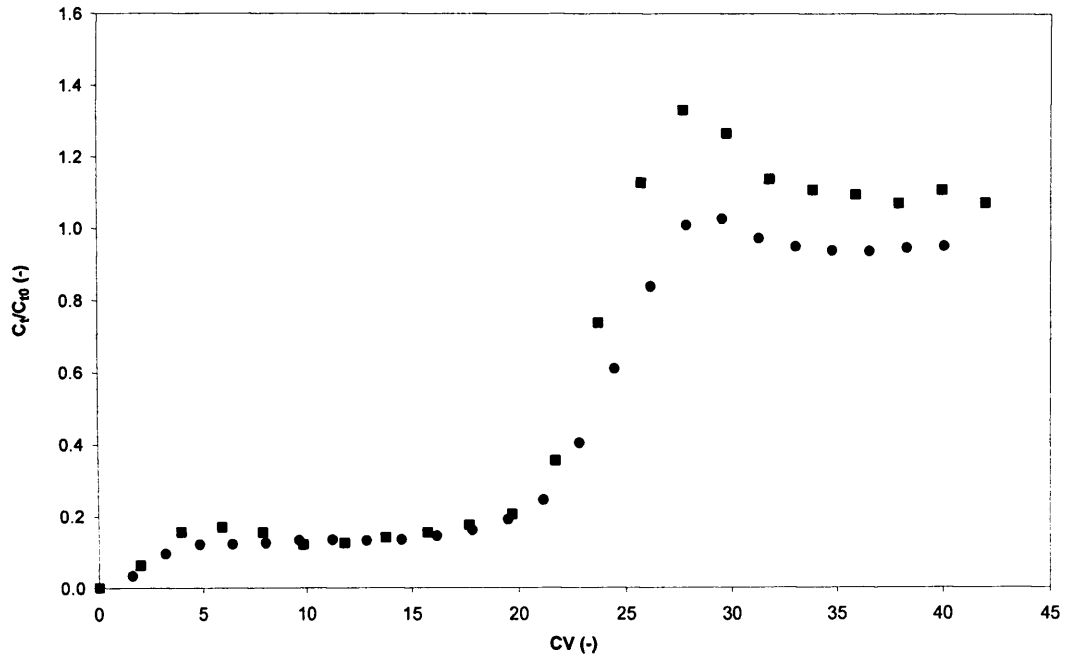

Figure 5.3. The adsorption of Fab' from a clarified *E. coli* homogenate to SP Sepharose FF at linear velocities of 100 (■) and 300 (●) cm/h.

The breakthrough curve at 100 cm/h gives a breakthrough concentration significantly greater than the feed concentration before falling down to a concentration just higher than the feed concentration. This trend is typical of multicomponent systems where there is competition between several species for adsorbent binding sites. This phenomenon has been reported by several authors (Gu *et al.*, 1990; Gu, 1995; Fargues *et al.*, 1998; Staby *et al.*, 1998).

The "roll up" of Fab' is caused by displacement due to a competing component having a higher affinity for the adsorbent than Fab'. Gu (1995) explains the mechanism behind this displacement effect. The concentration front of component 1, in this case Fab', which has a weaker affinity, migrates through the column faster than the concentration front of component 2. As a result of this difference in migration rate, the Fab' initially occupies a disproportionate number of binding sites. As the concentration front of component 2 catches up it causes the displacement of a proportion of the Fab', due its higher affinity, leading to the concentration of Fab' in the outlet exceeding the initial feed concentration. The Fab' concentration finally approaches the inlet concentration as an equilibrium is reached and each component occupies its share of the binding sites. In this case component 2 can be any one of a large number of contaminants in the homogenate feed. A possible reason for the

observed "roll up" being more pronounced at 100 cm/h could be due to the increased residence time which enables the Fab' to occupy more binding sites, and therefore more Fab' is then displaced by the other components.

Figure 5.4 shows the breakthrough curves for the lysate feedstock at 100 and 300 cm/h. Due to the low Fab' concentration and limited feedstock it was not possible to load to 100% breakthrough. It is however still evident that the linear velocity has minimal effect on the Fab' breakthrough, certainly to a breakthrough capacity of 10%.

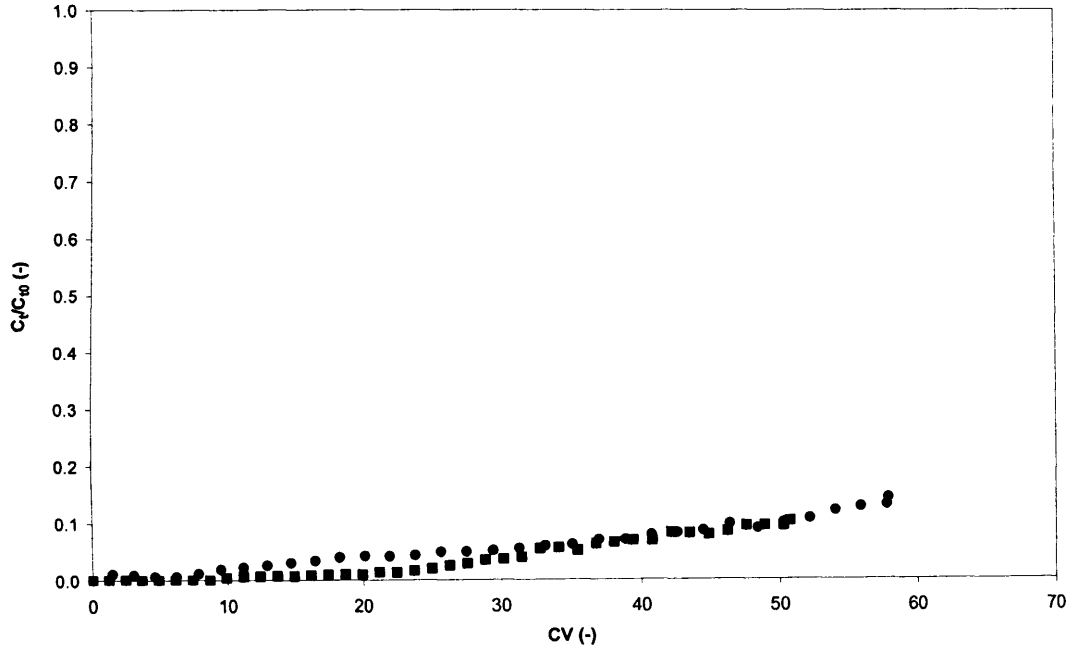

Figure 5.4. The adsorption of Fab' from a clarified *E. coli* lysate to SP Sepharose FF at linear velocities of 100 (■) and 300 (●) cm/h.

Figure 5.5 compares the effect of linear velocity on Fab' breakthrough for both clarified feedstocks. As the concentration of the feedstocks differed, plotting dimensionless concentration against the mass of Fab' applied allows direct comparison of the feedstocks as it removes any discrepancies in the feed Fab' concentration.

It is interesting to note that the initial breakthrough and plateau observed in the homogenate is not present in the case of the lysate. The breakthrough curves for the two feedstocks at both linear velocities tested appear to converge after 20 mg of Fab' is applied to the column.

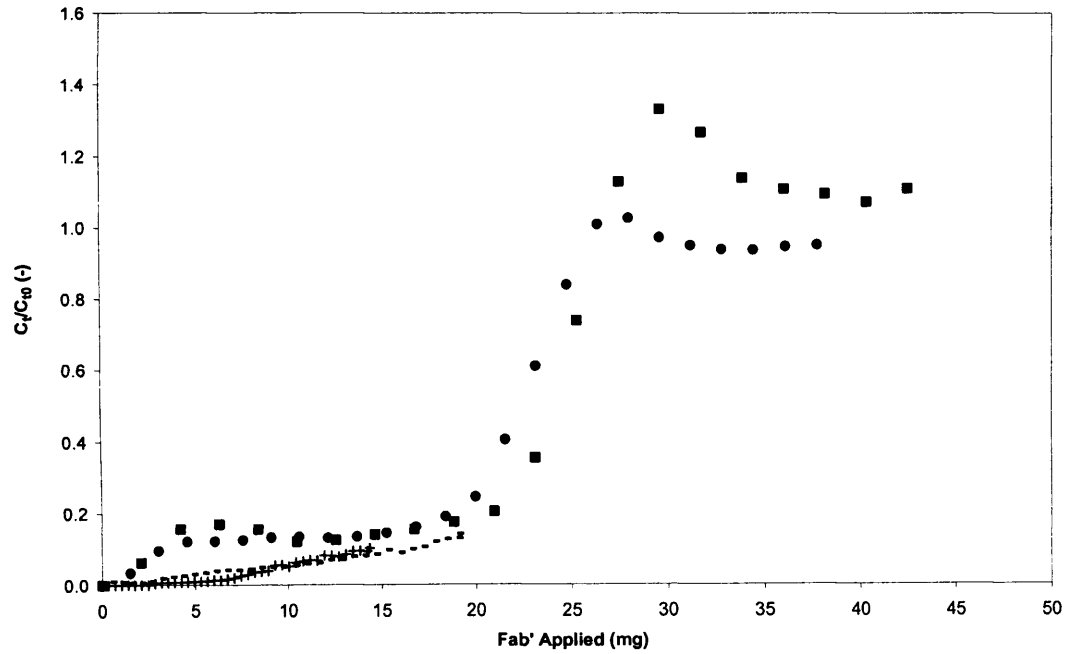

Figure 5.5. Comparing the adsorption of Fab' to SP Sepharose FF from clarified *E. coli* homogenate, at 100 (■) and 300 (●) cm/h and clarified lysate at 100 (+) and 300 (-) cm/h.

Table 5.2 compares the dynamic binding capacity (DBC), measured at 1, 5, 10 and 50% product breakthrough, of both feedstocks at each linear velocity. Binding capacity data is used industrially during process development to assess adsorbent performance (Staby *et al.*, 2004). In the case of the homogenate the binding capacity is not significantly affected by the linear velocity. There appears to be a slight increase in the DBC with increasing linear velocity, but as the values are so low this increase in DBC could be assumed to be insignificant. It is reasonable to conclude that in this specific case increasing the linear velocity causes a minor affect on the DBC but does not significantly reduce the column performance.

However, in the case of the lysate there is a slight decrease in DBC with increasing linear velocity, as is expected. A possible reason for the trends observed in this study could be that under the conditions used the binding of Fab' from the homogenate is hindered by the presence of contaminants released during cell disruption. The effect of these contaminants on the adsorption of Fab' is greater than the effect of linear velocity.

When comparing the two feedstocks it is clear that the binding capacity for the lysate feed is significantly higher than that of the homogenate. This is to be expected as the lysate contains substantially fewer contaminants than the homogenate, as previously

discussed in Chapter 4, and therefore fewer species competing for adsorbent binding sites.

Table 5.2. Binding capacity (mg/mL SP) at various product breakthrough levels for clarified feedstocks at increasing linear velocities. All runs performed in a column of 15 cm bed height (2.95 mL CV) and constant feed ionic strength. 3.2 mS/cm ± 0.1

	% Breakthrough			
Linear velocity	**1**	**5**	**10**	**50**
(cm/h)	**Dynamic Binding Capacity (mg/mL SP)**			
Homogenate				
100	0.11	0.55	0.96	7.98
300	0.15	0.64	1.02	7.45
Lysate				
100	1.79	3.11	4.86	-
300	0.82	3.09	5.59	-

5.2.2 The effect of feedstock solids concentration on Fab' breakthrough

Fab' breakthrough curves were obtained as described in Section 2.4.2.1. Approximately 9 and 10 CV of unclarified homogenate feed were loaded at linear velocities of 150 and 460 cm/h, respectively. The intended linear velocities were 100 and 300 cm/h, however, the presence of cell debris and the increased operating pressure appeared to affect the performance of the sample pump on the ÄKTA Explorer and resulted in flow rates higher than those intended. It was not possible to load the unclarified lysate feed onto the packed bed column as the system pressure limit was instantly triggered. The main reason for this is probably the mean particle diameter (d_{50}) of the lysed cells was too large for the solution to pass through the packed bed. As discussed in Chapter 3, the method of cell disruption had a major effect on the d_{50} of the *E. coli* cells. The d_{50} for the homogenate was found to be 0.37 μm after 5 passes at 500 bar through the Lab 60 (APV Ltd., Crawley, UK) high pressure homogeniser, whereas the d_{50} for the lysed cells was 0.76 μm.

The impact of loading unclarified homogenate, with a solids concentration of 11% (ww/v), on the system pressure drop is presented in Figure 5.6 which presents the pressure drop as a function of linear velocity and level of clarification. As

expected, loading unclarified material onto a packed bed caused a significant increase in the back-pressure, as well as compression of the packed bed and a system pressure limit trigger. However, it was still possible to load as much as 9 column volumes.

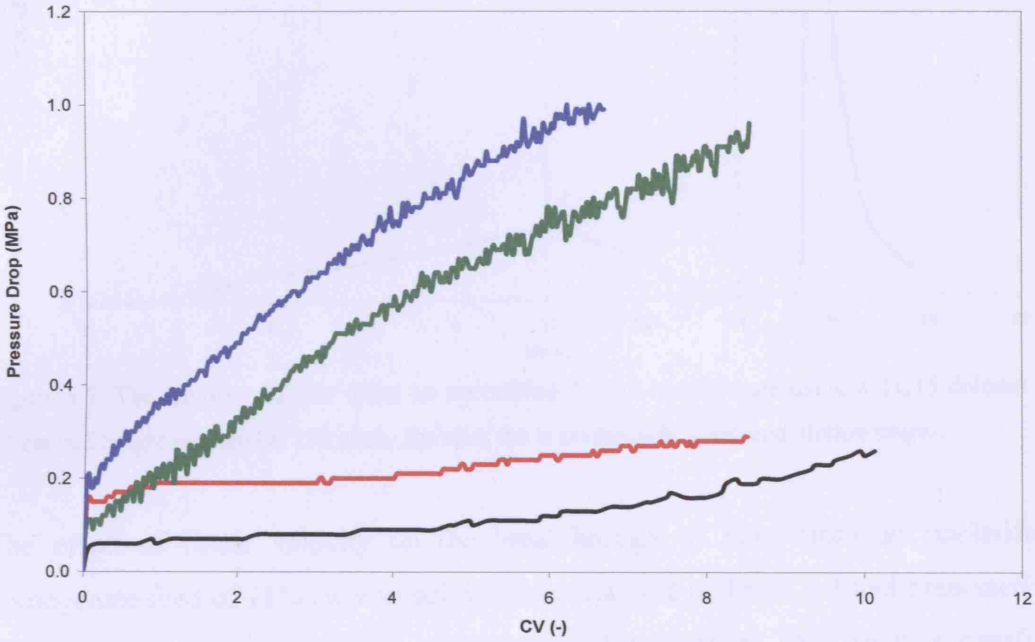

Figure 5.6. The impact of linear velocity and homogenate feed clarification on the pressure drop of the TC15 column. Clarified 100 (black line) and 300 (red line) cm/h and unclarified 150 (green line) and 460 (blue line) cm/h.

Figure 5.7 shows an example chromatogram for the purification of Fab' from an unclarified *E. coli* homogenate performed at 150 cm/h. When compared to Figure 5.2, the purification of Fab' from a clarified *E. coli* homogenate, it is noticeable that the presence of cell debris has affected the elution profile, with the elution peak appearing to have broadened. As presented in Table 5.3, which summarises the experimental conditions of the runs performed, bed compression of 7% (1.1 cm) of the initial packed bed height was observed and the loading of Fab' was interrupted by the system pressure alarm.

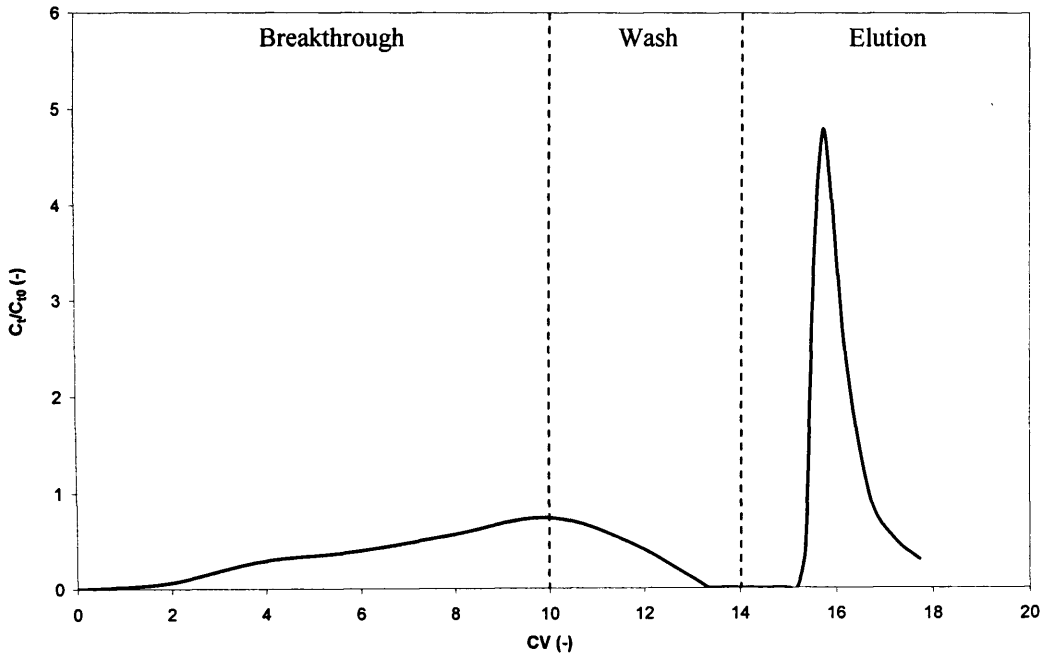

Figure 5.7. The recovery of Fab' from an unclarified *E. coli* homogenate using a TC15 column of 15 cm bed height operated at 150 cm/h, showing the breakthrough, wash and elution stages.

The effect of linear velocity on the breakthrough of Fab' from an unclarified homogenate feed of 11% (ww/v) solids is summarised in Table 5.3 and presented in Figure 5.8 where a comparison with the breakthrough of Fab' from a clarified homogenate is made.

Table 5.3. Experimental conditions and outputs for the recovery of Fab' from unclarified *E. coli* feedstocks as a function of linear velocity.

Linear Velocity (cm/h)	BT %	Residence Time (min)	% Solids (ww/v)	CV Loaded (-)	Fab' Applied (mg)	Comp'n (%)	Overpres' (>1 MPa)
Homogenate							
150	75	5.9	11	10	19.9	7	✗
460	60	2.0	11	9	20.0	4	✓
Lysate							
100	0	7.4	7	<1	-	0	✓
300	0	2.9	7	<1	-	0	✓

Table 5.3 shows that the system pressure limit of 1 MPa was reached when loading unclarified homogenate at 460 cm/h, after a total of 9 CV were loaded. The greatest degree of bed compression was observed at the lowest linear velocity, 150 cm/h. A possible reason for this could be the gradual rearrangement of the bed structure and the stabilisation of the adsorbent packing.

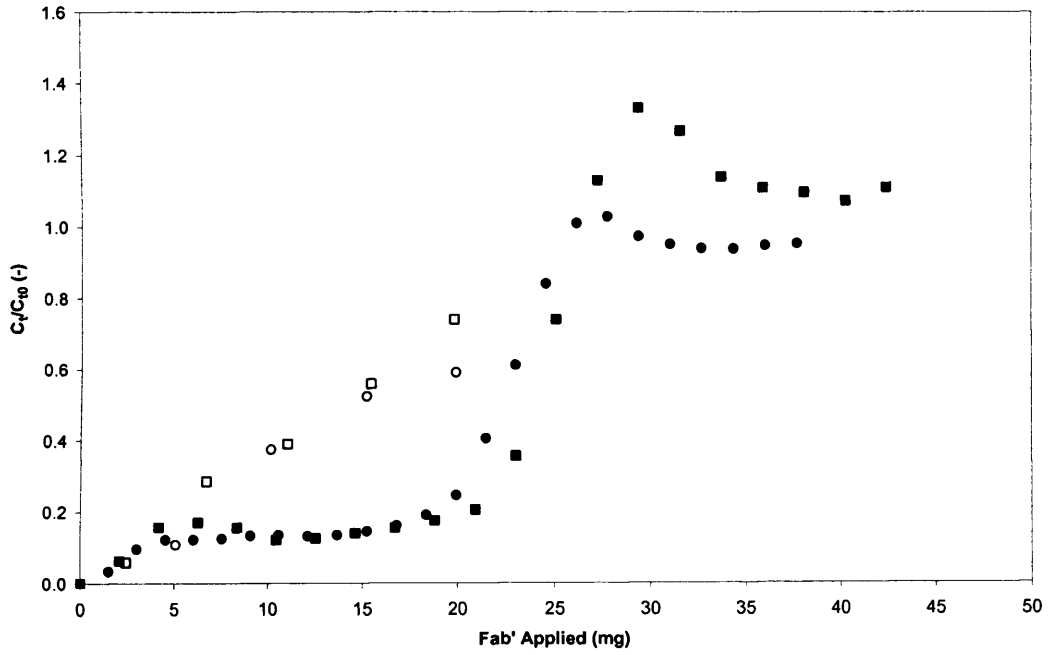

Figure 5.8. Comparing the breakthrough curves of Fab' from clarified and unclarified *E. coli* homogenate feedstocks to SP Sepharose FF at various linear velocity i) clarified; 100 (■) and 300 (●) cm/h and ii) unclarified; 150 (□) and 460 (○) cm/h.

Figure 5.8 compares the Fab' breakthrough curves as a function of linear velocity for both the clarified and unclarified homogenate feedstock. The breakthrough curves for the unclarified homogenate appear to be linear and unaffected by the increase in linear velocity, with the curves at 150 and 460 cm/h overlapping. A possible reason for this was given in Section 5.2.1.

Table 5.4 shows the effect of linear velocity on the binding capacity of Fab' when purified from an unclarified homogenate, measured at 1, 5, 10, and 50% product breakthrough. The dynamic binding capacity increased with increasing linear velocity, which was unexpected. This could be explained by the degree of bed compression observed in these experiments. The adsorbent used in this study was SP

Sepharose Fast Flow (GE Healthcare, Uppsala, Sweden), a spherical, highly cross-linked agarose-based adsorbent made up of 6% agarose. Despite the high degree of cross-linking, SP Sepharose FF is a compressible adsorbent.

As seen in Table 5.3 bed compression of 7% of the initial bed height was observed at 150 cm/h. Colby *et al.* (1996a) concluded that the compression of a packed bed of SP Sepharose Big-Beads (6% agarose) had no significant effect on the system behaviour. However, they report that increased compression leads to two competing mechanisms which lead to minor variations in breakthrough curves. Firstly, bed compression causes a reduction in the void volume which can result in a premature breakthrough and acceleration of the curve development. Secondly, external film mass transfer is increased which enhances the mass transfer between the mobile phase and the adsorbent, resulting in a delayed breakthrough curve. Colby *et al.* (1996a) stated that the appearance of delayed breakthrough curves in their work indicated that compression-induced increases in external film mass transfer were the dominant mechanism in their system. The increase in binding capacity with increasing linear velocity observed in this study could be attributed to the premature breakthrough at 150 cm/h caused by bed compression and the resulting reduction in void volume.

Table 5.4. Binding capacity (mg/mL SP) for unclarified homogenate at increasing linear velocities. Experiments performed in a 15 cm bed height column (2.95 mL CV) and feed ionic strength of 3.2 mS/cm.

	% Breakthrough			
Linear velocity	**1**	**5**	**10**	**50**
(cm/h)	**Dynamic Binding Capacity (mg/mL SP)**			
Homogenate				
150	0.14	0.68	1.07	4.30
460	0.16	0.78	1.51	4.35

In order to compare the binding capacity of the clarified and unclarified homogenate feeds, data at the lowest linear velocity was used. At 1, 5 and 10% breakthrough the dynamic binding capacity is not significantly affected by the presence of cells and cell debris. This confirms the trends observed in Figure 5.8 which shows that the breakthrough curves are almost identical up to a breakthrough of 20%. Above 20%

the breakthrough of Fab' from the unclarified feed continues to increase linearly, whereas the breakthrough of Fab' from the clarified feed plateaus for several column volumes. At 50% product breakthrough the DBC drops from 7.98 to 4.30 mg/mL SP in the presence of cell and cell debris. The reason for the reduced binding capacity, as discussed in Chapter 4, is likely to be the blockage of pores and binding sites caused by the cell debris, as well as the fact that the cell debris competes with the adsorbent for Fab'.

An important aspect of this study is the partition of Fab' between the feedstock supernatant and cell debris. The binding of Fab' to the cell debris could potentially have a major impact on Fab' recovery and therefore it is important to determine, not only if it is possible to load the unclarified material onto a packed bed, but also if packed bed chromatography is able to recover Fab' from the cell debris. The method of total available Fab' measurement, as described in Chapter 3, was used to determine the partitioning of Fab' as the homogenate was loaded onto the column.

In order to measure the concentration of debris-bound Fab' the solids concentration (% ww/v) of each fraction of the flowthrough was measured as described in Section 2.3.1.1. Normalising the flowthrough solids concentration results in a solids breakthrough curve, as seen in Figure 5.9, which presents the dimensionless solids concentration as a function of linear velocity and column volumes loaded. Figure 5.9 also shows the cumulative solids concentration collected from the flowthrough. At both linear velocities tested the first CV has a low solids concentration due to the dilution caused by the equilibration buffer present within the packed bed. The solids concentration (% ww/v) appears to plateau at a level below the maximum, which suggests that not all of the solids being loaded exit the column. This could be attributed to errors in the measurement of the solids concentration (% ww/v) as well as the accumulation of cell debris both at the top of, and within the packed bed. The increase in solids concentration at both 150 and 460 cm/h is slow and gradual, taking 4 CV to reach 90 and 120% breakthrough respectively. A breakthrough of 120% may be due to experimental error, as the solids concentration measurements were based on single measurements of the flowthrough fractions. It is also essential to ensure

that the feedstock is continuously mixed during the loading step to prevent solids settling and ensure the solids concentration is constant throughout the loading step.

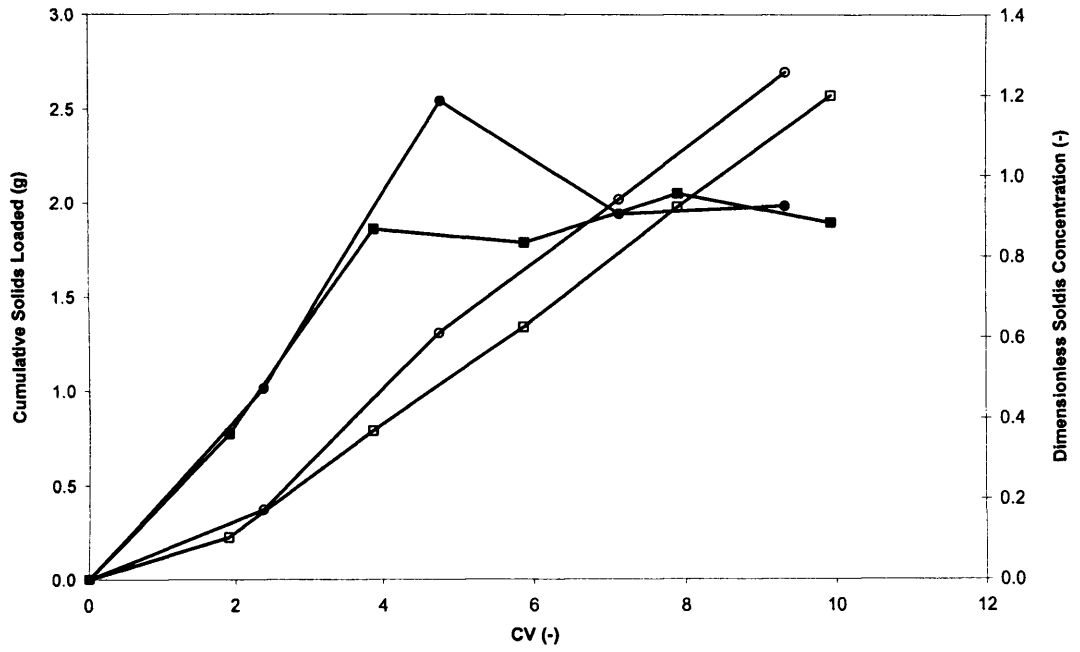

Figure 5.9. The impact of linear velocity on the breakthrough of homogenate cell debris through a TC15 column of 15 cm bed height. Dimensionless solids concentration (ww/v) at 150 (■) and 460 (●) cm/h and cumulative flowthrough solids at 150 (□) and 460 (○) cm/h.

At the point when the loading of unclarified feedstock was stopped, the cumulative mass of solids collected in the flowthrough reached 79 and 87 % at 150 and 460 cm/h respectively. This result confirms that there is accumulation of cell debris within the packed bed column.

Figure 5.10 shows a photograph of the top of the packed bed during the loading step, where the accumulation of cell debris on the surface of the packed bed is highlighted.

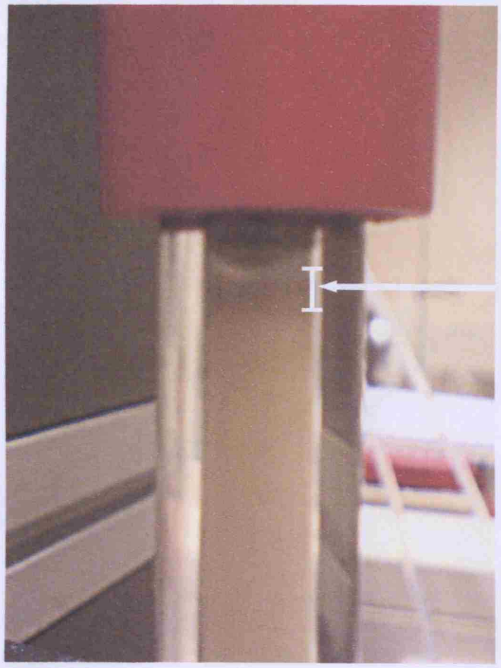

Figure 5.10. A photograph showing the bed compression and accumulation of cell debris.

Figure 5.11 shows the dimensionless debris-bound Fab' concentration (C_d/C_{d0}) as a function of linear velocity. From this figure it is clear to see that Fab' is indeed being recovered from the cell debris and that the linear velocity does not significantly affect the recovery of Fab' from cell debris. At both linear velocities tested there appears to be a plateau between 3 and 6 CV where C_d/C_{d0} appears to be constant, this is then followed by a sharp increase as the number of column volumes being loaded increases. Although the results shown in Figure 5.11 are based on single measurements, the method of debris-bound Fab' measurement was shown in Section 3.2.3.2 to be highly reproducible with a coefficient of variance of 1.4%.

With regards to column chromatography, measuring C_d/C_{d0} may not fully describe the mechanism of Fab' recovery from the cell debris as the first 3 CV loaded may have a low solids concentration due to dilution caused by the equilibration buffer, as shown in Figure 5.9. As C_d/C_{d0} does not take into account the mass of cell debris from which the Fab' has been eluted these dilute fractions would suggest that the debris-bound Fab' concentration is lower than it actually is. Calculating the mass of Fab' per gram of cell debris gives a more accurate debris-bound Fab' concentration. In order to avoid confusion with C_d (mg Fab/mL solution) this concentration was defined as C_f(mg Fab/g debris).

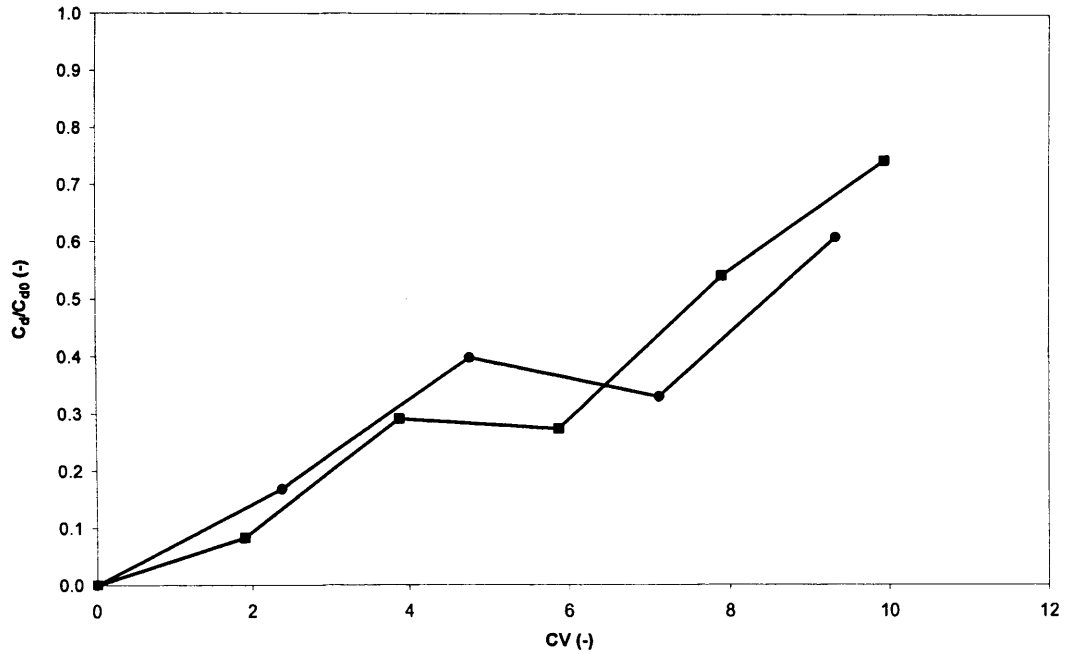

Figure 5.11. The impact of linear velocity on the concentration of debris-bound Fab'. 150 (■), and 460 (●) cm/h.

Figure 5.12 compares the two methods of debris-bound Fab' measurement and confirms that C_d is indeed affected by dilution caused by the equilibration buffer, as the difference between the two methods is greatest within the first 3 CV loaded, i.e. the period when dilution and incomplete debris breakthrough is occurring.

Figure 5.13 presents the dimensionless C_f as a function of linear velocity and shows that C_f/C_{f0} drops significantly as the unclarified homogenate is loaded onto the column, confirming that recovery of Fab' from the cell debris is occurring. As more homogenate is loaded C_f/C_{f0} increases to a plateau at around 30% before the concentration of Fab' per gram of cell debris rises sharply again. Figure 5.13 appears to consist of three distinct phases: I) rapid recovery of Fab' from the cell debris, II) an equilibrium phase, and III) an adsorption phase where Fab' is being re-adsorbed by the debris. This three phase pattern of Fab' desorption/adsorption by the debris can be explained by the binding capacity of the adsorbent, as presented in Figure 5.14. As the packed bed is challenged with the unclarified homogenate, Fab' is rapidly desorbed from the debris and adsorbed by the fresh adsorbent (phase I). The second phase is caused by a period of constant binding, where the concentration of Fab' bound to the cell debris remains constant as the adsorbent continues to bind Fab' from both the supernatant and cell debris. The third phase, the rapid increase in

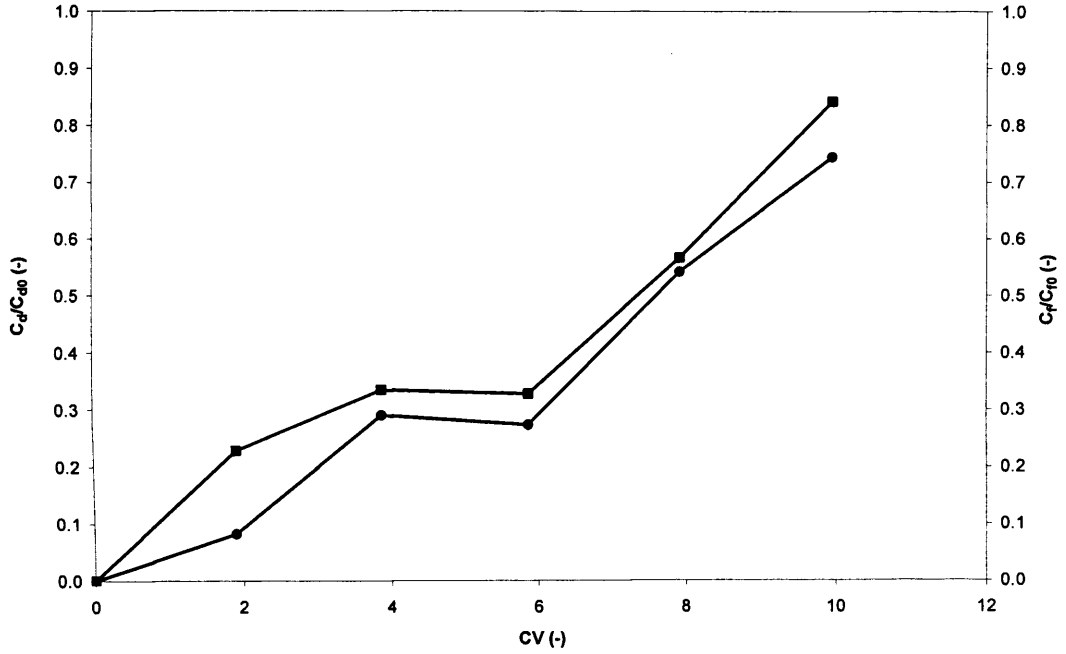

Figure 5.12. Comparing the two methods of debris-bound Fab' measurements showing C_d/C_{d0} (•) and C_f/C_{f0} (■). Feed loading linear velocity of 150 cm/h.

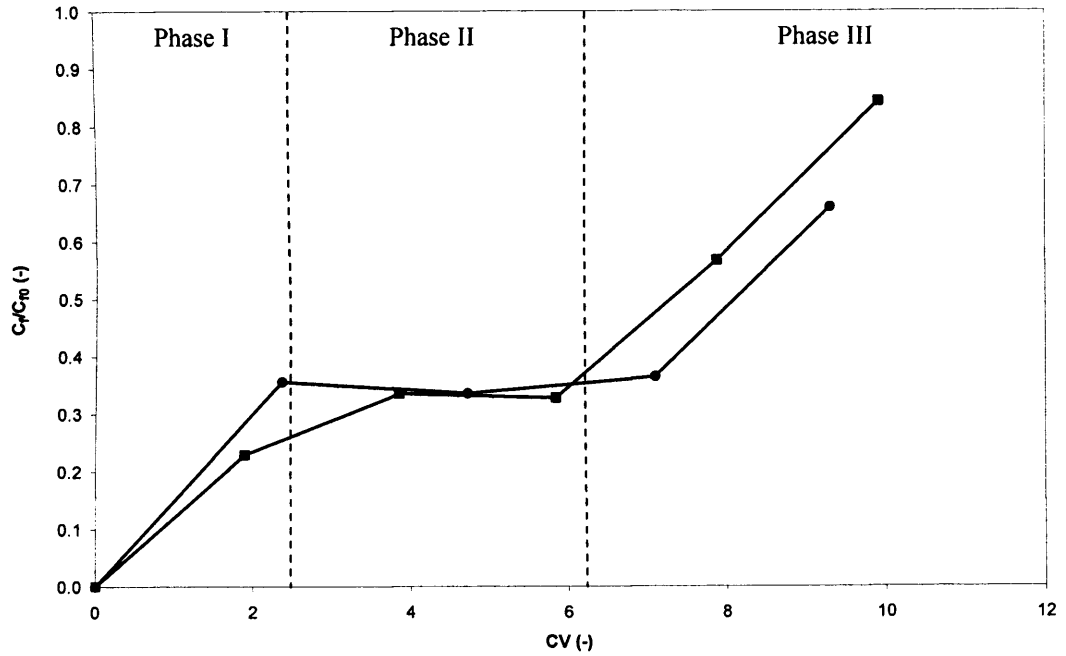

Figure 5.13. The impact of linear velocity on the concentration of debris-bound Fab' (C_f) as measured by the C_f method. 150 (■) and 460 (•) cm/h.

debris-bound Fab', is due to the fact that the adsorbent has reached its maximum dynamic binding capacity and so Fab' from the supernatant is being re-adsorbed by the cell debris. This is presented in Figure 5.15 which shows the partitioning of Fab' when unclarified homogenate is loaded onto the packed bed at a linear velocity of 150 cm/h. It is evident that as the unclarified homogenate is loaded onto the column, more Fab' is adsorbed from the supernatant than from the cell debris. This can be seen by the fact that C_s/C_{s0} reaches 4%, meaning that 96% of Fab' in the supernatant is adsorbed, as compared to 77% of Fab' from the cell debris. This is to be expected due to the affinity of the Fab' to the cell debris. This affinity and the interaction between the cell debris and Fab' leads to the supernatant Fab' concentration rising sharply while the debris-bound Fab' concentration plateaus before eventually rising as the adsorbent reaches it maximum capacity.

The effect of solids concentration on the binding of Fab' to SP Sepharose has been described in detail in Section 4.2.4.

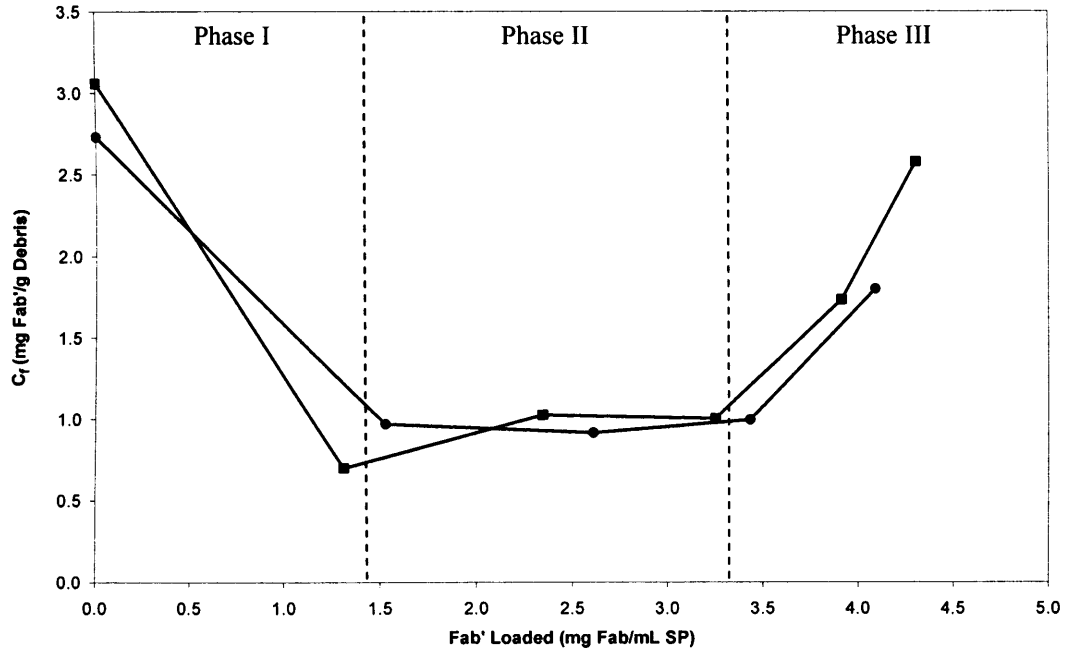

Figure 5.14. The impact of linear velocity on the concentration of debris-bound Fab' (C_f) as a function of Fab' loaded onto the adsorbent SP Sepharose FF. Feed loaded at 150 (■) and 460 (●) cm/h.

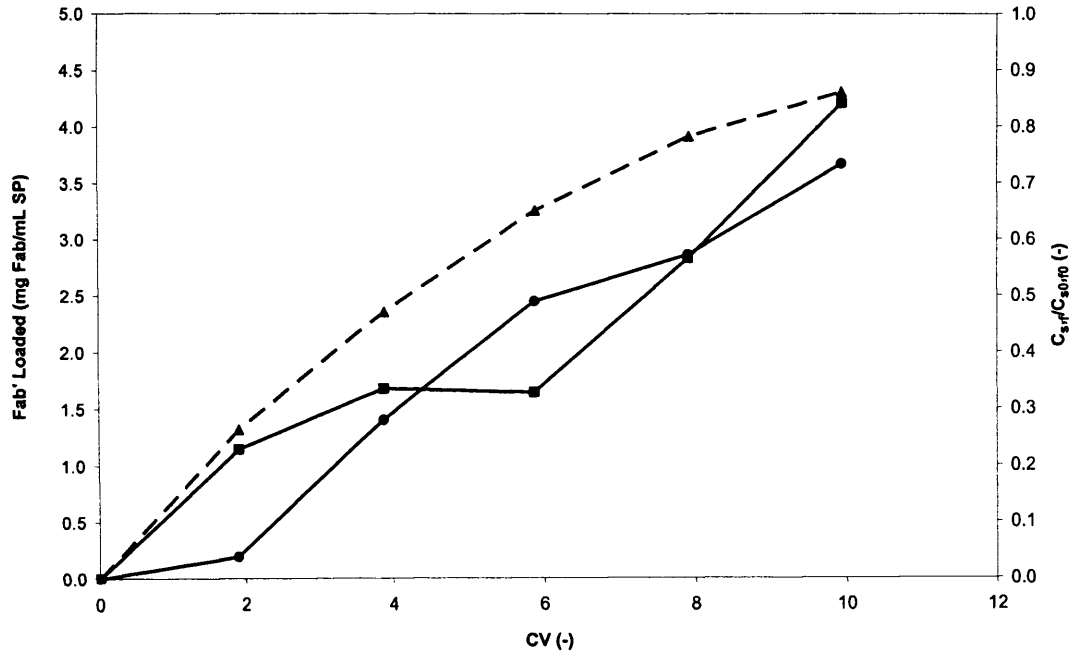

Figure 5.15. The partitioning of Fab' during the recovery from unclarified *E. coli* homogenate, showing the dimensionless supernatant (C_s) (●) and debris-bound (C_f) (■) concentration, as well as the concentration of Fab' loaded onto SP Sepharose FF (▲), when loaded at 150 cm/h.

5.2.3 *The effect of feedstock ionic strength on Fab' breakthrough*

Clarified homogenate was used to obtain full breakthrough curves at a range of feedstock ionic strengths, as described in Section 2.4.2.1. Figure 5.16 shows the breakthrough curves obtained at 300 cm/h and at feedstock ionic strengths ranging from 2.9 to 8.5 mS/cm. As described in Chapter 3 the ionic strength of the feedstock affects the initial Fab' concentration. To account for this difference in initial concentration a dimensionless concentration is plotted against mass Fab' applied to the column.

The feedstock ionic strength significantly affects the binding of Fab' to the cation exchanger SP Sepharose FF. At 7.0 and 8.5 mS/cm the breakthrough curves are very steep, becoming almost vertical initially, indicating that virtually no Fab' is being adsorbed. As the feed ionic strength decreases the plateau observed and discussed earlier becomes more pronounced, so too does the "roll up" or displacement effect first presented in Figure 5.3. Decreasing the ionic strength from 3.6 to 2.9 mS/cm does not significantly affect the shape of the breakthrough curve, but merely the length of the plateau.

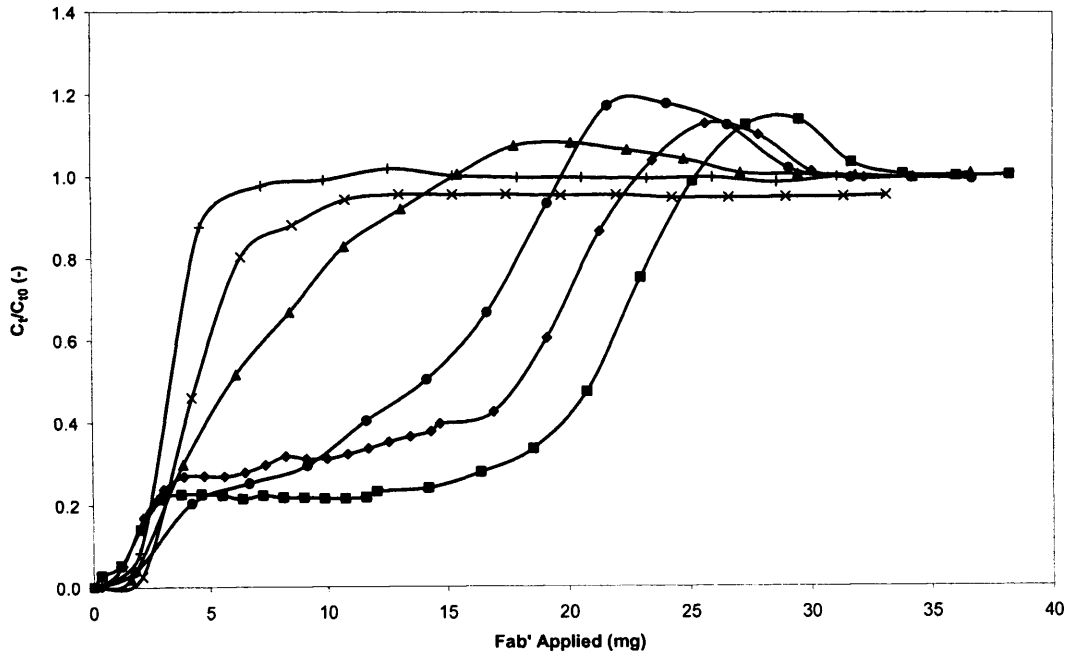

Figure 5.16. The effect of the ionic strength of a clarified *E. coli* homogenate on the breakthrough curves of Fab' loaded at 300 cm/h. Feedstock ionic strength: 2.9 (■), 3.2 (♦), 3.6 (●), 5.0 (▲), 7.0 (x) and 8.5 (+) mS/cm.

The fact that the displacement effect discussed earlier becomes more pronounced as the ionic strength of the feedstock falls confirms the theory described earlier. At a high feedstock ionic strength Fab' is unable to occupy any binding sites on the adsorbent, allowing the competing species to bind. As the ionic strength decreases Fab' is more likely to bind to the adsorbent, thus increasing the competition for binding sites. 5.0 mS/cm appears to be the ionic strength at which Fab' begins to compete with the contaminants for binding sites.

Table 5.5 shows the effect of feedstock ionic strength on the dynamic binding capacity at 1, 5, 10 and 50% product breakthrough. There appears to be no clear trend in the dynamic binding capacity below 10% breakthrough, which may be as a result of the difficulty in accurately calculating the DBC at such low Fab' concentrations. As a result, the dynamic binding capacity at 50% product breakthrough was used to investigate the effect of feedstock ionic strength on the adsorption of Fab'. It is clear to see that the DBC is significantly affected by the feedstock ionic strength. Figure 5.17 shows that the dynamic binding capacity, at 50% product breakthrough, and feedstock ionic strength are related by a power law equation. The dynamic binding capacity is high at low ionic strengths but drops off

quickly with increasing ionic strength. Although it was not possible to determine the maximum static binding capacity from the equilibrium adsorption isotherms in Chapter 3 the dynamic binding capacity shows agreement with the trends observed in the isotherm data. Explanations for the decreased binding capacity have already been discussed in Section 4.2.3 and include the shielding of binding sites by the salt ions.

Table 5.5. Binding capacity (mg/mL SP) for clarified *E. coli* homogenate at increasing ionic strength. All runs performed in a 15 cm bed height column (2.95 mL CV) operated at 300 cm/h.

	% Breakthrough			
Ionic Strength (mS/cm)	**1**	**5**	**10**	**50**
	Dynamic Binding Capacity (mg/mL SP)			
2.9	0.10	0.56	0.71	7.27
3.2	0.34	0.59	0.71	6.15
3.6	0.21	0.86	1.09	4.80
5.0	0.37	0.82	0.95	2.11
7.0	0.27	0.74	0.82	1.47
8.5	0.10	0.51	0.90	1.22

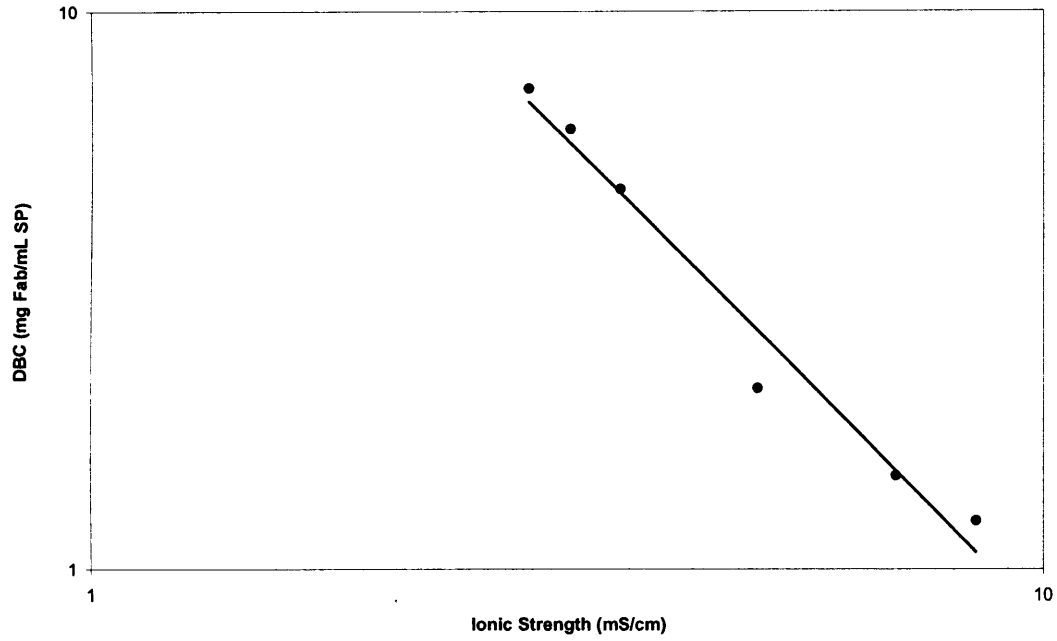

Figure 5.17. The dynamic binding capacity, at 50% product breakthrough, of Fab' on SP Sepharose FF as a function of feedstock ionic strength. The linear regression equation was DBC = 43.24*(I) – 1.73, with an $R^2 = 0.973$.

5.2.4 *The effect of column packing and wall support on Fab' breakthrough and system pressure*

Section 5.2.2 showed that it was possible to load an unclarified homogenate of 11% solids concentration (ww/v) onto a laboratory scale packed bed column and achieve a degree of adsorption comparable with that of a clarified feed when loaded to 20% breakthrough. The effect on the pressure drop and bed compression was also investigated. When operating at a linear velocity of 150 cm/h it was possible to load 10 CV of the homogenate without reaching the system pressure limit of 1 MPa, however 7% bed compression was observed. The experiments discussed thus far in the chapter have been performed using columns packed at a linear velocity 20% greater than the operating velocity in order to ensure no bed compression occurs during the loading of the feed. Although an acceptable packing method, this may not be representative of industrial scale packed bed chromatography. As stated in Section 5.1.2 u_{crit} is used to determine the linear velocity required for column packing and feed loading. Section 5.2.4.1 presents the results for the determination of u_{crit} for SP Sepharose FF packed in an XK16 column (GE Healthcare, Uppsala, Sweden). Section 5.2.4.2 describes the results of homogenate loading experiments performed using chromatographic columns packed using linear velocities based on u_{crit}. Finally, Section 5.2.4.3 describes the use of the Stickel model, as described in Section 5.1.2.1, to obtain a laboratory scale mimic of industrial scale column packing.

5.2.4.1 *The determination of u_{crit}*

The critical velocity was determined as described in Section 2.4.2.2.1. Figure 5.18 shows the pressure drop and bed height as a function of the normalised linear velocity. The linear velocity has been normalised by dividing by u_{crit}. The nonlinear pressure-flow profile observed is typical of compressible adsorbents (Sofer and Nystrom, 1989).

The dashed line (---) in Figure 5.18 represents the point at which the critical bed compression (λ_{crit}) was reached. Stickel *et al.* (2001) define λ_{crit} as

$$\lambda_{crit} = \frac{L_0 - L_{crit}}{L_0} \qquad 5.2$$

where L_0 is the gravity settled bed height and L_{crit} is the bed height at which u_{crit} occurs. Under the conditions used in this study λ_{crit} was found to be 0.16, which is in agreement with the findings of Tran and Joseph *et al.* (2007). Bed compression and linear velocity were found to be linearly related up to the critical velocity. The critical velocity is the velocity at which the slope of the pressure-flow curve becomes infinite (Stickel *et al.*, 2001), and was found to be 1540 cm/h, as illustrated in Figure 5.18 with the dashed line (···).

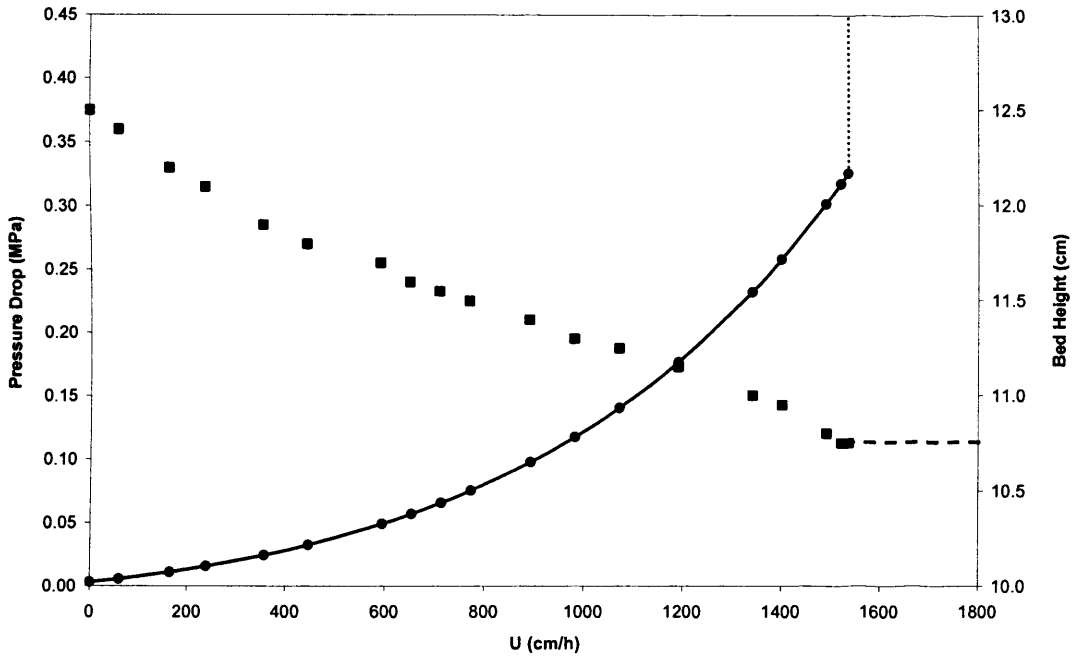

Figure 5.18. The effect of linear velocity on the pressure drop (●) and bed height (■) of a packed bed of SP Sepharose FF packed in a 1.6 cm diameter XK16 column. The point at which the critical velocity occurs is illustrated with the dashed lines.

Section 5.2.4.2 uses the experimentally determined u_{crit} to obtain column packing and loading velocities used for the loading of an unclarified homogenate feedstock.

5.2.4.2 *The effect of column packing and loading velocity on Fab' breakthrough*

Determining u_{crit} for SP Sepharose FF packed in an XK16 column (both from GE Healthcare, Uppsala, Sweden) made it possible to calculate the linear velocity required for optimal column packing and feedstock loading. As stated in Section 5.2.1, Sofer and Hagel (1997) suggest that columns should be packed at a flow rate approximately 90% of u_{crit}. The operating flow rate should then be no more than 80% of the packing flow rate. In this section of the study the linear velocity used for column packing was 1230 cm/h, 80% of the experimentally determined u_{crit}. The loading of unclarified homogenate was then performed at two linear velocities. Firstly, at 985 cm/h, which was just below the recommended maximum (80% of the packing velocity), and secondly, at 300 cm/h, which was chosen so that a comparison between the breakthrough curves obtained in this section and those in Section 5.2.2 could be made. This would highlight any affect column packing may have had on the loading of unclarified homogenate. Table 5.6 shows the loading velocity of the two runs performed in cm/h as well as a percentage of u_{crit}. Other experimental conditions and parameters, such as the residence time and level of Fab' breakthrough achieved are also presented.

Table 5.6. Experimental conditions and outputs for the recovery of Fab' from an unclarified *E. coli* feedstock of 9% solids (ww/v) when loaded onto a column packed at 80% of u_{crit}. The effect of loading linear velocity is presented.

Loading Velocity		Packed bed height (cm)	BT %	Residence Time (min)	CV Loaded (-)	Fab Applied (mg)	Compression (%)
cm/h	% of U_{crit}						
985	0.64	11.3	25	0.69	1.1	19.2	-
300	0.20	11.6	49	2.32	4.7	80.7	3

Figure 5.19 and Figure 5.20 show the dimensionless Fab' and cell debris concentration, as well as the pressure drop for the loading of unclarified homogenates at 985 and 300 cm/h, respectively. The x-axis for both charts has been fixed to 5 CV for easier visual comparison.

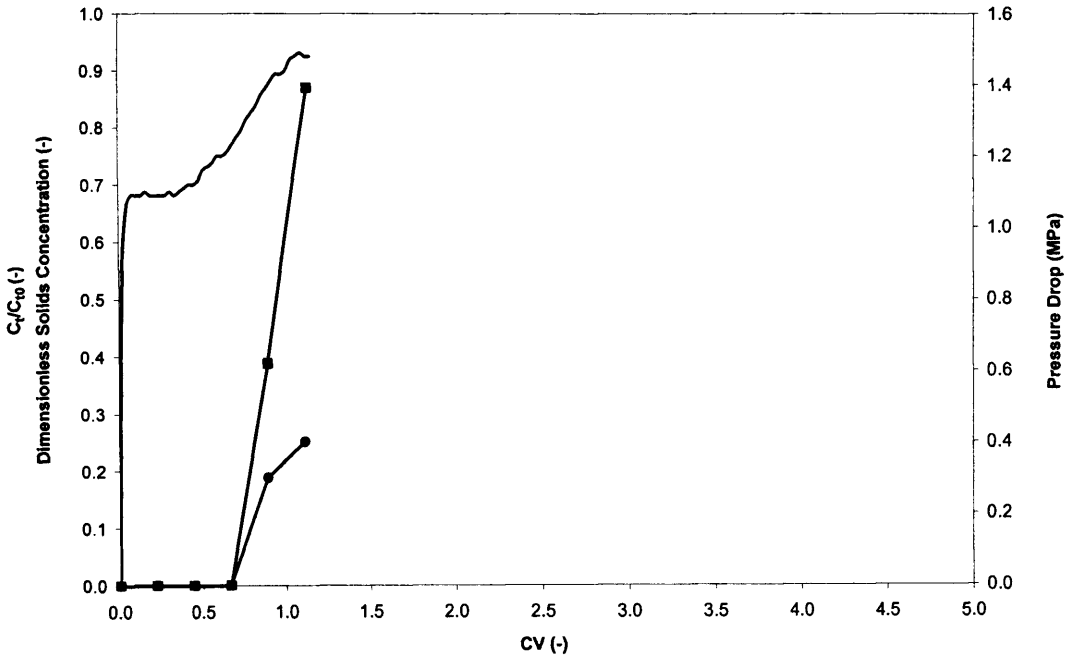

Figure 5.19. The breakthrough of Fab' (●) and cell debris (■) shown with the pressure drop (-) obtained when an XK16 column packed at 80% u_{crit} is then loaded with unclarified *E. coli* homogenate at 985 cm/h (64% u_{crit}).

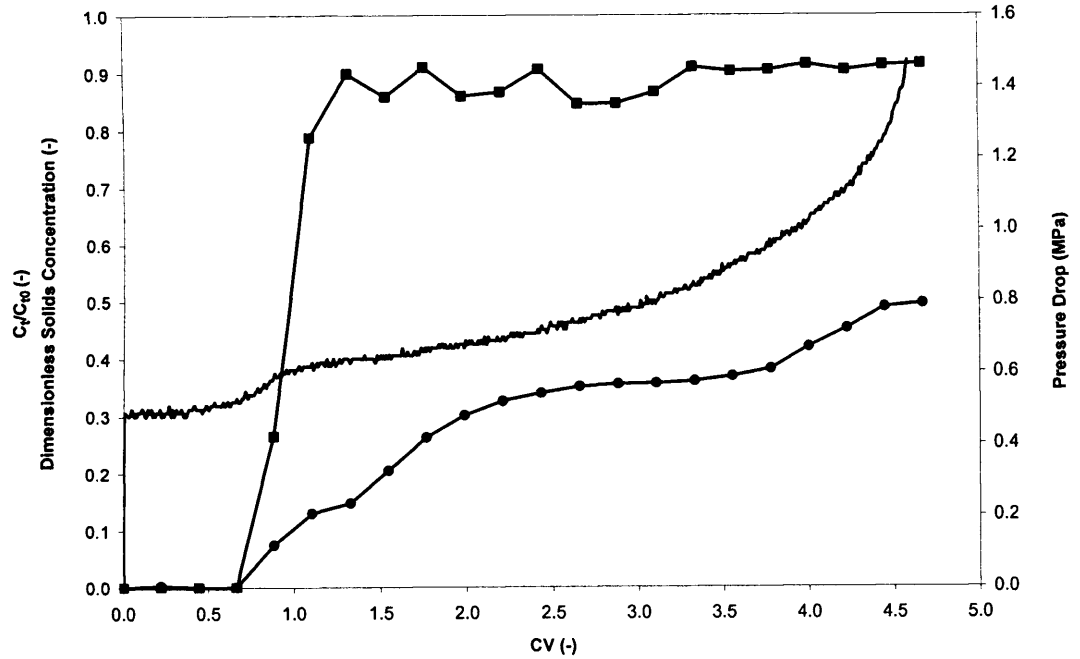

Figure 5.20. The breakthrough of Fab' (●) and cell debris (■) shown with the pressure drop (-) obtained when an XK16 column packed at 80% u_{crit} is then loaded with unclarified *E. coli* homogenate at 300 cm/h (20% u_{crit}).

Figure 5.19 shows that loading unclarified homogenate at a linear velocity of 985 cm/h has an instant and dramatic effect on the pressure drop, causing the system pressure limit of 1.5 MPa to be reached after 1 CV. At 300 cm/h, Figure 5.20, the increase in pressure is more gradual, with nearly 5 times as much material being loaded before the pressure increases to the system limit. The increase in the pressure drop appears to be related to an apparent accumulation of cell debris within the column, as seen by the dimensionless solids concentration reaching a plateau at approximately 90%. The initial breakthrough of Fab' occurs simultaneously, however, at 985 cm/h the level of breakthrough achieved after 1 CV is greater, once again indicating that the linear velocity affects the breakthrough of Fab'.

Figure 5.21 shows the partitioning of Fab' during the loading of unclarified homogenate at 300 cm/h. In this case it is clear to see that the breakthrough of Fab' occurs as a result of the change in concentration in both the supernatant and debris. However, the concentration of debris-bound Fab' appears to remain constant whereas an increase in the supernatant concentration results in the second phase of the breakthrough. As previously explained, this is due to the strong interactions between the cell debris and Fab'.

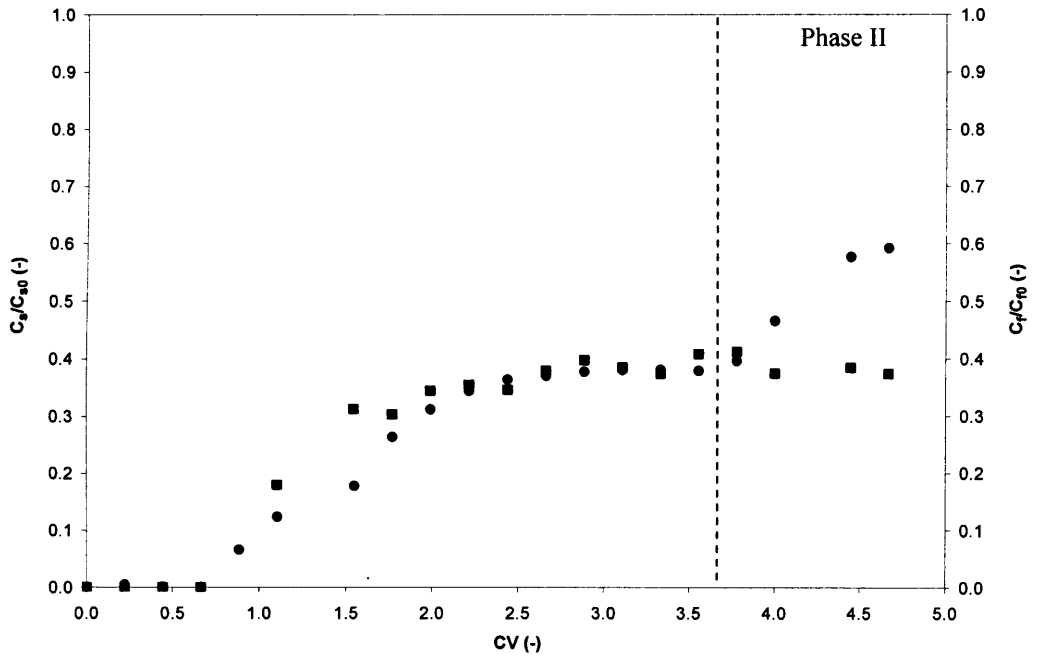

Figure 5.21. The partitioning of supernatant (●) and debris-bound (C_f) (■) Fab' in an unclarified *E. coli* homogenate loaded onto an XK16 column at 300 cm/h.

It is interesting to note that Figure 5.20 and Figure 5.21 show a significant plateau during the breakthrough of Fab', not previously observed during the loading of unclarified homogenate using the Tricorn-15 column (Section 5.2.2). This would lead one to believe that the increased bed compression resulting from the higher packing velocity increases Fab' binding and delays the breakthrough. However, Figure 5.22 compares the breakthrough curves obtained in the Tricorn-15 column in Section 5.2.2 and the breakthrough curve obtained in the XK16 column at 300 cm/h. Although there is a plateau and a period of sustained adsorption, the breakthrough curve actually occurs earlier in the compressed XK16 column. This result confirms the theory discussed in Section 5.22, regarding the findings of Colby *et al.* (1996a) who reported two competing mechanisms which lead to minor variations in breakthrough curves. In Section 5.2.2 a premature breakthrough at 150 cm/h was attributed to a reduction in void volume caused by bed compression. Bed compression can cause adsorbent bead deformation as well as a reduction in the surface area available for product adsorption (Colby *et al.*, 1996a) and lead to the early breakthrough observed in this study.

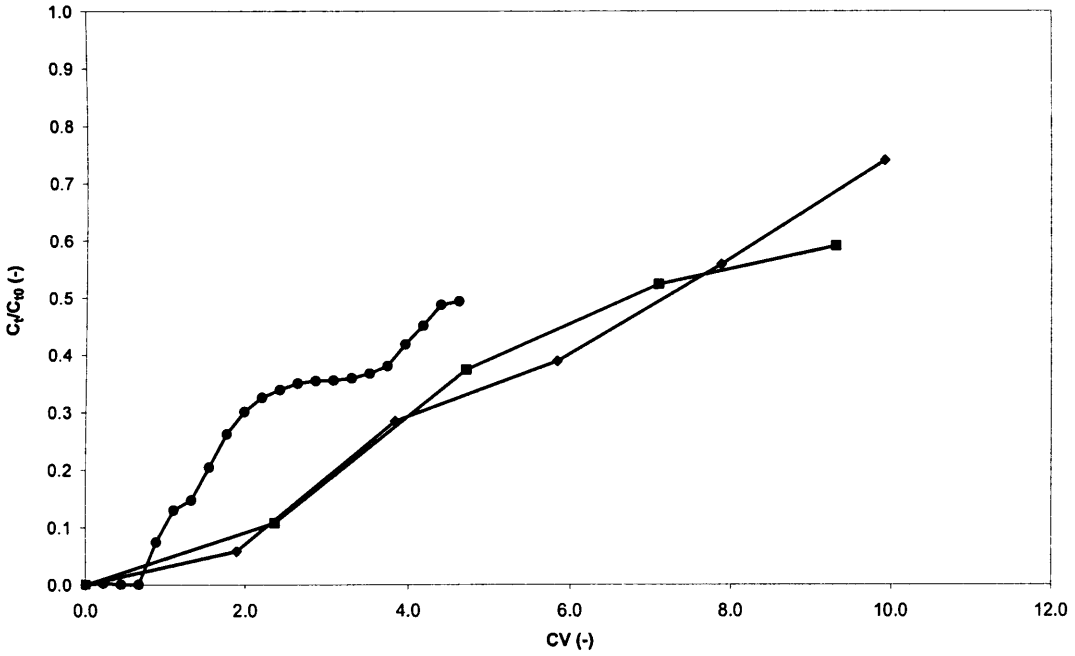

Figure 5.22. Comparing the breakthrough curves for Fab' achieved in a laboratory packed Tricorn 15 (TC15) column to that of a compressed XK16 packed at 80% u_{crit}. Columns: TC15 at 150 cm/h (♦), TC15 at 460 cm/h (■) and XK16 at 300 cm/h (●).

5.2.4.3 *Laboratory scale prediction of industrial scale chromatography*

In order to investigate the feasibility of scaling-up the purification of Fab' from an unclarified homogenate feedstock the approach put forward by Stickel *et al.* (2001) was used to obtain a laboratory scale prediction of the critical velocity for an industrial scale column. As described in Section 5.1.2, the Stickel model is an empirical model which correlates the effect of wall support and adsorbent compressibility.

The purification of Fab' from an unclarified homogenate feedstock was shown to be possible using a laboratory scale packed bed, given pressure and Fab' breakthrough limits. Figure 5.8 showed that up to a Fab' breakthrough of 15-20% the presence of cell debris did not significantly affect the performance of the adsorption process. Using higher linear velocities during the packing of the adsorbent reduced the number of column volumes which could be loaded and led to a premature breakthrough curve, though it was still possible to load unclarified material onto the packed bed. One reason for this is the wall affects in a laboratory scale column provide significant support to the packed bed. Loading unclarified feedstocks onto a packed bed results in compression, as observed in this study. However, the support provided by the walls of the column delay the onset of compression (Colby *et al.*, 1996b). Wall support and wall effects are more significant in smaller diameter columns, which often leads to problems with pressure drop when laboratory scale processes are scaled-up.

It was assumed that the process was being scaled-up to a 100 cm diameter column with a settled bed height of 15 cm. Using Equation 5.1 and the empirical constants m and b reported by Stickel the critical velocity for the industrial scale column was obtained. Stickel reports an m value for Phenyl Sepharose 6FF at 6 °C of 1058 cm^2/h. This was deemed appropriate due to the structural similarities between the SP Sepharose FF (6%) used in this study and Phenyl Sepharose 6FF. However, the b constant, which is a measure of the compressibility of an adsorbent, is greatly influenced by operating conditions. As the b constant reported by Stickel is for Phenyl Sepharose 6FF at 6 °C it was necessary to modify this value to account for

the difference in operating temperature. From the data in Stickel *et al.* (2001) it appears that increasing the operating temperature from 6 to 22 °C leads to an increase in the *b* constant for Sepharose 4FF of approximately 1300 cm^2/h. A similar increase was applied to account for the temperature difference.

The u_{crit} for the industrial scale column was estimated to be approximately 400 cm/h. It was assumed that the industrial scale column would be operated at a linear velocity of 300 cm/h. Therefore, for the industrial scale column the ratio between the operating (u_{op}) and critical velocity (u_{crit}) was 0.75.

In order to obtain a laboratory scale u_{op} which would result in the prediction of the pressure drop of the industrial scale column, the same ratio of u_{op} to u_{crit} was used. The experimentally determined u_{crit} was used to obtain a u_{op} of 1155 cm/h. The laboratory scale column was then packed at a linear velocity of 1380 cm/h, which was 20% greater than the u_{op}. Theoretically, the resulting packed bed resembled an industrial scale column in terms of its packing, porosity and wall support.

The purification of Fab' from an unclarified homogenate was then attempted at an operating velocity of 1155 cm/h, however, the system pressure limit was reached after 0.8 CV. This result indicates that although it may be possible to load unclarified material onto a laboratory scale packed bed column, using the Stickel model to obtain a mimic of industrial scale columns shows that scale-up of such a process would be unsuccessful. The reduced wall support and increased back pressure of an industrial scale column would lead to the blockage of the packed bed column during the loading of an unclarified feedstock. This indicates that either the feedstock must be clarified prior to loading onto the packed bed, resulting in reduced Fab' yields, or an alternative mode of operation be used for the capture of Fab'.

5.3 Summary

The use of laboratory scale columns to recover antibody fragments from various feedstocks was presented in this chapter. The effect of linear velocity, ionic strength and feed solids concentration on the adsorption of antibody fragments, using packed bed columns was investigated. The linear velocity at which the feedstock was loaded appeared to have a minor affect on the breakthrough curves, but did not significantly affect the column performance. This would suggest that the time required for the

chromatography step can be reduced without adversely affecting the purification. However, loading unclarified material onto a packed bed column lead to compression of the adsorbent, over-pressuring of the system and a significant decrease in the dynamic binding capacity. The use of the Stickel model for predicting the pressure drop for industrial scale columns indicated that although it is possible to load low volumes of unclarified homogenate onto a laboratory packed bed, the process could not be successfully scaled-up due to the reduced wall support and increased back pressure experienced at industrial scale. This would lead to a reduction in the bed porosity and prevent the loading of particulate material.

Having shown that the use of packed bed columns for the recovery of Fab' from unclarified feedstock has significant limitations, notably the backpressure, the following chapter (Chapter 6) investigates the use of stirred tank batch adsorption as a viable alternative process option. A microwell scale batch system is presented and the effect of feedstocks properties on the performance of the adsorption process is described, along with a geometric scale-up of the batch system.

6 Scale-down batch adsorption of Fab' antibody fragments from *E. coli* feedstocks

Abstract

The results from the previous chapter highlighted the limitations of using packed bed columns for the processing of unclarified feedstocks. This chapter explores the use of stirred tank batch adsorption as an alternative method of purification of antibody fragments from unclarified feedstocks.

A scale-down method, utilising microplate technology, is described along with attempts to scale-up to laboratory scale stirred tanks. The effects of key process variables, including mixing conditions, phase ratio, feedstock ionic strength and solids concentration on the adsorption of antibody fragments are presented.

The results show that the use of batch adsorption for the recovery and initial purification of Fab' from unclarified feedstocks is a viable alternative to the use of packed beds. The scale-up of the stirred tank process from microwell through to laboratory scale stirred tanks was found to be feasible and successful.

6.1 Introduction

The use of batch adsorption in bioprocessing has been discussed in Chapter 1. In this chapter batch adsorption, preformed in microwell filterplates and modified stirred cells, was used in order to capture Fab' from various *E. coli* feedstocks. Section 6.1.1 describes the use of microwell plates in chromatographic process development.

6.1.1 Microwell batch adsorption

Chromatographic process development has traditionally been a tedious, time consuming exercise, complicated by the availability of a large number of adsorbents, and the wide range of possible operating conditions and process variables (Rege *et al.*, 2006). Consequently the comprehensive screening of the desired

adsorbents and conditions often requires large volumes of the final product. The use of automated high throughput process screening (HTPS) performed in microwell plates can overcome these problems and accelerate process development. There are several examples of microwell HTPS of chromatographic processes in the literature (Welch *et al.*, 2002; Thiemann *et al.*, 2004; Follman *et al.*, 2004; Bastek *et al.*, 2004; Bensch *et al.*, 2005; Rege *et al.*, 2006). Rege *at al.* (2006) used HTPS to determine rapidly the sequence of chromatographic steps required to achieve high purities of their product. The purification of α-amylase was screened using 11 different adsorbents under different pH binding conditions. The results of the screening experiments resulted in single-band purities of the protein. Welch *et al.* (2002) showed how a 96-well microwell plate containing 95 different adsorbents could be used to evaluate a vast number of adsorbent chemistries and conditions and greatly speed up the development process.

In this chapter microwell HTPS techniques are developed and used to evaluate the impact of feedstock ionic strength and solids concentration, as well as the adsorbent phase ratio. The adsorption of Fab' from *E. coli* feedstocks is then scaled up to laboratory scale stirred tanks.

6.2 Results and discussion

Section 6.2.1 describes the use of a bespoke microwell filterplate for the screening of feedstock properties and binding conditions. The use of a small scale laboratory stirred tank for the adsorption of Fab' from unclarified feedstocks is described in Section 6.2.2. Finally, Section 6.2.3 compares the performance of the microwell and stirred tank systems and describes how well the microwell system predicts the behaviour of the stirred tank.

As the volume of diafiltered unclarified lysate was limited, it was not possible to perform all the experiments with both feedstocks. As a result, the majority of the results presented in this chapter are for experiments performed with an *E. coli* homogenate.

6.2.1 Microwell filterplate adsorption

A custom made 800 µL microwell filterplate was constructed and operated as described in Section 2.4.1. The microwell plate was mixed on an Eppendorf Thermomixer (Eppendorf UK Ltd, Cambridge, UK). The rotational speed required to achieve sufficient mixing to suspend the adsorbent was determined experimentally and the results presented in Section 6.2.1.1. The effects of the phase ratio (Section 6.2.1.2), feedstock solids concentration (Section 6.2.1.3), and feedstock ionic strength (Section 6.2.1.4) are also presented here.

As described in Section 2.4.1.1 the filterplate is constructed using a stainless steel mesh which has 25 µm pores. This allows the feedstock to pass through into collection plates whilst the adsorbent is retained. As the adsorbent is equilibrated with 3 x 0.5 mL 20 mM Sodium Acetate prior to the addition of the feedstock, any adsorbent particles smaller than 25 µm are removed, ensuring that the feedstock collected after adsorption is free of any adsorbent beads. When unclarified feedstocks are used, a 100 µL sample is spun in a bench top centrifuge and the supernatant assayed for Fab'. The cell pellet is then resuspended in 100 µL 1 M NaCl, as described in Section 2.3.5.2 and Section 3.2.3.1 to measure the debris-bound Fab' concentration (C_d). Due to the small volume of feedstock used in these experiments (200 µL) and the fact that the solids concentration within the microwell was constant and not subject to dilution, as was the case with the packed beds, measuring C_d was more appropriate than determining C_f (Section 5.2.2).

6.2.1.1 The effect of rotational speed on Fab' adsorption

Figure 6.1 shows the effect of increasing rotational speed on the adsorption of Fab', from two homogenate feedstocks, to SP Sepharose FF at a phase ratio of 0.25. The unclarified feedstock was mixed at each rotational speed for 1 min before the feedstock was separated from the adsorbent by vacuum filtration and collected. To assess the effect of rotational speed on the adsorption of Fab' the clarified homogenate feedstock was mixed at each rotational speed for 0.5 min before being

separated from the adsorbent. A control was performed which involved adding the feedstock to the adsorbent with the mixer stationary.

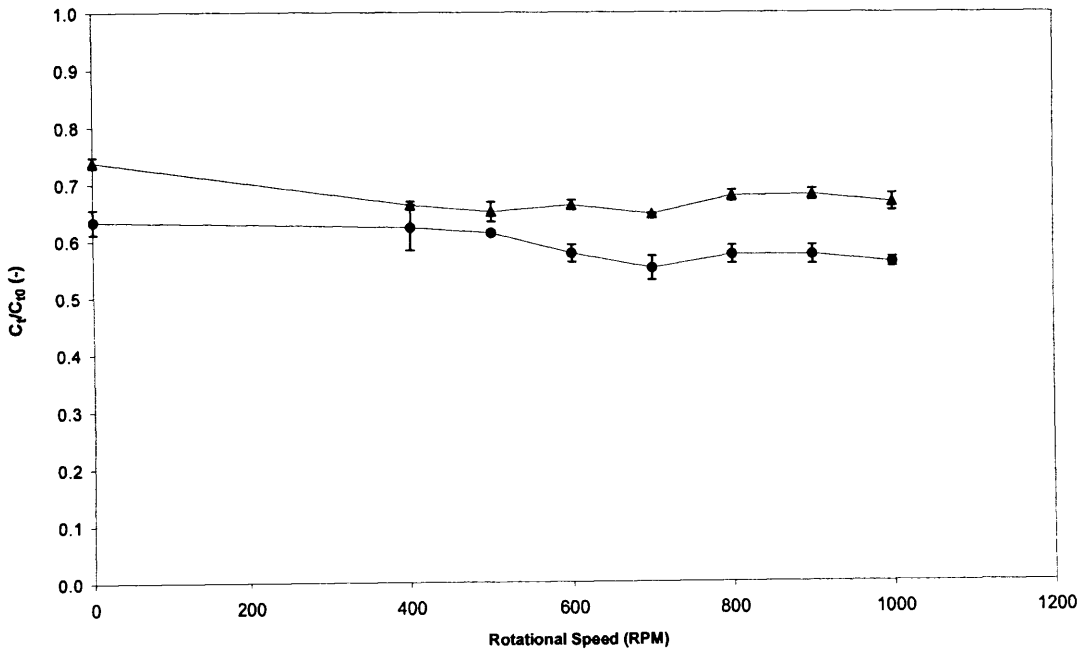

Figure 6.1. The effect of Thermomixer rotational speed on the adsorption of Fab' from clarified homogenate mixed for 0.5 min (•) and unclarified homogenate mixed for 1.0 min (▲). Feedstock ionic strength 3.4 mS/cm, pH 5.8. 200 µL feedstock contacted with 50 µL SP Sepharose FF (V_m/V_l = 0..25).

It is clear from Figure 6.1 that the adsorption of Fab' to SP Sepharose FF occurs rapidly and with little need for mixing. Mixing the clarified homogenate and adsorbent at 1,000 rpm for 0.5 min results in 44% of the available Fab' being adsorbed, compared to 37% with no mixing. 33% of available Fab' is adsorbed from the unclarified homogenate when mixed at 1,000 rpm for 1 min, as compared to 26% with no mixing. This finding confirms the results in Chapter 5 which suggested that the adsorption of Fab' to SP Sepharose FF was not mass transfer limited.

It is evident that at a phase ratio of 0.25 increasing the level of mixing beyond 500 rpm has no significant effect on the adsorption of Fab' from the unclarified homogenate. For the clarified homogenate this threshold occurs at 700 rpm. However, as this study will include experiments with higher phase ratios it was decided that a rotational speed of 1,000 rpm would be used for all microwell batch

adsorption experiments, in order to ensure complete suspension of the adsorbent and feedstock solutions.

6.2.1.2 *The effect of phase ratio*

Microwell batch adsorptions were performed as described in Section 2.4.1.5 at phase ratios ranging from 0.1 to 0.3 for the *E. coli* homogenate feedstock (Figure 6.2) and 0.01 to 0.03 for the lysate feed (Figure 6.3). As stated in Section 2.4.1.5 the lysate experiments were performed prior to the optimisation of the MWFP method.

As expected, increasing the phase ratio leads to an increased adsorption of Fab'. However, increasing the volume of adsorbent affects the suspension and mixing of the adsorbent and feedstock. At high phase ratios of 0.5 (results not shown) incomplete adsorbent suspension and Fab' adsorption was observed. Increasing adsorbent volume also affects the productivity of the adsorption process and the volume used must be selected with many factors being considered, such as the Fab' concentration, adsorbent binding capacity, and adsorbent cost.

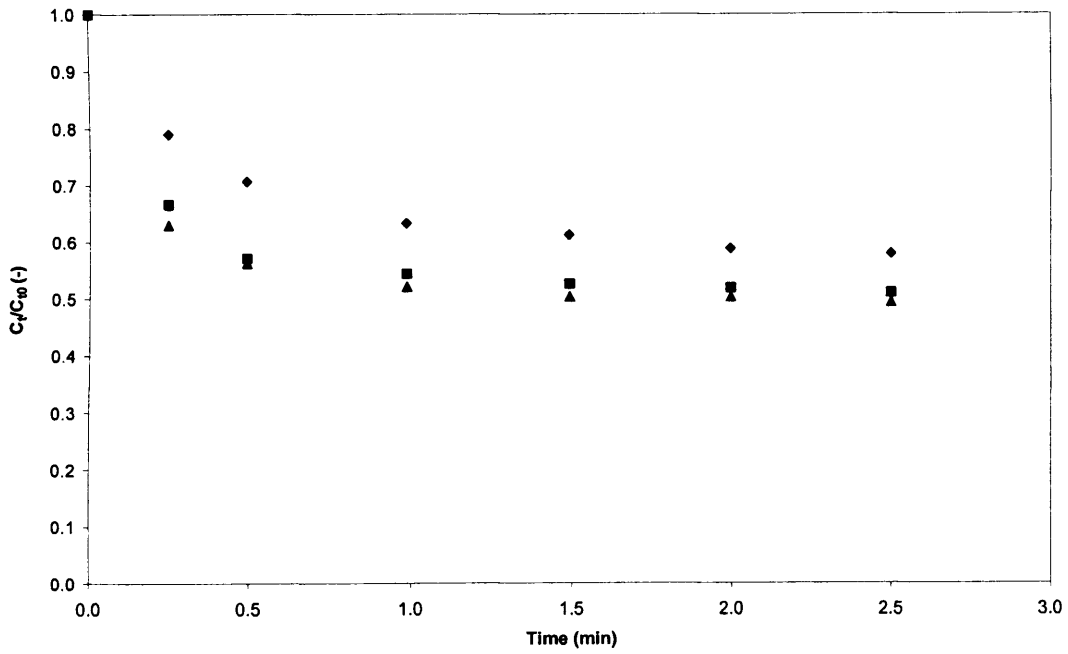

Figure 6.2. Fab' uptake curves for clarified homogenate at phase ratios of 0.1 (♦), 0.2 (■) and 0.3 (▲). Homogenate load volume 200 µL, 3.4 mS/cm, pH 5.8. Adsorptions performed in microwell filterplate mixed at 1,000 rpm on Thermomixer.

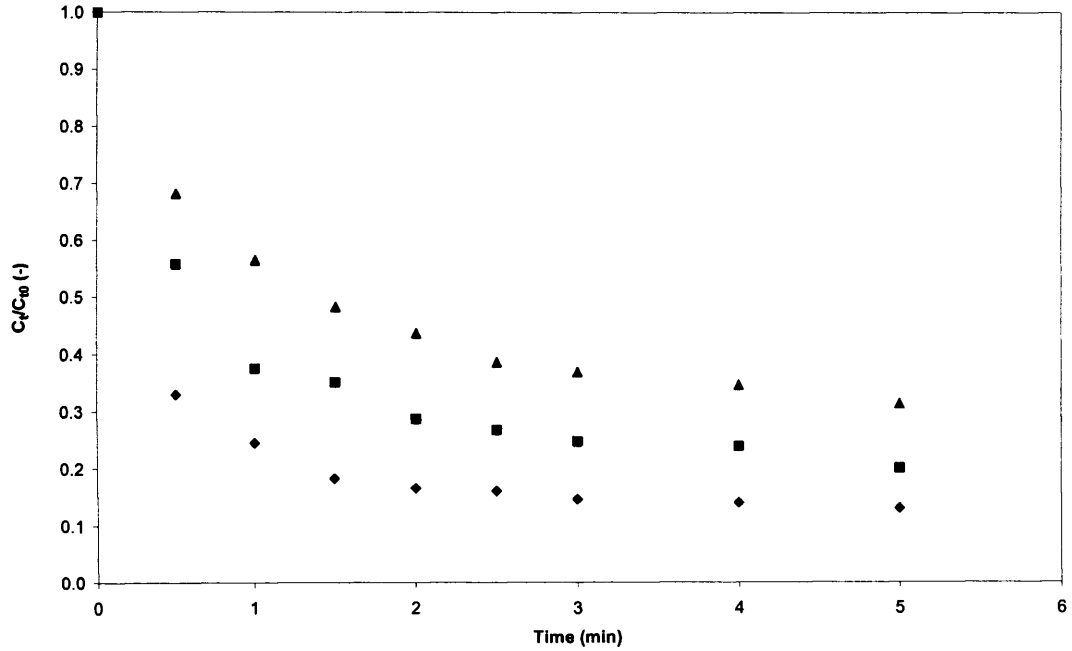

Figure 6.3. Fab' uptake curves for clarified lysate at phase ratios of 0.01 (▲), 0.02 (■) and 0.03 (●). Adsorbent volume 10 μL, 3.2 mS/cm, pH 5.5. Adsorptions performed in microwell filterplate mixed at 1,000 rpm on an Eppendorf Thermomixer.

6.2.1.3 The effect of feedstock solids concentration

The effect of solids concentration on the adsorption of Fab' from an unclarified homogenate feedstock is presented in Figure 6.4. Each data point in the figure is an individual batch adsorption and the error bars shown represent the standard deviation of three replicates. The presence of cell debris appears to affect slightly the initial rate of Fab' adsorption. However, after approximately 2 min the level of adsorption achieved in both the clarified and unclarified systems is almost identical. The delay in the rate of Fab' adsorption observed in the unclarified system is most likely to be caused by the blockage of binding sites by the cell debris particulates. This is to be expected as given a sufficient length of time and mixing Fab' molecules should come in to contact with adsorbent binding sites, despite any temporary blockage of sites caused by the cell debris. Figure 6.4 also highlights one of the advantages of batch adsorption systems, the rapid rate of adsorption, as the equilibrium appears to be reached within 2 min.

Figure 6.5 presents the partitioning of Fab' between the supernatant and cell debris when performed in batch mode using a microwell filterplate.

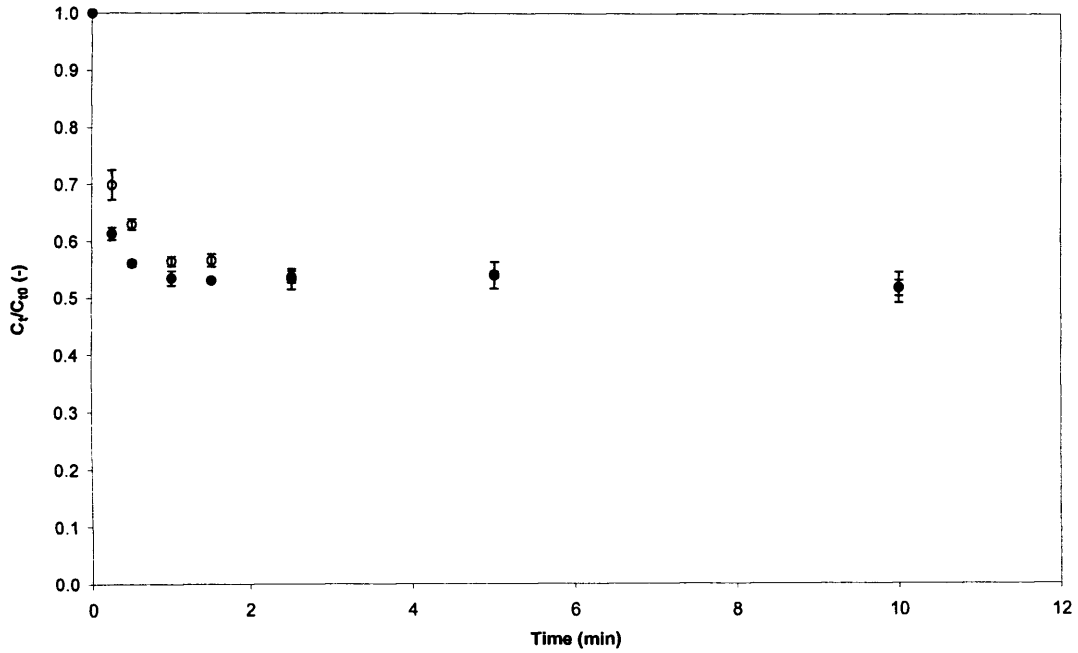

Figure 6.4. The adsorption of Fab' onto 60 µL SP Sepharose FF from a clarified (•) and unclarified (○) *E. coli* homogenate performed in batch mode using an 800 µL microwell filterplate. The homogenate ionic strength was 3.2 mS/cm and load volume of 200 µL ($V_m/V_l = 0.3$).

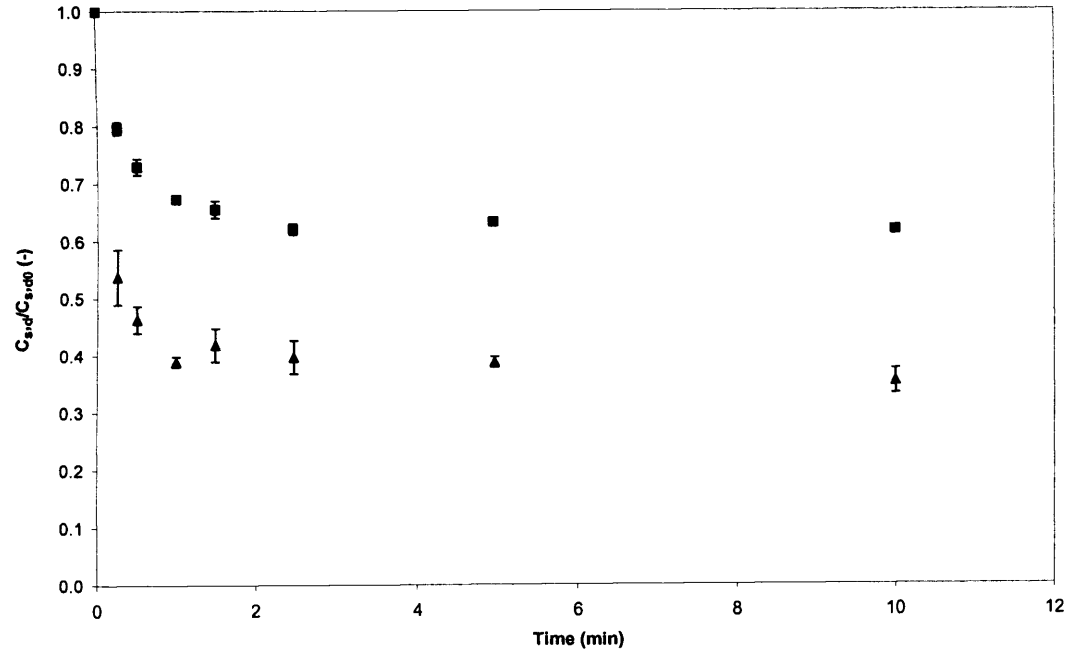

Figure 6.5. Comparing Fab' uptake from an unclarified homogenate feed with a solids concentration of 9.5% (ww/v). The supernatant (C_s) (■) and debris-bound (C_d) (▲) Fab' concentrations are shown as a function of time.

Figure 6.5 shows that debris-bound Fab' is recovered when the adsorption of Fab' from an unclarified homogenate is performed in batch mode. Prior to the addition of the adsorbent 37% of the total available Fab' was bound to the cell debris. At the end of the adsorption phase this had dropped to 26% confirming that the debris-bound Fab' was being partitioned to the adsorbent phase. At equilibrium approximately 75% of the debris-bound Fab' is removed from the debris. The equilibrium level is determined by many factors, such as the feedstock ionic strength and pH, as well as the adsorbent volume and equilibration conditions.

It is difficult to compare the partition of Fab' achieved in batch mode to that achieved in a packed bed column as the equilibrium obtained is not the same. Loading a column to saturation (100% product breakthrough) does not result in the same equilibrium as that achieved in a stirred tank. Adsorbent at equilibrium in a stirred tank may still contain many free binding sites and be far from saturated. However, any difference in the partitioning of Fab' observed between the two systems could be explained by the way the adsorbent and Fab' are contacted. Within the tightly packed structure of the packed bed the debris-bound Fab' may not be fully exposed to the binding sites on the adsorbent due to a shielding effect caused by neighbouring cell debris particulates. As a result of this it is possible that cell debris can flow through the packed bed having had very little, or no contact with the adsorbent. However, in a stirred tank there is more free space and vigorous mixing which ensures that the adsorbent and cell debris are well mixed and there is sufficient time and opportunity for adsorption. This would lead to greater level of partitioning of the Fab' from the cell debris.

This section has shown that it is possible to investigate the effect of feedstock properties and adsorption conditions using a microwell filterplate, using minimal volumes of valuable feedstock. Section 6.2.2 describes the scale-up of the experiments discussed in Section 6.2.1 using modified laboratory stirred tanks, and investigates the use of stirred tank batch adsorption as an alternative to packed bed column chromatography.

6.2.2 *Stirred tank batch adsorption*

As described in Section 2.4.3.1 two Amicon Stirred Cells, model 8050 (50 mL volume) and model 8200 (200 mL volume), (Millipore UK Ltd, Watford, UK) were modified to incorporate a stainless steel mesh instead of an ultrafiltration membrane. The mesh retains the adsorbent whilst allowing the buffers or feedstock to drain out of the stirred cell. The magnetic stirrer was replaced by a Eurostar Digital Overhead Stirrer (IKA Works, Inc, Wilmington, USA) and a custom made 4-blade pitched-blade impeller. The impeller diameter was designed to be 85% of the diameter of the stirred cell. This ratio was maintained when the stirred cell was scaled-up.

6.2.2.1 *Assessing the damage caused to adsorbent by agitator*

The mixing of the adsorbent-feedstock slurry using an overhead stirrer can damage the adsorbent particles. The use of magnetic stirrers is generally avoided when suspending chromatographic media as the adsorbents are prone to physical breakage and grinding. Table 6.1 summarises the results of a study investigating the damage caused by several laboratory impellers and a magnetic stirrer. No significant change in the particle size distribution of the adsorbent beads was observed. For reference purposes a sample of adsorbent was deliberately crushed. Figure 6.6 shows the particle size distribution of the fresh and crushed SP Sepharose FF. As expected, crushing the adsorbent beads produces a significant number of small particles. Since this feature was not seen during batch studies one can conclude that the adsorbent is extremely robust and mechanically stable.

Confirmation that the 4-blade pitched-blade impeller used in the batch adsorption experiments did not affect the particle size distribution of the adsorbent was achieved as described in Section 2.4.3.3. A 50% (v/v) slurry of the adsorbent was stirred in the 20 mL stirred tank for 2 min at stirrer speeds ranging from 100 to 1,000 rpm. The particle size distribution was then measured using the Malvern Mastersizer 2000 (Malvern Instruments, Worcestershire, UK). As expected, there was no significant effect on the particle size distribution. The d_{50} for the fresh adsorbent beads was

91.4 μm. The average d_{50} for the agitated adsorbent samples was found to be 91.6 μm with a standard deviation of 0.6 μm.

Table 6.1. The impeller type, stirrer speed and length of mixing used to assess the damage caused to adsorbent beads during agitation in a 20 mL stirred tank. The particle size distribution of the adsorbent, suspended in equilibration buffer, was measured at the time specified below.

Stirrer	Speed (RPM)	Time (min)
6-blade Rushton	1,500	80
3-blade Marine	1,500	80
4-blade Pitched-blade	1,000	15
Magnetic	Level 8	25

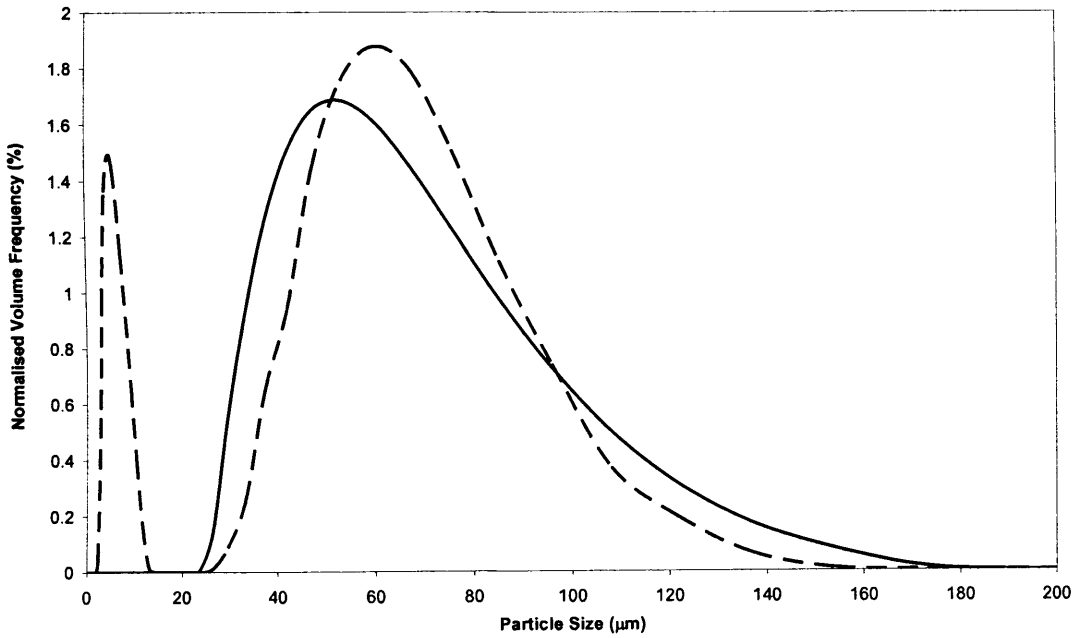

Figure 6.6. The particle size distribution of fresh (—) and crushed (---) SP Sepharose FF.

6.2.2.2 The effect of agitation on Fab' adsorption

Figure 6.7 shows the effect of increasing stirrer speed on the adsorption of Fab' from an unclarified *E. coli* lysate feedstock, to SP Sepharose FF at a phase ratio of 0.3. The unclarified lysate was mixed at stirrer speeds ranging from 50-500 rpm for 2 min before being separated from the adsorbent by vacuum filtration and collected in a

collection plate. As this particular experiment was performed before the method of total available Fab' measurement was developed, only the supernatant Fab' concentration was measured, and is shown in Figure 6.7. It is clear to see that increasing the stirrer speed from 50 to 150 rpm leads to an increase in the degree of Fab' adsorbed from the supernatant. Beyond this point, an increase in stirrer speed did not significantly affect the degree of Fab' adsorption. Due to these findings the stirrer speed for all stirred tank batch adsorptions was fixed at 300 rpm.

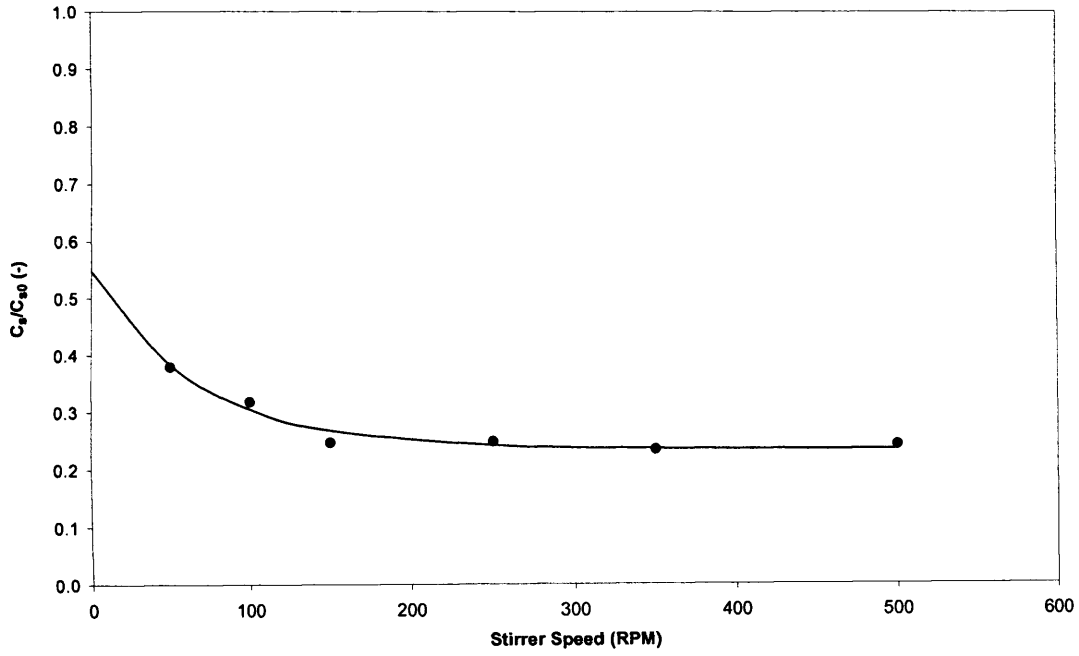

Figure 6.7. The effect of stirrer speed on the batch adsorption of Fab' from an unclarified *E. coli* lysate of 10% solids (ww/v), at pH 5.6 and ionic strength of 3.1 mS/cm. 1.5 mL SP Sepharose FF was mixed with 15 mL of lysate (V_m/V_l = 0.3) using a 4-blade pitched-blade impeller for 2 min at stirrer speeds ranging from 50 to 500 rpm.

6.2.2.3 The effect of phase ratio

The effect of phase ratio on the adsorption of Fab' from an unclarified *E. coli* homogenate is presented in Figure 6.8. As described in Section 2.4.3.5 15 mL of the homogenate feedstock was mixed with 1.5, 4.5 and 7.5 mL SP Sepharose FF, giving phase ratios of 0.1, 0.3 and 0.5 respectively. Figure 6.8 shows that the initial rate of adsorption is affected by the adsorbent volume, however, the highest initial rate of adsorption was achieved when the phase ratio was 0.3, and not 0.5 as expected. This

was attributed to the difficulty in mixing and fully suspending such a high slurry concentration. However, once the adsorbent is fully suspended and the slurry is well mixed the greatest degree of Fab' adsorption is achieved at a phase ratio of 0.5.

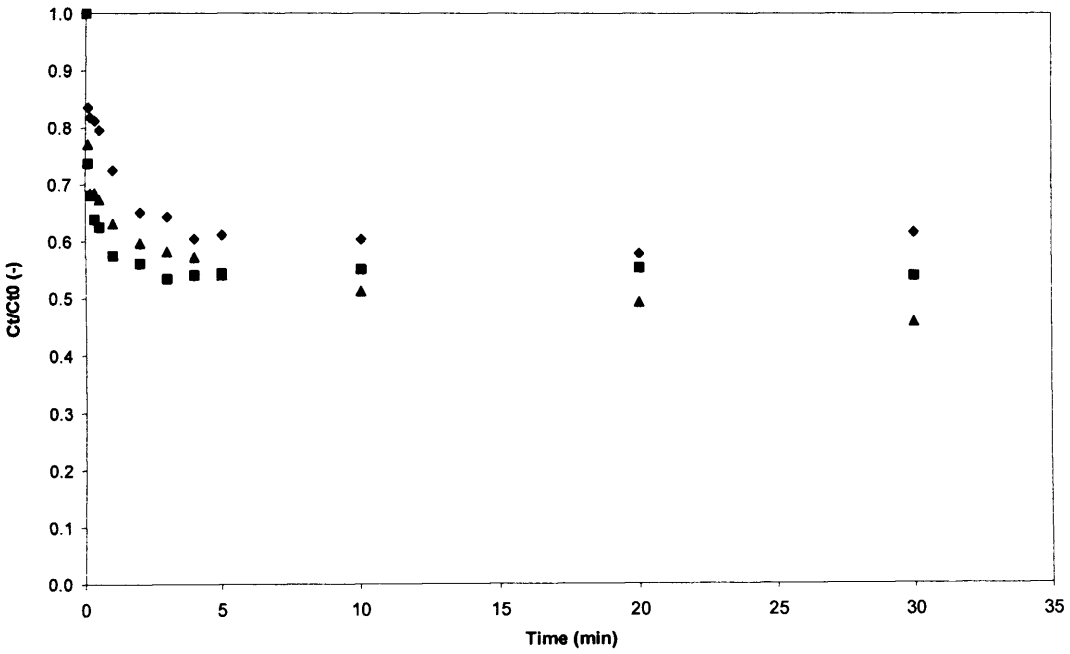

Figure 6.8. The effect of phase ratio on the batch adsorption of Fab' from an unclarified *E. coli* homogenate onto SP Sepharose FF. 15 mL homogenate of 9.5% (ww/v) solids concentration and ionic strength 3.2 mS/cm mixed with 1.5, 4.5 and 7.5 mL adsorbent, giving phase ratios of 0.1 (♦), 0.3 (■) and 0.5 (▲), mixed with a 4-blade pitched-blade impeller stirred at 300 rpm.

Figure 6.9 shows the complete batch adsorption process performed in the 20 mL stirred tank. As described in Section 2.4.3.2 15 mL of unclarified homogenate was mixed with 4.5 mL SP Sepharose FF, giving a phase ratio of 0.3. At the end of the adsorption phase the feedstock was drained from the stirred tank and discarded. (In an optimised industrial system this could be recycled with fresh adsorbent to recover the remainder of the Fab'. This was not within the scope of this study and therefore not deemed necessary.) Once the homogenate had been drained 3 buffer volume (BV) washes using 20 mM Sodium Acetate were performed to remove cell debris and unbound contaminants prior to elution. In order to assay the homogenate Fab' concentration samples of the slurry were removed at certain time intervals, therefore reducing the total system volume. As a result the volume of elution buffer used was calculated based on the initial volume less that removed for assaying. In this specific

case 12.8 mL of 1 M NaCl was used to elute the Fab' from the adsorbent. Figure 6.9 shows that 49% of the available Fab' was bound by the adsorbent, and of the Fab' bound, 89% was recovered. Therefore, the overall yield was 43%. Yields achieved in batch adsorption are typically lower than that of a packed bed column and protein capture is often incomplete as the adsorption approaches equilibrium (Chase, 1994).

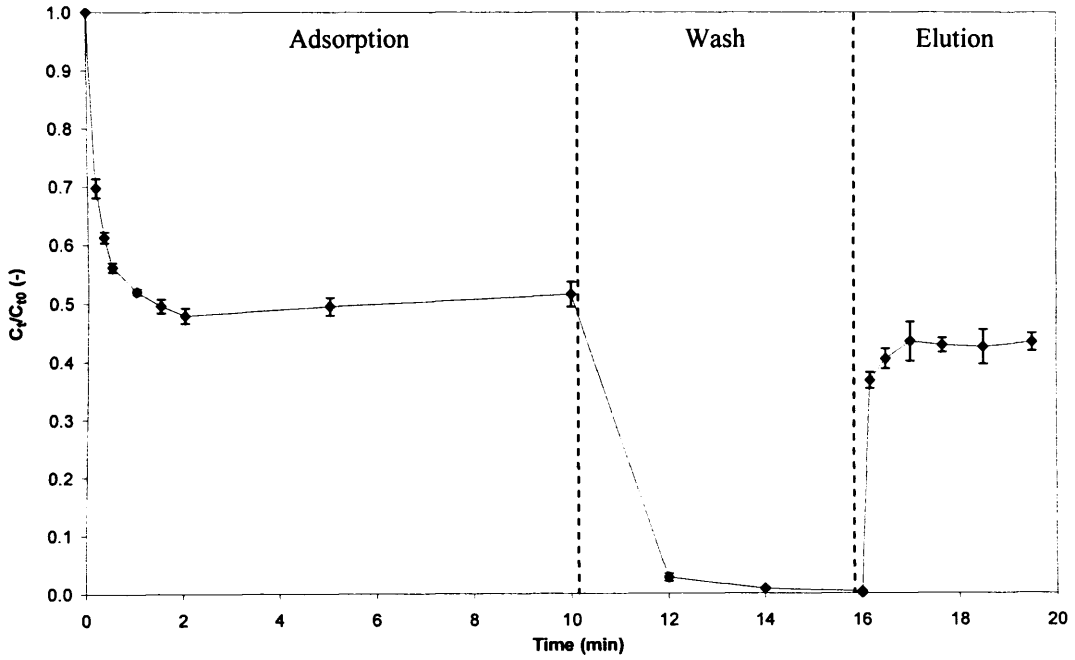

Figure 6.9. The complete Fab' adsorption process performed in a 20 mL stirred tank. 15 mL of unclarified homogenate, 9.5% (ww/v) solids concentration, pH 5.8, ionic strength 3.2 mS/cm, contacted with 4.5 mL SP Sepharose FF ($V_m/V_l = 0.3$) using a 4-blade pitched-blade impeller at 300 rpm. Three batch volume (3 x 1 BV) washes performed prior to elution with 12.8 mL 1 M NaCl. Wash and elution stages also mixed at 300 rpm with 4-blade pitched-blade impeller.

6.2.2.4 The effect of feedstock solids concentration

Stirred tank batch adsorption using the 20 mL stirred tank were performed as described in Section 2.4.3.6 and the results shown in Figure 6.10. 15 mL of the clarified and unclarified homogenate feedstock were mixed with 4.5 mL of adsorbent (phase ratio 0.3) at 300 rpm with a 4-blabe pitched-blade impeller. It is clear from Figure 6.10 that the presence of cell debris affects the initial rate of Fab' adsorption, but does not significantly affect the overall degree of Fab' adsorption.

Figure 6.10 shows an unexpected uptake profile for the clarified homogenate system, where a sharp drop in the supernatant Fab' concentration is followed by a gradual

rise to an equilibrium concentration which appears to be similar to that of the unclarified system. A possible explanation for this rise in Fab' concentration with time could be a displacement effect similar to that observed in the packed bed chromatography experiments. However, in this case the displacement is not caused by components migrating through the packed bed at different rates, but possibly due to the difference in the rate at which various components diffuse into the pores of the adsorbent. It is possible that in the case of the clarified feedstock Fab' binds rapidly, occupying available binding sites. The component which causes Fab' to be displaced may be a molecule with a higher affinity, however due its size and charge does not diffuse as fast as Fab', resulting in a delay in Fab' displacement. Possible reasons for the displacement being observed only in the clarified feed include the fact that the initial Fab' adsorption is hindered by the presence of cell debris and insufficient mixing of the slurry. However, after 5 min both the clarified and unclarified systems appear to have reached a similar equilibrium, indicating that the presence of the cell debris does not significantly hinder the overall degree of Fab' adsorption.

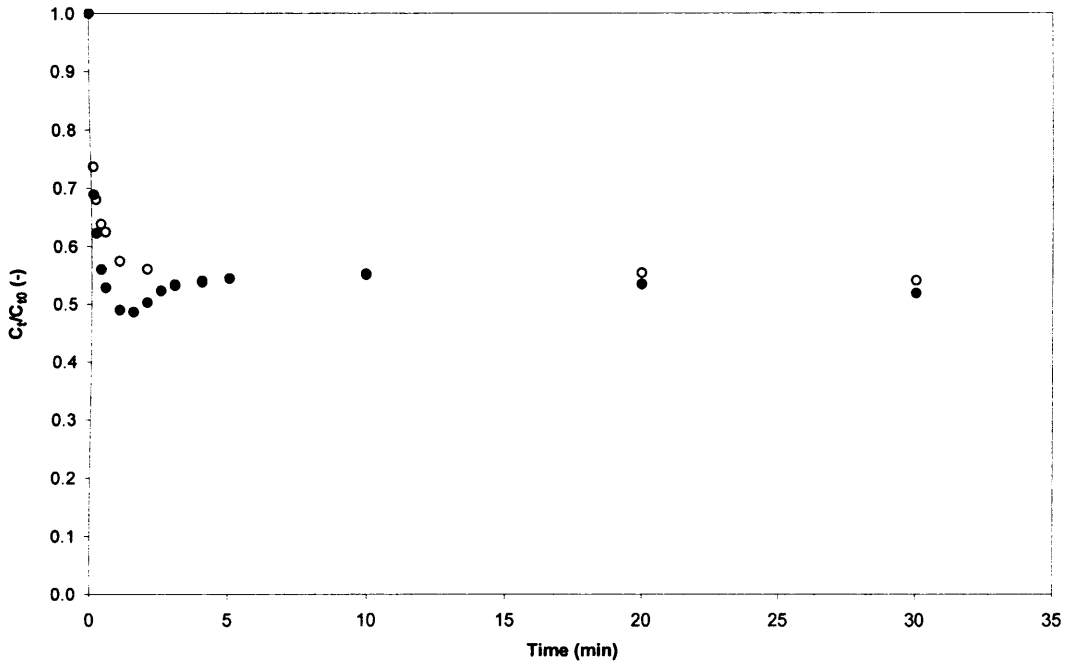

Figure 6.10. The effect of solids concentration on the adsorption of Fab' from a clarified (•) and unclarified (○) (9.5% (ww/v) solids concentration) homogenate. Adsorption performed in a 20 mL stirred tank. 15 mL of homogenate, pH 5.8, ionic strength 3.2 mS/cm contacted with 4.5 mL SP Sepharose FF ($V_m/V_l = 0.3$) using a 4-blade pitched-blade impeller at 300 rpm.

Figure 6.11 shows the partitioning of Fab' when purified from an unclarified homogenate in a 20 mL stirred tank. At the start of the adsorption stage 34% of the total available Fab' was bound to the cell debris. This then dropped to 22% when the adsorption was complete. In this case the debris-bound Fab' concentration fell by 64%.

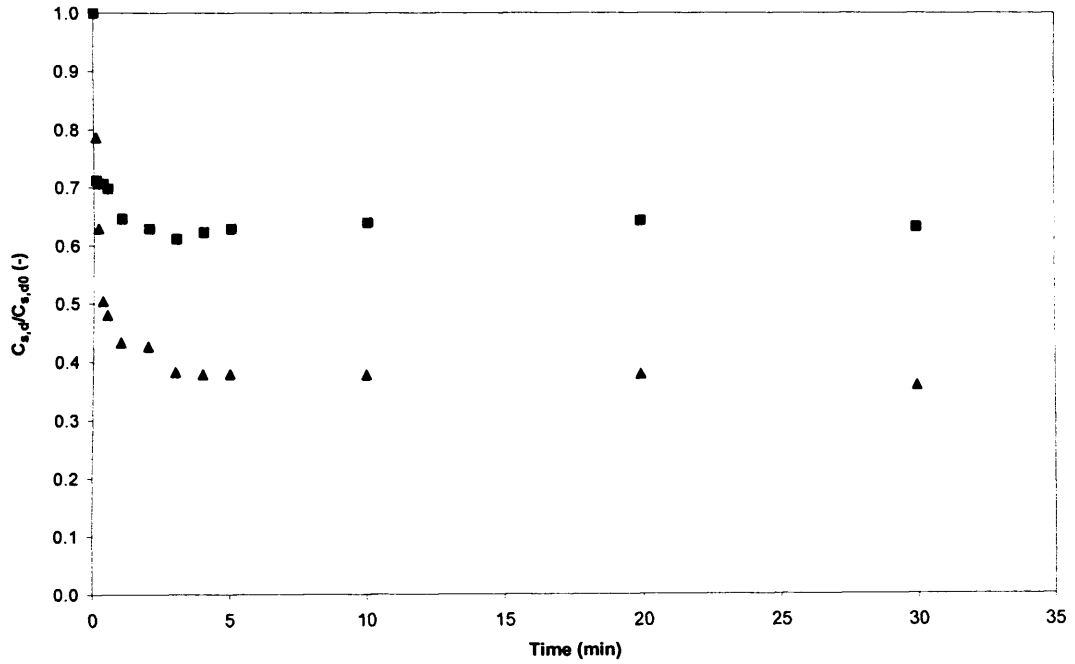

Figure 6.11. The partitioning of Fab' during stirred tank batch adsorption of an unclarified homogenate feedstock of 9.5% (ww/v) solids concentration, pH 5.8 and ionic strength 3.2 mS/cm. The dimensionless supernatant (■) and debris-bound (▲) Fab' concentrations are shown as a function of adsorption time. 15 mL homogenate mixed with 4.5 mL adsorbent at 300 rpm.

As with the results of the microwell filterplate adsorptions it is surprising to see the debris-bound Fab' concentration falls more than that of the supernatant Fab' concentration. One would expect Fab' free in solution to be bound preferentially, as was the case in the packed bed columns where the adsorption of supernatant Fab' was greater than that of debris-bound Fab'. It is not possible to determine if the Fab' being removed from the cell debris is being bound directly to the adsorbent, or if it is being pulled back into solution as a result of the supernatant Fab' concentration falling as Fab' is bound by the adsorbent. It is quite likely that Fab' is going back into solution to adjust the equilibrium position between the supernatant, debris and adsorbent. As discussed previously, the position of equilibrium is affected by many

factors, including the feedstock ionic strength and adsorbent volume. Figure 6.12 presents the effect of phase ratio on the recovery of debris-bound Fab' from an *E. coli* homogenate. It is clear that beyond a certain phase ratio, an increase in adsorbent volume no longer improves the recovery of debris-bound Fab'. When this result is considered with the results presented in Figure 6.8 it is evident that increasing the phase ratio from 0.3 to 0.5 does not significantly improve the adsorption of Fab' from an unclarified homogenate. Such an increase in the phase ratio would have a significant affect on the throughput of the purification process and results such as these would aid in the design of an adsorption process. (The impact of phase ratio and solids concentration on the throughput of the process is described in further detail in Chapter 7.)

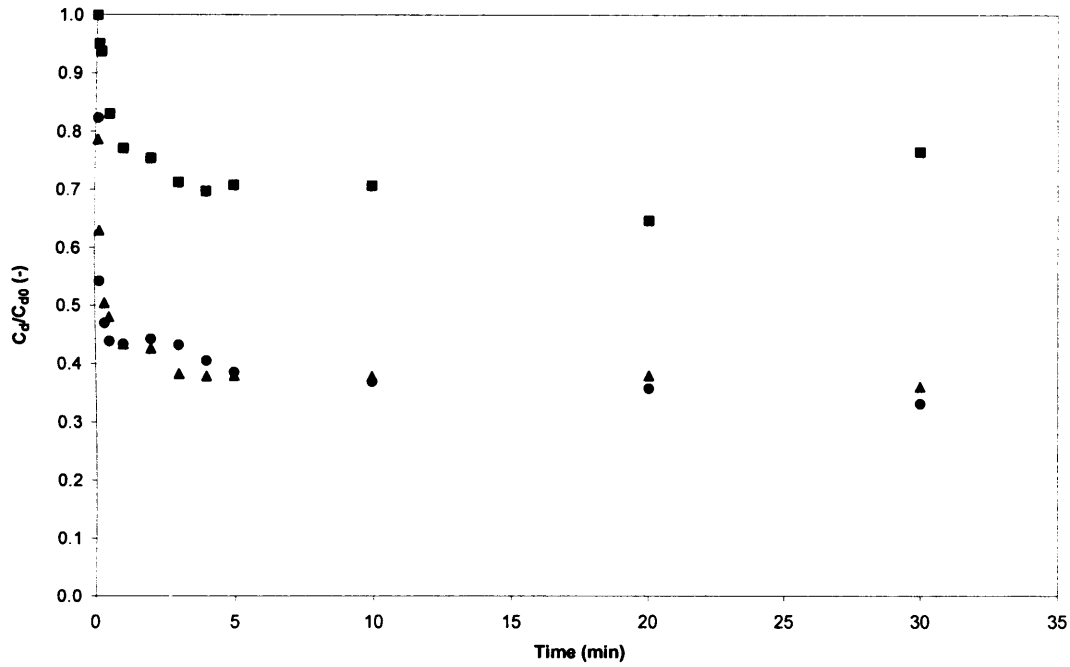

Figure 6.12. The effect of phase ratio on the liberation of debris-bound Fab' from an unclarified *E. coli* homogenate of 9.5% (ww/v) solids concentration and ionic strength 3.2 mS/cm, at phase ratios of 0.1 (■), 0.3 (▲) and 0.5 (●).

Adsorption of Fab' from a clarified and unclarified *E. coli* lysate was performed in a 20 mL stirred tank as described in Section 2.4.3.6. The effect of solids concentration on the batch adsorption of Fab' is presented in Figure 6.13. The presence of cell debris significantly affects Fab' adsorption, as can be seen by the difference in the

uptake curves between the clarified and unclarified feedstocks. The effect of solids concentration on the adsorption of Fab' has been described previously.

When comparing the effect of solids concentration on the batch adsorption of Fab' from the clarified and unclarified feedstocks, it is important to note that the Fab' concentration of the lysate is approximately 30% of that of the homogenate. This, along with the fact that the lysate contains fewer contaminants, may explain why complete Fab' adsorption was achieved in the clarified lysate. As the phase ratio for both the homogenate and lysate stirred tank systems was the same, 0.3, the same volume of adsorbent was challenged with a lower mass of Fab', therefore resulting in a lower dimensionless concentration at equilibrium. The equilibrium was achieved after 1 min in the case of the clarified lysate, compared to 3 min for the unclarified.

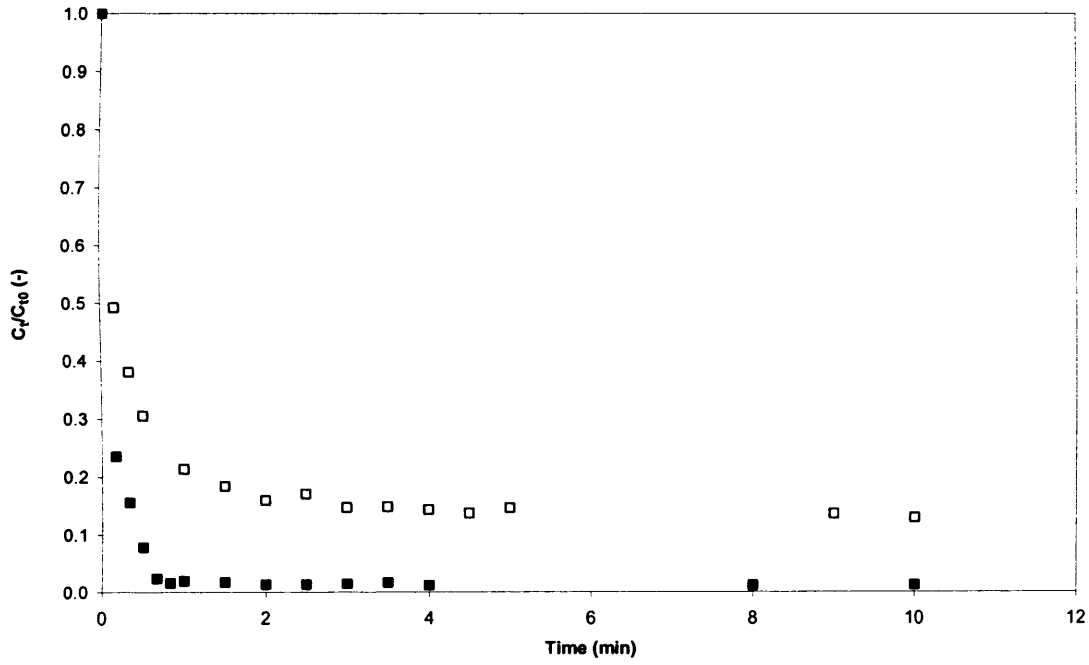

Figure 6.13. The effect of solids concentration on the adsorption of Fab' from a clarified (•) and unclarified (○) (7% solids concentration (ww/v)) *E. coli* lysate. Adsorption performed in a 20 mL stirred tank. 15 mL of lysate, pH 5.5, ionic strength 3.4 mS/cm contacted with 4.5 mL SP Sepharose FF (V_m/V_l = 0.3) using a 4-blade pitched-blade impeller at 300 rpm.

6.2.2.5 The effect of feedstock ionic strength

Unclarified homogenate at a range of ionic strengths was used to obtain uptake curves for the adsorption of Fab' using a 20 mL stirred tank as described in

Section 2.4.3.6. Figure 6.14 shows the effect of feedstock ionic strength on the adsorption of Fab' from an unclarified *E. coli* homogenate at 3.2, 5.0 and 8.5 mS/cm. As expected, the adsorption of Fab' is significantly affected by ionic strength, and an increase in the feedstock ionic strength leads to a decrease in the adsorption performance. These results are in agreement with the findings of the equilibrium isotherm and packed bed studies discussed in Chapter 4 and Chapter 5 respectively.

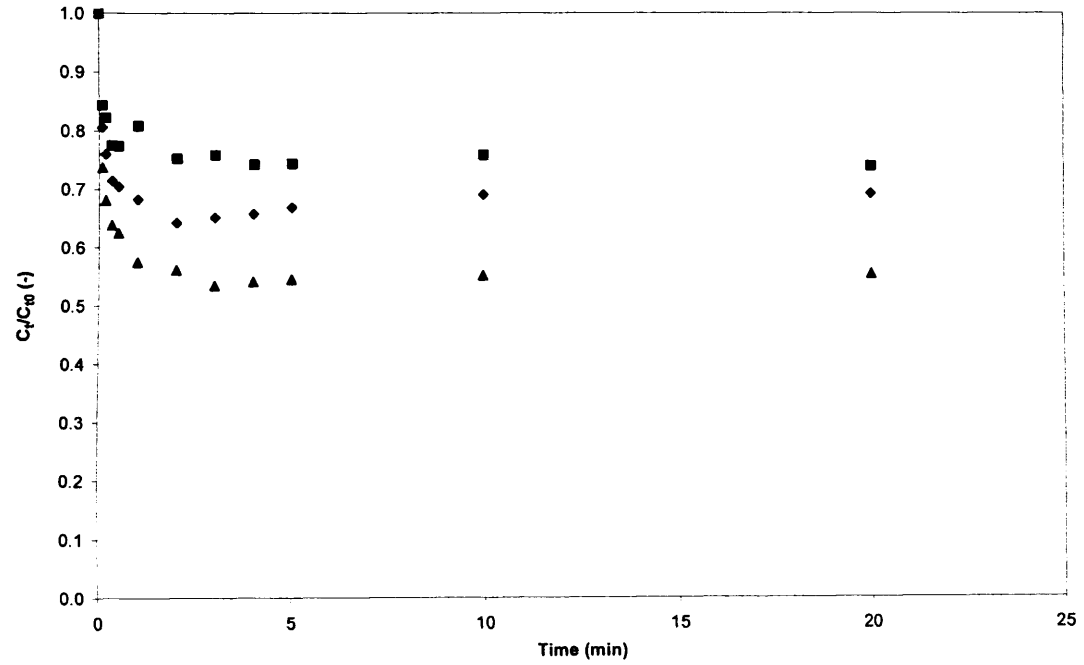

Figure 6.14. The effect of feedstock ionic strength on the adsorption of Fab' from an unclarified *E. coli* homogenate at 3.2 (▲), 5.0 (♦) and 8.5 (■) mS/cm, pH 5.8 and solids concentration of 9.5% (ww/v). 15 mL of feedstock was mixed at 300 rpm using a 4-blade pitched-blade impeller with 4.5 mL adsorbent ($V_m/V_l = 0.3$).

6.2.2.6 Geometric scale-up of stirred tank batch adsorption

Stirred tank batch adsorptions were performed using a modified 200 mL stirred cell, as described in Section 2.4.3.7. In order to allow a direct comparison with the small scale stirred tank (20 mL) the phase ratio and impeller to tank diameter ratio were kept constant. The rate of agitation, type of agitator and equilibration conditions were kept constant when scaling up to the 200 mL stirred tank. Figure 6.15 shows the complete process for the adsorption of Fab' from an unclarified *E. coli* homogenate, performed in the 200 mL stirred tank. Due to volume limitations a 9-fold scale-up

was performed, using 135 mL of homogenate, contacted with 40.5 mL of adsorbent and mixed at 300 rpm with a 4-blade pitched-blade impeller. In this case the adsorption stage was allowed to continue to ensure that the equilibrium was achieved. As a purification process it would be more efficient to drain the feedstock and stop the adsorption after approximately 5 min when the initial period of adsorption appears to plateau. There is some evidence of the displacement effect observed previously in the clarified homogenate, as discussed in Section 6.2.2.4.

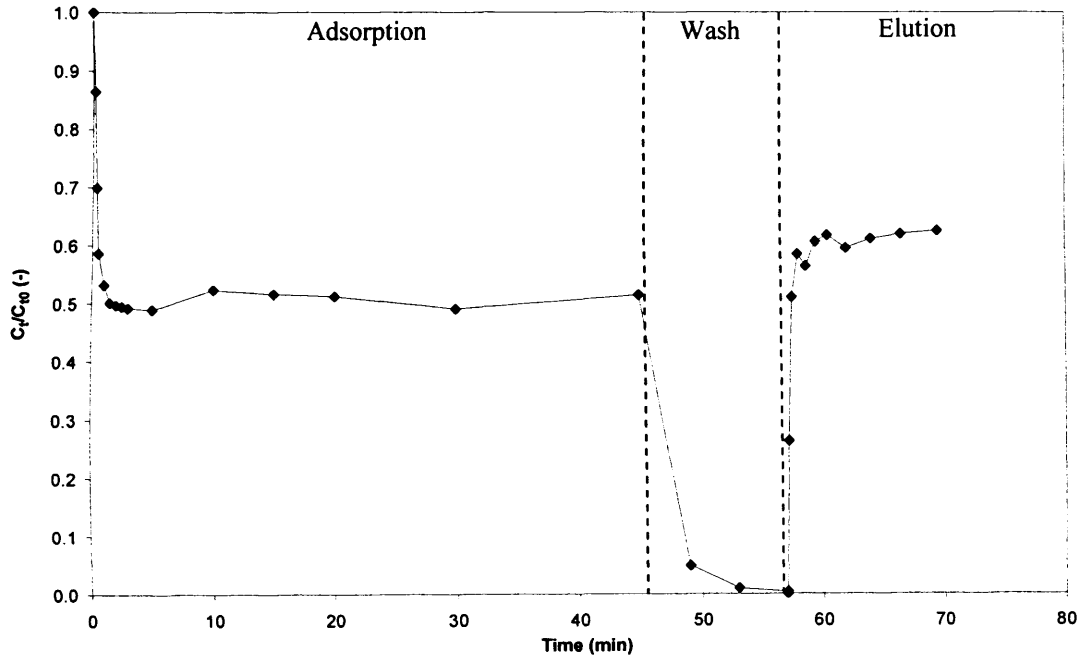

Figure 6.15. The complete Fab' adsorption process performed in a 200 mL stirred tank. 135 mL of unclarified homogenate, 9.5% solids concentration (ww/v), pH 5.8, ionic strength 3.2 mS/cm, contacted with 40.5 mL SP Sepharose FF (V_m/V_l = 0.3) using a 4-blade pitched-blade impeller at 300 rpm. Three 100 mL washes performed prior to elution with 120 mL 1 M NaCl. Wash and elution stages also mixed at 300 rpm with 4-blade pitched-blade impeller.

Figure 6.16 compares Fab' uptake curves for clarified and unclarified homogenate, performed in the 200 mL, scaled-up, stirred tank. The displacement effect is once again evident in the clarified homogenate uptake curve, however, after an extended period of adsorption the equilibrium achieved by both feedstocks is almost identical. 46% of the available Fab' was adsorbed from the clarified feedstock, compared to 49% in the unclarified. This result shows that the presence of cell debris does not affect the overall equilibrium and adsorption of Fab' from an *E. coli* homogenate.

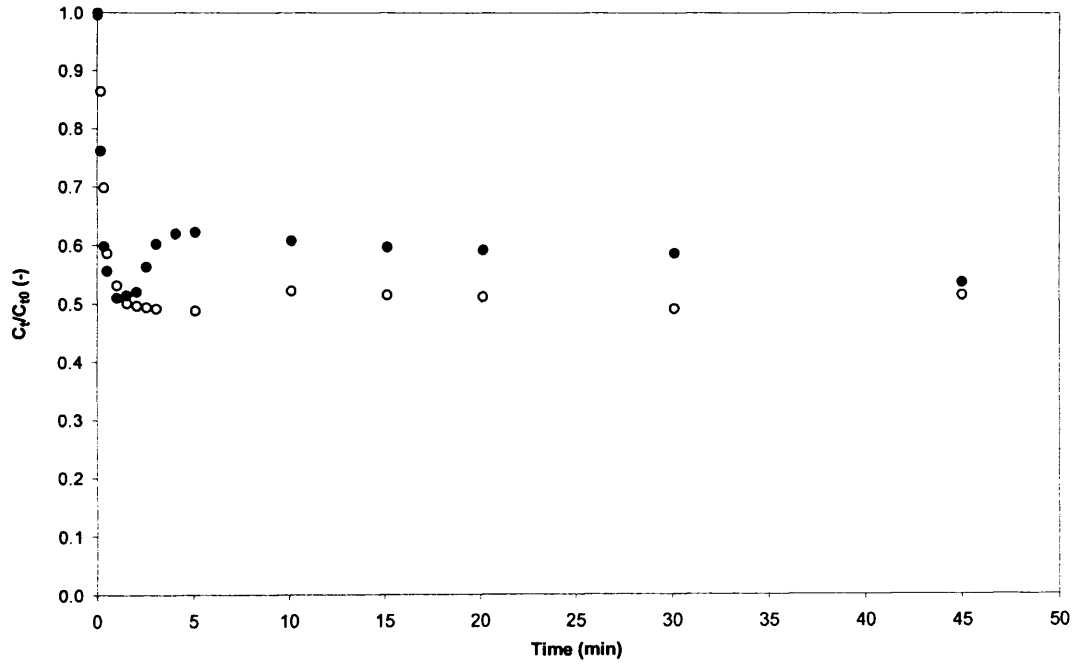

Figure 6.16. The effect of solids concentration on the stirred tank batch adsorption of Fab' onto SP Sepharose FF performed in a 200 mL stirred tank. 135 mL of clarified (•) and unclarified (○) homogenate, 9.5% solids concentration (ww/v), pH 5.8 and ionic strength 3.2 mS/cm, contacted with 40.5 mL SP Sepharose FF ($V_m/V_l = 0.3$) using a 4-blade pitched-blade impeller at 300 rpm.

Comparing the uptake curves of the 15 and 135 mL (feedstock load volume) stirred tank batch adsorptions shows that the geometric scale-up of this process is achievable and the uptake curves show good agreement. The first 10 min of the adsorption phase of the capture of Fab' from the clarified and unclarified homogenate feedstocks at both scales is presented in Figure 6.17 and Figure 6.18, respectively. For both the clarified and unclarified feedstocks the rate of Fab' adsorption, as well as the equilibrium, is almost identical at both scales, indicating that the scale-up rules used in this study lead to a successful scale-up of this purification scheme. The time taken to achieve equilibrium is also identical between the two scales of stirred tank tested. This would indicate that following these scale-up rules it would be possible to achieve large scale Fab' adsorption within the same length of time. This would give the stirred tank batch adsorption system a significant advantage over a process stream utilising packed bed chromatography. Chapter 7 compares process streams utilising either packed bed chromatography or stirred tank batch adsorption in detail.

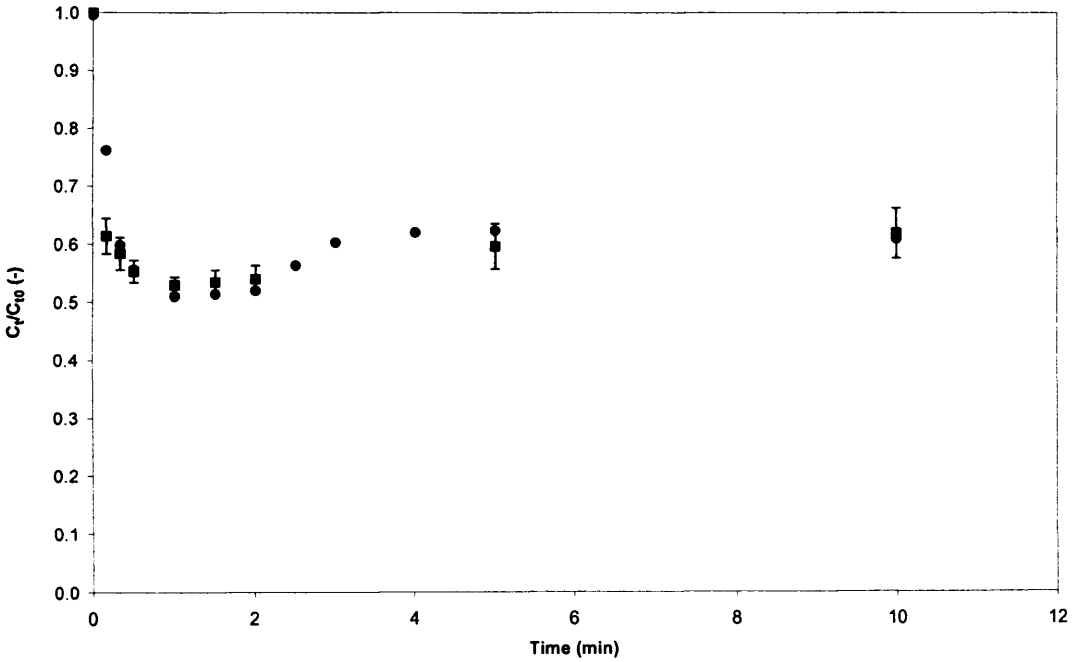

Figure 6.17. The scale-up of stirred tank batch adsorption of Fab' from clarified homogenate onto SP Sepharose FF performed in a 20 (■) and 200 (●) mL stirred tank. 15 and 135 mL of feed, pH 5.8 and ionic strength 3.2 mS/cm, contacted with 4.5 and 40.5 mL SP Sepharose FF, respectively, (V_m/V_l = 0.3) using a 4-blade pitched-blade impeller at 300 rpm.

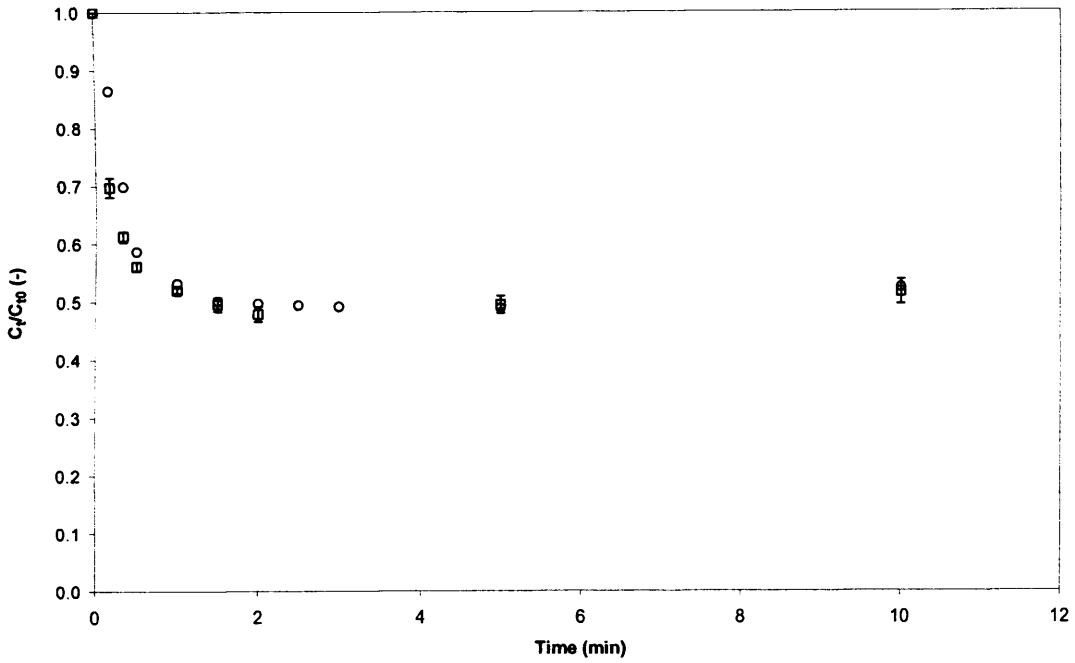

Figure 6.18. The scale-up of stirred tank batch adsorption of Fab' from unclarified homogenate onto SP Sepharose FF performed in a 20 (□) and 200 (○) mL stirred tank. 15 and 135 mL of feed, 9.5% solids concentration (ww/v), pH 5.8 and ionic strength 3.2 mS/cm, contacted with 4.5 and 40.5 mL SP Sepharose FF, respectively, (V_m/V_l = 0.3) using a 4-blade pitched-blade impeller at 300 rpm.

6.2.3 *Comparing microwell and laboratory scale stirred tank adsorption*

The objective of this chapter was to investigate the use of stirred tank batch adsorption as an alternative to column chromatography for the purification of Fab' from unclarified feedstocks. In addition, microwell batch adsorptions were used to investigate the effect of feedstock properties on the adsorption of Fab' and rapidly provide experimental data which can be used to design purification schemes, using minimal volumes of the potentially valuable, and limited, product. It is therefore essential to assess the microwell predictions and compare the results to those of the laboratory stirred tank used in this study. Figure 6.19 compares the first 10 min of the uptake curves for the microwell filterplate and 200 mL stirred tank batch adsorptions of Fab' from a clarified *E. coli* homogenate. The initial phase of the adsorption is almost identical, with both systems reaching approximately 50% adsorption after 2 min. At this point the displacement effect observed in the stirred tank leads to an increase in the unbound Fab' concentration. The displacement effect is not observed in the microwell batch adsorptions. The final equilibrium achieved in the microwell and stirred tank adsorptions shows a difference of only 2%.

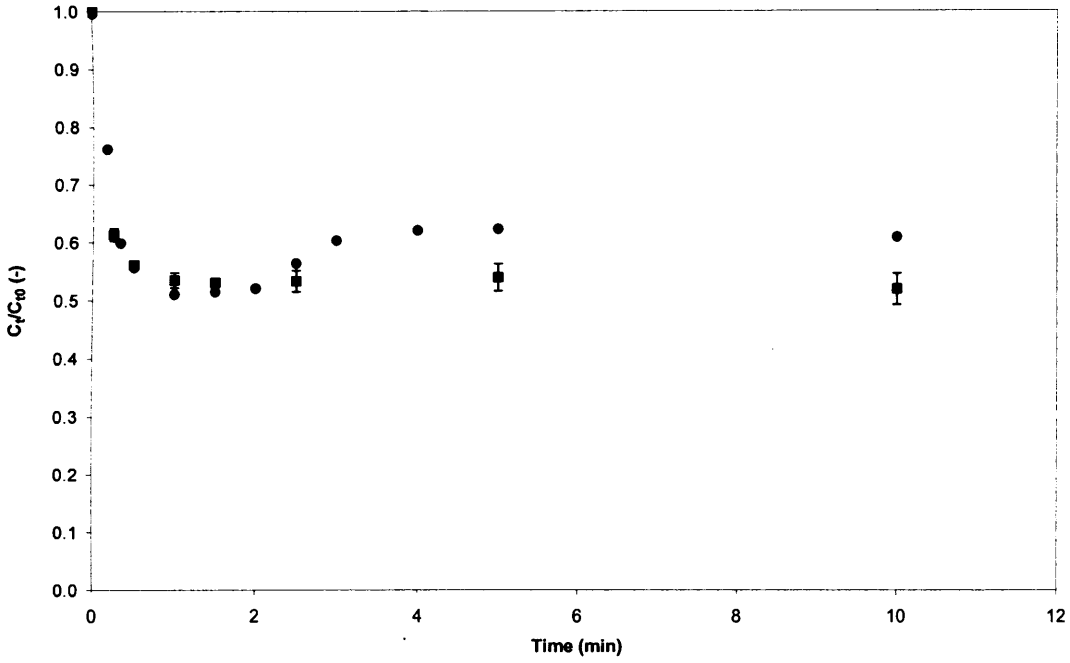

Figure 6.19. The scale-up of batch adsorption of Fab' onto SP Sepharose FF performed in a 0.8 mL microwell (■) and 200 mL stirred tank (●). 0.2 and 135 mL of clarified homogenate, pH 5.8 and ionic strength 3.2 mS/cm, contacted with 0.06 and 40.5 mL SP Sepharose FF, respectively, ($V_m/V_l = 0.3$).

Figure 6.20 presents the first 10 min of the uptake curves for the microwell filterplate and 200 mL stirred tank batch adsorptions of Fab' from an unclarified homogenate feedstock. In this case the initial rate of adsorption is slightly different, with the rate of Fab' adsorption being greater in the stirred tank. This is likely to be due to the difference in the way the systems are mixed. It is likely that mixing and suspending the unclarified feed-adsorbent slurry is more challenging in the microwell filterplate, as opposed to the stirred tank mixed with a pitched-blade impeller. The Fab' concentration for both systems after 10 min is identical and the equilibrium concentration in the 200 mL stirred tank only differs by 1%. Therefore, it is clear to see that it is possible to increase the feedstock load volume from 0.2 to 135 mL, which represents a 675-fold scale up, and achieve the same degree of adsorption, allowing the accurate prediction of the behaviour of a stirred tank batch adsorption using a microwell filterplate.

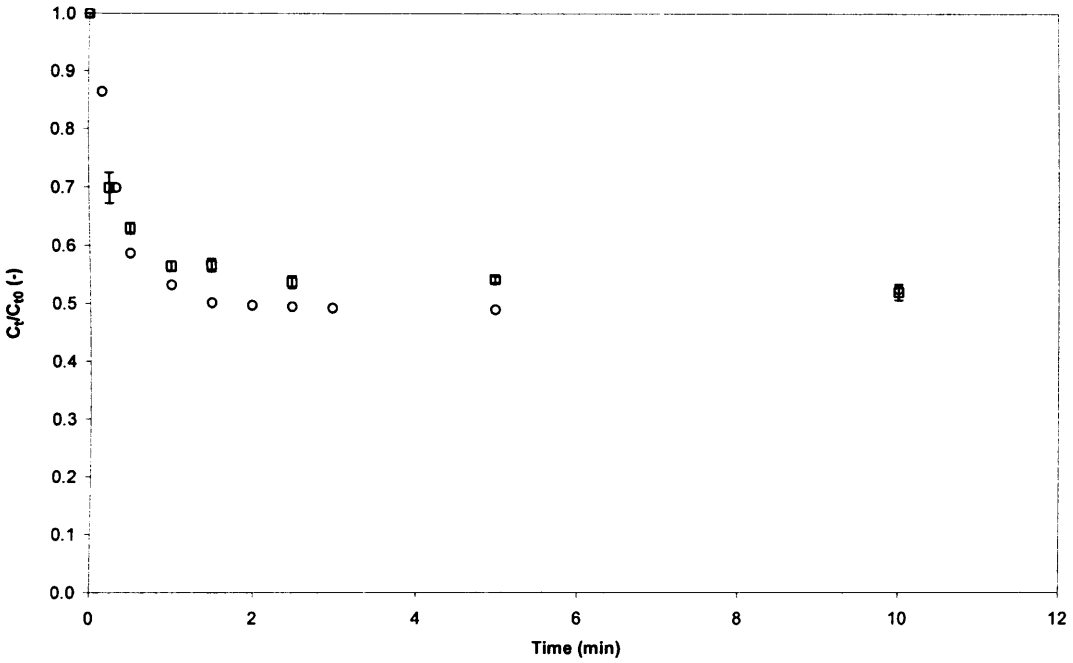

Figure 6.20. The scale-up of batch adsorption of Fab' onto SP Sepharose FF performed in a 0.8 mL microwell (□) and 200 mL stirred tank (○). 0.2 and 135 mL of unclarified homogenate, pH 5.8 and ionic strength 3.2 mS/cm, contacted with 0.06 and 40.5 mL SP Sepharose FF ($V_m/V_l = 0.3$), respectively.

6.3 Summary

The use of stirred tank batch adsorption as an alternative to packed bed chromatography has been evaluated in this chapter. Although the conditions for adsorption were not optimised, the use of batch adsorption was shown to be a viable alternative to conventional packed beds for the recovery and initial purification of Fab' from unclarified feedstocks. The advantages of using batch adsorption, which include the potential removal of all feedstock pre-treatment steps prior to purification, could possibly lead to improved process efficiency. The use of microwell plates as an ultra scale-down tool for the development of batch adsorption systems was shown to be feasible and scaleable to laboratory scale stirred tanks.

The results from Chapters 4, 5 and 6 can be used to generate Windows of Operation which can be used by design engineers to select operating variables which result in predetermined process performance criteria being achieved. The generation and use of such Windows of Operation is now discussed in Chapter 7.

7 A comparison and visualisation of the performance of various process options for the primary recovery and initial capture of Fab' using Windows of Operation

Abstract

The use of computer aided process design has become increasingly common and important in the biopharmaceutical industry. The need for improved and accelerated process development has lead manufacturers to use process simulation and optimisation tools to evaluate process options.

Using the model developed in Chapter 4 and the experimental observations made throughout this study, this chapter provides a review of various process options and flowsheets for the recovery of Fab' from *E. coli* cell disruptates. The impact of the cell disruption method, the number of adsorption cycles and how they are scheduled, as well as the mode of chromatographic operation, on the total process time, yield and throughput is discussed and visualised through the use of Windows of Operation. The Windows of Operation were used to evaluate the alternative process options and to identify the differences in processing efficiently by highlighting the combination of operating variables which result in an operating region that yields the required performance outputs and how these differ between the options selected.

7.1 Introduction

The increasingly high demand for biopharmaceuticals and antibodies in particular, as well as the financial pressures on manufacturers, makes it essential to improve the speed of process development. The cost of development and commercialisation of a new product can be as high as $800 million (Rathore *et al.*, 2004), with the process taking up to 12 years to complete (Petrides *et al.*, 2002). The industry increasingly utilises process simulation and modelling tools to evaluate various process options and speed up the development process (Petrides *et al.*, 2002).

The use of scale-down methods to obtain data which assess the effects of operating conditions on the adsorption of Fab' has been described in the previous chapters. This section of work will use data from the equilibrium isotherms obtained in Chapter 4 to predict the performance of various process options for the purification of Fab' from *E. coli* disruptates. In addition this chapter provides an indication of the manner with which the results reported in this thesis may be drawn together in order to draw process-wide insights.

The equations developed in Chapter 4 form the basis of a comprehensive model which enables the evaluation of several adsorptive process options, utilising various unit operations for the primary recovery and initial capture of Fab' expressed in *E. coli*. The model provides a powerful tool capable of evaluating a wide range of process variables including:

- The method of cell disruption, including the length of the lysis procedure
- Feedstock properties, such as solids concentration, ionic strength and initial Fab' concentration
- The number and duration of unit operations
- The phase ratio (matrix volume/feed load volume) employed during adsorption
- The number of cycles needed for Fab' adsorption
- The consequences of Fab' partitioning and binding to cell debris.

As described in Chapter 4 the model is capable of calculating the total process yield (%) and throughput (g Fab'/h) based on the results of the adsorption isotherms. The process yield and throughput may then be used to assess process performance through the use of Windows of Operation, a visualisation tool capable of identifying suitable operating conditions. The Windows of Operation are then used as part of a process optimisation scheme in order to select a process route capable of meeting pre-determined performance criteria.

To highlight the various process options available during the preparation of feedstocks and the primary recovery and initial purification of Fab', Section 7.1.1 summarises the process options used during this study. Section 7.1.2 then describes the development of Windows of Operation.

7.1.1 *Process options utilised in this study*

The Fab' used in the study is expressed periplasmically in *E. coli*, hence the first unit operation to consider is the method of cell disruption. The two methods utilised in this study were high pressure homogenisation and heat lysis. As with all unit operations, each has its advantages and disadvantages. High pressure homogenisation is a relatively simple and rapid procedure, and when performed in RO water, yields a solution of low ionic strength, suitable for ion exchange adsorption without the need for diafiltration or buffer exchange. However, high pressure homogenisation releases all the cell contents into solution, resulting in a highly contaminated feedstock. The heat lysis method used is a lengthy process, taking up to 16 h to complete, at a temperature of 60 °C. The resulting lysate though is relatively pure, containing very few contaminants, as described in Chapter 3. However, the lysis buffers used result in a solution of high ionic strength, not suitable for ion exchange without the prior use of diafiltration. Diafiltration of the unclarified lysate was carried out using a hollow fibre membrane, a process which adds to the total pre-treatment time.

As described in previous chapters the antibody fragment used throughout this study binds to the *E. coli* cell debris; it partitions. Clarification of the feedstock during the primary recovery of Fab', and therefore the removal of cell debris, would lead to the loss of debris-bound Fab' and have a significant impact on the total process yield. In order to avoid the loss of debris-bound Fab', the initial purification of Fab' from unclarified feedstocks was evaluated. Chapter 4 presented the results of the relevant adsorption isotherms, which indicated that the presence of cell debris compromised the adsorption of Fab' onto an ion exchange adsorbent. The initial purification of Fab', from both clarified and unclarified feedstocks using packed bed columns was investigated in Chapter 5. The results showed that it is possible to recover Fab' from an unclarified homogenate using loosely packed laboratory columns, however, when a column packing procedure designed to mimic large scale column packing was used the homogenate was found to block the column and recovery of Fab' from an unclarified feedstock was not possible. This suggested that industrial scale purification of Fab' from an unclarified feedstock using packed bed columns would be precluded and instead the use of primary recovery unit operations such as

centrifugation and filtration prior to packed bed adsorption would be essential. The use of batch adsorption removes the need for any feedstock clarification and combines primary recovery and initial purification. Chapter 6 showed that it is possible to use stirred tank batch adsorption for the primary recovery of Fab' from unclarified feedstocks. However, in the case of the homogenate, it was only possible to adsorb approximately 50% of the total Fab' loaded in a single adsorption cycle.

It is evident that for the recovery of this particular Fab' there exist numerous process options and trade-offs and the selection of individual unit operations can have significant impacts on the overall process. For example, as the results of Chapter 4 showed, the distribution coefficients of the lysate feedstock are significantly greater than those of the homogenate, indicating that the adsorption of Fab' is more favourable from the lysate. However, the time taken to carry out the lysis and diafiltration in preparation for ion exchange adsorption would significantly impact the process throughput. The analysis and evaluation of such trade-offs implicit in the various process options are the aim of this chapter. To facilitate the rapid, visual evaluation of the various process options and the necessary trade-offs, Windows of Operation are developed and compared.

7.1.2 The generation of Windows of Operation

The use of Windows of Operation as a visualisation tool, capable of aiding the design and comparison of alternative bioprocess options has been reported previously (Woodley and Titchener-Hooker, 1996; Zhou and Titchener-Hooker, 1999; King *et al.*, 2004; Nealon *et al.*, 2005; Salte *et al.*, 2006).

The generation of a Window of Operation firstly requires the selection of the process variables which are used to define the horizontal and vertical axis of the plots. As a Window of Operation can be used as a design and optimisation tool, the process variables which are chosen to define the axis must be easily altered and controlled in order to allow the optimisation of the process. For the purpose of this study the phase ratio of the adsorption step (V_m/V_l) and the feedstock solids concentration (% ww/v) were chosen as the process variables.

The Windows of Operation developed in this chapter portray the performance of the entire process being evaluated, from the method of cell disruption, the solid/liquid separation, right through to the mode of operation of the adsorptive step. The performance parameters of total process yield and throughput were obtained through the use of the models developed and presented in Chapter 4. Using the software program Origin™ (Microcal Software Inc., Northampton, USA) the total process yield and throughput were correlated with the solids concentration and phase ratio. These data were then used to obtain 2-D contour plots, where the total process yield and throughput are displayed as a function of solids concentration and phase ratio.
In order to obtain realistic, feasible operating conditions, Windows of Operation often include operational constraints. For example, the maximum operating flow rates for centrifuges and a processing time limit were the constraints used by Salte *et al.* (2006), whereas, Nealon *et al.* (2005) incorporated the lower limits of liquid handling accuracy for a robotic liquid dispenser. For a batch adsorption system the phase ratio may be constrained due to financial or physical reasons, such as the mixing and suspension of the adsorbent/feedstock slurry. As a result the Windows of Operation developed in this chapter will be constrained by the phase ratio and centrifuge performance, as defined by the maximum flow rate.

[The focus of this chapter is solely to consider the range of process options available. Although other factors such as the economics, detailed scheduling, equipment footprint and adsorbent deterioration are important and will ultimately influence the decision-making process, this type of analysis is not within the scope of this chapter.]

7.2 Results and discussion

The results of this chapter are presented as a series of case studies, investigating various process options. Case Study 1 (Section 7.2.1) evaluates and compares high pressure homogenisation and heat cell lysis as methods of cell disruption, and also investigates the effect of feedstock solids concentration and the adsorbent phase ratio on pre-selected performance parameters. The general process flowsheets and assumptions on which all the case studies are based on are also outlined in Case Study 1. Case Study 2 (Section 7.2.2) presents the results of an optimisation of the

batch adsorption process. Case Study 3 (Section 7.2.3) compares the use of stirred tank batch and packed bed adsorption. Finally, a model sensitivity analysis, evaluating the effect of lysis time and Fab' partitioning on the process flowsheets is presented in Case Study 4 (Section 7.2.4).

Although the effect of ionic strength on ion exchange adsorption was investigated in detail in previous chapters, it was decided that the process options being evaluated in this chapter should focus on the effect of solids concentration and feedstock clarification. These factors were deemed to have a greater impact on the process being considered, especially due to the dominating loss of debris-bound Fab' occurring through clarification.

Figure 7.1 shows a simplified version of the process flowsheet, on which the case studies were based. It was assumed the process consists of a cell disruption method which gives 1,000 L of feedstock, then depending on the disruption method, a number of pre-treatment steps followed by purification, or alternatively, primary recovery and initial purification using stirred tank batch adsorption.

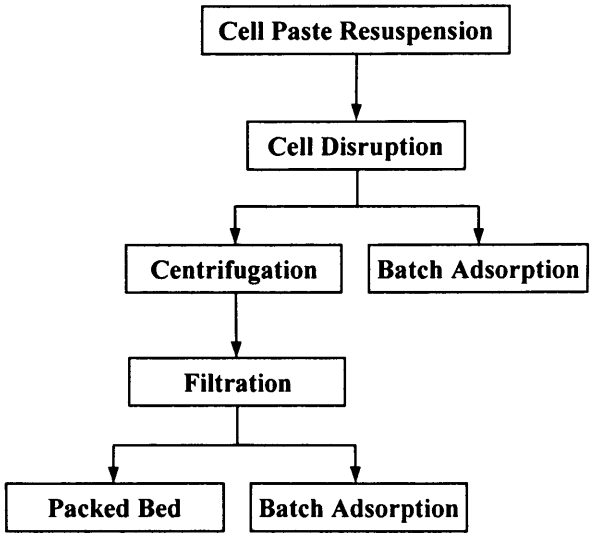

Figure 7.1. Flowsheet options for the primary recovery and initial purification of Fab', expressed in the periplasm of *E. coli.*

7.2.1 *Case Study 1: the effect of cell disruption methods, solids concentration and adsorbent phase ratio on the batch adsorption of Fab'.*

The aim of this case study is to outline the general assumptions used to develop the model, highlight the differences between the process flowsheets utilising either high pressure homogenisation or heat lysis, and describe the process behind constructing Windows of Operation, with the aim of selecting the most efficient process flowsheet.

Figure 7.2 shows the flowsheets for processes utilising either high pressure homogenisation or heat lysis for the release of periplasmically expressed Fab'. The reasons for using each unit operation and the impact they have on the process are described in Sections 7.2.1.1 to 7.2.1.4. Section 7.2.1.5 discusses how the performance parameters are obtained, and Section 7.2.1.6 uses those performance parameters to develop and compare Windows of Operation for both process flowsheets.

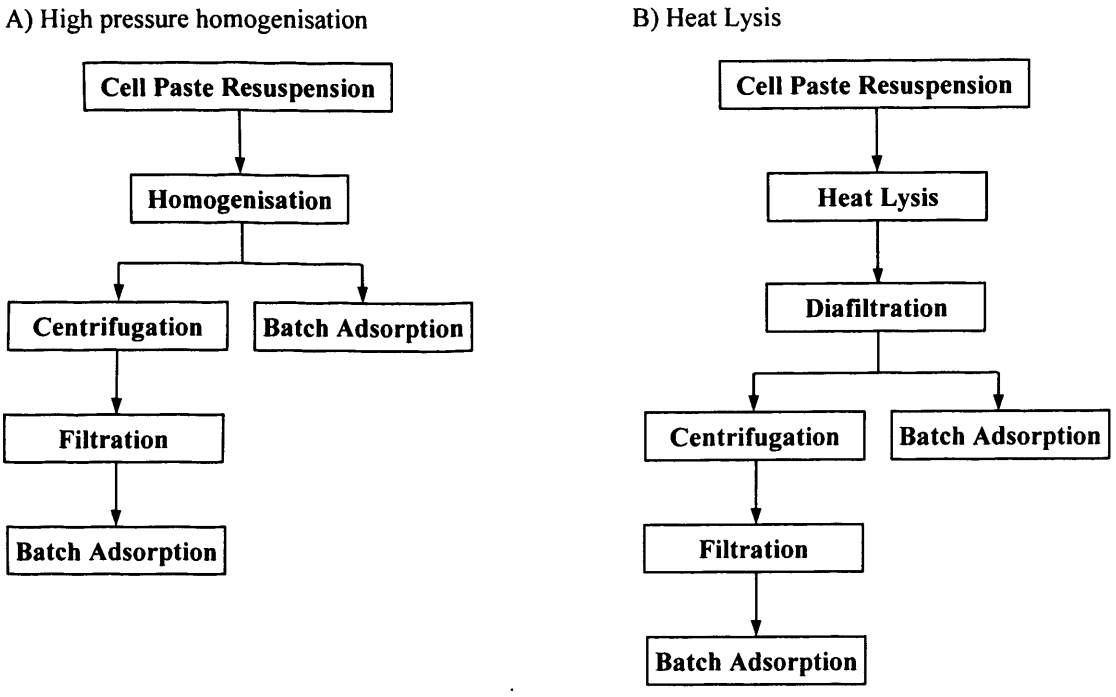

Figure 7.2. The impact of cell disruption methods on the flowsheet options for the primary recovery and initial purification of Fab', expressed in the periplasm of *E. coli.* Due to the use of high ionic strength lysis buffers, the lysis process route requires an additional diafiltration step to prepare the feedstock for ion exchange adsorption.

7.2.1.1 *Liquid handling and transfer*

Due to the assumption that large volumes of feedstocks and buffers are being handled, the time required to fill and drain storage and reactor tanks must be included. The time taken to transfer the feedstocks from one unit operation to another, for example from the homogeniser to the centrifuge, is also included. In all cases it was assumed that a pump operating at 6,000 L/h was available to transfer all the process fluids.

7.2.1.2 *Cell disruption*

As shown in Figure 7.2 it is assumed that both process flowsheets start with the harvested cell paste being resuspended, either in RO water (or a low ionic strength buffer) in preparation for high pressure homogenisation, or in a lysis buffer, prior to heat lysis. The total volume of the resulting feedstock is 1,000 L. As one of the main variables being evaluated is feedstock solids concentration, the mass of cells resuspended results in a feed solids concentration of 10% (ww/v) for both the homogenate and lysate feed. In order to obtain the same solids concentration for the adsorption stage it may be necessary to use a larger mass of cell paste for the homogenate, as the process of high pressure homogenisation decreases the solids concentration to a greater extent than the lysis. This will result in a difference in the feedstock Fab' concentration, however, the model is able to predict and account for differences in initial concentration. The homogenisation and lysis procedures are assumed to last 4 and 16 h respectively. As the ionic strength of the lysate is too high for ion exchange adsorption, a diafiltration step is included and is assumed to last 4 h.

7.2.1.3 *Feedstock solids concentration*

In order to evaluate the effect of feedstock solids concentration on the process performance, it was assumed that feed solutions of varying solids concentration were prepared using an Alfa Laval BTUX 510 (AL-510) disc-stack centrifuge. The centrifugation conditions, i.e. the flow rate and centrifugation time, required to

achieve certain clarification efficiencies were calculated based on the USD work carried out by Salte (2006) who used the Sigma theory (Ambler, 1961; Maybury *et al.*, 1998) to compare the performance of centrifuges of different size and design (refer to Appendix A1). The Sigma theory states that each centrifuge has a unique Sigma factor (Σ), defined as "the surface area of a gravity settling tank required to give the equivalent separation performance to the particular centrifuge. Salte (2006) presents predicted $V_{lab}/t_{lab}\Sigma_{lab}$ data for the laboratory scale clarification of both *E. coli* lysate and homogenate, where V_{lab} is the volume of liquid in the laboratory spin tube, t_{lab} is residence time in the laboratory centrifuge, and Σ_{lab} is the equivalent settling area. Using Equation 5.1 such data can be used to predict the separation performance of the AL-510 centrifuge, and obtain the volumetric flow rates needed to achieve the desired levels of clarification.

$$\frac{V_{lab}}{t_{lab}\Sigma_{lab}} = \frac{Q}{c\Sigma} \qquad 5.1$$

where Q is the volumetric flow rate, and c is a correction factor which accounts for differences in the flow patterns between different centrifuge designs. Given that the $c\Sigma$ value for the AL-510 is known to be 42,400 m^2 calculating the required volumetric flow rates is straightforward.

An increase in the process throughput could be achieved by processing the feedstock through the centrifuge at the maximum flow rate, although this would result in a poorly clarified feed. When comparing the clarification efficiencies achievable for the homogenate and lysate, it is evident that the lysate is easier to clarify. Figure 7.3 shows how the solids concentration of both the homogenate and lysate feedstocks decreases with time. Reducing the solids concentration of the lysate requires less time than the homogenate. Figure 7.4 shows how the solids concentration is affected by the flow rate of the centrifuge. As expected, the greater the flow rate, the less efficient the clarification. When operating at the maximum flow rate it is evident that the clarification of the lysate is more efficient than that of the homogenate. In order to obtain feedstocks virtually free of particulates (0.01% solids ww/v) a filtration step is included in the process after the centrifugation stage, and is sized based on a process duration of 2 h.

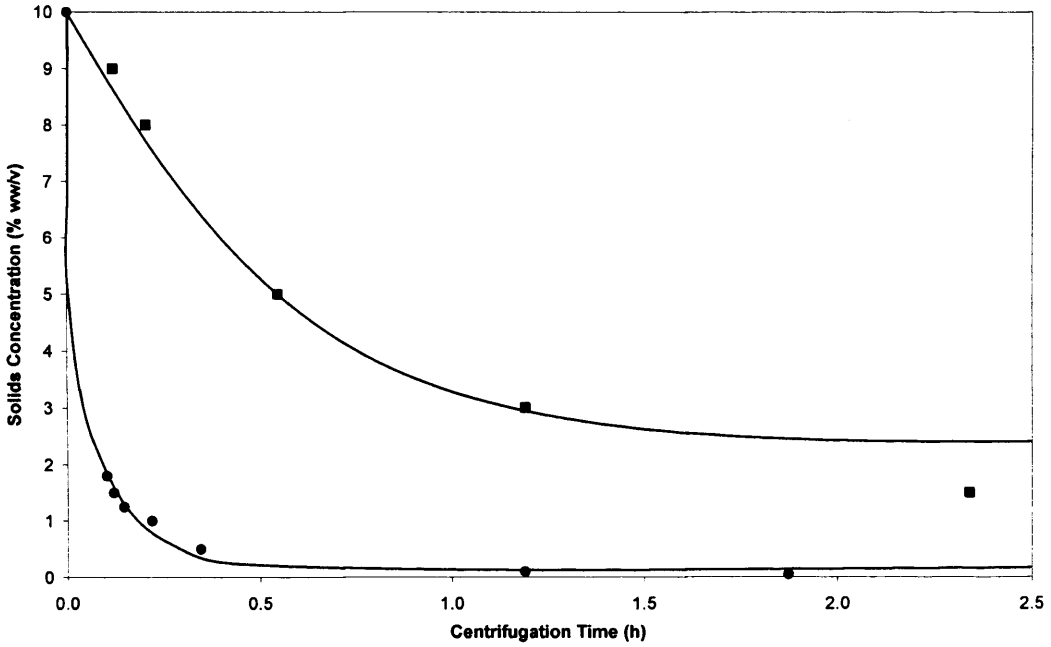

Figure 7.3. The effect of centrifugation time on the solids concentration of *E. coli* homogenate (■) and lysate (●) feedstocks of 10% (ww/v) initial feedstock solids concentration. For the purpose of the model centrifugation was assumed to have been performed using an Alfa Laval BTUX 510 disc-stack centrifuge.

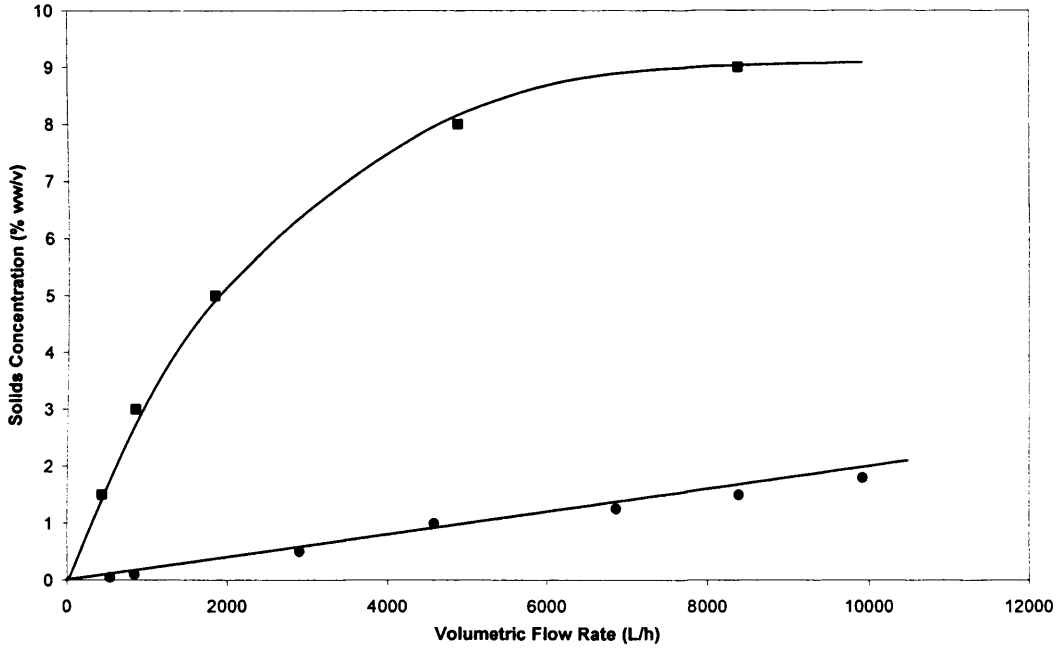

Figure 7.4 The effect of the volumetric flow rate of the Alfa Laval BTUX 510 disc-stack centrifuge on the solids concentration of *E. coli* homogenate (■) and lysate (●) feedstocks of 10% (ww/v) initial feedstock solids concentration.

It was assumed that the volume of the feedstock decreases after centrifugation and filtration as a result of the loss of solids. Table 7.1 and Table 7.2 show the unit operations, and the time required for each, to prepare the homogenate and lysate feedstocks, respectively. It is clear to see that although the lysate requires a shorter centrifugation time, the lengthy lysis procedure, coupled with the addition of the diafiltration step, results in a significantly longer time for feedstock preparation.

As previously stated, clarification of both feedstocks leads to the loss of Fab' due to Fab' being bound to cells or cell debris. The extent to which Fab' binds to cells or cell debris depends on many factors, including the method of cell disruption; as shown in Figure 7.5. It is clear to see that when complete clarification of the diafiltered lysate is achieved more than 70% of the total available Fab' is lost with the cells removed during centrifugation and filtration, as compared to approximately 40% of the total Fab' available in the homogenate. This would clearly have a major impact on the process performance.

Table 7.1. The unit operations utilised in the pre-treatment and preparation of an *E. coli* homogenate feedstock, and the resulting process time and feedstock properties.

		Pre-adsorption Process Time (h)				
Solids Concentration (% ww/v)	**Volume (L)**	**Homog'**	**Cent'**	**Filt'**	**Fluid Transfer**	**Total Time**
10	1,000	4	0.0	0	0.7	4.7
9	990	4	0.1	0	0.7	4.8
8	980	4	0.2	0	0.7	4.9
5	950	4	0.6	0	0.7	5.2
3	930	4	1.2	0	0.7	5.9
1.5	915	4	2.3	0	0.7	7.0
0.01	900	4	2.3	2	1.0	9.3

Table 7.2. The unit operations utilised in the pre-treatment and preparation of an *E. coli* lysate feedstock, and the resulting process time and feedstock properties.

		Pre-adsorption Process Time (h)					
Solids Concentration (% ww/v)	Volume (L)	Heat Lysis	DF	Cent'	Filt'	Fluid Transfer	Total Time
10	1,000	16	4	0.0	0	1.0	21.0
1.8	918	16	4	0.1	0	1.0	21.1
1.0	910	16	4	0.2	0	1.0	21.2
0.5	905	16	4	0.3	0	1.0	21.3
0.1	901	16	4	1.2	0	1.0	22.2
0.05	900	16	4	1.9	0	1.0	22.9
0.01	900	16	4	1.9	2	1.3	25.2

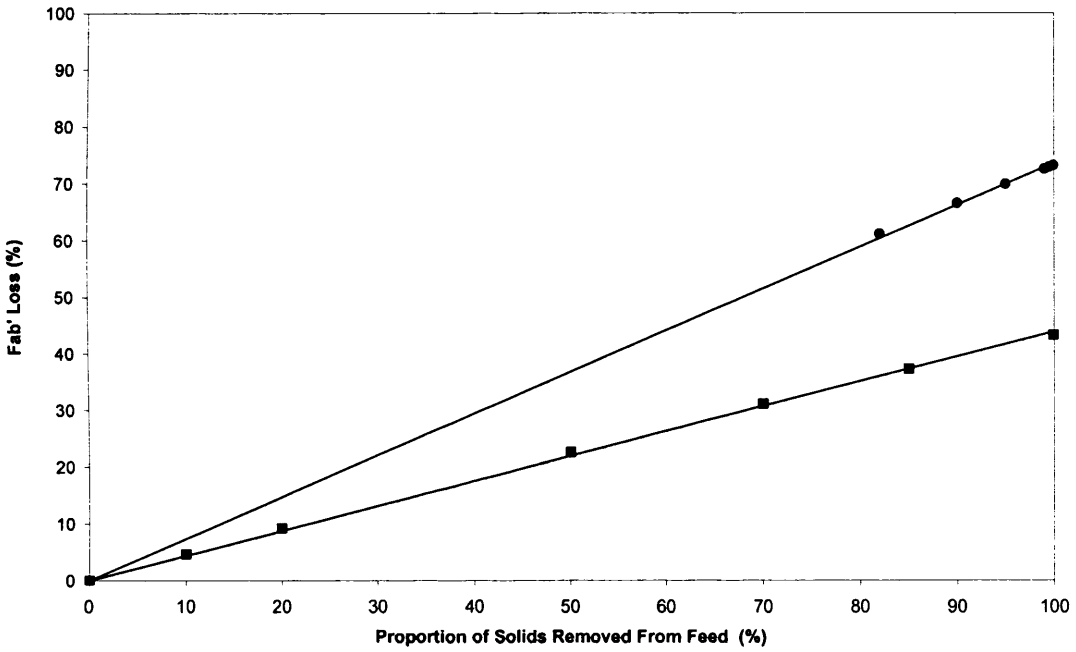

Figure 7.5. The loss of total available Fab' due to the clarification of *E. coli* homogenate (■) and diafiltered lysate (●) feedstocks. (Maximum proportion of solids removed is 99.99%)

7.2.1.4 Stirred tank batch adsorption

The process model developed in this thesis incorporates stirred tank batch adsorption with the main assumptions being that the adsorbent is used only once, and as such a CIP time is not included. Based on repeated experimental observations the adsorption process includes the following stages: equilibration steps lasting 10 min

each, one adsorption step lasting 30 min, wash steps lasting 10 min each and finally, an elution step lasting 10 min. Figure 7.6 shows the adsorptive process flowsheet for the recovery of Fab' from a feedstock with a solids concentration of 10% (ww/v), at a phase ratio of 0.5 (1,000 L feedstock load volume contacted with 500 L adsorbent). Once again, based on repeated experimental observations the adsorption flowsheet is based on the assumptions that the process includes two separate adsorbent equilibration steps using 1 adsorbent, or batch volume (BV) buffer each, a wash cycle using two wash steps, of 1 BV buffer each, if the solids concentration is less than or equal to 1% (ww/v) and three wash steps, of 1 BV buffer each, if the solids concentration is greater than 1% (ww/v) and finally, one elution step using 1 BV buffer.

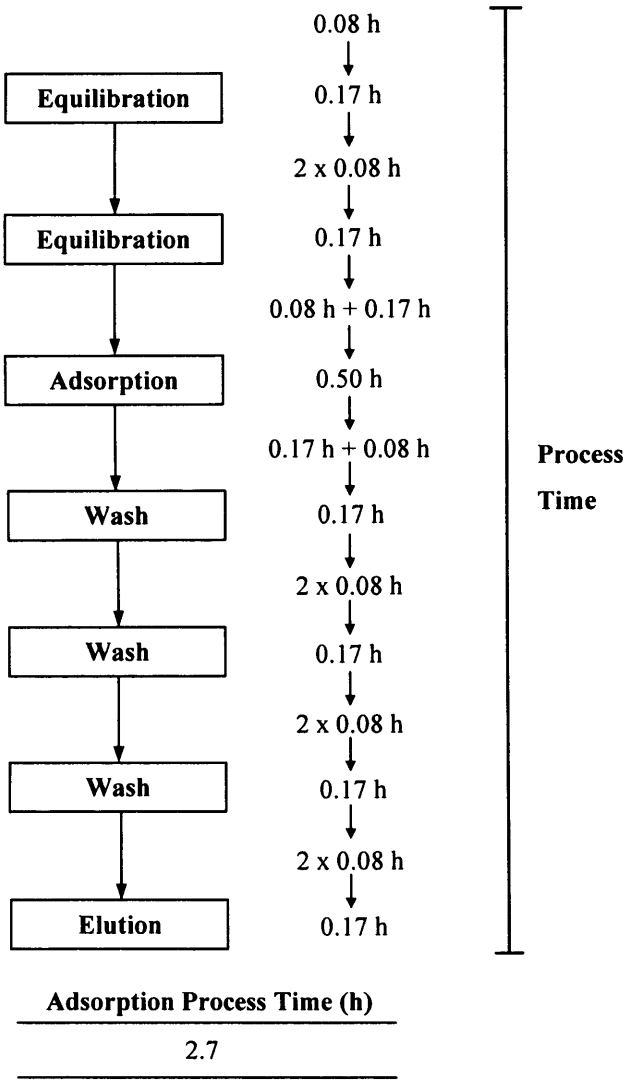

Figure 7.6. Process flowsheet for the adsorptive stage of the recovery of Fab' from 1,000 L of a generic feedstock of 10% (ww/v) solids concentration using a single cycle batch adsorption at a phase ratio of 0.5. The process times shown include the time required to fill, drain, and mix the process liquids.

7.2.1.5 *Process performance - total process yield, time and throughput*

Equation 4.29 was used to calculate the process yield, where R, the percentage Fab' recovered, is assumed to be 0.9 due to losses during the wash and elution stages. The total process time, which includes the time needed for liquid transfer, the unit operations used, as well as the adsorptive process time, is used to calculate the total process throughput, using Equation 4.30. Table 7.3 shows the effect of homogenate feedstock solids concentration and volume, as well as phase ratio on the total process time. When compared to the lysate feedstock process, shown in Table 7.4, the impact the long lysis procedure has on the overall process time is clear to see.

Table 7.3. The effect of homogenate feedstock load volume and solids concentration, as well as adsorbent phase ratio on the total process time. The total time includes all liquid transfer, unit operations and a single cycle batch adsorption process.

Solids Conc' (% ww/v)	**0.01**	**1.5**	**3.0**	**5.0**	**8.0**	**9.0**	**10.0**
Feed Volume (L)	**900**	**915**	**930**	**950**	**980**	**990**	**1,000**
V_m/V_l	**Total Process Time (h)**						
0.10	11.1	9.0	7.8	7.2	6.9	6.8	6.7
0.30	11.4	9.3	8.2	7.6	7.3	7.2	7.1
0.50	11.7	9.7	8.6	8.0	7.7	7.6	7.5
0.75	12.1	10.2	9.1	8.4	8.2	8.1	8.0
1.00	12.4	10.6	9.5	8.9	8.7	8.6	8.5

Table 7.4. The effect of lysate feedstock load volume and solids concentration, as well as adsorbent phase ratio on the total process time. The total time includes all liquid transfer, unit operations and a single cycle batch adsorption process.

Solids Conc' (% ww/v)	**0.01**	**0.05**	**0.1**	**0.5**	**1.0**	**1.8**	**10.0**
Feed Volume (L)	**900**	**900**	**901**	**905**	**910**	**918**	**1,000**
V_m/V_l	**Total Process Time (h)**						
0.10	26.9	24.6	24.0	23.1	23.0	23.1	23.0
0.30	27.2	24.9	24.3	23.4	23.3	23.4	23.4
0.50	27.5	25.2	24.6	23.7	23.6	23.8	23.8
0.75	27.9	25.6	24.9	24.1	24.0	24.3	24.3
1.00	28.3	26.0	25.3	24.5	24.4	24.7	24.8

The process yield and throughput were used to evaluate the different process options and to measure the process performance. Figure 7.7 and Figure 7.8 show the effect of feedstock solids concentration and clarification on the total process yield and throughput, respectively, of processes using batch adsorption, at a phase ratio of 0.5. It is evident from Figure 7.7 that the highest yield is achieved when Fab' is recovered from unclarified feedstocks. It is interesting to note that at a phase ratio of 0.5 the highest yield achievable is over 80% in the case of the lysate and approximately 65% for the homogenate. This was expected as the lysate is a much purer feed than the homogenate, containing very few contaminants. However, despite the higher yield, the lysate process option has a much lower process throughput, as already stated, due to the lengthy lysis time and addition of a diafiltration step. In an initial capture step this is generally not a problem, however, it is always advantageous to separate the product from contaminants, such as protease enzymes, as rapidly as possible. The drop in the throughput observed in the homogenate feedstock is due to the addition of a filtration step at the end of centrifugation, in order to achieve a highly clarified homogenate solution.

Figure 7.7 and Figure 7.8 can be used in the decision making process when designing a process flowsheet, however these figures only show the results obtained from one phase ratio and do not illustrate how the operating conditions, in this case the phase ratio and solids concentration, can be combined to achieve pre-determined performance parameters. The model is, however, capable of generating data for any phase ratio, and solids concentration but plotting such large amounts of data in the form of Figure 7.7 and Figure 7.8 would be impractical and would still not identify suitable operating conditions for a given process objective. To overcome this Windows of Operation can be used as a design tool to identify and visualise the suitable operating conditions.

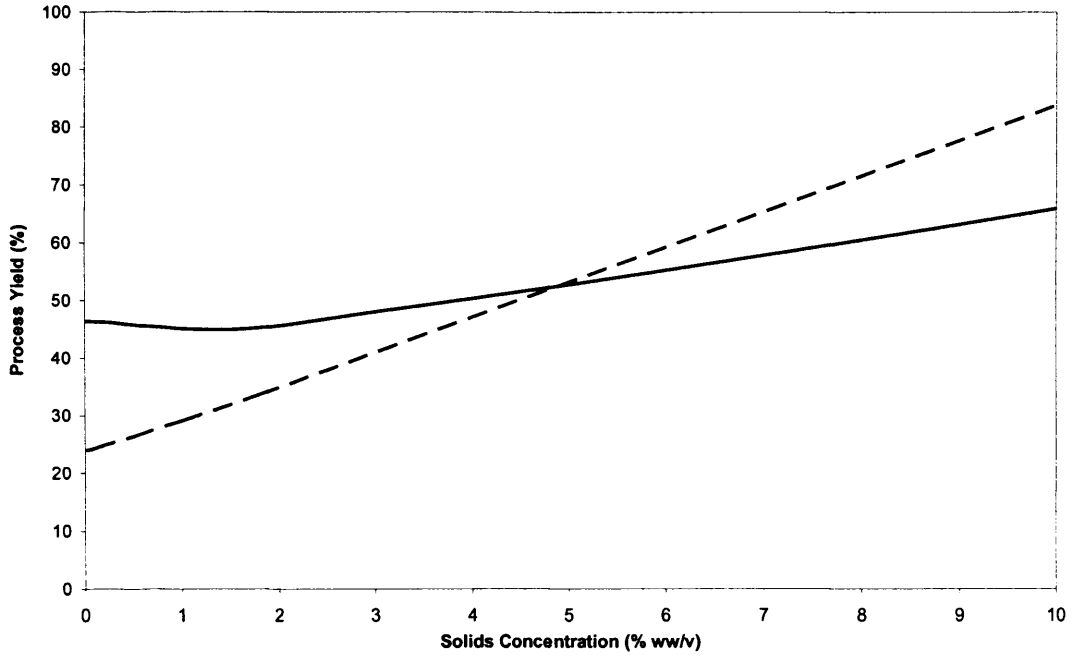

Figure 7.7. The effect of clarification of homogenate (—) and lysate (---) feedstocks of 10% (ww/v) solids concentration, on the total process yield of a process flowsheet utilising a single cycle batch adsorption at a phase ratio of 0.5

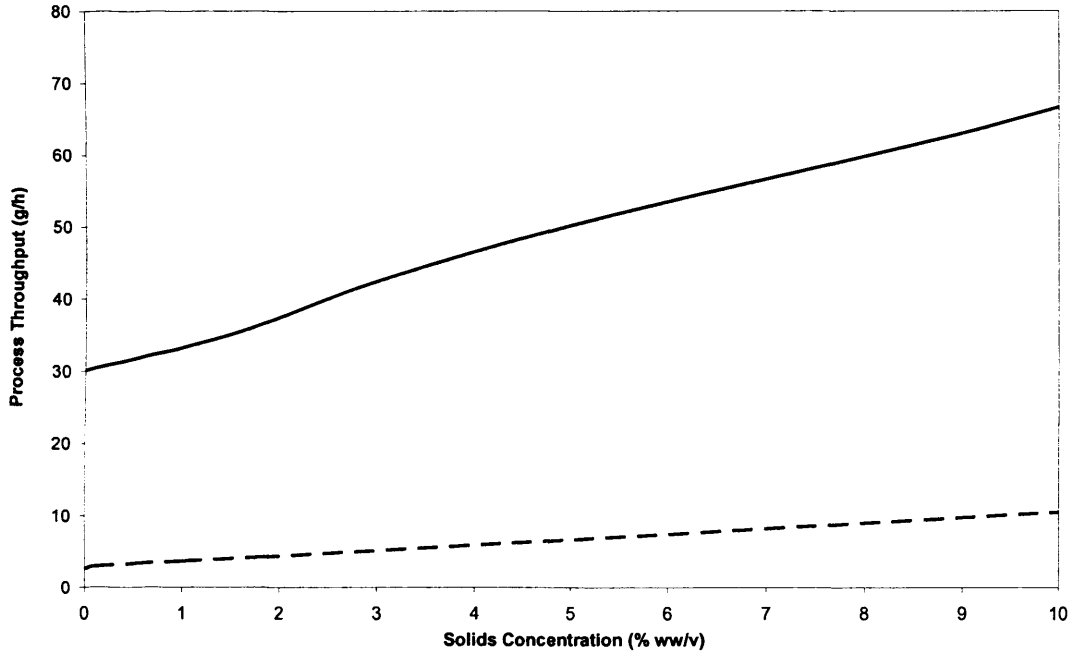

Figure 7.8. The effect of clarification of homogenate (—) and lysate (---) feedstocks of 10% (ww/v) solids concentration, on the total process throughput of a process flowsheet utilising a single cycle batch adsorption at a phase ratio of 0.5.

7.2.1.6 *Windows of Operation*

The development and generation of a single Window of Operation for the primary recovery and initial purification of Fab' from an *E. coli* homogenate, based on the process and assumptions outlined so far in this case study, is presented in Figures 7.9 a) - f). The completed Window of Operation for the primary recovery and initial purification of Fab' from an *E. coli* lysate is shown in Figure 7.10.

Figure 7.9 a) and Figure 7.9 b) show the 2-D contour plots for the total process yield and throughput, respectively, as a function of phase ratio and feedstock solids concentration. In this case it is clear to see that both the yield and throughput decrease with decreasing solids concentration, i.e. increasing clarification, which is to be expected due to the loss in debris-bound Fab'. Figure 7.9 c) shows how overlapping the 2-D contour plots can help to identify rapidly operating conditions which give a certain combination of yield and throughput.

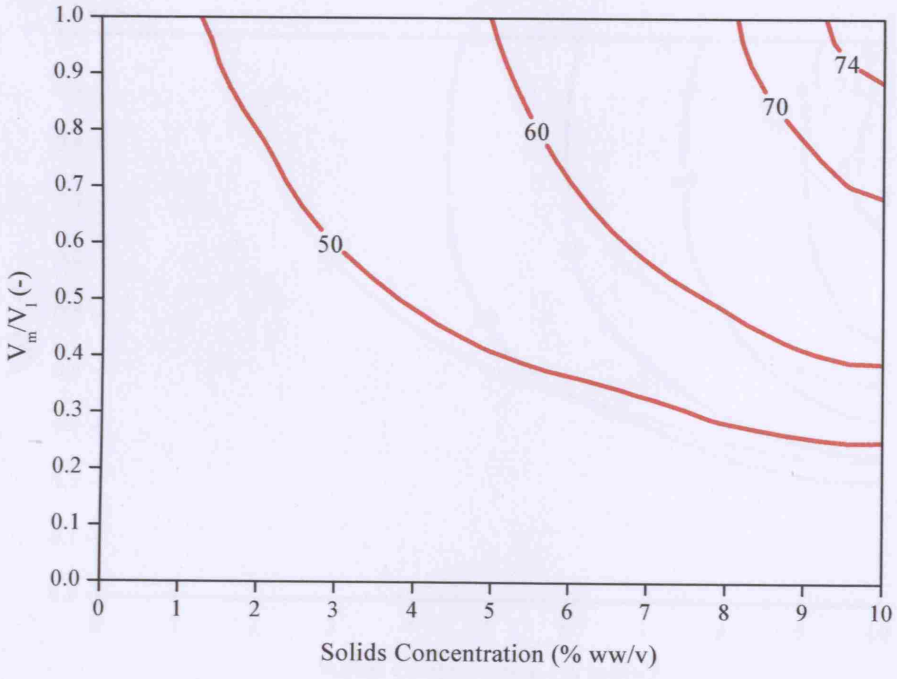

Figure 7.9 a). Development of the Window of Operation for the primary recovery and initial purification of Fab' from an *E. coli* homogenate feedstock with an initial solids concentration of 10% (ww/v) using a single cycle batch adsorption process. Step 1: a 2-D contour plot showing the total process yield (%) as a function of solids concentration and phase ratio.

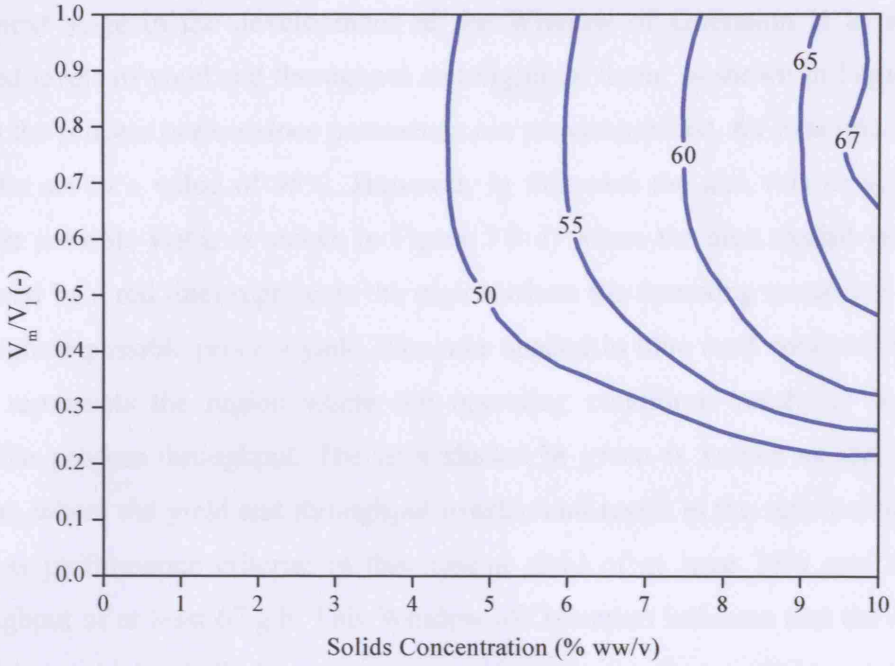

Figure 7.9 b). Development of the Window of Operation for the primary recovery and initial purification of Fab' from an *E. coli* homogenate feedstock with an initial solids concentration of 10% (ww/v) using a single cycle batch adsorption process. Step 2: a 2-D contour plot showing the total process throughput (g/h) as a function of solids concentration and phase ratio.

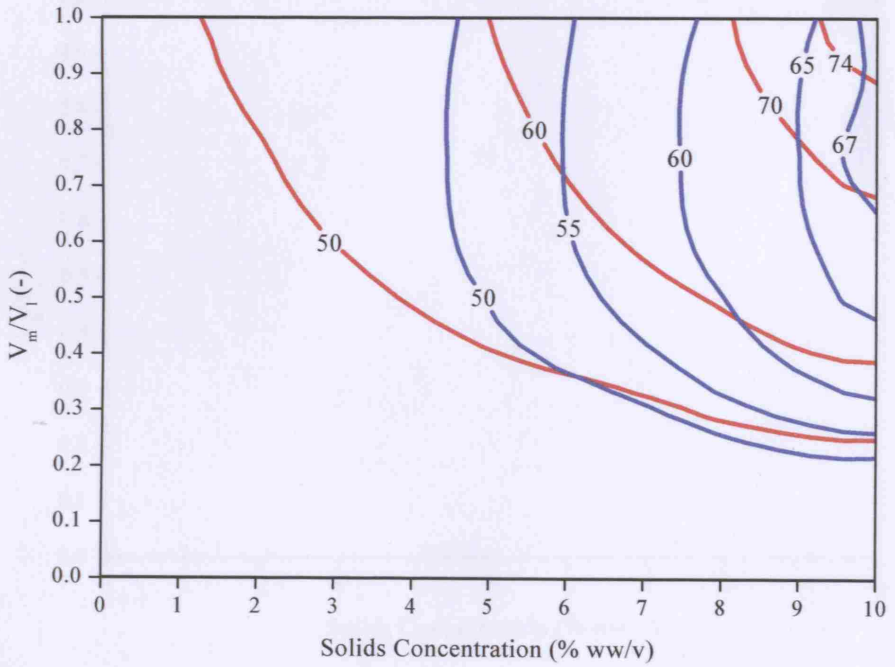

Figure 7.9 c). Development of the Window of Operation for the primary recovery and initial purification of Fab' from an *E. coli* homogenate feedstock with an initial solids concentration of 10% (ww/v) using a single cycle batch adsorption process. Step 3: the overlapped 2-D contour plots showing the total process yield (%) (red) and throughput (g/h) (blue). The operating conditions which result in the desired combined levels of yield and throughput can now be visualised and identified.

The next stage in the development of the Window of Operation is to select the desired levels of yield and throughput and highlight them, as shown in Figure 7.9 d). Often the process performance parameters are pre-determined, for example, the yield may be set to a value of 95%. However, in this case the aim was to achieve the highest possible yield, as shown in Figure 7.9 d) where the area shaded in red (and enclosed by a red line) represents the region where the operating conditions result in the highest possible process yield. The area shaded in blue (and enclosed by a blue line) represents the region where the operating conditions result in the highest possible process throughput. The area shaded in green is known as the operating region, where the yield and throughput overlap and result in the satisfaction of both process performance criteria; in this case a yield of at least 74% *and* a process throughput of at least 67 g/h. This Window of Operation indicates that the operating conditions which satisfy the performance criteria are an adsorption process utilising a phase ratio > 0.9 and a homogenate feedstock with a solids concentration approximately > 9.7%.

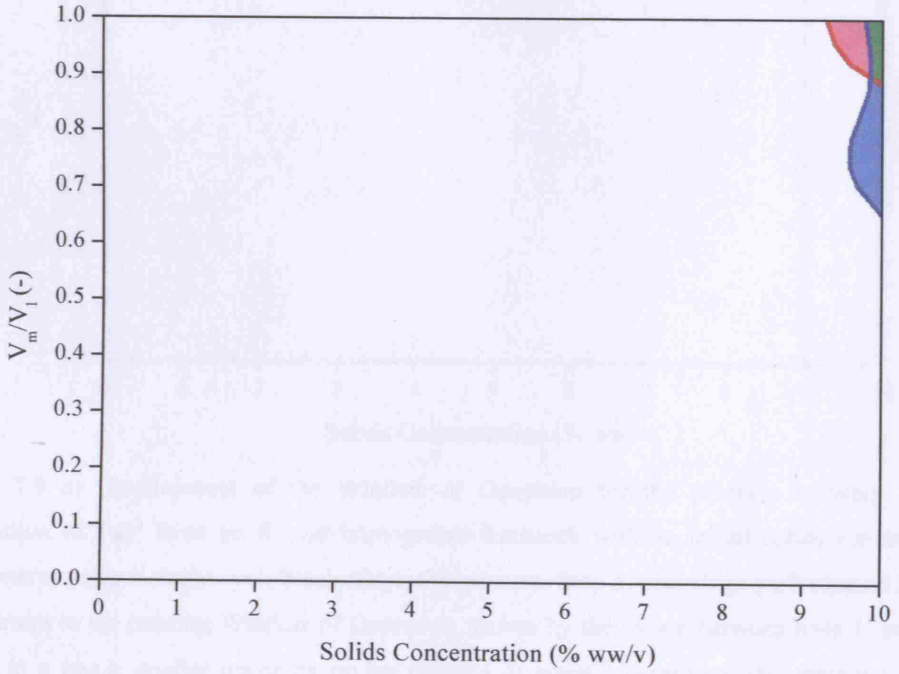

Figure 7.9 d) Development of the Window of Operation for the primary recovery and initial purification of Fab' from an *E. coli* homogenate feedstock with an initial solids concentration of 10% (ww/v) using a single cycle batch adsorption process. Step 4: the visualisation of the operating region (shaded in green), identifying the operating conditions which result in a process yield of 74% (area shaded red) and process throughput of 67 g/h (area shaded blue).

In order to complete the Window of Operation, operational constraints are applied. Figure 7.9 e) shows how the maximum volumetric flow rate of the centrifuge used during the preparation of the feedstock impacts the Window of Operation. Operating the Alfa Laval BTUX 510 at its maximum flow rate of 10,000 L/h results in a feedstock with a solids concentration of 9% (ww/v). This means that it is not possible to obtain a partially clarified homogenate feedstock with a solids concentration between 9 and 10% (ww/v), as shown by the region between lines 1) and 2) in Figure 7.9 e). The area to the right of line 2) represents the unclarified feed. If the performance parameters remain fixed at a yield of 74% and a throughput of 67 g/h, the operating region becomes much smaller and the operating conditions are restricted to the use of unclarified homogenate (10% ww/v).

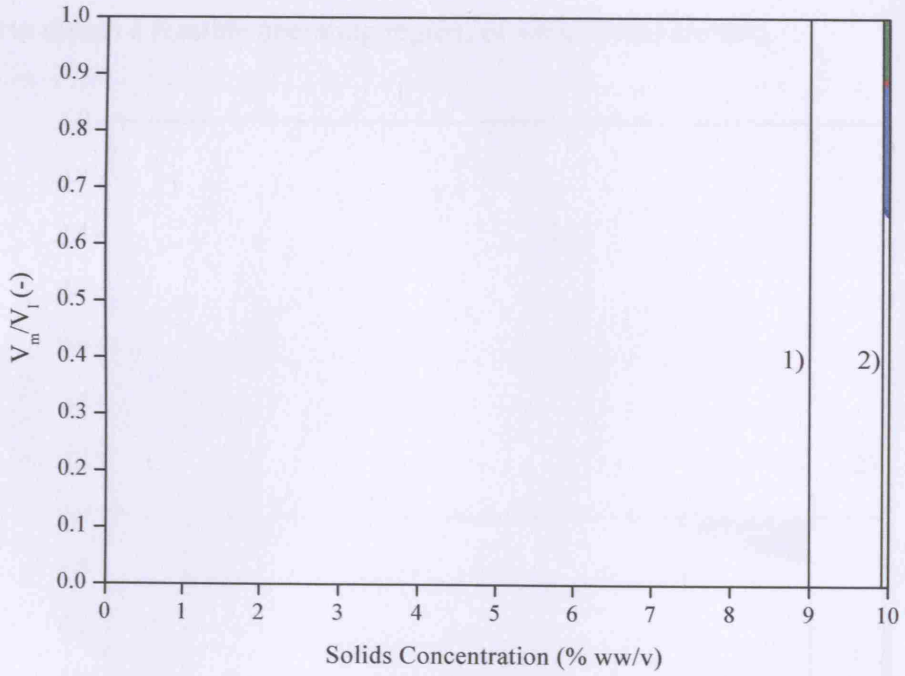

Figure 7.9 e) Development of the Window of Operation for the primary recovery and initial purification of Fab' from an *E. coli* homogenate feedstock with an initial solids concentration of 10% (ww/v) using a single cycle batch adsorption process. Step 5: centrifuge performance is added as a constraint to the existing Window of Operation, shown by the region between lines 1) and 2). This results in a much smaller operating region (shaded in green), identifying the operating conditions which result in a process yield of 74% (area above red line) and a process throughput of 67 g/h (area shaded blue). This constraint restricts the process to the use of unclarified homogenate.

The Window of Operation presented in Figure 7.9 e) indicates that the desired levels of Fab' yield and process throughput can be achieved through the processing of an

unclarified homogenate, with the use of batch adsorption at a phase ratio approximately ≥0.9. However, such a high phase ratio would be very difficult to mix and suspend and is rather unrealistic. As a result, the phase ratio is limited to ≤0.30 (a phase ratio utilised in Chapter 6) and a second constraint is applied to the Window of Operation, shown by area above line 3) in Figure 7.9 f).

Having applied this constraint, maintaining the levels of yield and throughput at 74% and 67 g/h, respectively, results in no feasible operating region. It is therefore necessary to lower the performance criteria to levels which do give a feasible operating region. Figure 7.9 f) shows the completed Window of Operating for the primary recovery and initial purification of Fab' from an *E. coli* homogenate. As a result of the operational constraints applied to the process, the process performance parameters of yield and throughput are reduced to 50% and 50 g/h, respectively, in order to obtain a feasible operating region, of which there are two.

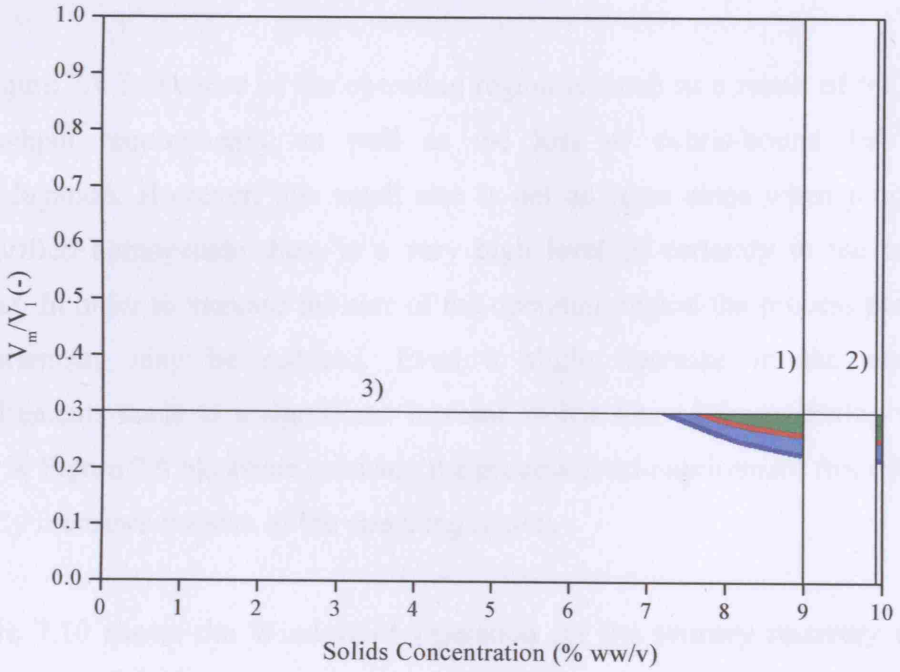

Figure 7.9 f) Development of the Window of Operation for the primary recovery and initial purification of Fab' from an *E. coli* homogenate feedstock with an initial solids concentration of 10% (ww/v), using a single cycle batch adsorption process. Step 6: a constraint limiting the adsorption step phase ratio to ≤0.30 is added, as shown by the area above line 3). The performance parameters are reduced to give a feasible operating region (shaded in green) identifying the operating conditions which result in a process yield of 50% (area above red line) and a process throughput of 50 g/h (area shaded blue).

This Window of Operation shows that during the purification of Fab' from an *E. coli* homogenate, performed using stirred tank batch adsorption, it is possible to achieve a process yield and throughput of 50% and 50 g/h, respectively, from both an unclarified and partially clarified (~7.8-9.0% solids concentration (ww/v)) feedstock. This highlights the trade-offs between the clarification process and the adsorption stage. Although clarification of the feedstock improves the adsorption of Fab' onto the ion exchange adsorbent, the time lost through centrifugation, and the loss of debris-bound Fab', impact both the total process yield and throughput. The Window of Operation shows that although it is possible to achieve the same level of yield and throughput in both an unclarified and partially clarified feedstock, the adsorption of Fab' from a partially clarified feedstock requires a larger volume of adsorbent, as seen by the slight increase in the minimum phase ratio needed. This would indicate that the primary recovery and initial purification of Fab' from an *E. coli* homogenate is most efficiently performed without any feedstock clarification.

In Figure 7.9 f) the size of the operating region is small as a result of the yield and throughput requirements, as well as the loss of debris-bound Fab' through centrifugation. However, this small size is not an issue since when processing an unclarified homogenate there is a very high level of certainty in the operational output. In order to increase the size of the operating region the process performance requirements may be reduced. Even a slight decrease in the performance requirements leads to a significant increase in the size of the operating region, as seen in Figure 7.9 b), where reducing the process yield requirement from 67 to 65 % greatly increases the size of the operating region.

Figure 7.10 shows the Window of Operation for the primary recovery and initial purification of Fab' from an *E. coli* lysate feedstock, using a single adsorption cycle in a stirred tank batch adsorption process.

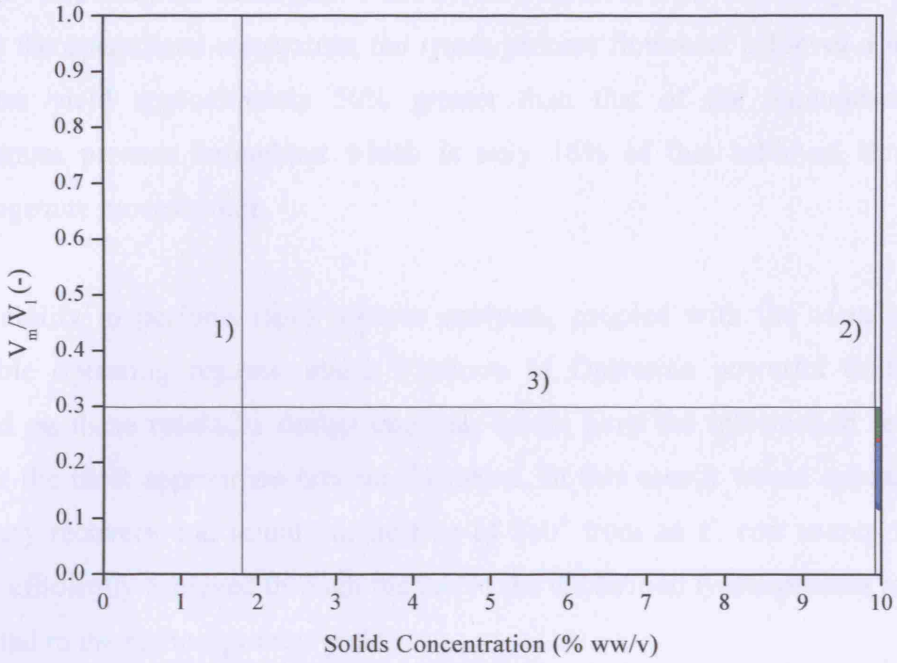

Figure 7.10. Window of Operation for the primary recovery and initial purification of Fab' from an *E. coli* lysate feedstock with an initial solids concentration of 10% (ww/v) using a single cycle batch adsorption process. Operational constraints including the centrifuge performance, shown by the region between lines 1) and 2), and limiting the adsorption step phase ratio to ≤0.3, as shown by the area above line 3) are applied. The feasible operating region (shaded in green) identifies the operating conditions which result in a process yield of 72% (area above red line) and a process throughput of 8 g/h (area shaded blue).

As discussed previously, the flow rate limits on the Alfa Laval BTUX 510 centrifuge, coupled with the ease with which the lysate is clarified, means that it is not possible to obtain a partially clarified lysate feedstock with a solids concentration ≥1.8% (ww/v). Therefore, the centrifuge performance constraint for the lysate window reduces the feasible operating region significantly, as shown by the area between lines 1) and 2) in Figure 7.10. As with the homogenate window, a phase ratio constraint of ≤0.3 is applied and shown by the area above line 3). As a result of the operational constraints applied, the maximum process yield and throughput, which result in a feasible operating region, are 72% and 8 g/h, respectively, shown as the area shaded green in Figure 7.10. Unlike the Window of Operation for the homogenate process, there is only one operating region in Figure 7.10. However, once again, the highest Fab' yield was achieved when no feedstock clarification was applied.

When comparing the homogenate and lysate processes it is interesting to note that, given the operational constraints, the lysate process flowsheet achieves a maximum process yield approximately 50% greater than that of the homogenate but a maximum process throughput which is only 16% of that achieved through the homogenate process route.

The ability to perform rapid process analyses, coupled with the visualisation of feasible operating regions, make Windows of Operation powerful design tools. Based on these results, a design engineer would have the information required to select the most appropriate process flowsheet. In this case it would appear that the primary recovery and initial purification of Fab' from an *E. coli* source would be most efficiently achieved through the use of the unclarified lysate process route, as it resulted in the highest process yield.

7.2.2 Case Study 2: the optimisation of the batch adsorption process

The results of Case Study 1 indicated that given the operational constraints the adsorption of Fab' through the use of a single batch adsorption cycle was incomplete. The purification of Fab' from the unclarified homogenate and lysate feedstocks, where losses due to centrifugation are avoided, results in process yields of 50 and 72%, respectively. The aim of the next case study was to describe the optimisation of the adsorption process achieved through the use of an increased number of adsorption cycles.

7.2.2.1 Process flowsheets and assumptions

Figure 7.11 shows how the number of adsorption cycles, and the way the cycles are scheduled, affects the adsorptive process flowsheet for the recovery of Fab' from a feedstock with a solids concentration of 10% (ww/v), at a phase ratio of 0.3. The three adsorption flowsheets are based on the same set of assumptions outlined in Section 7.2.1.4, however with an additional adsorption cycle, where necessary.

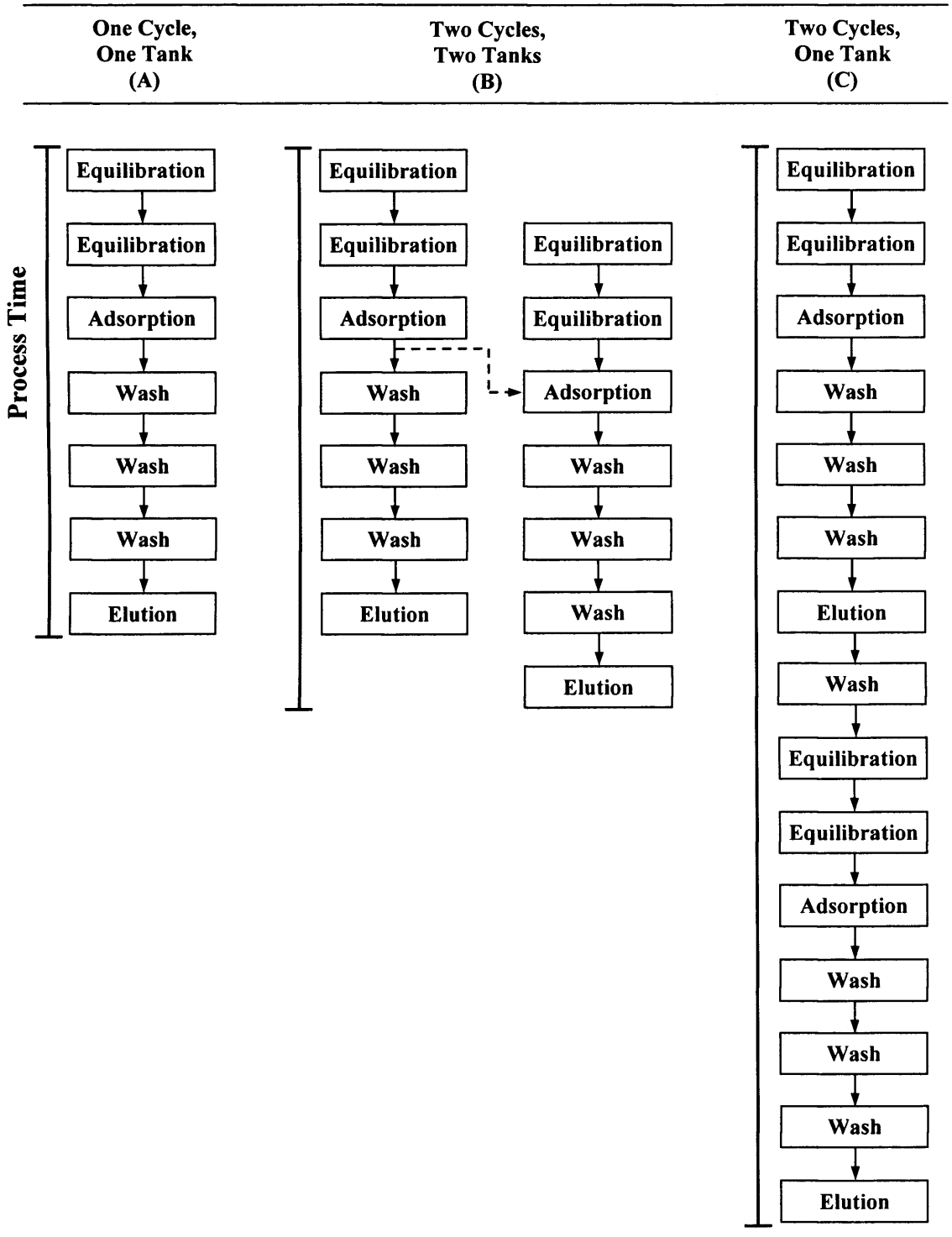

Figure 7.11. The process flowsheets and time for the adsorptive stage of the recovery of Fab' from a generic feedstock of 10% (ww/v) solids concentration using stirred tank batch adsorption at a phase ratio of 0.3 (using a feedstock load volume of 1,000 L and batch (adsorbent) volume of 300 L). In situation B where two tanks are used, each tank is operated at a phase of ratio of 0.3, giving a combined system phase ratio of 0.6.

Column A in Figure 7.11 represents the simplest mode of operation which is one adsorption cycle performed in one reactor tank. At the end of the adsorption process the feedstock, which may still contain Fab', can be transferred to a tank containing pre-equilibrated adsorbent, as shown in column B of Figure 7.11. The two tanks then run in parallel and as the two batches are staggered, the effect on the total process time is effectively only the addition of one extra step (including the time to drain the buffers). The same phase ratio is used in each tank, for example 0.3 in Figure 7.11, however, the total system phase ratio is the combination of the two tanks, i.e. 0.6. The third option is to carry out two adsorption cycles using one tank, as shown in column C of Figure 7.11. It is assumed that CIP would not be needed but an extra wash step was included between the two cycles prior to the re-equilibration of the same adsorbent.

7.2.2.2 Windows of Operation

The method of constructing Windows of Operation described in Section 7.2.1.6 was used to obtain a set of windows which provide a rapid visual evaluation of the various adsorption process options. As stated in Section 7.2.1.6 the Windows of Operation in this study are compared on the basis of the maximum achievable process yield (%) and throughput (g Fab'/h), given the operational constraints.

Figure 7.12 a)-c) and Figure 7.13 a)-c) present the Windows of Operation for the primary recovery and initial purification of Fab' from an *E. coli* homogenate and lysate feedstock, respectively, and show how the number of adsorption cycles affects the operating region and the performance parameters of yield and throughput. For ease of comparison Figure 7.9 f) and Figure 7.10 are presented again as Figure 7.12 a) and Figure 7.13 a), respectively.

Table 7.5 summarises the maximum achievable process yield and throughput for each of the adsorption process options outlined in Figure 7.11, with the corresponding operating conditions which result in the feasible operating regions. In order to minimise the batch and adsorbent volumes, the minimum possible phase ratio which results in the operating region is presented.

Table 7.5. The maximum achievable process yield (%) and throughput (g/h) for the three adsorption processes outlined in Figure 7.11, including the operating conditions which give the feasible operating regions in the Windows of Operation shown in Figure 7.12 and Figure 7.13. In process A the adsorption is performed as one cycle in one tank. Process B consists of two cycles performed in parallel in two tanks and, finally, process C consists of two cycles performed in series in one tank.

	Homogenate			Lysate		
Ads' Process	**A**	**B**	**C**	**A**	**B**	**C**
Yield (%)	50	69	69	72	84	84
Thr'put (g/h)	50	70	54	8	11	10
	Feasible Operating Conditions					
Minimum V_m/V_l (-)	~0.24	~0.45	~0.24	~0.24	~0.55	~0.27
Solids (% ww/v)	10 / 7.8-9.0	10 / 7.8-9.0	10 / 8.2-9.0	10	10	10

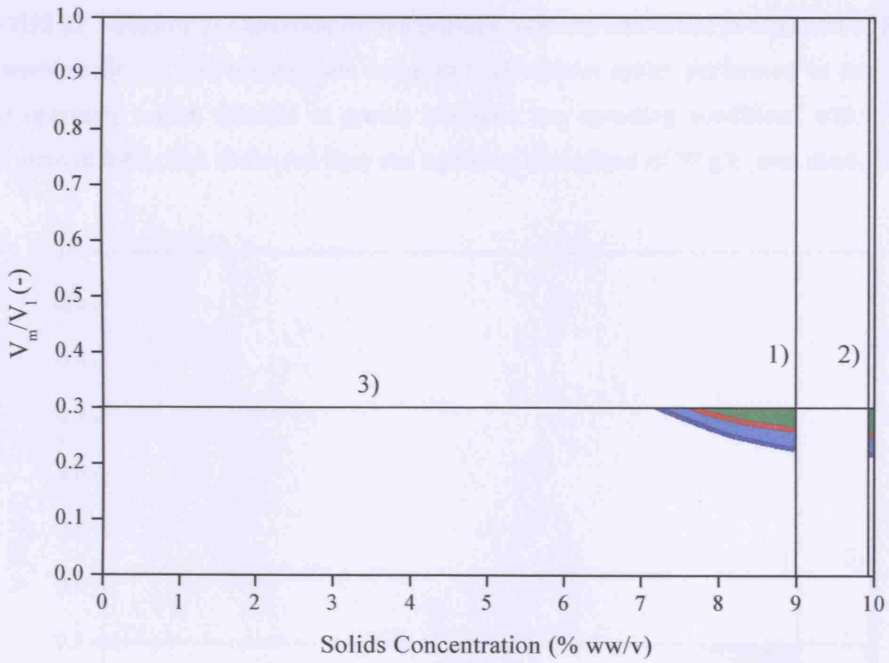

Figure 7.12 a). Window of Operation for the primary recovery and initial purification of Fab' from a 10% (ww/v) solids *E. coli* homogenate using a single cycle batch adsorption process. The feasible operating region (shaded in green) identifies the operating conditions which result in a process yield of 50% (area above red line) and a process throughput of 50 g/h (area shaded blue).

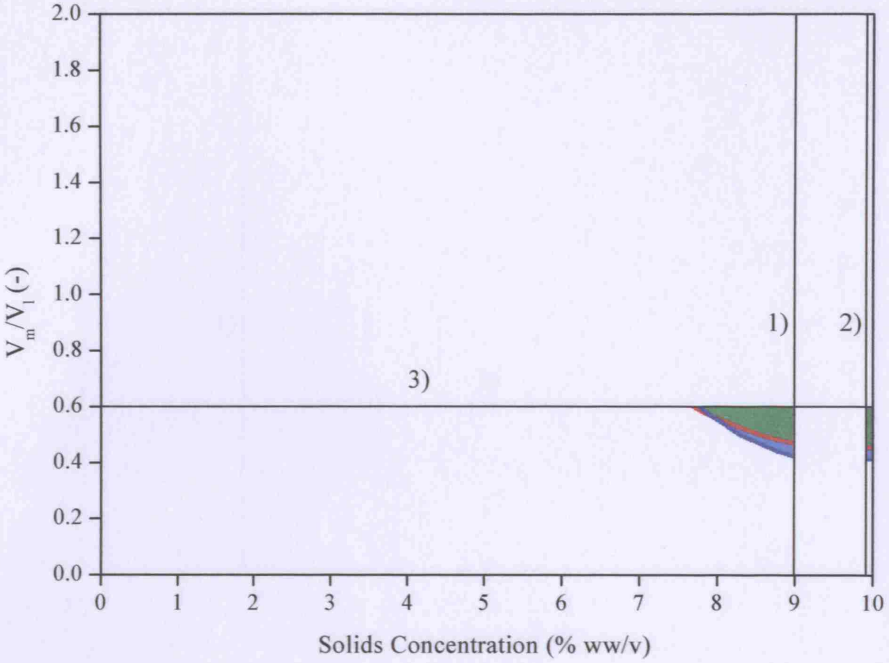

Figure 7.12 b). Window of Operation for the primary recovery and initial purification of Fab' from a 10% (ww/v) solids *E. coli* homogenate using two adsorption cycles performed in two tanks. The feasible operating region (shaded in green) identifies the operating conditions which result in a process yield of 69% (area above red line) and a process throughput of 70 g/h (area shaded blue).

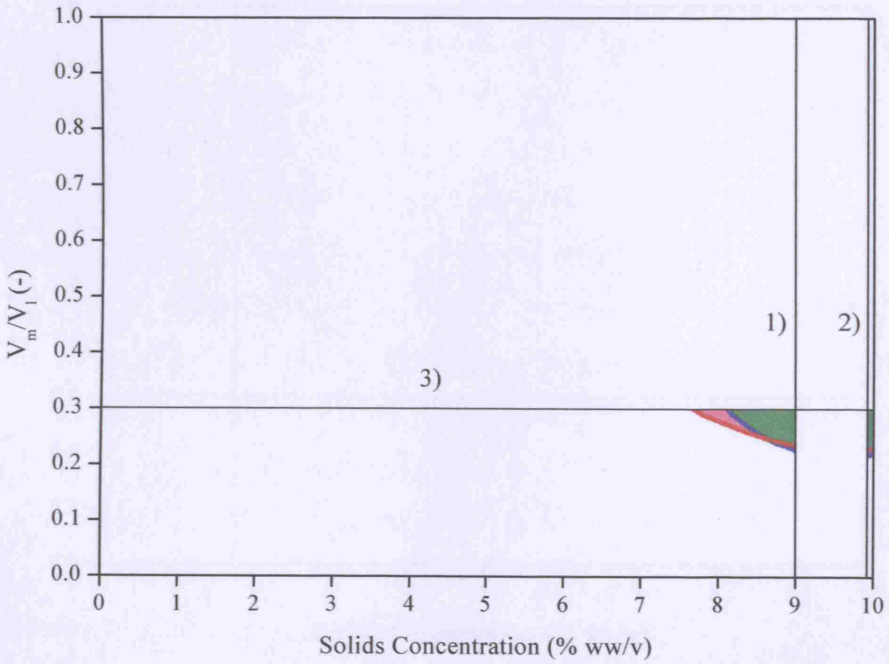

Figure 7.12 c). Window of Operation for the primary recovery and initial purification of Fab' from a 10% (ww/v) solids *E. coli* homogenate using two adsorption cycles performed in series in one tank. The feasible operating region (shaded in green) identifies the operating conditions which result in a process yield of 69% (area above red line) and a process throughput of 54 g/h (area shaded blue).

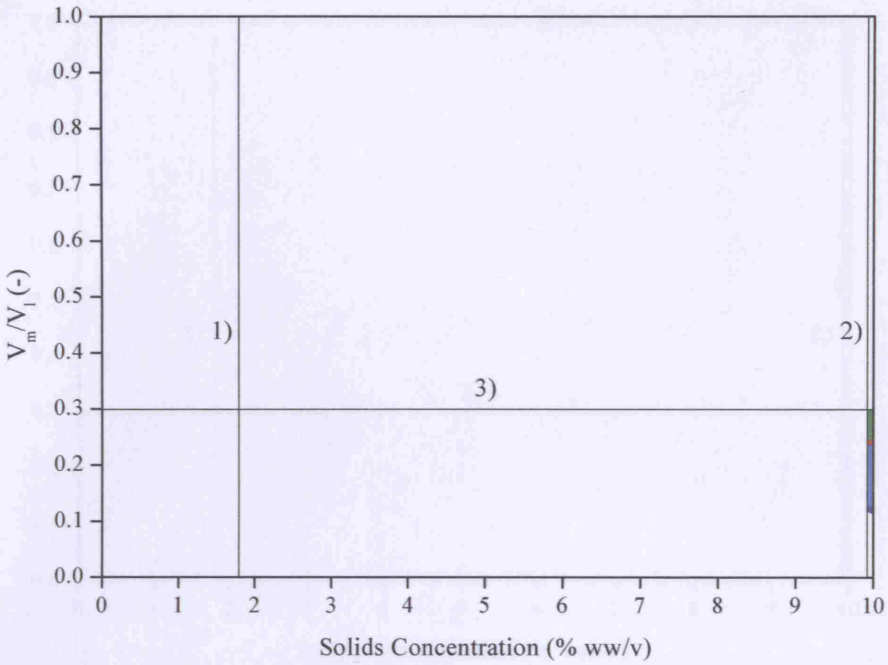

Figure 7.13 a). Window of Operation for the primary recovery and initial purification of Fab' from a 10% (ww/v) solids *E. coli* lysate using a single cycle batch adsorption process. The feasible operating region (shaded in green) identifies the operating conditions which result in a process yield of 72% (area above red line) and a process throughput of 8 g/h (area shaded blue).

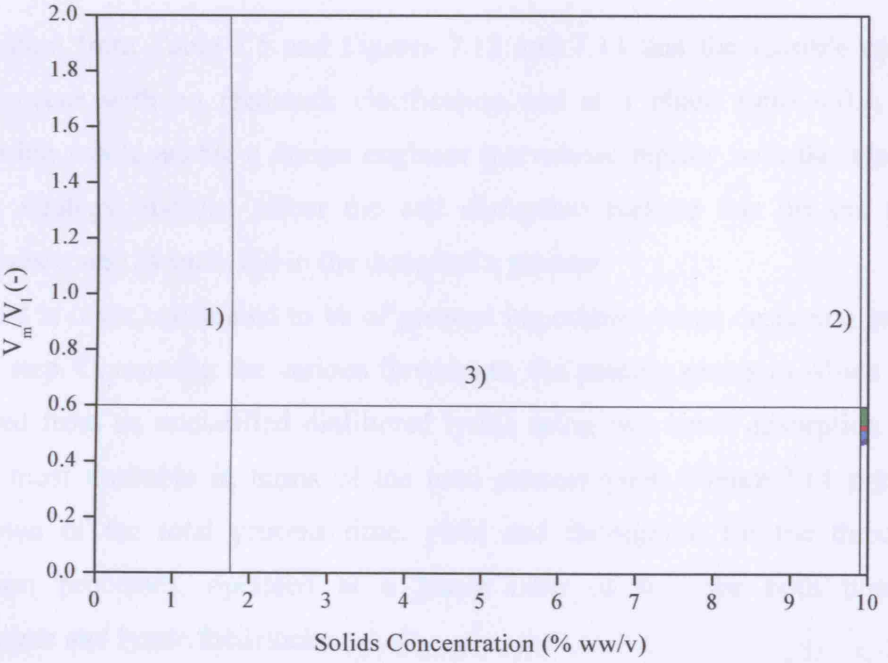

Figure 7.13 b) Window of Operation for the primary recovery and initial purification of Fab' from a 10% (ww/v) solids *E. coli* lysate using two adsorption cycles performed in two tanks. The feasible operating region (shaded in green) identifies the operating conditions which result in a process yield of 84% (area above red line) and a process throughput of 11 g/h (area shaded blue).

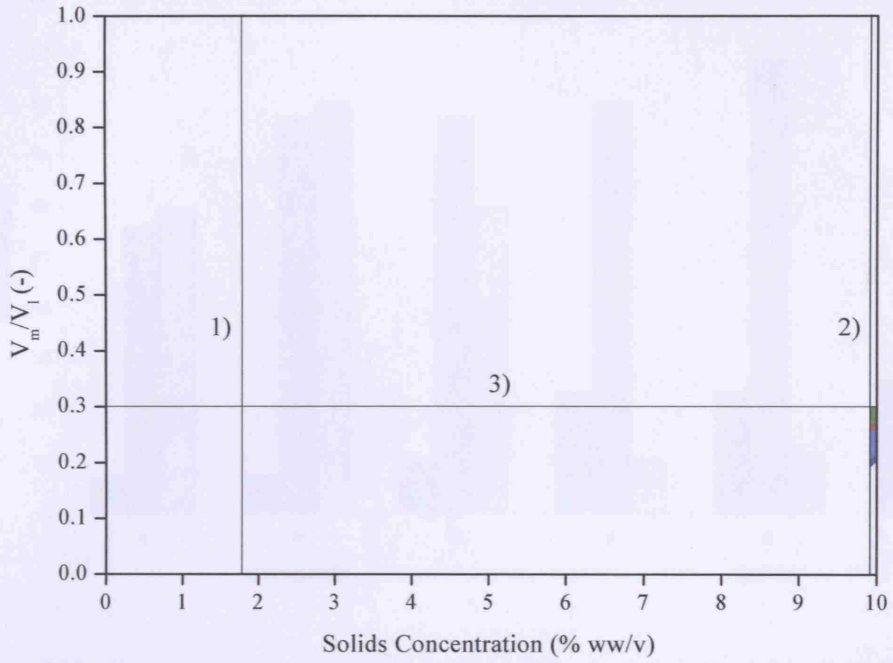

Figure 7.13 c). Window of Operation for the primary recovery and initial purification of Fab' from a 10% (ww/v) solids *E. coli* lysate using two adsorption cycles performed in series in one tank. The feasible operating region (shaded in green) identifies the operating conditions which result in a process yield of 84% (area above red line) and a process throughput of 10 g/h (area shaded blue).

It is evident from Table 7.5 and Figures 7.12 and 7.13 that the feasible operating regions occur with no feedstock clarification and at a phase ratio < 0.3. Such information would enable a design engineer to evaluate rapidly both the adsorption process strategy and the effect the cell disruption method has on the process performance, and as such, aid in the design of a process.

The yield is often considered to be of greatest importance when designing an initial capture step. Comparing the various flowsheets, the process routes in which Fab' is recovered from an unclarified diafiltered lysate using two batch adsorption cycles, are the most desirable in terms of the total process yield. Figure 7.14 presents a breakdown of the total process time, yield and throughput for the three batch adsorption processes, operated at a phase ratio of 0.3, for both unclarified homogenate and lysate feedstocks.

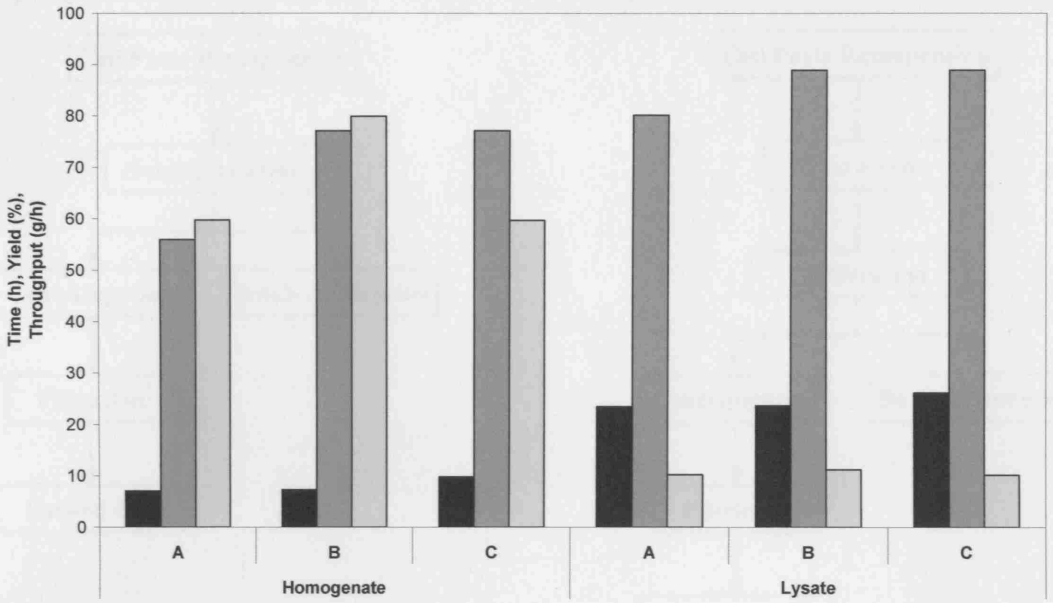

Figure 7.14. The process time (■), yield (■) and throughput (■) for Fab' adsorption processes utilising unclarified homogenate and lysate feedstocks. During process A the adsorption is performed as a single cycle in one tank. Process B consists of two cycles performed in parallel in two tanks and, finally, process C consists of two cycles performed in series in one tank. The phase ratio for adsorption process A and C is 0.3 and 0.6 for B (0.3 + 0.3).

It is clear to see in Figure 7.14 that the process routes which utilise cell lysis suffer from significantly extended process times and reduced throughput, when compared to those utilising high pressure homogenisation. Despite the lower process yields, the homogenisation routes may be more desirable in a situation where the stability of the product demands a short process time. The use of the model developed in this study, combined with Windows of Operation, enables such trade-offs to be assessed and their affects on the process to be visualised, allowing rapid evaluation.

7.2.3 Case Study 3: Comparing the use of batch and packed bed adsorption

This case study provides an evaluation of two process flowsheets, one utilising stirred tank batch adsorption, and the other packed bed adsorption. The comparison will be based solely on the process parameters of yield, throughput, and total time. Once again, the method of cell disruption will also be included in the analysis. Figure 7.15 shows the two process flowsheets being evaluated.

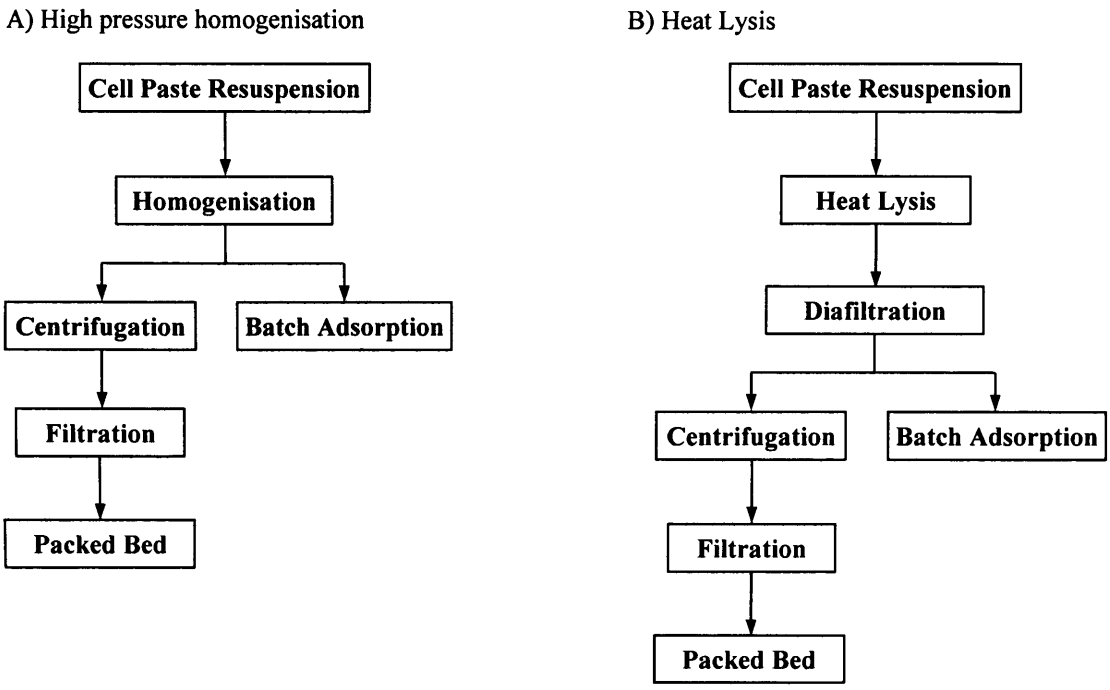

Figure 7.15. Flowsheet options for the primary recovery and initial purification of Fab', expressed in the periplasm of *E. coli.* In order to prepare the feedstocks for packed bed adsorption, centrifugation and filtration are essential unit operations which must be included in the process route. The lysis route requires an additional diafiltration step to reduce the ionic strength in preparation for ion exchange adsorption.

7.2.3.1 Process flowsheets and assumptions

The batch adsorption process used in this case study was based on the assumptions described in Section 7.2.2.1. The feedstocks being processed were assumed to be unclarified and to have a solids concentration of 10% (ww/v), giving a load volume of 1,000 L. The batch adsorption was performed with a phase ratio of 0.1 and consists of two cycles carried out in series in one tank (process C in Figure 7.11). In this example the phase ratio for the batch adsorption system was assumed to be 0.1 so that the phase ratios of the two processes would be comparable.

The packed bed route includes a centrifugation and filtration step to obtain feedstocks with a solids concentration of 0.01% (ww/v). It is assumed that the removal of solids leads to a reduction in the volume of the feedstock being processed and as a result the volume being loaded is assumed to be 900 L. The column used is assumed to have a 0.9 m diameter and column volume (CV) of 95 L, giving a phase

ratio of 0.1. The process time for the packed bed route was calculated based on the following assumptions:

- Equilibration lasting 30 min
- Two adsorption cycles loaded at 300 cm/h
- 5 CV wash
- 3 CV elution
- No CIP
- Percentage Fab' recovery, R = 0.95

7.2.3.2 Process time, yield and throughput

The results of the comparison study are presented in Table 7.6. It is evident that in this case, the use of stirred tank batch adsorption has significant advantages over the use of packed bed columns.

Table 7.6. Results of Case Study 3. Process flowsheets based on either stirred tank batch adsorption or packed bed adsorption were assessed, along with the impact of cell disruption methods. The feedstocks used in the batch adsorption study were assumed to have a solids concentration of 10% (ww/v) and a volume of 1,000 L. The feedstocks used in the packed bed study were clarified and had a solids concentration of 0.01% (ww/v) and a volume of 900 L. The processes were compared based on the total process time, yield and throughput.

	Batch Adsorption		**Packed Bed**	
	Homogenate	**Lysate**	**Homogenate**	**Lysate**
Time (h)	8.9	25.3	11.9	26.8
Yield (%)	52.4	84.5	48.4	25.5
Thr'put (g/h)	44.5	9.9	31.0	2.8

The lower yields observed in the packed bed flowsheets are due to the loss of debris-bound Fab', as a result of clarification of the feedstocks. When combined with the increased process time, required for centrifugation and filtration, the resulting throughput is significantly lower. However, there are many factors which contribute to the total process time. As described in Section 7.2.1.1 the model incorporates liquid transfer times as well as the time required for the unit operations and the adsorption process. In this case, the adsorption process time for packed beds is in fact

shorter than that of batch systems. Rather it is the additional unit operations used in the pre-treatment of the feedstocks that results in the increased process time.
The low yield observed in the homogenate batch system is due to the low phase ratio, resulting in the incomplete binding of Fab'. A possible explanation why a similarly low yield was not observed in the lysate batch system is the fact that the lysate contains fewer contaminants than the homogenate.

Based on the results of this case study, given the assumptions made, the primary recovery and initial purification of Fab' is most efficiently achieved through the processing of an unclarified lysate using batch adsorption.

7.2.4 Case Study 4: Model sensitivity analysis – the effect of lysis time and Fab' partitioning

The aim of this case study was to assess the sensitivity of the model to changes in the process and feedstock properties. The batch adsorption processes used in this case study were based on the assumptions described in Section 7.2.2.1 and the Windows of Operation were constructed as described in Section 7.2.1.6.

7.2.4.1 The effect of a reduced lysis time

This section describes the effect of lysis time on the total process throughput, and shows how decreasing the lysis time impacts the feasible operating region of the Window of Operation. For ease of comparison Figure 7.13 b) is presented in this section as Figure 7.17 a).
As discussed in the previous case studies, the length of the lysis procedure significantly impacts the total process time and throughput. A process flowsheet which includes the lysis step must also include diafiltration in order to reduce the ionic strength. In this case these two unit operations cause an increase in the process time of 16 h, when compared to the homogenate flowsheet (homogenisation assumed to last 4 h in Section 7.2.1). As Figure 3.6 showed, the concentration of Fab' begins to stabilise approximately 4 h into the lysis procedure, and therefore, it may be possible to reduce the length of the lysis protocol. Although the quality of the Fab'

obtained during the lysis procedure improves over time it was assumed, for the purpose of this investigation, that the quality and concentration of Fab' available after 4 h of lysis is the same as that present in the lysate after 16 h. (In order to improve the accuracy of this assumption, the quality of the Fab' obtained over the course of the lysis procedure could be monitored experimentally to determine the point at which the quality of Fab' becomes constant.)

Figure 7.16 shows how the length of the lysis procedure effects the total process throughput of a process recovering Fab' from an unclarified lysate using a batch adsorption process consisting of two cycles performed in two tanks (process B in Figure 7.11). In this case, a decrease in the lysis time from the standard 16 h to a minimum of 4 h, results in a doubling of process throughput.

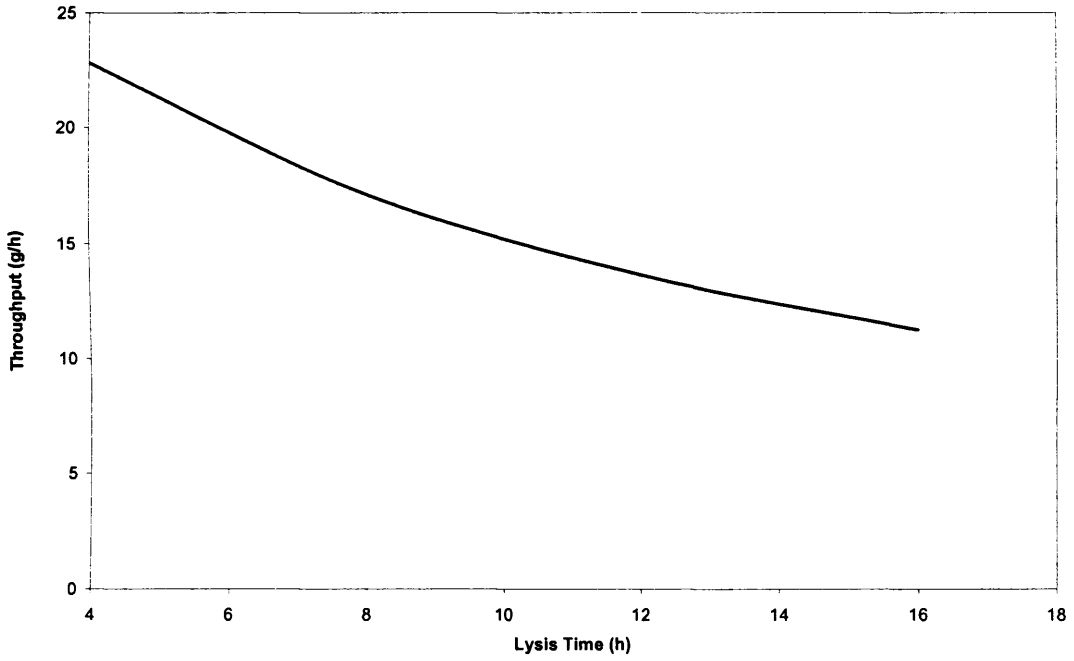

Figure 7.16. The effect that lysis procedure length has on the total process throughput of a process recovering Fab' from an unclarified lysate, with a solids concentration of 10% (ww/v), using a batch adsorption process consisting of two cycles performed in two tanks, with a combined phase ratio of 0.6 (each tank has a phase ratio of 0.3).

Figure 7.17 a) shows the Window of Operation for a process which includes a 16 h lysis procedure and adsorption comprising of two cycles, performed in two tanks. The performance parameters of yield and throughput were 84% and 11 g/h,

respectively. Figure 7.17 b) presents the Window of Operation for the same process, however, with a reduced lysis time of 4 h. The performance parameters remain the same, fixed at 84% and 11 g/h. It is clear to see that although the operating region remains the same size, due to the yield remaining constant, the region which represents the satisfaction of the throughput requirement (shaded in blue) has now increased in size, indicating it is now easier to achieve the required throughput.

Although decreasing the lysis time improves the throughput of the process flowsheet utilising that unit operation, the throughput is still significantly lower than that of a process which uses homogenisation as oppose to lysis, as show in Figure 7.18.

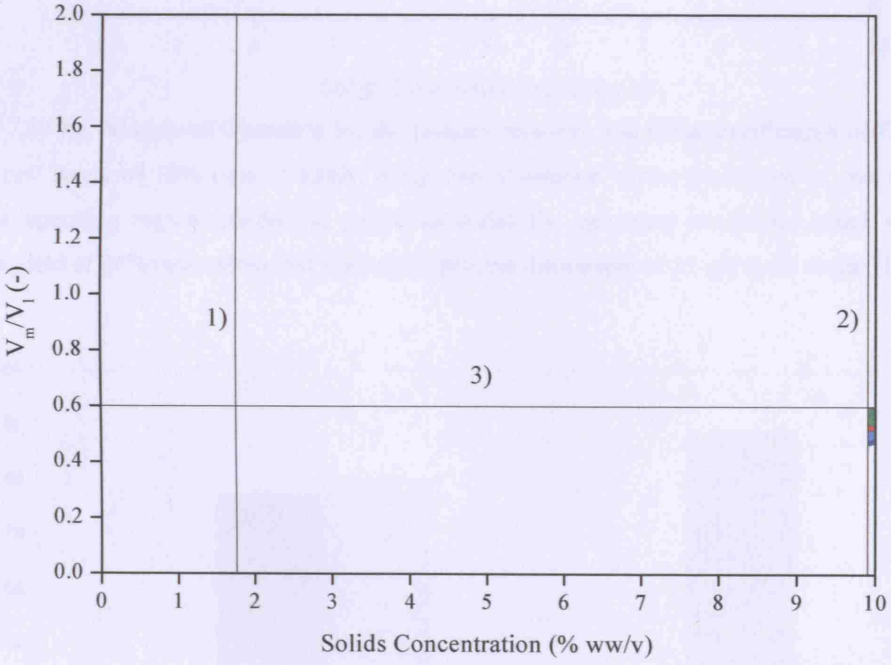

Figure 7.17 a). Window of Operation for the primary recovery and initial purification of Fab' from a 16 h *E. coli* lysate of 10% (ww/v) solids, using two adsorption cycles performed in two tanks. The feasible operating region (shaded in green) identifies the operating conditions which result in a process yield of 84% (area above red line) and a process throughput of 11 g/h (area shaded blue).

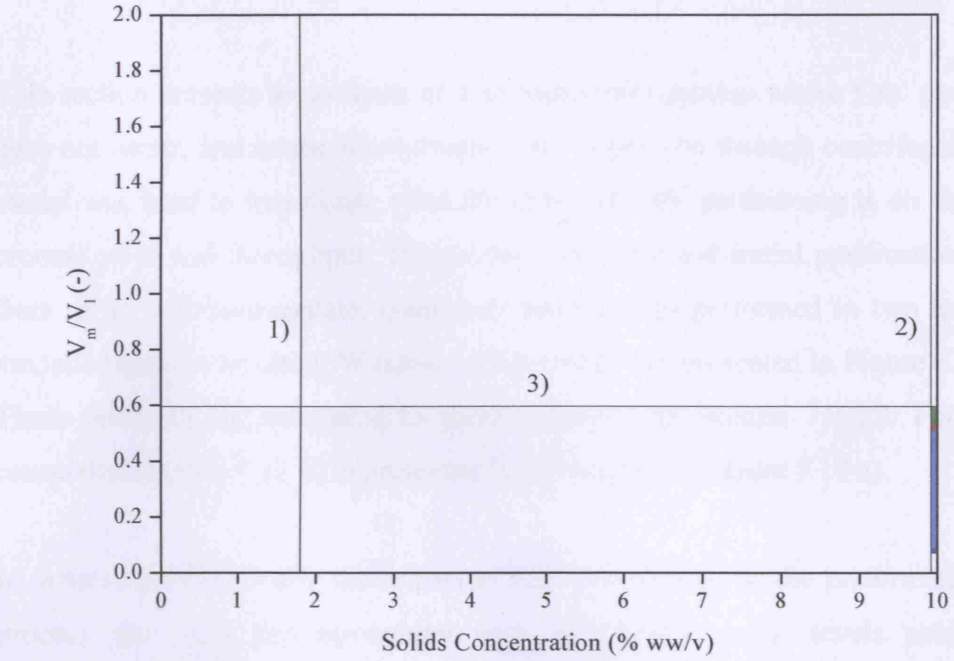

Figure 7.17 b). Window of Operation for the primary recovery and initial purification of Fab' from a 4 h *E. coli* lysate of 10% (ww/v) solids, using two adsorption cycles performed in two tanks. The feasible operating region (shaded in green) identifies the operating conditions which result in a process yield of 84% (area above red line) and a process throughput of 11 g/h (area shaded blue).

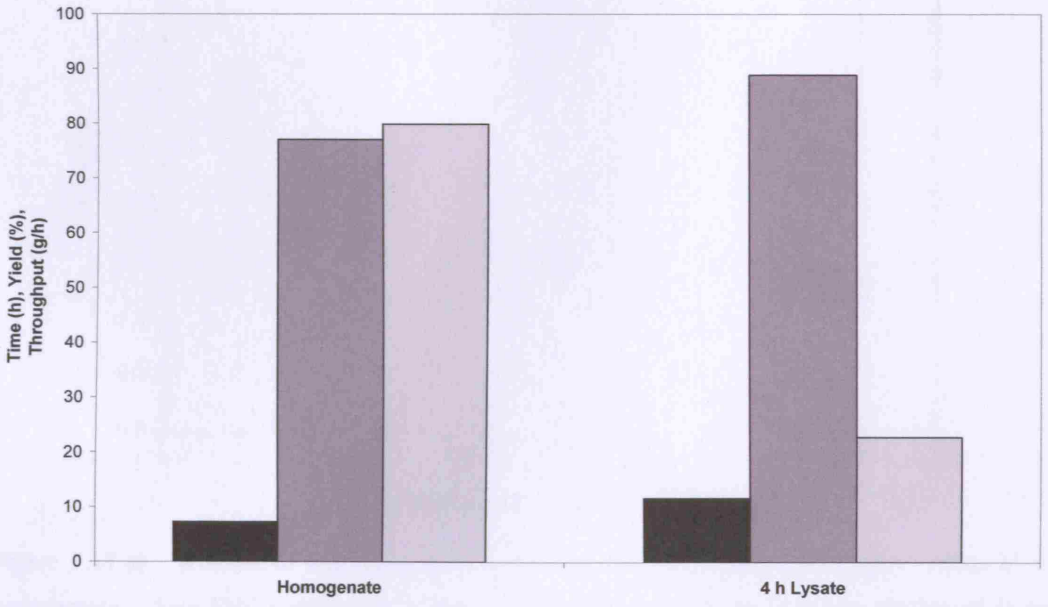

Figure 7.18. Comparing the process time (■), yield (■) and throughput (■) for two Fab' adsorption processes utilising either an unclarified homogenate or a diafiltered 4 h lysate. Both feedstocks have a solids concentration of 10% (ww/v), and the adsorption process consists of two adsorption cycles performed in two tanks, with a combined phase ratio of 0.6 (each tank has a phase ratio of 0.3).

7.2.4.2 Fab' partitioning

This section presents an analysis of a hypothetical situation where Fab' partitioning does not occur, and hence debris-bound Fab' is not lost through centrifugation. The model was used to investigate what the effect of Fab' partitioning is on the overall process yield and throughput. The primary recovery and initial purification of Fab' from an *E. coli* homogenate, using two batch cycles performed in two tanks, was modelled and the resulting Windows of Operation are presented in Figure 7.19 a)-b). These windows are compared to those presented in Section 7.2.2.2. For ease of comparison Figure 7.12 b) is presented in this section as Figure 7.19 a).

In order to present clearly the impact of Fab' partitioning on the performance of the process, the yield and throughput were maintained at the levels presented in Table 7.5, i.e. a yield of 69% and a throughput of 70 g/h.

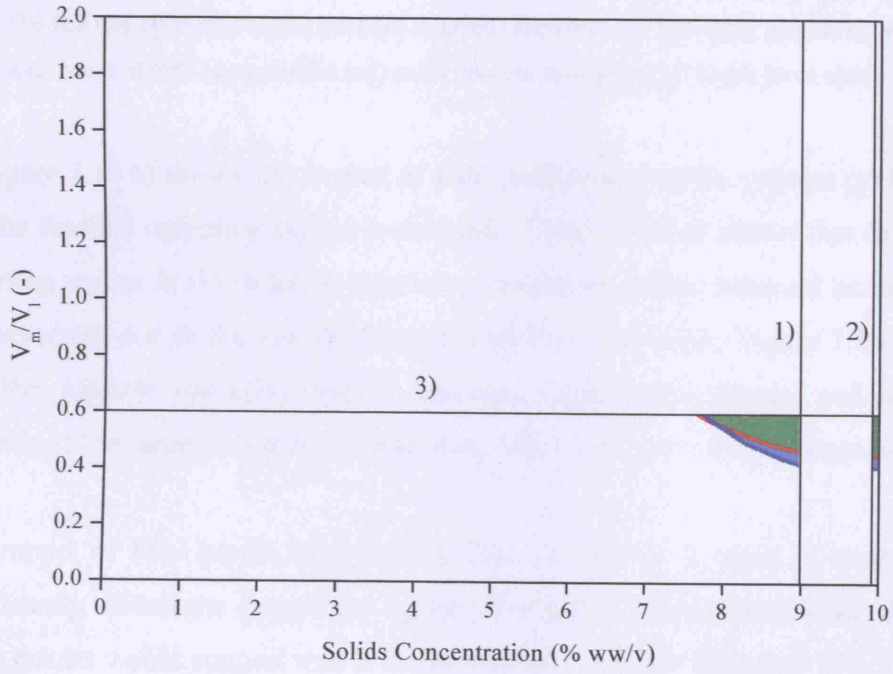

Figure 7.19 a). Window of Operation for the recovery of Fab' from a 10% (ww/v) solids *E. coli* homogenate, where Fab' partitioning DOES occur, using two adsorption cycles performed in two tanks. The feasible operating region (shaded in green) identifies the operating conditions which result in a process yield of 69% (area above red line) and a process throughput of 70 g/h (area shaded blue).

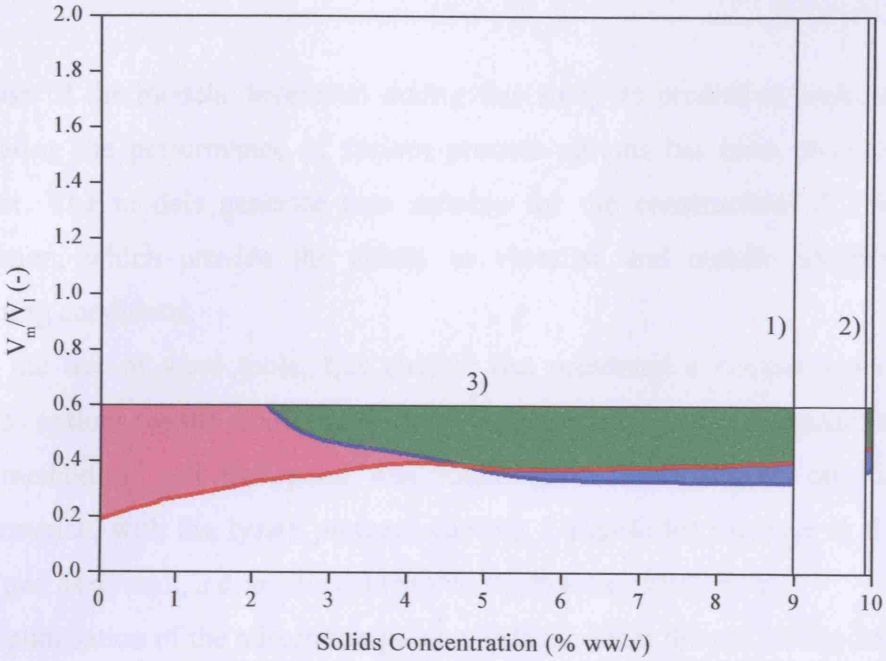

Figure 7.19 b). Window of Operation for the recovery of Fab' from a 10% (ww/v) solids *E. coli* homogenate, where Fab' partitioning does NOT occur, using two adsorption cycles performed in two tanks. The feasible operating region (shaded in green) identifies the operating conditions which result in a process yield of 69% (area shaded red) and a process throughput of 70 g/h (area above blue line).

As Figure 7.19 b) shows, the impact of Fab' partitioning on the process performance, and the feasible operating region is dramatic. Figure 7.19 a) shows that the feasible operating region is restricted to operating conditions where minimal centrifugation had occurred, due to the loss of debris-bound Fab'. However, Figure 7.19 b) shows that the feasible operating region becomes significantly larger, and spans the majority of the range of solids concentration when Fab' partitioning is not occurring.

The impact of Fab' partitioning and the loss of Fab' as a result of centrifugation significantly affects the design and operation of a downstream processing flowsheet. These results would suggest that it is essential to assess the tendency of a product to bind to cell debris prior to designing a process route, as this could have major impacts on the process yield.

7.3 Summary

The use of the models developed during this study as predictive tools, capable of evaluating the performance of various process options has been presented in this chapter. The models generate data suitable for the construction of Windows of Operation, which provide the ability to visualise and rapidly identify suitable operating conditions.

With the use of these tools, this chapter has presented a comparison of various process options for the recovery of Fab' from both an *E. coli* homogenate and lysate. The method of cell disruption was found to have an impact on the process performance, with the lysate protocol causing a significant increase in the process time, and as a result, a dramatic decrease in the process throughput.

The optimisation of the adsorption process indicated that the use of two batch cycles performed in two separate tanks gave the highest yield and throughput, and was the most desirable batch process option.

A process flowsheet incorporating the use of batch adsorption was also found to be more favourable, in terms of process time, yield and throughput, than an alternative process which utilised packed bed adsorption. This was mainly due to the loss of debris-bound Fab' and the necessity to clarify the feedstocks prior to loading onto a packed bed.

A sensitivity analysis found that the model was able to predict the effect of decreasing the lysis protocol time, as well as the effect of Fab' partitioning. Decreasing the length of the lysis procedure from 16 to 4 h lead to a 100% increase in the total process throughput. Fab' partitioning was found to affect significantly the operating region of a Window of Operation, and in a situation where the product was not binding to the cell debris, the process yield and throughput of a clarified feedstock were found to be greater.

8 Commercial benefits of implementing batch adsorption through the use of process optimisation tools

8.1 Introduction

The importance of getting a product to market as quickly as possible, coupled with the need to reduce production costs and improve process outputs, places significant pressures on manufacturers to employ rapid process development and explore alternative production methods. As stated in Chapter 7, development and commercialisation of a new product can cost as much as $800 million and take up to 12 years to complete. An additional concern to the biopharmaceutical industry is the knowledge that up to 85% of products in development will fail, often after undergoing clinical trials, and that significantly more money is spent on developing these failed drugs than on those that reach the market (Petrides *et al.,* 2002). Therefore, the implementation of any tools which could speed up process development and reduce the costs would be of great benefit to the industry.

This thesis has developed selected scale-down methods capable of rapidly evaluating various process parameters and combined those methods with the use of an optimisation model and Windows of Operation in order to identify an optimal process flowsheet. The use of batch adsorption as a viable alternative to conventional packed beds was examined from a process perspective.

This chapter aims to provide a qualitative analysis of the impact adopting such small scale process development and batch adsorption might have on a biopharmaceutical manufacturing process.

8.2 Process optimisation

The ability to evaluate large numbers of process parameters rapidly and cost-effectively has become an essential part of process development and

optimisation. The use of high throughput process screening (HTPS) provides the means to perform many hundreds, or even thousands of screening experiments which could help to accelerate process development, and reduce costs and the time to market.

Once the data required has been generated optimisation tools, such as computer aided process design (CAPD) can be used to simulate various process options and optimise the design and operation of the process.

8.2.1 High throughput process screening (HTPS)

Process development has historically been a process of trial and error and involved numerous experiments, often requiring large volumes of the final product. This approach to process development is costly, time consuming and the amount of data collected can be quite limited. Quite often in the early stages of drug discovery the aim is merely to produce enough material for pre-clinical and clinical phase I trials, and as a result the process may not be scalable or sufficiently robust (Sofer and Hagel, 1997). The development of a process which is scalable, robust and complies with FDA regulations requires time, sophisticated equipment, skilled staff, and of course, money (Pallapothu *et al.*, 2006). High throughput process screening can alleviate the burden on process development. The use of HTPS, quite often performed using microwell plates and automated robotic devices, provides a means to perform thousands of experiments in parallel, enabling the cheap and rapid evaluation of numerous process parameters and conditions. Automated HTPS using robots such as the Genesis (Tecan, Männedorf, Switzerland), the Multimek (Beckman-Coulter Inc., CA, USA) or the Gilson 215 liquid handler (Gilson Inc., WI, USA), can significantly speed up the development process, reducing the burden of manual labour, improving reproducibility, increasing throughput and reduce buffer requirements and cost. HTPS also enables characterisation of the total process and can provide vast amounts of data which can be stored as a detailed database, outlining the effect of process parameters and process integration. There are several examples of HTPS of chromatographic processes in literature (Welch *et al.*, 2002; Thiemann *et al.*, 2004; Follman *et al.*, 2004; Bastek *et al.*, 2004; Bensch *et al.*, 2005; Rege *et al.*, 2006). Incorporating the HTPS methods developed in this thesis into the

early stages of a development pipeline of a new pharmaceutical product would ultimately lead to cheaper, faster and more robust process development.

8.2.2 Computer aided process design

Chapter 7 showed how a mathematical model can be used to evaluate various process options. Process flowsheets for the initial recovery of Fab' from an unclarified feedstock utilising either packed beds or batch adsorption were compared. The model allowed the flowsheets to be compared rapidly and with no further experimentation. Through the use of mathematical models and simulations the number of labour-intensive experiments can be reduced, resulting in a shorter development time and reduced costs (Karlsson *et al.*, 2004). Simulation tools can be used from the moment an idea is generated right through to the design of the facility and large scale manufacturing (Petrides *et al.*, 2002). There are numerous examples of models being used to simulate and optimise both process development and large scale production of biopharmaceuticals (Katti and Jagland, 1998; Rouf *et al.*, 2001a; Rouf *et al.*, 2001b; Petrides *et al.*, 2002; Karlsson *et al.*, 2004; Mustafa *et al.*, 2006; Chhatre *et al.*, 2007). Process modelling is also used to evaluate the economic benefits of various process options (Novais *et al.*, 2001; Sinclair and Monge, 2002; Rathore *et al.*, 2004; Farid *et al.*, 2005; Lim *et al.*, 2006).

It is evident that the use of process simulation tools can have significant impacts on the development and commercialisation of a biopharmaceutical product.

8.3 Batch adsorption

Section 7.2.3 compared batch adsorption and packed beds from a process perspective, comparing the process time, yield and throughput. Based on the results of the process model used, the batch adsorption route was found to achieve greater process yields and throughput. This section aims to compare the two processes from a more commercial perspective.

Figure 8.1 compares the conventional packed bed route to that of the alternative stirred tank batch adsorption which may prove more desirable than packed beds, especially when large volumes of feedstock are being processed.

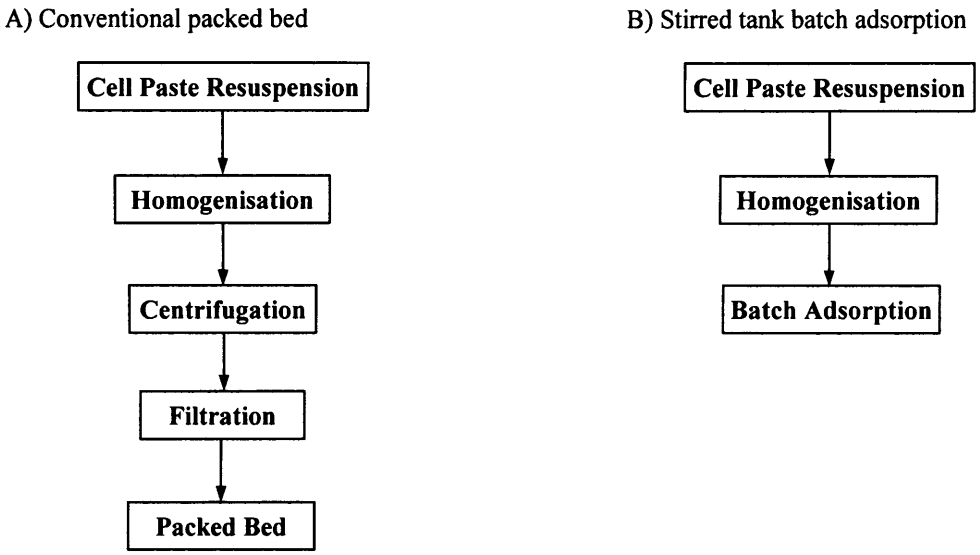

Figure 8.1. Flowsheet options for the primary recovery and initial purification of Fab' from an *E. coli* homogenate. In order to prepare the feedstocks for packed bed adsorption, centrifugation and filtration are essential unit operations which must be included in the process route.

When compared to conventional packed beds, stirred tank batch adsorption is a very straight forward and simple process. There are no sophisticated column packing methods which need to be mastered and no packing tests are necessary. Despite this, batch adsorption processes have traditionally used stirred tanks which are often open to the environment, are labour intensive and difficult to validate (Levison *et al.*, 1993), and their use in biopharmaceutical manufacturing has been limited. However, the recent introduction of Batch Columns (Bio-Rad, California, USA) is an indication of the commercial viability of batch adsorption for use within the industry. The Bio-Rad Batch Columns provide a fully automated and contained system which is easy to validate, as there is no manual filling and emptying of the media, and the system is completely sealed. An example of how the industry is beginning to adopt batch adsorption is CAF-DCF (Brussels, Belgium), the fractionation department of the Belgian Red Cross. CAF-DCF has a fully validated batch adsorption system using the Bio-Rad Batch Columns, handling up to 1250 kg/day plasma.

As seen in Chapter 6, the adsorption stage of a batch adsorption can be very fast. Levison *et al.* (1993) reported that the adsorption stage of a batch system lasted 30-60 min regardless of scale. Processing large volumes of material in a packed bed would take significantly longer and would therefore affect the operation and

scheduling of the process. Packed beds are also problematic when handling viscous or particulate-containing feedstocks, and so the conventional route requires substantial feedstock pre-treatment prior to the adsorption step. The lack of feedstock pre-treatment in a process utilising batch adsorption not only leads to an increase in the process yield, due to the removal of two unit operations, but also the process throughput.

There are also economic benefits when using batch adsorption instead of packed beds. The process flowsheet in Figure 8.1 shows that the batch route has removed the need for centrifugation and filtration. The cost savings can be significant, not only in terms of capital investment but also running costs associated with operating a centrifuge and filtration rig, which would include labour costs. Further savings can be made through the use of cheaper single-use adsorbents (Sofer and Hagel, 1997). The methods employed during this study used standard adsorbents designed for use in packed bed columns. These adsorbents are precision engineered, often to a specific particle diameter and have very high mechanical and chemical stability. The chemical stability is essential due to the repeated exposure to harsh cleaning agents used during cleaning-in-place (CIP) and adsorbent regeneration. The cost of the adsorbents used in batch adsorption can be less than that of those used in packed beds. Single-use adsorbents which lack the geometric refinement and rigidity essential to packed bed columns could be used in process scale batch adsorption (Lyddiatt, 2002).

8.4 Summary

Using the batch-based HTPS methods developed in this thesis optimisation of the batch adsorption method would be significantly faster, and cheaper, than the process development of a column based approach. The implementation of batch adsorption would also have both process and commercial benefits, and may lead to a reduction in the development and production costs.

9 Bioprocess Validation

9.1 Introduction

In order to get a product to market comprehensive validation must be performed by the manufacturer and documented evidence submitted to regulatory authorities. The US Food and Drug Administration (FDA) defines validation as "establishing documented evidence which provides a high degree of assurance that a specific process will consistently produce a product meeting its predetermined specifications and quality characteristics". Validation is often considered an expensive, time consuming drain on resources, and nothing more than yet another bureaucratic obstacle. However, validation should be seen as an opportunity to increase process understanding, improve product quality and reduce costs by ensuring that processes are operating under optimum conditions.

The aim of this chapter is not to provide a detailed and comprehensive review of validation, but to provide a brief description of the factors and processes which would have to be considered when attempting to validate the processes described in this thesis. Section 9.2 describes the general validation of a biopharmaceutical product. Section 9.3 discusses the validation issues surrounding a process designed to capture Fab' directly from an unclarified feedstock through the use of batch adsorption, as described in Section 7.2.3 and Figure 7.15 (flowsheet A - high pressure homogenisation).

9.2 General validation considerations

In order to validate fully a biopharmaceutical product many factors such as the process, equipment, quality systems and the cleaning must be taken into consideration. As a rule, anything which may impact the process and the final product quality must be validated.

9.2.1 *Validation master plan (VMP)*

The first step towards successful process validation is the generation of a validation master plan (VMP). The use of a VMP is not compulsory, but it is usually the first document the regulatory authorities will ask to see during an inspection. It is therefore very important to make sure the VMP is as comprehensive and detailed as possible. There is no standard structure which a VMP should take, however typically it would include the following:

- An introduction which clearly defines the project goals, the regulatory and compliance objectives, as well as a definition of the objectives of the VMP itself and the roles of personnel involved
- An operating description which details all the equipment, facilities and utilities used during the process, as well as a description of the flow of personnel, materials and products
- A validation policy which describes the policies for validation and revalidation of processes, methods and cleaning
- A detailed schedule and a description of the scope of the validation of critical components
- A description of the maintenance of rooms, systems, computers and software and all equipment
- A description of documentation such as standard operating procedures (SOPs), batch records, personnel training, calibration and certification

9.2.2 *Process validation*

Process validation is needed to ensure strict control of manufacturing processes in order to avoid any changes in the quality of the final product. The production and analytical methods, as well as equipment and materials used must be characterised. Any changes or deviations from the validated process must be documented and re-validated.

9.2.3 *Equipment qualification*

Equipment qualification consists of four main stages. Firstly, design qualification (DQ) provides verification that the equipment design is cGMP and VMP compliant, is calibratable and that the required utilities are available and validated. Installation qualification (IQ) then ensures that all critical equipment has been commissioned and installed correctly. Operational qualification (OQ), which is often combined with IQ, demonstrates the functionality of the equipment and ensuring that they operate within critical design limits. Finally, performance qualification (PQ) provides evidence that the process is robust and reliable and will consistently produce the desired product.

9.2.4 *Quality systems validation*

A VMP specific to the quality systems could also be implemented. For example, the specificity, accuracy, precision and reproducibility of all assays used must be established and documented. All equipment used in QC must be listed, calibrated and well maintained.

9.2.5 *Cleaning process validation*

Standard operating procedures (SOPs) for the cleaning process must be established, and the reproducibility of the methods tested and documented. The endpoint of the cleaning process must be clearly defined and the sampling methods used to determine the level of contamination must be validated.

9.3 Validating the direct capture of Fab' from an unclarified feedstock through the use of batch adsorption

This section describes the validation considerations for a process designed to combine the primary recovery and initial purification of Fab' from an unclarified *E. coli* homogenate. As described in Section 7.2.3 and Figure 7.15 (flowsheet A - high pressure homogenisation) the process consists of cell disruption by means of high pressure homogenisation and direct capture through the use of batch adsorption.

The batch adsorption is performed in a stirred tank and utilises single-use ion exchange adsorbents.

9.3.1 Cell disruption

The main concern during cell disruption is the degree of cell disruption and the level of contamination caused by the release of cellular products. The release of nucleic acids affects the performance of anion exchangers, and so the concentration of nucleic acids must be monitored (Sofer and Hagel, 1997).

9.3.2 Batch adsorption

There are similarities between validating batch adsorption and chromatography. The validation of chromatography involves the qualification of the equipment and the process, the definition of acceptance criteria for the adsorbents, as well as the validation of the cleaning procedures (Sofer and Hagel, 1997).

9.3.2.1 Equipment qualification

The typical equipment used during batch adsorption includes the adsorption tanks, pumps, valves and stirrers. The manufacturer of the specialist tanks (tanks with a mesh, similar to the modified Amicon Stirred Cell described in Section 2.4.4.1), would have to be validated and ensure that the design and installation of the equipment meets DQ/IQ requirements, as set out in the VMP. OQ tests would ensure the stirred tank system as a whole functions as required, within the critical design limits. This would include testing the stirrer, pumps, valves and control systems, including any computers and software. Unlike a packed bed system there are no OQ tests to assess the column packing, as this is not relevant to a stirred tank. However, the efficiency and reproducibility of the mixing could be assessed through the use of mixing tests (Doran, 2002).

9.3.2.2 *Performance qualification*

The performance qualification (PQ) of the batch adsorption system would demonstrate that the process performs consistently and reliably. The process would be assessed on performance parameters such as the yield, product purity, impurity reduction and stability of the process intermediates and bulk product. In order to validate the reproducibility of the process three consecutive full scale runs must all meet predefined performance criteria.

9.3.2.3 *Adsorbents qualification*

The first step in adsorbent qualification is to use vendors that provide either a regulatory support file (RSF) or drug master file (DMF) (Gavin *et al.*, 2006). These files provide information regarding the separation performance, binding capacity, characterisation of lot reproducibility and leachables (Sofer and Hagel, 1997). Lot reproducibility is often detailed in a certificate of analysis (CoA) which is supplied with the adsorbent. Without such data files, the manufacturer must take the responsibility, cost and burden to perform the necessary tests in order to qualify the adsorbents. The binding capacity of the adsorbent must be tested as it affects the separation performance. It can in fact be used to qualify lot reproducibility as it is an indicator of pore-size distribution and product-accessible surface area (Gavin *et al.*, 2006).

Although the adsorbents used in this study are assumed to be disposable, the problem of leachables would also have to be considered. Adsorbents are known to breakdown during their use, releasing components of the media such as the ligand. This may occur at any time during the process, including storage and even during product elution. It is essential to determine when during the process the leaching is occurring and to characterise the leachables. Adsorbent vendors would perform some form of characterisation and the information would be included in the RSF or DMF (Gavin *et al.*, 2006).

9.3.2.4 Cleaning validation

Cleaning validation requires a clearly defined objective, such as the consistent reduction of product residuals and cleaning agents to a predetermined level. The use of SOPs which clearly state the concentration of cleaning agents, the residence time, temperature, pressure and flow rate, as well as the number of wash and rinse cycles, must be demonstrated. In this case, the cleaning and sanitisation of the storage and adsorption tanks must be validated and the surfaces tested through the use of swabs and qualified QC assays. The safety, efficacy and compatibility of the cleaning agents must also be assessed.

The cleaning of adsorbents is a critical element of chromatographic cleaning validation, however in this case the adsorbent is assumed to be disposable, removing the need for cleaning and cleaning validation.

9.4 Summary

The validation of biopharmaceutical product manufacturing is clearly more than just a bureaucratic obstacle, it is an essential part of process development and manufacturing. The validation process benefits both the manufacturer and the consumer as it ensures the product is of the highest possible quality and safety.

The validation of batch adsorption systems differs slightly from a conventional packed bed process. However, with the use of a well structured validation master plan, validation of such processes can easily be achieved.

10 Conclusions

The aim of this thesis was to evaluate alternative adsorptive process options for the recovery of antibody fragments from crude *E. coli* feedstocks. Scale-down methods, including microwell batch adsorptions, have been developed and applied in order to assess rapidly a range of process options and feedstock properties. The work has highlighted and addressed some of the challenges related to the recovery of antibody fragments through the use of conventional downstream methods.

As one of the first unit operations used during the recovery of periplasmically expressed antibody fragments the method of cell disruption can have a significant impact on the subsequent separation process. The use of high pressure homogenisation and selective periplasmic release were found to have a significant impact on the properties of the resulting feedstock. High pressure homogenisation yields a solution of low ionic strength, however, due to the release of all cell contents, the feedstock contains many contaminants, which may complicate subsequent purification steps. Although the lysate resulting from the periplasmic extraction was relatively pure, containing only few contaminants, the lysis buffers used resulted in the feedstock having a high ionic strength. Ion exchange adsorption of the antibody fragments from the homogenate was possible without the need for any reduction in the feedstock ionic strength. However, in order to purify the antibody fragments from the lysate hollow fibre diafiltration was needed to reduce the ionic strength. Reducing the ionic strength of the unclarified feedstocks was found to increase the level of debris-Fab' interactions, which would have a significant impact on the design of the purification route.

The effect of process variables, such as the feedstock ionic strength and solids concentration, on the adsorption of antibody fragments was investigated through the use of adsorption isotherms. Adsorption isotherms performed at small scale in a custom built microwell plate showed how decreasing the feedstock ionic strength and solids concentration can significantly improve the adsorption of Fab' onto SP Sepharose FF. A decrease in the ionic strength of the clarified homogenate, from 8.5

to 3.2 mS/cm, lead to a 7-fold increase in the distribution coefficient (K), whereas the same reduction in the ionic strength of the clarified lysate lead to a 36-fold increase. Clarification of the homogenate and lysate feedstocks lead to a 1.7- and 3-fold increase in K, respectively. The results of the isotherms also confirmed that the lysate contained fewer contaminants than the homogenate, as seen by the higher distribution coefficients, indicating a greater degree of adsorption.

Laboratory scale packed bed columns were used to investigate the affect of feedstock properties on the adsorption of Fab' from a range of *E. coli* feedstocks. The results of the packed bed studies confirmed the findings of the adsorption isotherms; the presence of the cell debris adversely affects the adsorption of Fab', causing the breakthrough curves to appear linear, and reducing the ionic strength of the feedstock leads to improved Fab' binding and a delayed breakthrough. At 50% product breakthrough the dynamic binding capacity (DBC) was found to drop from 7.98 to 4.30 mg/mL SP in the presence of cells and cell debris. The DBC for a clarified homogenate, measured at 50% product breakthrough was found to increase 6-fold as a result of decreasing the feedstock ionic strength from 8.5 to 2.9 mS/cm.
Although it was possible to load unclarified feedstocks onto a laboratory packed bed column, doing so caused bed compression, over-pressuring of the system and resulting in a significant decrease in the dynamic binding capacity. The Stickel model (Stickel *et al.*, 2001) was used to obtain a laboratory scale packed bed column which had the packing structure of an industrial scale packed bed. This packing mimic would remove any wall support artefact and give an indication if whether loading unclarified feedstocks at large scale would be feasible. The results indicated that, for this biotypical feed, without the wall support experienced at small scale, and the reduced bed porosity, loading of an unclarified feedstock at industrial scale would not be possible.

Due to the limitations of the packed bed columns and the associated loss of product through feedstock clarification, the use of stirred tank batch adsorption as an alternative to packed bed chromatography was investigated. The presence of homogenate cell debris was not found to significantly affect the degree of Fab' adsorption when performed in both a microwell and stirred tank. The use of stirred

tank batch adsorption was shown to be a viable alternative to conventional packed beds for the recovery and initial purification of Fab' from unclarified feedstocks.
The results also showed that it is possible to scale-up successfully the batch adsorption process from a microwell plate using 0.2 mL feedstock per well to a stirred tank with a volume of 135 mL. The use of ultra scale-down microwell batch adsorptions allows the rapid evaluation of feedstock properties and process variables, whilst utilising minimal volumes of the feedstock.

The results of the adsorption isotherms were used to develop a process model capable of evaluating the performance of a wide range of process options for the recovery of Fab' from *E. coli* feedstocks. The process model was used to generate data which enabled the construction of Windows of Operation, and therefore, the visualisation and rapid identification of suitable operating conditions. The Windows of Operation were used to compare various process options, including: flowsheets incorporating high pressure homogenisation or periplasmic cell lysis, optimisation of the batch adsorption process, flowsheets utilising either stirred tank batch adsorption or packed bed chromatography, and finally, the impact the length of cell disruption has on the process yield and throughput. The results suggest that the use of periplasmic extraction causes a significant increase in the process time as a result of the lengthy extraction process, coupled with the need for diafiltration in order to reduce the feedstock ionic strength. For the preparation of a clarified feedstock ready for ion exchange adsorption, a process utilising periplasmic cell lysis was found to take almost 3 times longer than a process utilising high pressure homogenisation, leading to a lower process throughput. The results of the batch adsorption optimisation suggested that using two adsorption cycles, performed in two separate tanks resulted in the highest process yield and throughput.

A process incorporating batch adsorption was more favourable than one utilising packed bed chromatography, in terms of process yield and throughput. This was primarily due to the feedstock pre-treatment steps resulting in product losses and extended processing times.

This study has highlighted the benefits of batch-based high-throughput process screening and how the use of such small scale methods, coupled with Windows of Operation and process modelling, could significantly speed up process development, as well as reduce costs associated with conventional development methods. The implementation of stirred tank batch adsorption could potentially provide both process and commercial benefits, leading to a reduction in production costs and improved process yields.

11 Future Work

This thesis has investigated the use of batch adsorption, high-throughput process screening, process modelling, and the use of Windows of Operation for the recovery and initial purification of Fab' from crude *E. coli* feedstocks. The results indicate areas which could benefit from further investigation. This chapter will describe some of the possible future work which could be of interest and importance.

11.1 Batch Adsorption

The results of this study have shown that the scale-up of batch adsorption from microwell to laboratory scale stirred tanks is possible and reproducible. However, in order to evaluate the use of batch adsorption as a viable industrial alternative to packed bed columns further scale-up studies should be performed to determine whether large scale recovery of Fab' from unclarified feedstocks is possible. This could either be performed in specialised equipment, such as the Bio-Rad Batch Columns, or in modified stirred tanks. The main aim would be to assess the levels of purity, yield and throughput achieved by batch adsorption, and compare them to those of a process utilising packed bed chromatography. Another aim would be to compare the large scale data to that of the microwell batch adsorptions in order to determine whether or not ultra scale-down methods can accurately predict large scale batch-based separation.

11.2 High-throughput process screening (HTPS)

The HTPS methods developed in this thesis have focussed on evaluating a range of feedstock properties and operating variables, such as the adsorbent phase ratio. These methods could also be applied to the screening of various adsorbent matrices in order to develop a Fab' purification sequence, where the yield and purity is assessed at each stage. For example, high salt tolerant matrices could be used in order to remove the need for diafiltration, or a purification route consisting of several ion exchange steps or one protein A step could be assessed. The data from such experiments could

be used to assess various combinations of adsorbents and sequence orders in order to obtain optimal Fab' recovery.

11.3 Process modelling

For the purpose of this study the process model developed in this thesis provided sufficient accuracy for the comparison of different process options. However, the model could be expanded and developed further to include other process variables such as adsorbent re-use and deterioration, CIP times, scheduling (including operator shifts) as well as an economic analysis of the various options being considered. This would provide more information as a basis from which process decisions can be made.

11.4 Windows of Operation

The validation of the Windows of Operation developed in this thesis, through the use large scale batch adsorptions, would provide interesting information regarding the accuracy and robustness of the Windows of Operation approach. For example, the verification of a given operating region could be achieved by processing the relevant feedstock at the suggested phase ratio. To test the robustness of the operating region, operating conditions beyond the boundaries of the operating region could be chosen and the resulting levels of process yield and throughput compared.

Appendix A1: Sigma calculations for centrifuges

Although not used directly in this thesis, the following section provides a brief description of the equations used in the Sigma theory, and has been taken from Salte (2006).

A1.1 Sigma equations

A1.1.1 Sigma factor

The general equation for the Sigma factor is given by Equation A1.1 (Ambler, 1959):

$$\Sigma = \frac{V\omega^2 r_e}{g s_e} \qquad \text{A1.1}$$

where V is the volume of liquid in the bowl, $\omega = 2\pi N$, N is the rotational speed, g is acceleration due to gravity, r_e is the effective radius of the centrifuge and s_e is the effective settling distance. Specific expressions for the calculation of Σ values for laboratory batch centrifuges, and disc-stack machines are given below.

Each centrifuge design has a unique expression for the Σ factor. The Σ factor a laboratory centrifuge, Σ_{lab}, is defined by Equation A1.2.

$$\Sigma_{lab} = \frac{V_{lab}\omega^2(3-2x-2y)}{6g\ln(\frac{2r_o}{r_o+r_i})} \qquad \text{A1.2}$$

where V_{lab} is the volume of feed material in laboratory tube, $\omega = 2\pi N$, N is the rotational speed, r_i is the inner radius (the distance between the centre of rotation and the top of the liquid), r_o is the outer radius (the distance between the centre of rotation and the bottom of the tube), g is the acceleration due to gravity, and x and y

are the fractional times required for acceleration and deceleration, respectively (Maybury *et al.*, 1998).

For a disc-stack centrifuge (for example, the Alfa Laval BTUX 510), the expression for Σ_{ds} is given by Equation A1.3.

$$\Sigma_{ds}= \frac{2\pi N_{AD}\omega^2(r_2^3 - r_1^3)}{3g\tan\theta} f_1 \qquad \text{A1.3}$$

where N_{AD} is the number of active discs, r_1 and r_2 are the inner and outer disc radius, respectively, θ is the half disc angle and f_1 is the correction factor for spacer caulks (assume $f_1 = 1$).

A1.2 USD predictions

Using Figures A1.1 and A1.2, both modified from Salte (2006), and Equation 5.1 it is possible to compare the separation performance of centrifuges of different size and design. In this case the $V_{lab}/t_{lab}\Sigma_{lab}$ data acquired through extrapolation is used to predict the volumetric flow rates which result in the desired levels of clarification when using the large scale Alfa Laval BTUX 510 centrifuge.

A1.2.1 Example calculation

The predicted clarification efficiency for an *E. coli* homogenate of 10% solids concentration (ww/v) is shown in Figure A1.1. As an example, a clarification level of 80% corresponds to a $V_{lab}/t_{lab}\Sigma_{lab}$ value of approximately $0.037\text{x}10^{-7}$ m/s. Multiplying this value by the $c\Sigma$ value (Equation 5.1) for the Alfa Laval BTUX 510, which is 42,400 m^2, gives a volumetric flow rate of 565 L/h. Operating this centrifuge at the calculated flow rate would then result in a clarification level of 80%.

The predicted clarification efficiency for an *E. coli* lysate of ~9% solids concentration (ww/v) is shown in Figure A1.2, and a similar approach to the one described above was used for this feed stream.

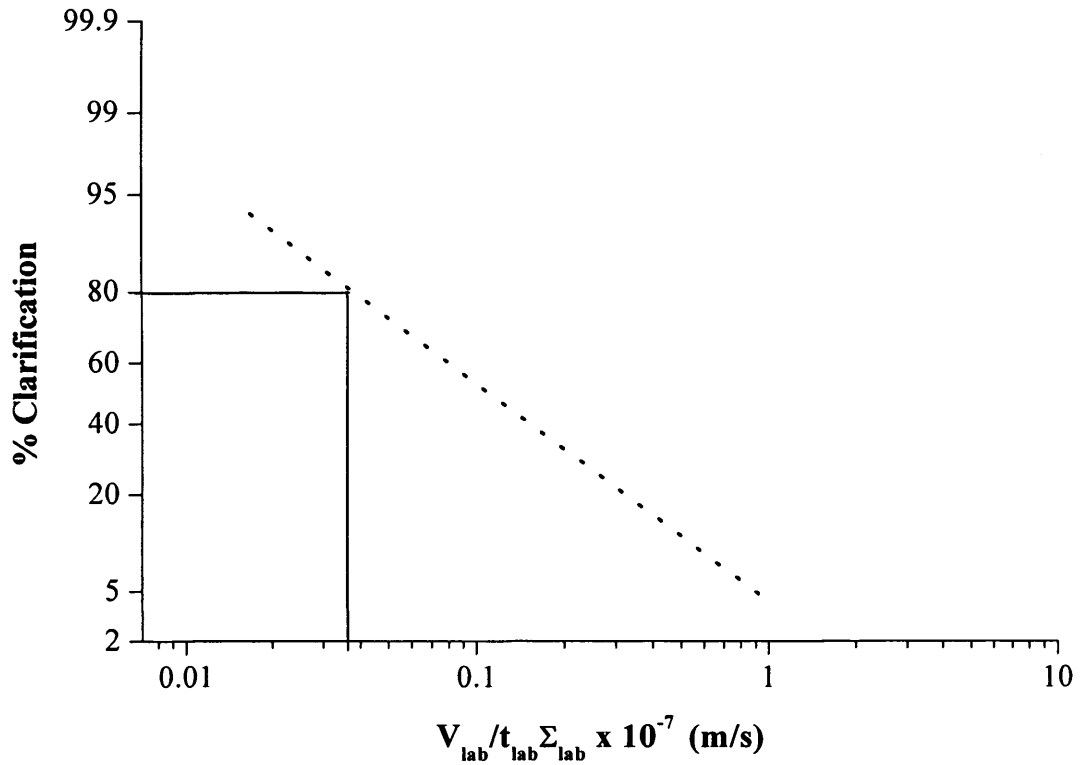

Figure A1.1. Figure A1.1. Predicted clarification efficiency for an *E. coli* homogenate of 10% (·····) (ww/v) solids concentration. Predictions were based on USD methodology using a 0.9% (ww/v) solids concentration feed as described by Salte (2006).

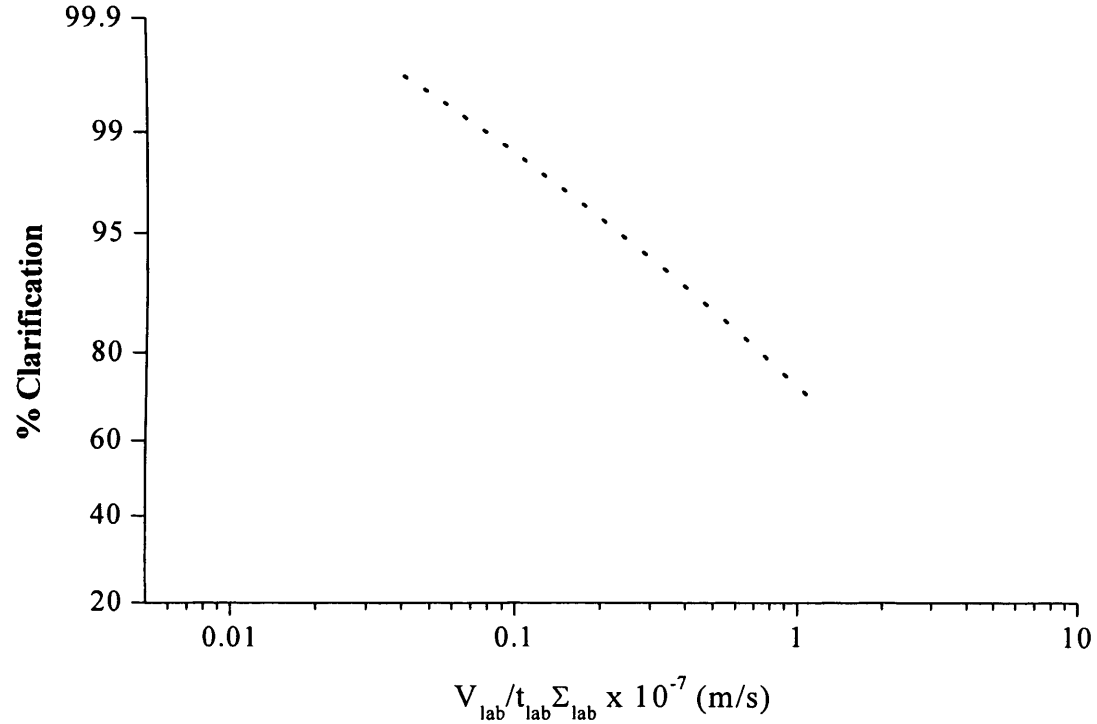

Figure A1.2. Predicted clarification efficiency for periplasmically lysed *E. coli* cells of ~9% solids concentration (ww/v) (·····). Figure modified from Salte (2006).

References

Aldridge, S. (2006) Downstream processing needs a boost. Genetic Engineering and Biotechnology News **26** (1) January 2006

Ambler, C.M. (1959) The theory of scaling up laboratory data for the sedimentation type centrifuge. Journal of Biochemical and Microbiological Technology and Engineering **1**: 185-205

Annadurai, G. and Krishnan, M.R.V. (1997) Batch equilibrium adsorption of reactive dye onto natural biopolymer. Iranian Polymer Journal **6** (3): 169-175

Andersen, D.C., Reilly, D.E. (2004) Production technologies for monoclonal antibodies and their fragments. Current Opinion in Biotechnology **15**: 456-462

Anspach, F.B., Curbelo, D., Hartmann, R., Garke, G. and Deckwer, W-D. (1999) Review: Expanded-bed chromatography in primary protein purification. Journal of Chromatography A **865**: 129-144

Barnfield-Frej, A-K. (1996) Expanded bed adsorption for recovery of renatured human recombinant interleukin 8 from *Escherichia coli* inclusion bodies. Bioseparation **6**: 265-271

Barnfield-Frej, A-K., Hjorth, R., Hammarstrom, A. (1994) Pilot scale recovery of recombinant annexin V from unclarified Escherichia coli homogenate using expanded bed adsorption. Biotechnology and Bioengineering **44**: 922-929

Bastek, P., Molner, K., Kelley, B., Coffman, J. (2004) High-throughput screening of resins and excipients for chromatographic process development. Presented at ACS National Meeting, Anaheim, CA, USA

Bensch, M., Wierling, P.S., von Lieres, E., Hubbuch, J. (2005) High throughput screening of chromatographic phases for rapid process development. Chemical Engineering and Technology **28** (11): 1274-1284

Bayramoglu, G., Yalçin, E. and Arica, M.Y. (2005) Adsorption of serum albumin and γ-globulin from single and binary mixture and characterization of pHEMA-based affinity membrane surface by contact angle measurements. Biochemical Engineering Journal **26** (1): 12-21

Beacham, I.R. (1979) Periplasmic enzymes in gram-negative bacteria. International. Journal of Biochemistry **10** (11): 877-883

Belter P.A., Cussler, E.L. and Hu, W.S. (1988) Bioseparations: Downstream Processing for Biotechnology. John Wiley & Sons, New York.

Berry, M.J., Davies, J. (1992) Use of antibody fragments in immunoaffinity chromatography: Comparison of Fv fragments, V_H fragments and paralog peptides. Journal of Chromatography A **597**: 239-245

Bird, R.E., Hardman, K.D., Jacobson, J.W., Johnson, S., Kaufman, B.M., Lee, S.M., Lee, T., Pope, S.H., Riordan, G.S. and Whitlow, M. (1988) Single-chain antigen binding proteins. Science **242**: 423-426

BioPharm International (2003) The BioPharm International Guide to columns July 2003. Column Packing for Process-Scale Chromatography: Guidelines for Reproducibility

Blank, G.S., Zapata, G., Fahrner, R., Milton, M., Yedinak, C., Knudsen, H., Schmelzer, C. (2001) Expanded bed adsorption in the purification of monoclonal antibodies: a comparison of process alternatives. Bioseparation **10**: 65-71

Bonnerjea, J., Oh, S., Hoare, M., Dunnill, P. (1986) Protein purification: the right step at the right time. Bio/Technology **4**: 954-958

Bowering, L.C., Bracewell, D.G., Keshavarz-Moore, E., Hoare, M., Weir, A.N.C. (2002) Comparison of techniques for monitoring antibody fragment production in *E. coli* fermentation cultures. Biotechnology Progress **18**: 1431-1438

Brinkmannn, U., Di Carlo, A., Vasmatzis, G., Kurochkina, N., Beers, R., Lee, B., Pastan, I. (1997) Stabilization of a recombinant Fv fragment by base-loop interconnection and V_H-V_L permutation. Journal of Molecular Biology **268**: 107-117

Brooks, C.A. and Cramer, S.M. (1992) Steric Mass-Action ion exchange: displacement profiles and induced salt gradients. American Institute of Chemical Engineers Journal **38** (12): 1969-1978

Brunauer, S., Emmet, P.H. and Teller, E. (1938) Adsorption of gases in multimolecular layers. Journal of the American Chemical Society **60** (2): 309-319

Chang, C., Lenhoff, A. (1998) Comparison of protein adsorption isotherms and uptake rates in preparative cation-exchange materials. Journal of Chromatography A **827**: 281-293

Chang, Y-K., Horn, J-T., Huanga, R-Z., Lin, S-Y. (2006) Direct recovery of clotting factor IX from unclarified human plasma by expanded bed ion exchange chromatography. Biochemical Engineering Journal **30**: 138-146

Chase, H.A. (1994) Purification of proteins by adsorption chromatography in expanded beds. Trends in Biotechnology **12**: 296-303.

Chase, H.A. and Draeger, N.M. (1992). Expanded bed adsorption of proteins using ion-exchangers. Separation Science and Technology **27** (14): 2021-2039

Chhatre, S., Francis, R., O'Donovan, K., Titchener-Hooker, N.J., Newcombe, A.R., Keshavarz-Moore, E. (2007) A decision-support model for evaluating changes in biopharmaceutical manufacturing processes. Bioprocess and Biosystems Engineering **30**: 1-11

Chen, L-H., Huang, Q., Wan, L., Z, L-Y., Li, S-F., Li, Y-P., Lu, X-F., Cheng, J-Q. (2006a) Expression, purification, and in vitro refolding of a humanised single-chain Fv antibody against human CTLA4 (CD152). Protein Expression and Purification **46**: 495-502

Chen, W-D., Huc, H-H., Wang, Y-D. (2006b) Analysis of steric mass-action model for protein adsorption equilibrium onto porous anion-exchange adsorbent. Chemical Engineering Science **61**: 7068-7076

Colby, C.B., O'Neill, B.,K., Vaughan, F., Middelberg, A.P.J. (1996a) Simulation of compression effects during scaleup of a commercial ion-exchange process. Biotechnology Progress **12**: 662-681

Colby, C.B., O'Neill, B.,K., Middelberg, A.P.J. (1996b) A modified version of the volume-averaged continuum theory to predict pressure drop across compressible packed beds of Sepharose Big-Beads SP. Biotechnology Progress **12**: 92-99

Dainiak, M.B., Kumar, A., Plieva, F.M., Galaev, I.Y., Mattiasson, B. (2004). Integrated isolation of antibody fragments from microbial cell culture fluids using supermacroporous cryogels. Journal of Chromatography A **1045**: 93-98

Data File HiTrap Protein G. GE Healthcare, Uppsala, Sweden.

Data File Malvern Mastersizer 2000: The science behind the technology. Malvern Instruments

De Neve, M., De Loose, M., Jacobs, A., Van Houdt, H., Kaluza, B., Weidle, U., Van Montagu, M., Depicker, A. (1993) Assembly of an antibody and its derived antibody fragment in Nicotiana and Arabidopsis. Transgenic Research **2**: 227-237.

Dechow, F. J. (1989) Separation and purification techniques in biotechnology. Noyes Publications, New Jersey.

Derrick, J.P. and Wigley, D.B. (1994) The third IgG-binding domain from streptococcal protein G. An analysis by X-ray crystallography of the structure alone and in a complex with Fab. Journal of Molecular Biology **243** (5): 906-918

Doran, P.M. (2002) Bioprocess Engineering Principles. Academic Press Ltd. San Diego.

Drager, R.R. and Regnier F.E. (1986) Application of the stoichiometric displacement model of retention to anion-exchange chromatography of nucleic acids. Journal of Chromatography A **359**: 147-155

DrugResearcher.com (2005) Worldwide antibody market to reach $26 billion. DrugResearcher.com article 02/06/2005

Dziennik, S.R., Belcher, E.B., Barker, G.A., Lenhoff, A.M. (2005) Effects of ionic strength on Lysozyme uptake rates in cation exchangers. 1: Uptake in SP Sepharose FF. Biotechnology and Bioengineering **91** (2): 139-153

Evans, D. and Das, R. (2005) Monoclonal antibody therapies: evolving into a $30 billion market. DataMonitor, London, UK

Expanded Bed Adsorption Handbook (EBA). GE Healthcare. Code No 18-1124-26 Edition AA.

Fahrner, R.L., Blank, G.S., Zapata, G.A. (1999) Expanded bed protein A affinity chromatography of a recombinant humanized monoclonal antibody: process development, operation, and comparison with a packed bed method. Journal of Biotechnology **75**: 273-280

Farid, S.S., Washbrook, J., Titchener-Hooker, N.J. (2005) Combining multiple quantitative and qualitative goals when assessing biomanufacturing strategies under uncertainty. Biotechnology Progress **21** (4): 1183-1191

Fargues, C., Bailly, M., Grevillot, G. (1998) Asorption of BSA and Hemoglobin on hydroxyapatite support: Equilibria and multicomponent dynamic adsorption. Adsorption **4** (5): 5-16

Fee, C.J. and Chand, A. (2005) Design considerations for the batch capture of proteins from raw whole milk by ion exchange chromatography. Chemical Engineering and Technology **28** (11): 1360-1366

Ferreira, G.N.M., Cabral, J.M.S., Prazeres, D.M.F. (2000) Studies on the batch adsorption of plasmid DNA onto anion-exchange chromatographic supports. Biotechnology Progress **16**: 416-424

Feuser, J., Halfar, M., Lutkemeyer, D., Ameskamp, N., Kula, M.-R., Thömmes, J. (1999a) Interaction of mammalian cell culture broth with adsorbents in expanded bed adsorption of monoclonal antibodies. Process Biochemistry **34**: 159-165

Feuser, J., Walter, J., Kula, M-R., Thömmes, J. (1999b) Cell/adsorbent interactions in expanded bed adsorption of proteins. Bioseparation **8**: 99-109

Finette, G.M.S., Mao, Q-M., Hearn, M.T.W. (1997) Comparative studies on the isothermal characteristics of proteins adsorbed under batch equilibrium conditions to ion-exchange, immobilised metal ion affinity and dye matrices with different ionic strength and temperature conditions. Journal of Chromatography A **763**: 71-91

Fiedler, U., Phillips, J., Artsaenko, O., Conrad, U. (1997) Optimization of scFv antibody production in transgenic plants. Immunotechnology **3**: 205-216.

French, C., Keshavarz-Moore, E., Ward, J.M. (1996) Development of a simple method for the recovery of recombinant proteins from the *Escherichia coli* periplasm. Enzyme and Microbial Technology **19**: 332-338

Frenken, L.G.J., Hessing, J.G.M., Van den Hondel, C.A.M.J.J., Verrips, C.T. (1998) Recent advances in the large-scale production of antibody fragments using lower eukaryotic microorganisms. Research in immunology **149**: 589-599

Freundlich, H.M.F. (1906) Over the adsorption in solution. Journal of Physical Chemistry **57** (A): 385-470

Freyre, F.M., Vazquez, J.E., Ayala, M., Canaan-Haden, L., Bell, H., Rodriguez, I., Gonzalez, A., Cintado, A., Gavilondo, J.V. (2000) Very high expression of an anti-carcinoembryonic antigen single chain Fv antibody fragment in the yeast *Pichia pastoris*. Journal of Biotechnology **76**: 157–163

Follman, D.K., Fahrner, R.L. (2004) Factorial screening of antibody purification processes using three chromatography steps without protein A. Journal of Chromatography A **1024**: 79-85

Gavin, D., Gagnon, P. (2006) Building process control into chromatographic purification of viruses, part 1. BioProcess International November 2006

Giles, C. H., MacEwan, T. H., Nakhwa, S. N., Smith, D. (1960) Studies in adsorption. Part XI. A system of classification of solution adsorption isotherms, and its use in diagnosis of adsorption mechanisms and in measurement of specific surface areas of solids. Journal of the American Chemical Society: 3973-3993

Glockshuber, R., Malia, M., Pfitzinger, I. and Plückthun, A. (1990) A comparison of strategies to stabilize immunoglobulin Fv-fragments. Biochemistry **29**: 1362-1367

Gonzalez, Y., Ibarra, N., Gomez, H., Gonzalez, M., Dorta, L., Padilla, S., Valdes, R. (2003) Expanded bed adsorption processing of mammalian cell culture fluid: comparison with packed bed affinity chromatography. Journal of Chromatography B **784**: 183 187

Goyal, D., Sahoo, D.K., Sahni, G (2006) Hydrophobic interaction expanded bed adsorption chromatography (HI-EBAC) based facile purification of recombinant Streptokinase from E. coli inclusion bodies. Journal of Chromatography B In Press, Corrected Proof, Available online 26 December 2006

Gronenborn, A.M. and Clore, G.M. (1993) Identification of the contact surface of a Streptococcal Protein G domain complexed with a human Fc fragment. Journal of Molecular Biology **233** (3): 331-335

Gu, T., Tsao, G.T., Tsai, G-J., Ladisch, M.R. (1990) Displacement effect in multicomponent chromatography. American Institute of Chemical Engineering Journal **36** (8): 1156-1162

Gu, T. (1995) Mathematical Modelling and Scale Up of Liquid Chromatography. Springer Press, Berlin.

Hahn, R., Schlegel, R., Jungbauer, A. (2003) Comparison of protein A affinity sorbents. Journal of Chromatography B **790**: 35-51

Harinarayan, C., Mueller, J., Ljunglof, A., Fahrner, R., Van Alstine, J., van Reis, R. (2006) An exclusion mechanism in ion exchange chromatography. Biotechnology and Bioengineering **95** (5): 775-787

Hashim, M. A., Chu, K-H., Tsan, P-S. (1995) Effects of ionic strength and pH on the adsorption equilibria of Lysozyme on ion exchangers. Journal of Chemical Technology and Biotechnology **62**: 253-260

Hjorth, R. (1997) Expanded bed adsorption in industrial bioprocessing: recent developments. Trends in Biotechnology **15**: 230-235

Humphreys, D.P., Heywood, S.P., King, L.M., Bowering, L.C., Turner, J.P., Lane, S.E. (2004) Engineering of *Escherichia coli* to improve the purification of periplasmic Fab' fragments: changing the p*I* of the chromosomally encoded PhoS/PstS protein. Protein Expression and Purification **37**: 109-118

Huston, J.S., Levinson, D., Mudgett-Hunter, M., Tai, M-S., Novotny, J., Margolies, M.N., Ridge, R.J., Bruccoleri, R.E., Haber, E., Crea, R., Oppermann, H. (1998) Protein engineering of antibody binding sites: Recovery of specific activity in an anti-digoxin single-chain Fv analogue produced in *Escherichia coli*. Proceedings of the National Academy of Sciences of USA **87** (16): 5879-5883

Ishihara, T., Yamamoto, S. (2005) Optimization of monoclonal antibody purification by ion-exchange chromatography: Application of simple methods with linear gradient elution experimental data. Journal of Chromatography A **1069**: 99-106

Janson, J-C. and Jönsson, J-Å (1998) Introduction to chromatography, in Protein Purification: Principles, High Resolution Methods and Applications (J-C. Janson and L. Rydén, Eds.). John Wiley & Sons, New York.

Johnson, B.H. and Hecht, M.H. (1994) Recombinant proteins can be isolated from *E. coli* cells by repeated cycles of freezing and thawing. Bio/Technology **12**: 1357-1360

Joosten, V., Lokman C., van den Hondel, C. and Punt, P.J. (2003) The production of antibody fragments and antibody fusion proteins by yeasts and filamentous fungi. Microbial Cell Factories **2**: 1-15

Jozwik, M., Kaczmarski, K., Freitag, R. (2005) Evaluation of the Langmuir formalism for modelling the adsorption isotherms of proteins and polyelectrolytes in simulations of ion exchange chromatography. Chemical Engineering and Technology **28** (11): 1346-1359

Kaltenbrunner, O., Jungbauer, A. (1996) Adsorption isotherms in protein chromatography. Combined influence of protein and salt concentration on adsorption isotherm. Journal of Chromatography A **734**: 183-194

Karlsson, D., Jakobsson, N., Axelsson, A., Nilsson, B. (2004) Model-based optimisation of a preparative ion-exchange step for antibody purification. Journal of Chromatography A **1055**: 29-39

Katti, A.M. and Jagland, P. (1998) Development and optimisation of industrial scale chromatography for use in manufacturing. Analusis Magazine **26** (7): 38-46

Keshavarz-Moore, E., Hoare, M., Dunnill, P. (1990) Disruption of baker's yeast in a high-pressure homogeniser: New evidence on mechanism. Enzyme and Microbial Technology **12**: 764 770

King, J.M.P., Griffiths, P., Zhou, Y., Titchener-Hooker, N.J. (2004) Visualising bioprocesses using '3D-Windows of Operation'. Journal of Chemical Technology and Biotechnology **79**: 518-525

Kleinig, A. R., O'Neill, B.K., Middelberg, A.P.J. (1996) The effect of homogeniser impact distance on the disruption of *E. coli.* Biotechnology Techniques **10** (3): 199-204

Kondo, A. and Fukuda, H. (1998) Effects of adsorption conditions on kinetics of protein adsorption and conformational changes at ultrafine silica particles Journal of Colloid and Interface Science **198**: 34–41

Kortt, A.A., Lah, M., Oddie, G.W., Gruen, C.L., Burns, J.E., Pearce, L.A., Atwell, J.L., McCoy, A.J., Howlett, G.J., Metzger, D.W., Webster, R.G., Hudson, P.J. (1997) Single-chain Fv fragments of anti-neuraminidase antibody NC10 containing five- and ten-residue linkers form dimers and with zero-residue linker a trimer. Protein Engineering **10** (4): 423-433

Lall, S.D., Eriho, B.E, Jay, J.M. (1989) Comparison for four methods for extracting periplasmic proteins. Journal of Microbiological Methods **9** (3): 195-199

Lam, K.S., Gustavson, D.R., Veitch, J.M., Forenza, S., Ross, J., Miller, D., Roach, J., Lebherz III, W.B., Poole, K. (1994) Large scale production and semi-purification of kedarcidin in a 1000 L fermentor. Journal of Industrial Microbiology **13**: 356-360

Lan, Q., Bassi, A. S., Zhu, J-X., Margaritis, A. (2001) A modified Langmuir model for the prediction of ionic strength on the equilibrium characteristics of protein adsorption onto ion exchange/affinity adsorbents. Chemical Engineering Journal **81**: 179-186

Langmuir, I. (1918) The adsorption of gases on plane surfaces of glass, mica and platinum. Journal of the American Chemical Society **40**: 1361-1403

Larrick, J.W., Thomas, D. (2001) Producing proteins in transgenic plants and animals. Current Opinion in Biotechnology **12**: 411-418

Lee, S-M., Gustafson, M.E., Pickle, D.J., Flickinger, M.C., Muschik, G.M., Morgan Jr., A.C. (1986) Large-scale purification of a murine antimelanoma monoclonal antibody. Journal of Biotechnology **4** (4): 189-204

Levison, P.R., Badger, S.E., Toome, D.W., Koscielny, M.L., Lane, L., Butts, E.T. (1992) Economic considerations important in the scale-up of an ovalbumin separation from hen egg-white on the anion-exchange cellulose DE92. Journal of Chromatography A **590**: 49-58

Levison, P.R., in: Ganetsos, G., Barker, P.E. (Editors) (1993) Preparative and production scale chromatography; Marcel Dekker, New York

Levison, P.R., Hopkins, A.K., Hathi, P., Badger, S.E., Mann, F., Dickson, N., Purdon, G. (2000) Suspended bed chromatography, a new approach in downstream processing. Journal of Chromatography A **890**: 45-51

Lian, L-Y., Barsukov, I.L., Derrick, J.P., Roberts, G.C.K. (1994) Mapping the interactions between streptococcal protein G and the Fab fragment of IgG in solution. Nature Structural Biology **1** (6): 355-357

Lim, A.C., Washbrook, J., Titchener-Hooker, N.J., Farid, S.S. (2006) A computer aided approach to compare the production economics of fed batch and perfusion culture under uncertainty. Biotechnology and Bioengineering **93** (4): 687 697

Lin, L-C., Putnam, F.W. (1978) Cold pepsin digestion: A novel method to produce the Fv fragment from human immunoglobulin M. Proceedings of the National Academy of Sciences of USA **75** (6): 2649-2653

Linden, T., Ljunglöf, A., Hagel, L., Kula, M-R., Thömmes, J. (2002) Visualizing patterns of protein uptake to porous media using confocal scanning laser microscopy. Separation Science and Technology **37**: 1-32

Ling, T.C., Lyddiatt, A., Carmichael, I., Purdon, G., Hathi, P., Levison, P.R. (2003) Direct enzyme adsorption from an unclarified microbial feedstock using suspended bed chromatography. Journal of Chromatography A **989**: 109-118

Ljunglöf, A, Lacki, K.M., Mueller, J., Harinarayan, C., Van Reis, R., Fahrner, R., Van Alstine, J. M. (2007) Ion exchange chromatography of antibody fragments. Biotechnology and Bioengineering **96** (3): 515-524

Loetscher, P., Mottlau, L., Hochuli, E. (1992) Immobilization of monoclonal antibodies for affinity chromatography using a chelating peptide. Journal of Chromatography A **595**: 113-119

Lyddiatt, A. (2002) Process chromatography: current constraints and future options for the adsorptive recovery of bioproducts. Current Opinion in Biotechnology **13**: 95-103

Maybury, J.P., Mannweiler, K., Titchener-Hooker, N.J., Hoare, M., Dunnill, P. (1998) The performance of a scaled-down industrial disc-stack centrifuge with a reduced feed material requirement. Bioprocess and Biosystems Engineering **18** (3): 191-199

Maynard, J., Georgiou, G. (2000) Antibody engineering. Annual Review of Biomedical Engineering **2**: 339-376

McDonald, J.R., Ong, M., Shen, C., Parandoosh, Z., Sosnowski, B., Bussel, S., Houston, L.L. (1996) Large-scale purification and characterization of recombinant fibroblast growth factor-saporin mitotoxin. Protein Expression and Purification **8**: 97-108

Mhatre, R., Nashabeh, W., Schmalzing, D., Yao, X., Fuchs, M., Whitney, D., Regnier, F. (1995) Purification of antibody Fab fragments by cation-exchange chromatography and pH gradient elution. Journal of Chromatography A **707**: 225-231

Melter, L., Ströhlein, G., Butte, A., Morbidelli, M. (2007) Adsorption of monoclonal antibody variants on analytical cation-exchange resin. Journal of Chromatography A **1154**: 121-131

Miyabe, K., Guichon, G. (2004) Characterisation of monolithic columns for HPLC. Journal of Separation Science **27**: 853-873

Moreira, M.J., Ferreira, L.M. (2005) Kinetic studies for sorption of amino acids using a strong anion-exchange resin. Effect of ionic strength. Journal of Chromatography A **1092**: 101-106

Mustafa, M.A., Washbrook, J., Titchener-Hooker, N.J., Farid, S.S. (2006) Retrofit decisions within the biopharmaceutical industry. An EBA case study. Food and Bioproducts Processing **84** (C1): 84–89

Naglak, T.J. and Wang, H.Y. (1990) Recovery of a foreign protein from the periplasm of *Escherichia coli* by chemical permeabilisation. Enzyme and Microbial Technology **12** (8): 603-611

Nature (2002) Magic bullets hit the target. Nature **417**: 584-586 6th June 2002

Nealon, A.J., Willson, K.E., Pickering, S.C.R., Clayton, T.M., O'Kennedy, R., Titchener-Hooker, N.J., Lye, G.J. (2005) Use of operating windows in the assessment of integrated robotic systems for the measurement of bioprocess kinetics. Biotechnology Progress **21**: 283-291

Neu, H.C., Heppel, L.A. (1965) The release of enzymes from *Escherichia coli* by osmotic shock and during the formation of spheroplasts. Journal of Biological Chemistry **24**: 3685-3692

Novais, J. (2001) Economic and engineering aspects of disposables-based bioprocessing. PhD thesis, University of London

Novais, J.L., Titchener-Hooker, N.J., Hoare, M. (2001) Economic comparison between conventional and disposables-based technology for the production of biopharmaceuticals. Biotechnology and Bioengineering **75** (2): 143-153

Pallapothu, M.K., Padia, J., Kayser, A. (2006) Integrated process design and development - Finding the optimal Window of Operation and steering clear of bottlenecks. Genetic Engineering Biotechnology News **26** (15) Sept. 2006

Peeters, K., De Wilde, C., De Jaeger, G., Angenon, G., Depicker, A. (2001) Production of antibodies and antibody fragments in plants. Vaccine **19**: 2756-2761

Petrides, D.P., Koulouris, A., Lagonikos, P.T. (2002) The role of process simulation in pharmaceutical process development and product commercialisation. Pharmaceutical Engineering **22** (1) Jan/Feb. 2002

Pierce, J.J., Turner, C., Keshavarz-Moore, E., Dunnill, P. (1997) Factors determining more efficient large-scale release of a periplasmic enzyme from *E. coli* using Lysozyme. Journal of Biotechnology **58**: 1-11

Pierce J.J., Fischer, E.J., Smith, M.P., Turner, C., Keshavarz-Moore, E., Dunnill, P. (1999) Purification of a periplasmic enzyme by a stirred adsorbent, and by expanded and packed bed. Bioprocess Engineering **20**: 449-457

Przybycien, T., Pujar, N., Steele, L.M. (2004) Alternative bioseparation operations: life beyond packed-bed chromatography. Current Opinion in Biotechnology **15**: 469-478

Quinones-Garcia, I., Raynor, I., Levison, P.R., Dickson, N., Purdom, G. (2001) Performance comparison of suspended bed and batch contactor chromatography. Journal of Chromatography A **908**: 169-178

Rathore, A. S., Latham, P., Kaltenbrunner, O., Curling, J., Levine, H. (2004) Costing issues in the production of biopharmaceuticals. BioPharm International, February 2004

Rege, K., Pepsin, M., Falcon, B., Steele, L., Heng, M. (2006) High-Throughput process development for recombinant protein purification. Biotechnology and Bioengineering **93** (4): 618-63

Rehm, H. J., Reed, G. (1993) Biotechnology: Volume 3, Bioprocessing. John Wiley & Sons, New York.

Roitt, I.M. (1991) Essential Immunology. Blackwell Scientific Publications, Oxford, UK

Roque, A.C.A., Lowe, C.R., Taipa, M.A. (2004) Antibodies and genetically engineered related molecules: Production and purification. Biotechnology Progress **20**: 639-654

Rouf, S.A., Douglas, P.L., Moo-Young, M., Scharer, J.M. (2001a) Computer simulation for large scale bioprocess design. Biochemical Engineering Journal **8**: 229-234

Rouf, S.A., Douglas, P.L., Moo-Young, M., Scharer, J.M. (2001b) Economics of fed batch operation: a computer aided approach. Bioprocess and Biosystems Engineering **24** (1): 65-71

Ryan, W., Parulekar, S.J. (1991) Recombinant protein excretion in *Escherichia coli* JM103 (pUC 8): Effects of plasmid content, ethylenediaminetetraacetate, and phenethyl alcohol on cell membrane permeability. Biotechnology and Bioengineering **37**: 430-444

Salte, H. (2006) Rapid evaluation of options for the primary recovery of antibody fragments expressed in high cell density cultures. PhD thesis, University of London

Salte, H., King, J.M.P., Baganz, F., Hoare, M., Titchener-Hooker, N.J. (2006) A methodology for centrifuge selection for the separation of high solids density cell broths by visualisation of performance using Windows of Operation. Biotechnology and Bioengineering **95** (6): 1218-1227

Sauer, T., Robinson, C.W., Glick, B.R. (1989) Disruption of native and recombinant *Escherichia coli* in a high-pressure homogenizer. Biotechnology and Bioengineering **33**: 1330-1342

Seidel-Morgenstern, A. (2004) Experimental determination of single solute and competitive adsorption isotherms. Journal of Chromatography A **1037**: 255-272

Selisko, B., Cosío, G., García, C., Becerril, B., Possani, D.L., Horjales, E. (2004) Bacterial expression, purification and functional characterization of a recombinant chimeric Fab derived from murine mAb BCF2 that neutralizes the venom of the scorpion Centruroides noxius Hoffmann. Toxicon **43** (1): 43-51

Sharma, S. and Agarwal, G.P. (2001) Interactions of proteins and metal ions: role of ionic strength and pH. Journal of colloid and interface science **243**: 61-72

Siddiqi, S.F., Titchener-Hooker, N.J., Shamlou, P.A. (1996) High Pressure disruption of yeast cells: The use of scale down operations for the prediction of protein release and cell debris size distribution. Biotechnology and Bioengineering **55**: 642 649

Sigma product information sheet – Sodium Acetate Trihydrate. Sigma-Aldrich. http://www.sigmaaldrich.com/catalog/search/ProductDetail/SIAL/S8625

Sinclair, A. and Monge, M. (2002) Quantitative economic evaluation of single use disposables in bioprocessing. Pharmaceutical Engineering **22** (3) May/June 2002

Skidmore, G.L., Horstmann, B.J., Chase, H.A. (1990) A Modelling single component protein adsorption to the cation exchanger S Sepharose® FF. Journal of Chromatography **488**: 113-128

Skidmore, G.L. and Chase, H.A. (1990) Two-component protein adsorption to the cation exchanger S Sepharose® FF. Journal of Chromatography **505**: 329-347

Smith, M.P., Bulmera, M.A., Hjorth, R., Titchener-Hooker, N.J. (2002) Hydrophobic interaction ligand selection and scale-up of an expanded bed separation of an intracellular enzyme from *Saccharomyces cerevisiae*. Journal of Chromatography A **968**: 121-128

Sofer, G. and Hagel, L. (1997) Handbook of Process chromatography: A Guide to Optimization, Scale-Up and Validation; Academic Press, San Diego.

Sofer, G.K. and Nystrom, L.-E. (1989) Process Chromatography; A Practical Guide: Academic Press, San Diego.

Staby, A., Johansen, N., Wahlstrom, H., Mollerup, I. (1998) Comparison of loading capacities of various proteins and peptides in culture medium and in pure state. Journal of Chromatography A **827**: 311-318

Staby, A., Sand, M-B., Hansen, R.G., Jacobsen, J.H., Andersen, L.A., Gerstenberg, M., Bruus, U. K., Jensen, I. H. (2004) Comparison of chromatographic ion-exchange resins III. Strong cation-exchange resins. Journal of Chromatography A **1034**: 85-97

Ståhlberg, J., Jönsson, B., Horváth, C. (1992) Combined Effect of Coulombic and van der Waals Interactions in the chromatography of Proteins. Analytical Chemistry **64**: 3118-3124

Stein, A. and Kiesewetter, A. (2007) Cation exchange chromatography in antibody purification: pH screening for optimised binding and HCP removal. Journal of Chromatography B **848**: 151-158

Stickel, J. J., Fotopoulos, A. (2001) Pressure-flow relationships for packed beds of compressible chromatography media at laboratory and production scale. Biotechnology Progress **17** (4): 744-751

Thiemann, J., Jankowski, J., Rykl, J., Kurzawski, S., Pohl, T., Wittmann-Liebold, B., Schlüter, H. (2004) Principle and applications of the protein-purification-parameter screening system. Journal of Chromatography A **1043**: 73-80

Thömmes, J., Bader, A., Halfar, M., Karau, A., Kula, R-M. (1996) Isolation of monoclonal antibodies from cell containing hybridoma broth using a protein A coated adsorbent in expanded beds. Journal of Chromatography A **752**: 111-122

Thömmes, J., Halfar, M., Gieren, H., Curvers, S., Takors, R., Brunschier, R., Kula, M-R. (2001) Human Chymotrypsinogen B Production from *Pichia pastoris* by Integrated Development of Fermentation and Downstream Processing. Part 2. Protein Recovery. Biotechnology Progress **17**: 503-512

Tran, R. and Joseph, J.R., Sinclair, A., Bracewell, D., Zhou, Y., Titchener-Hooker, N.J. (2007) A framework for the prediction of scale-up when using compressible chromatographic packings. Biotechnology Progress **23**: 413-442

Tsuchido, T., Katsui, N., Takeuchi, A., Takano, M., Shibaski, I. (1985) Destruction of the outer membrane permeability barrier of *Escherichia coli* by heat treatment. Applied and Environmental Microbiology **50** (2): 298-303

Ujam, L.B., Clemmitt, R.H., Chase, H.A. (2000) Cell separation by expanded bed adsorption: use of ion exchange chromatography for the separation of *E. coli* and *S. cerevesiae*. Bioprocess Engineering **23**: 245-250

US FDA (1987). Guidelines on general principles of process validation. Center for Drugs and Biologics, Center for Devices and Radiological Health, FDA, Rockville USA.

Valdes, R., Gomez, L., Padilla, S., Brito, J., Reyes, B., Alvarez, T., Mendoza, O., Herrera, O., Ferro, W., Pujol, M., Leal, V., Linares, M., Hevia, Y., Garcia, C., Mila, L., Garcia, O., Sanchez, R., Acosta, A., Geada, D., Paez, R., Vega J.L., Borroto, C. (2003) Large-scale purification of an antibody directed against hepatitis B surface antigen from transgenic tobacco plants. Biochemical and Biophysical Research Communications **308**: 94-100

Vaughan, T.J., Osbourn, J.K., Tepmest, P.R. (1998) Human antibodies by design. Nature Biotechnology **16**: 535-539

Velayudhan, A. and Horváth, C. (1988) Preparative chromatography of proteins: Analysis of the multivalent ion-exchange formalism. Journal of Chromatography A **443**: 13-29

Weir. A. N.C. and Bailey, N. A. (1997) Process for obtaining antibodies utilising heat treatment. US Patent 5,665,866

Weir, N.C., Nesbitt, A., Chapman, A.P., Popplewell, A.G., Antoniw, P., Lawson, A.D.G. (2002) Formatting antibody fragments to mediate specific therapeutic functions. Biochemical Society Transactions **30** (4): 512-516

Welch, C.J., Shaimi, M., Biba, M., Chilenski, J.R., Szumigala Jr, R.H., Dolling, U., Mathre, D.J., Reider, P.J. (2002) Microplate evaluation of process adsorbents. Journal of Separation Science **25**: 847-850

Whitlow, M., Bell, B.A., Feng, S-L., Filpula, D., Hardman, K.D., Hubert, S.L., Rollence, M.L., Wood, J.F., Schoot, M.E., Milenic, D.E., Yokota, T., Schlom, J. (1993) An improved linker for single-chain Fv with reduced aggregation and enhanced proteolytic stability. Protein Engineering **6** (8): 989-995

Whitlow, M., Filpula, D., Rollence, M.L., Feng, S-L., Wood, J.F. (1994) Multivalent Fvs: characterization of single-chain Fv oligomers and preparation of a bispecific Fv Protein Engineering **7** (8): 1017-1026

Wlad, H., Ballagi, A., Bouakaz, L., Gu, Z., Janson, J-C. (2001) Rapid two-step purification of a recombinant mouse Fab fragment expressed in *Escherichia coli.* Protein Expression and Purification **22**: 325-329

Woodley, J.M. and Titchener-Hooker, N.J. (1996) The use of Windows of Operation as a bioprocess design tool. Bioprocess Engineering **14**: 263-268

Yamamoto, S. (1995) Plate height determination for gradient elution chromatography of proteins. Biotechnology and Bioengineering **48**: 444-451

Yamamoto, S., Nakanishi, K., Matsuno, R., Kamikubo, T. (1983) Ion exchange chromatography of proteins-prediction of elution curves and operating conditions. II. Experimental verification. Biotechnology and Bioengineering **15**: 1373-1391

Yokota, T., Milenic, D.E., Whitlow, M., Schloml, J. (1992) Rapid tumor penetration of a single-chain Fv and comparison with other immunoglobulin forms. Cancer Research **52**: 3402-3408

Yu, P., Aristidou, A.A., San, K.S. (1991) Synergistic effect of glycine and bacteriocin release protein in the release of periplasmic protein in recombinant *E. coli*. Biotechnology Letters **13**: 311-316

Zanette, D., Dundon, W., Soffientini, A., Sottani, C., Marinelli, F., Akeson, A., Sarubbi, E. (1998) Human IL-1 receptor antagonist from *Escherichia coli*: Large scale microbial growth and protein purification. Journal of Biotechnology **64**: 187-196

Zhou, Y., Titchener-Hooker, N.J. (1999) Visualizing integrated bioprocess designs through 'Windows of Operation'. Biotechnology and Bioengineering **65**: 550-557

Zucker, A.R., Lacina, S.J., DasGupta, D.S., Fozzard, H.A., Mehlman D., Butler Jr, V.P., Haber, E., Smith, T.W. (1982) Fab fragments of digoxin-specific antibodies used to reverse ventricular fibrillation induced by digoxin ingestion in a child. Pediatrics **70** (3): 468-471